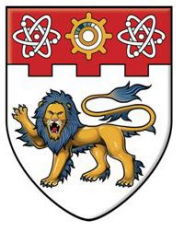

NANYANG TECHNOLOGICAL UNIVERSITY

Discovery of Novel Non-Immunosuppressive Immunophilin Ligands Modulating Functions of *Plasmodium* FKBP35 and Human FKBP38

Amaravadhi. V. K. Harikishore

School of Biological Sciences

Nanyang Technological University

2012

Contents

Acknowledgments

I express my sincere gratitude to my supervisor, A/Prof. Yoon Ho Sup, for his continuous guidance and support, which has been a source of inspiration to pursue my research work.

Many Thanks are due to my lab members especially Dr. Goutam Chakraborty, Dr. Reema Alag, Dr. Sreekanth Rajan, Dr. Souvik C, Dr. Ye Hong, Dr. Shin Joon, Dr. Choi Bo-Hwa, Mr. BaiHong, Mr. Lu Wei, Mr. Toan for their cooperation and help they extended during the course of my work.

I thank School of Biological Sciences, Nanyang Technological University, Singapore for providing PhD studentship without which this work would not have been possible.

I also take this opportunity to express my gratitude to my parents, siblings and friends for their unrelenting support.

Abstract

In this study, we highlight our efforts in developing novel ligands targeting *Plasmodium* FKBP35 (FK506 binding protein 35) and human FKBP38. Though both these proteins belong to the FK506-binding protein family and are intricately involved in the protein folding process, they differ in their enzymatic properties. *Plasmodium* FKBP35 exhibits canonical peptidyl-prolyl *cis-trans* isomerase (PPIase) activity, whereas human FKBP38 exhibits PPIase activity only in presence of co-factor Ca^{2+}-calmodulin. Inhibition of PPIase activity by FK506 and its analogs was shown not only to confer protection from neurodegenerative disorders but also to control infectious diseases such as malaria. In an attempt to identify novel ligands that could selectively bind to *Plasmodium* FKBP35 and human FKBP38, I have adopted different strategies such as de novo and analog based drug design to identify potential ligands that bind to FKBPs. Computational molecular modeling of X-ray crystal structures of *Plasmodium falciparum* FKBP35-FK506 complex and human FKBP38 has identified potential hits targeting the respective proteins. Our *in vitro* biochemical studies, nuclear magnetic resonance (NMR) binding, and X-ray crystallographic studies show that supradamal (SRA / D5) and D44 bind to Plasmodium FKBP35 inhibiting its PPIase activity and parasite growth. In order to understand the mode of action, we have solved the crystal structures of D44 and SRA in complex with *Plasmodium* FKBP35 (*falciparum* and *vivax* species) providing a structural basis for achieving selective inhibition of *Plasmodium* FKBPs.

I. Introduction

Immunophilins represent a group of cytosolic receptors which bind to either of the immunosuppressive drugs cyclosporine A (CsA) and FK506; and accordingly are known as cyclophilins (CyP) and FK506 binding proteins (FKBPs) respectively [1, 2]. Both FK506 and CsA bind to their cognate immunophilins forming FK506/FKBP or CsA/CyP binary complexes. The resulting binary complexes interact with calcineurin (CaN), a Ca^{2+}-calmodulin dependent protein serine/threonine phosphatase, and inhibit its phosphatase activity. As a consequence, the NF-AT (nuclear factor of activated T-cells) transcription factor cannot undergo dephosphorylation and its successive events like nuclear translocation and IL-2 activation are prevented. This leads to suppression of T-cell activation and thereby leading to immunosuppression [2-4] (Fig. 1).

Figure 1: Immunosuppressive actions of FK506 and CsA: Upon reaching intracellular region,

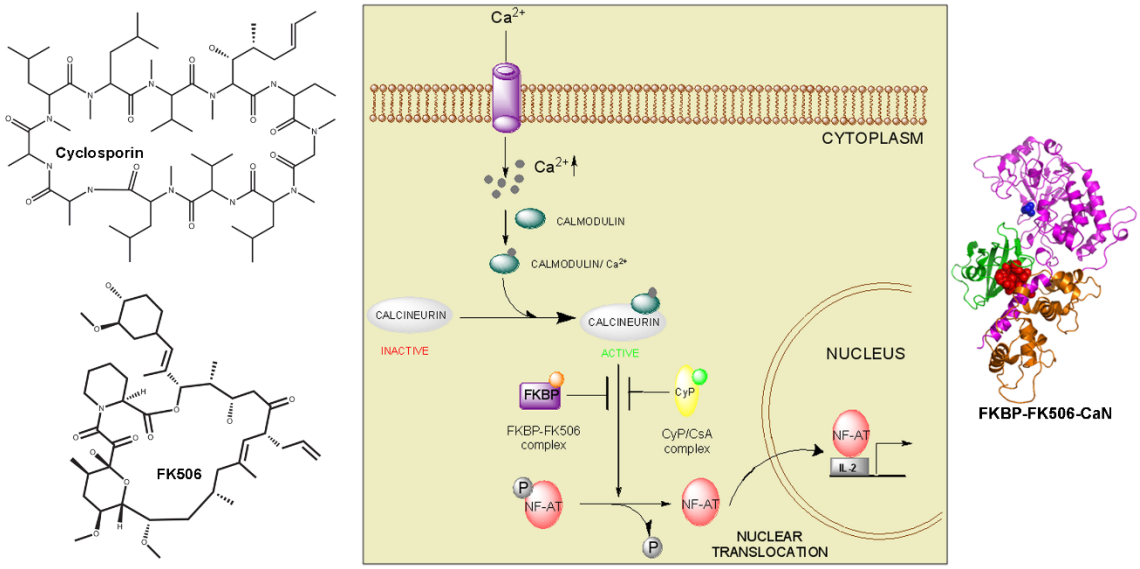

both the drugs bind to their cognate immunophilins forming binary complex(es). These complexes interact with Ca^{2+}-calmodulin activated calcineurin and form a ternary complex and prevent the dephosphorylation and nuclear translocation of NF-AT and thereby suppress IL-2 induced T-cell activation.

Both the PPIases - cyclophilins and FKBPs - exhibit a characteristic peptidyl-prolyl *cis-trans* isomerase (PPIase) or rotamase activity, a rate limiting step in the process of protein folding [5] (Fig. 2). PPIase(s) by catalyzing the *cis-trans* isomerization of the peptide bond preceding the proline in a polypeptide chain accelerate the slow steps of folding and assist in *de novo* protein folding. FKBPs play a key role as a helper protein assisting folding pathways by mediating the cellular responses to physiological signals and effectors. Thus FKBPs influence various biochemical processes like protein folding, aggregation, stability, receptor signaling, protein trafficking and transcription [6, 7] (Table 1)

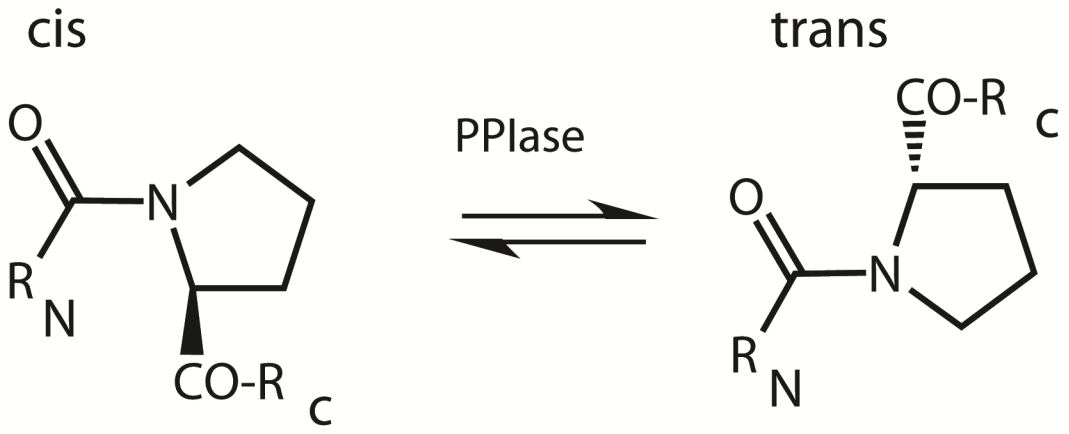

Figure 2: PPIase mediated *cis-trans* isomerization; the residue preceding proline isomerizes from *cis* form to *trans* form in presence of an FKBP or other PPIase. This *cis-trans* isomerization is a rate limiting step for the de novo protein folding. PPIases accelerate the slow steps of folding and thereby assist de novo protein folding.

I.1 FKBPs and their classification

In mammals, the FKBP family consists of more than 16 individual members classified according to their molecular masses, each possessing one or more FKBP domains complemented with tetratricopeptide repeat (TPR) domains, endoplasmic reticulum (ER) signal peptides, EF-hand motifs and/or calcium calmodulin binding regions.

Table I Pathophysiological roles of human FKBPs

Protein	Class/localation	PPIase domains	Extra domain (s)	Functions
FKBP12	Cytoplasmic	1		Ca^{2+} signaling, immune suppression, neurodegeneration.
FKBP12.6	Cytoplasmic	1		Ca^{2+} signaling.
FKBP25	Nuclear	1	DNA binding	Tumor suppression.
FKBP135	Nuclear	1	WH1, MT, DNA binding	Endosome transport/cytoskeletal organization.
FKBP36	TPR containing	1	TPR, LZ, CaM	Glyceraldehyde 3-phosphate dehydrogenase (GAPDH) inhibitor, spermatogenesis.
FKBP37	TPR containing	2	TPR, LZ, CaM	AH signaling, Hepatitis B suppression.
FKBP38	TPR containing	1	TPR, LZ, CaM, TM	Apoptosis, Neurodegeneration.
FKBP51	TPR containing	2	TPR, LZ, CaM	Hormone signaling, Cancer, Neurodegeneration.
FKBP52	TPR containing	2	TPR, LZ, CaM	Hormone signaling, Ca^{2+} signaling, neurodegeneration, Major mood disorders.
FKBP13	Secretory pathway	1		Complement system, Vesicular trafficking.
FKBP19	Secretory pathway	1	TM	Unknown.
FKBP22	Secretory pathway	1	EF hand	Cancer resistance.
FKBP23	Secretory pathway	1	EF hand	Chaperone regulation.
FKBP60	Secretory pathway	4	EF hand	Unknown.
FKBP65	Secretory pathway	4	EF hand	Osteogenesis, Chaperone, Proteostasis.

AH - aromatic hydrocarbon; MT - myosin tail; TPR - tetratricopeptide repeat; WH1 - Wasp homology domain, LZ - leucine zipper, CaM - calmodulin-binding domain, TM - transmembrane region, EF hand, Ca^{+2} binding domain.

Based on their cellular distribution, FKBPs are broadly divided into cytoplasmic FKBPs (FKBP12 & 12.6), nuclear FKBPs (FKBP13, FKBP25), and ER FKBPs (FKBP13, -19, -22, -60, -65). Based on presence of a particular polypeptide segment (ER signal or TPR), the members are called either ER signal peptide containing FKBPs (FKBP65)

or TPR containing chaperonic FKBPs (FKBP36, -38, -51, -52). Based on the ability to show PPIase and FK506 binding ability, FKBPs are also classified as canonical FKBPs (FKBP12, 12.6, FK1 domains of FKBP51, -52) or non-canonical FKBPs (FKBP38, FK2 domains of FKBP51, 52).

Within the different FKBP members, FKBP domain architecture is more diverse, ranging from a multiplicity of PPIase domains, calmodulin binding sites, TPR (tetratricopeptide repeat regions), trans-membrane (TM) motifs, EF hands, and leucine zippers to DNA binding domains [7, 8]. As shown in Fig. 3, the archetypical homolog FKBP12 possesses a singular PPIase domain, whereas proteins with higher molecular mass such as, FKBP38, -51, -52 and *Plasmodium* FKBP35 share a similar kind of domain arrangement, having a PPIase domain followed by three TPR domains and a putative calmodulin (CaM) binding domain. FKBP38 differs from other FKBPs in possessing an inactive PPIase domain and a trans-membrane (TM) motif. Larger immunophilins like FKBP51 and FKBP52 possesses two PPIase domains (the first copy is active whereas the second copy is inactive) followed by three TPR domains.

Sequence alignment of human and *Plasmodium* FKBP show that their FKBP domain is very much similar with few differences as shown in Fig. 4. (*) Marked residues are very much degenerate across both the species (human and plasmodium) whereas the (^) marked residues between 80 and 90 region vary between human and plasmodium FKBPs and could probably be useful in achieving selectivity between human and Plasmodium FKBPs.

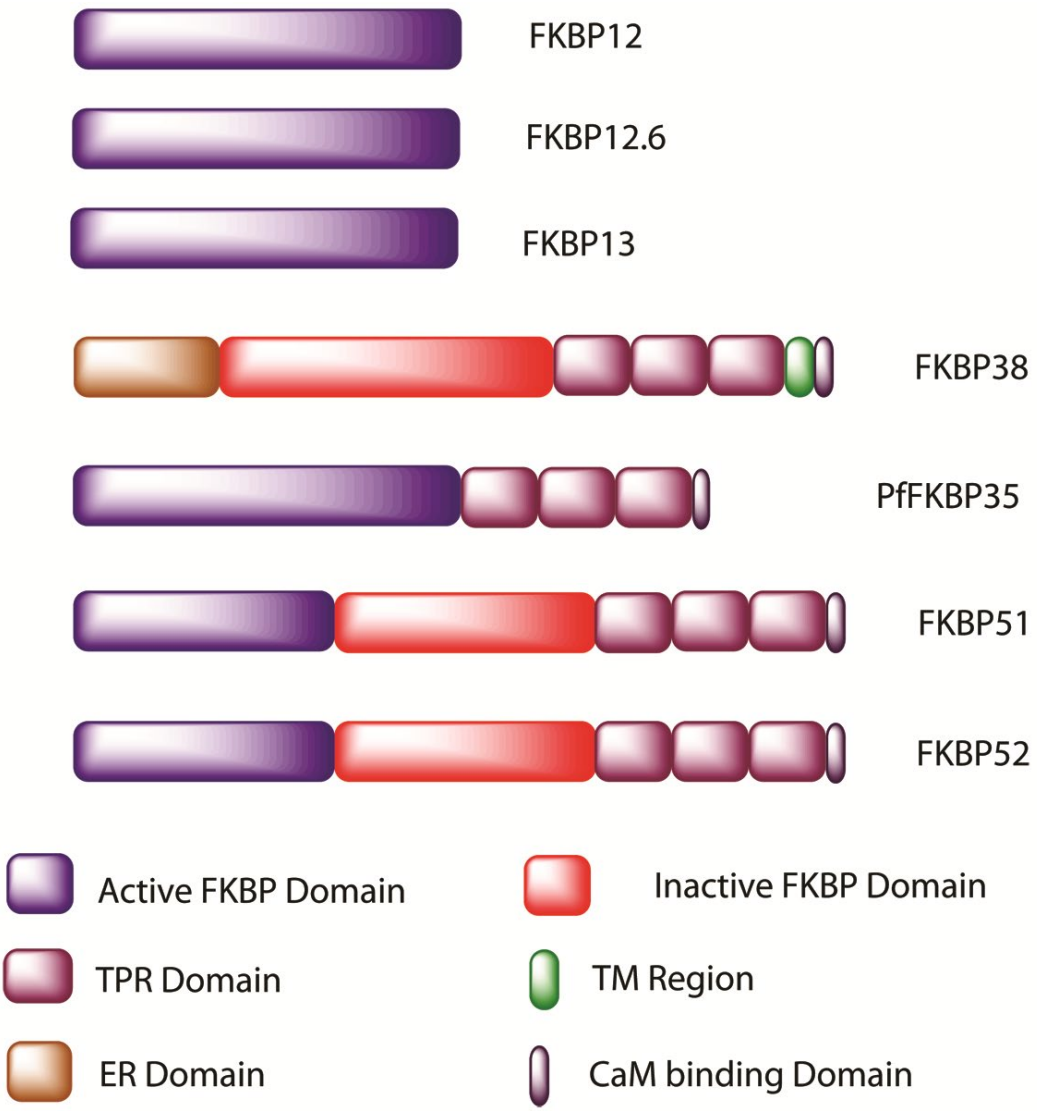

Figure 3: FKBPs domain architecture. Small molecular mass immunophilins such FKBP12, 12.6, 13 possess a single FKBP domain; FKBP25 possess a helix-loop-helix (HLH) structure at its N-terminal and an FKBP domain at C-terminal end; larger molecular mass immunophilins such as PfFKBP35, FKBP38, FKBP51 and FKBP52 possess multiple domains such active FKBP (FK1) and/or inactive FKBP (FK2) domains followed by TPR domains. FKBP38 in addition to FKBP domain and TPR domains also possesses a glutamine rich domain (ERD), leucine zipper (LZ), calmodulin binding domain and transmembrane regions.

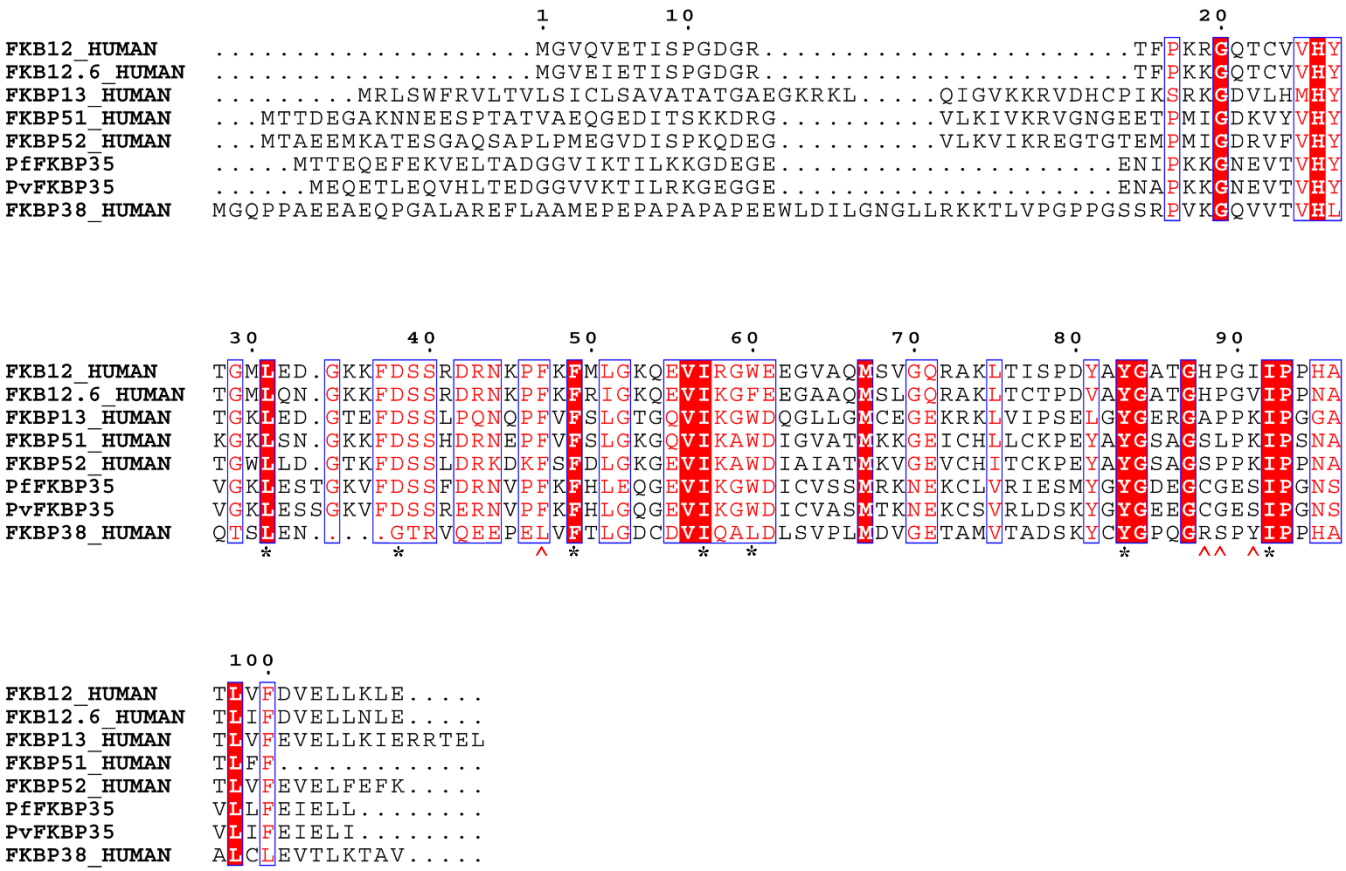

Figure 4: Sequence aligment of human and *Plasmodium* FKBP family members active domains. The most conserved residues are highlighted as * and the residues that vary between the *Plasmodium* FKBP and human FKBPs are highlighted as ^. These varying residues from 87 to 90 could be the probable residues for achieving selectivity between the human and parasite FKBPs

I.2 Substrate selectivity

PPIase family members such as FKBPs, cyclophilins and parvulins prefer a specific substrate to exhibit their catalytic efficiency. Cyclophilin family members show good catalytic efficiency with a slightly hydrophobic Ala residue at the Xaa–Pro position of the Succ-AXPF-pNA substrate. FKBPs prefer a more hydrophobic residue such as Phe or Leu at the Xaa-Pro position of AXPF substrate in comparison to cyclophilins. On the other hand parvulins prefer phosphorylated Ser-Pro or Thr-Pro motifs, whereas neither cyclophilin nor FKBPs can effectively catalyze isomerization of phosphorylated substrates [9, 10].

Steady state enzymatic kinetic studies measuring the catalytic efficiency of FKBP12 using different substrates (AXPF) with a residue varied at the Xaa (or P1) position preceding proline have shown the preferential selectivity towards hydrophobic residues. The catalytic efficiency of FKBPs is heavily dependent on the nature of side chain at position P1 of the substrate with either leucine or phenylalanine preceding the proline residue displaying catalytic efficiency 100 to 1000 fold higher than for substrates with charged or smaller side chains at this position [9, 11, 12]. This indicates that P1 amino acid substitutions with hydrophobic side chains like Leu, Ile, norleucine (Nle), Phe, and Val are better substrates as their side chains seem to have a better fitting into a hydrophobic groove than the charged residues like Lys, His and Glu.

Similarly, data from Zoldak and colleagues exploring the specificity of prolyl isomerases using fluorescent peptides indicated that not only charged residues but also the presence of proline at P1 position allows no enzymatic activity [13]. This lack of enzymatic activity with this peptide could be either due to its inhibitory effect on enzymatic activity of FKBPs or lack of binding. These kinetic studies have clearly demonstrated that by varying the P1 residue, one can effectively design a peptide that

could bind and inhibit the enzymatic activity. It remains to be seen whether this selectivity of substrate could present an avenue to achieve selective inhibitor among the FKBP family members.

I.3 Structural traits and important physiological roles of human FKBPs

I.3.1 FKBP1A / FKBP12

FKBP12 represents the archetypical member of FKBP family and is ubiquitously expressed. It possesses a single FK506 binding domain which catalyses PPIase (rotamase) activity. Binding of FK506 to this domain results in inhibition of rotamase activity.

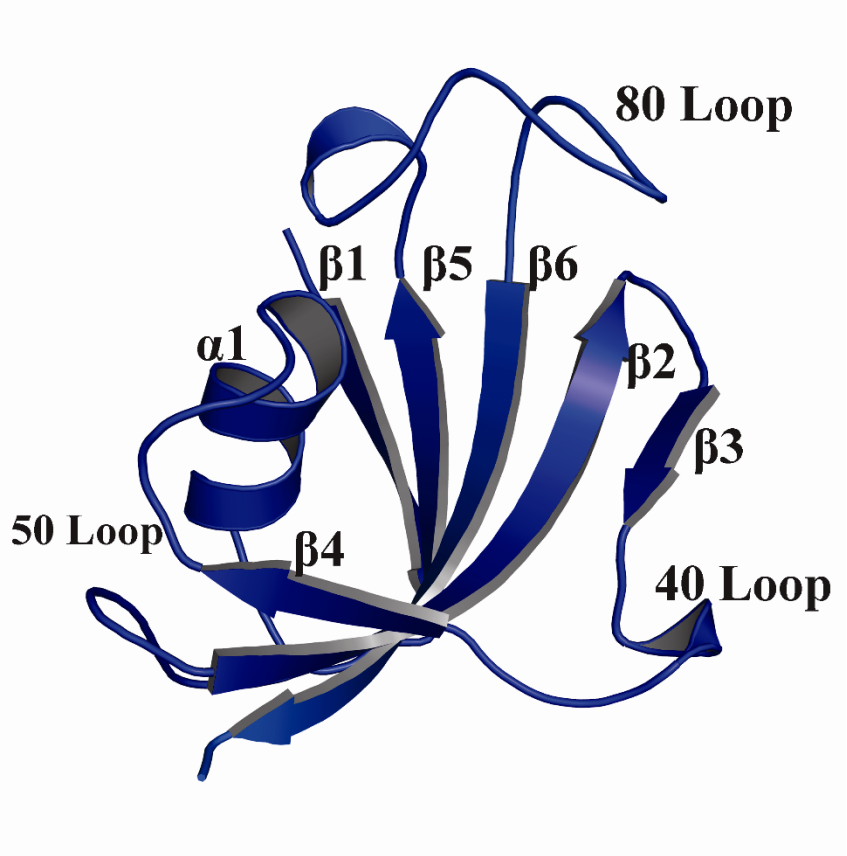

Figure 5: Structural role of the loops in FKBP; mainly the β4 - α1 helix (50-loop), β5 – β6 loop (80-loop) and β3 - β4 loop (40-loop) play an important role in ligand binding and PPIase enzymatic activity.

The FKBP12 structure has become well known for its typical fold, characterized by the presence of an amphiphilic six stranded anti-parallel β-sheets wrapped around a short α helix. The amphiphilic α-helix packs against the hydrophobic face of the β-sheet at an angle of 60º along the long axis; the β-sheet with its right handed twist wraps around the central α-helix forming a well defined hydrophobic groove. One of the notable features of the FKBP12 fold is the topological crossing of the loop (S8-G19 and L50-Q70) between the β1 and β2 strands and loop between β5 and the α1 helix, which is described as a rare feature among anti-parallel sheet structures. It has been suggested that this type of topological crossing of loops affects complex folding pathways and slows down the folding process or results in misfolded species that form kinetic traps on the folding pathway [14]. A buried water molecule in the FKBP12 structure is stabilized by hydrogen bonding to M49, L52, D54 and D60 residues and imparts structural stability as well as formation of the ligand binding pocket [15]. Loops composed of residues 39–46 (40-loop), 50–56 (50-loop), and 82–95 (80-loop) flank the FK506 binding pocket (Fig. 5). The side chains of Y26, F46, F99, V55 and I56 make up the hydrophobic groove with W59 of the α helix forming the canonical base for binding of the pipecoline moiety of FK506 [16].

I.3.2 Calcium Homeostasis

FKBP12 regulates several physiological processes either by rotamase activity or by mediating protein-protein interactions. As described previously (in chapter I), the FKBP12–FK506 binary complex interacts with calcineurin leading to inhibition of T-cell signaling and ultimately leading to immunosuppression. Irrespective of its rotamase activity, FKBP12 has been shown to interact with many physiological substrates and regulate their physiological activities. FKBP12 associates with the skeletal ryanodine

receptor (RyR1) and its close homolog inositol 1, 4, 5-triphosphate receptor (IP_3R) and regulates calcium release [17]. FK506 and rapamycin disrupt the IP_3R interaction and increase Ca^{2+} levels and regulate calcium homeostasis. The Leu-Pro (1400-1401) residues on IP_3R were mapped to be critical for interaction with FKBP12 [18].

I.3.3 Receptor Signaling / Inhibition of transforming growth factor β (TGF-β) signaling

FKBP12 also interacts with TGF-β type 1 receptor and this interaction is disrupted by high concentrations of FK506 (Fig. 6A). This suggests that the TGF-β type 1 receptors interaction site overlaps with FK506 binding site. Deletion or point mutations and co-immunoprecipitation studies have confirmed the specificity of this interaction. Point mutations such as K230R on TGF-β type 1 receptor and D37G on FKBP12 decrease the affinity between FKBP12-TGF-β type I receptor. Not only these point mutations but also the deletion of the first five residues on N-terminus of FKBP12 has reduced the affinity of type I receptors of TGF-β for FKBP12 [19]. Therefore, FKBP12 is considered to be a common inhibitor of TGF-β signaling. Point mutations such as G89P and I90K residues on FKBP12 have abolished its inhibitory effect on TGF-β signaling and inferred that the specific site for FKBP12-TGF-β resides on the 80-loop of FKBP12 [20].

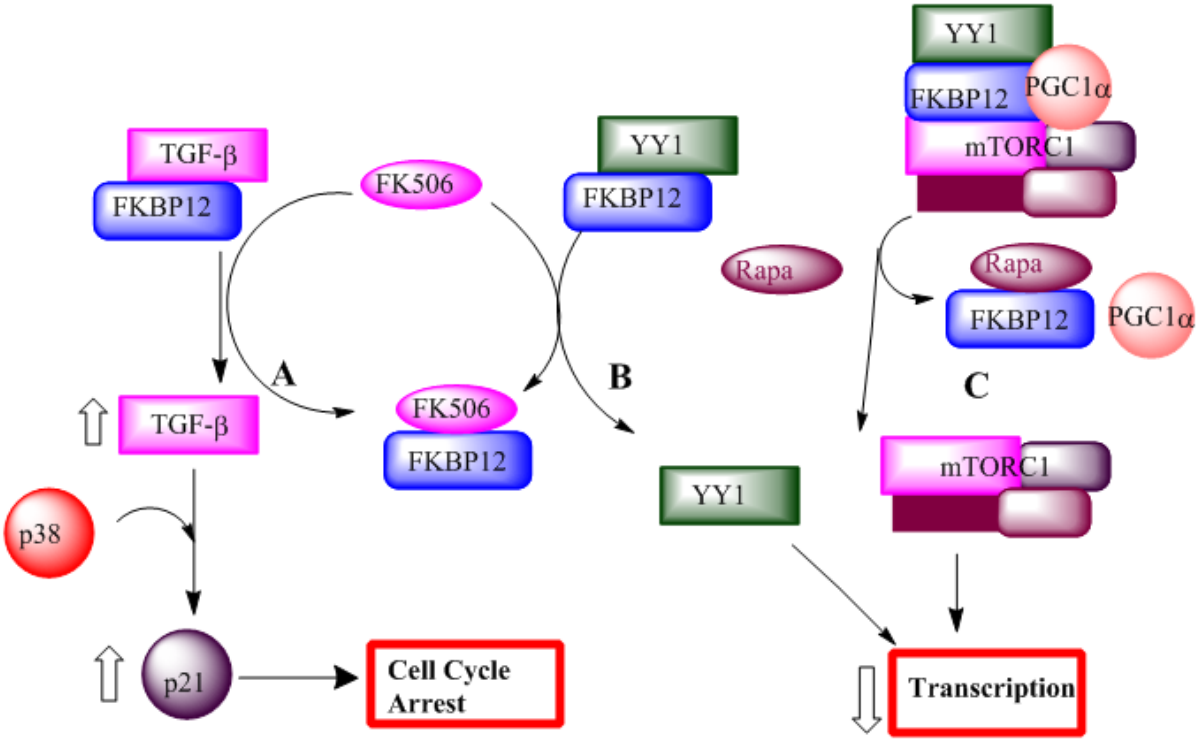

Figure 6: Important roles mediated by FKBP12. A) FKBP12 interacts with TGF-β family members and inhibits TGF-β signaling. FK506 disrupts FKBP12- TGF-β interactions and elevates TGF-β levels, which together with p38 enhances p21 levels and induce cell cycle arrest. B) FK506 disrupts FKBP12 and YY1 (Yin Yang 1) interaction, elevates YY1 levels, leading to transcriptional repression. C) Similarly, rapamycin/Rapa disrupts the YY1-FKBP12-mTORC1 and peroxisome proliferator-activated receptor gamma co-activator 1-alpha (PGC-1α) activation complex and blocks transcription.

I.3.4 Transcriptional Regulation

Transcriptional roles of FKBPs have emerged with the findings of interaction between FKBP12 and transcriptional repressor protein “yin-yang1” (YY1) through a yeast two-hybrid assay screen using YY1 as bait [21]. YY1 interacts with FKBP12 at the conserved PPIase domain and abrogates the repression activity of YY1 (Fig. 6B). Disruption of FKBP12 and YY1 interaction by FK506 or rapamycin indicates that this interaction site overlaps with the FK506 binding site and can be modulated by small

molecule inhibitors. Similarly, FKBP12 activated transcription when recruited to a target promoter through interaction with YY1. Addition of rapamycin to FKBP12 fused to a Gal4-DNA binding domain forced the fusion protein to the target promoter (in mammalian cells) and activated transcription [22]. FKBP12-TORC1 forms an activation complex with YY1 and peroxisome proliferator-activated receptor gamma coactivator 1-alpha (PGC-1α) and targets YY1 to its promoters [23]. Rapamycin disrupts these interactions and turns YY1 into a repressor (Fig. 6C). Based on these two studies, FKBP12 seems to be a part of the YY1/TORC1/PGC-1α activation complex. FK506 or rapamycin binds to FKBP12 disrupting the protein complex and releases FKBP12 from the promoter and thereby switches the YY1 from an activator to a repressor [24].

I.3.5 Depalmitoylation & α-synuclein aggregation

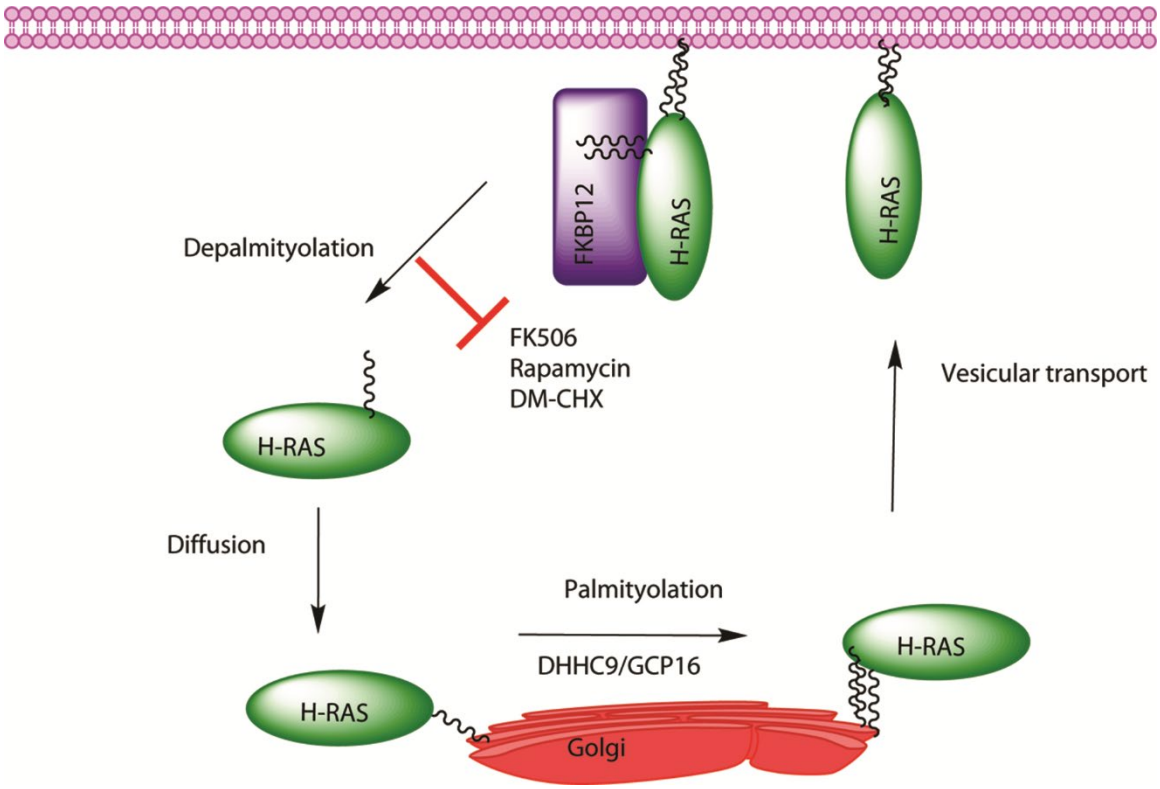

Figure 7: FKBP12 regulates depalmitoylation of H-RAS and is involved in recycling of H-RAS. FK506 or rapamycin and N-(N', N'-dimethylcarboxamidomethyl) cycloheximide (DM-CHX) inhibit the depalmitoylation process mediated by FKBP12.

FKBP12 negatively regulates H-Ras signaling by promoting depalmitoylation and retrograde trafficking of H-Ras via *cis-trans* isomerization of peptidyl-prolyl bonds in the proximity to acetylated cysteines (Fig. 7). PPIase inhibitors like FK506, N-(N',N'-dimethylcarboxamidomethyl)cycloheximide (DM-CHX), rapamycin inhibit the FKBP12 mediated negative regulation of H-Ras signaling and enhance early GTP loading of Ras in response to growth factors and thereby promotes H-Ras-dependent neurite outgrowth from PC12 cells [25, 26].

Recently, a comparative study of different PPIases such as FKBP12, -38, -52, -65, cyclophilin, and Pin1 by means of *in vitro* and neuronal cell model studies has shown that FKBP12 accelerates α-synuclein aggregation at sub-nanomolar concentrations more prominently than FKBP-38, -52, 65, cyclophilin or Pin1 [27]. This study reaffirms the earlier studies [28, 29] showing the promise of FKBP12 and 38 as attractive drug targets for neurodegenerative diseases.

I.4 FKBP1B/FKBP12.6

FKBP12.6 shares 83% identity with FKBP12 differing in only 18 out of 107 residues. The E31, D32 and W59 residues in FKBP12 are changed to Q31, N32 and F59, respectively. FK506 shows a lower affinity towards FKBP12.6 (IC_{50} 2.9 ± 0.4 nM) than FKBP12 but forms a ternary complex with calcineurin (IC_{50} 147 ± 17 nM) in a manner similar to FKBP12 [30, 31]. FK506 does not affect any positive or negative inotropic effect on cardiac contractility [32]. FKBP12.6 exclusively binds to sarcoplasmic reticulum (SR) Ca^{2+} release channels or ryanodine receptor (RyR2) and prevents SR

calcium leaks and regulates calcium homeostasis. There is much interest about the emerging diverse roles of FKBP12.6.

Earlier studies [33-42] have shown the role of FKBP12.6 in stabilizing the integrity of RyR2 receptors. Disruption of this interaction could lead to aggravating cardiac complications such as cardiac arrhythmia and tachycardia. For example, protein kinase A (PKA) induced hyperphosphorylation of RyR2 results in dissociation of FKBP12.6-RyR2 interaction and abnormal levels of SR Ca^{2+} leading to cardiac arrhythmia and sudden cardiac death [38]. This model proposes an attractive mechanism for increase in diastolic Ca^{+2} levels via the loss of FKBP12.6 but fails to explain the unaltered or elevated levels of FKBP12.6 in a model associated with arrhythmogenic cardiac disease assessing the effect of Ryr2 receptor mutations in mammalian cells [43-47]. This observation indicates that FKBP12.6 mediated regulation of Ryr2 receptors might not be a key player for arrhythmogenic cardiac disease [48]. FKBP12.6 knockout studies from several groups have highlighted the diverse roles of FKBP12.6. One FKBP12.6 gene knockout study has implicated FKBP12.6 in excitation-contraction (E-C) coupling* (*see Glossary). Depletion of FKBP12.6 produced increased Ca^{2+} spark duration and elevated calcium induced calcium release (CICR) leading to hypertensive cardiac hypertrophy in male mice but not in female mice. However, when female FKBP12.6$^{-/-}$ mice were treated with tamoxifen, an estrogen receptor antagonist, cardiac hypertrophy appeared in female mice (similar to male mice) indicating that the female sexual hormone estrogen plays a protective role in hypertrophic responses of the heart to Ca^{2+} dysregulation [49].

Another knockout study has showcased new roles for FKBP12.6. This study shows that depletion of FKBP12.6 in mice actually enhances glucose stimulated insulin secretion (GSIS) and displays hyperinsulinemia and resistance to high-fat diet-

induced hyperglycemia. Based on these data, it is also suggested that FKBP12.6 could be a potential target for treatment of type II diabetes [50, 51].

I.5 FKBP25

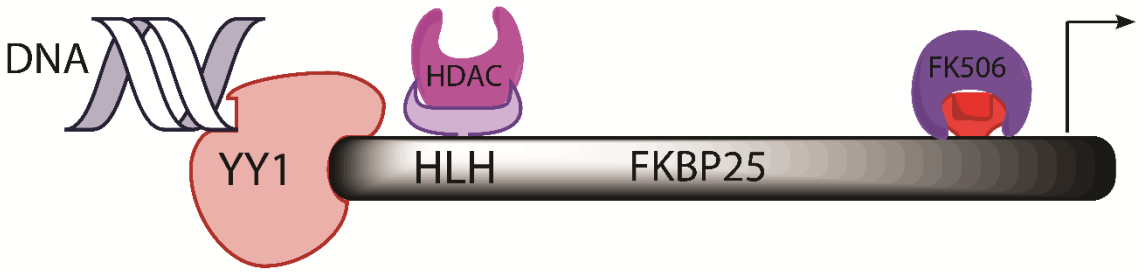

Figure 8: Domain structure of FKBP25 highlighting its interacting domains. FKBP25 interacts with HDAC and also functions as scaffolding protein mediating interaction with YY1 and DNA. The N-terminal domain (via helix-loop-helix structures) mainly mediates these actions while the FK506 binding domain is at the C-terminus.

FKBP family member FKBP25 interacts directly with both histone deacetylases (HDAC) and transcription factor YY1 through its N-terminal charged region. Interestingly, treatment with either rapamycin or FK506 has no effect on these interactions [52] (Fig. 8).

I.6 FKBP4/FKBP52

FKBP52 is a 52-kDa molecular mass chaperone - containing neuro-immunophilin that binds tightly to FK506 but does not show affinity to calcineurin and mediates its effects in a calcineurin independent manner [31]. FKBP52 is highly enriched in nervous tissues and plays an important role in mediating a protective role in neurodegenerative disorders [53-55]. Aberrations in protein folding (misfolding and aggregation) leads to formation of intra - or extra - neuronal accumulation of amyloid fibrils or neurofibrillary tangles which is a hallmark of neurodegenerative diseases like Alzheimer's disease

and Parkinson's disease. Chaperone machinery comprising molecular chaperones and co-chaperones forms the first line of defense against the misfolded, aggregation-prone proteins by maintaining protein quality control [56]. Co-chaperone FKBP52 physically binds to phosphorylated form of tau and co-localizes with tau in the distal part of neuronal axons and promotes microtubule assembly. Over-expression of FKBP52 in differentiated PC12 cells showed an "anti-tau" effect resulting in a reduced neurite outgrowth [57, 58]. Peptidyl-prolyl isomerase activity of FKBP52 modulates TRPC1 channel opening which in turn regulates myelin associated glycoprotein induced growth cone repulsions and thereby prevents axonal regeneration [59]. FKBP52 mediates multiple protein-protein interactions and positively modulates androgen, glucocorticoid, and progesterone receptor signaling [60] by associating with Hsp90 via its TPR domain and influences both receptor hormone binding and receptor sub-cellular location [61-64].

FKBP52 mediates important role in trafficking of signal proteins between the cytoplasm and nucleus. FKBP52 through its PPIase domain modulates the expression of dynamitin and its association with dynein motor protein and thereby enabling the dynein's cargoe formation [65]. FKBP52 binds to dynein motor protein and links the GR-Hsp90-Hsp70 hetermomeric complex with dynein motor protein and and transports cargoes-ligand-bound receptors such as p53 etc., via a retrograde pathway to the nucleus [66]. *si*RNA knock down of the FKBP52 gene has shown that FKBP52 modulates cortisol-hypothalamus pituitary adrenal (HPA) axis (Glossary) responses by eliciting cortisol levels to activate glucocorticoid receptor (GR) nuclear translocation, and consequent stimulation of GR-responsive genes leads to mood disorders or psychiatric conditions [67]. Regulating FKBP52 levels could have benefits for treatment of major depressive disorders and neurodegenerative diseases.

FKBP52 has two FKBP domains (FK1 and FK2), a 3-unit helical TPR domain together with an additional α helix ($\alpha 7$) (beyond the TPR motif) and a calmodulin binding domain [68]. Although FK1 and FK2 domains are architecturally similar, they show distinct biochemical characteristics.

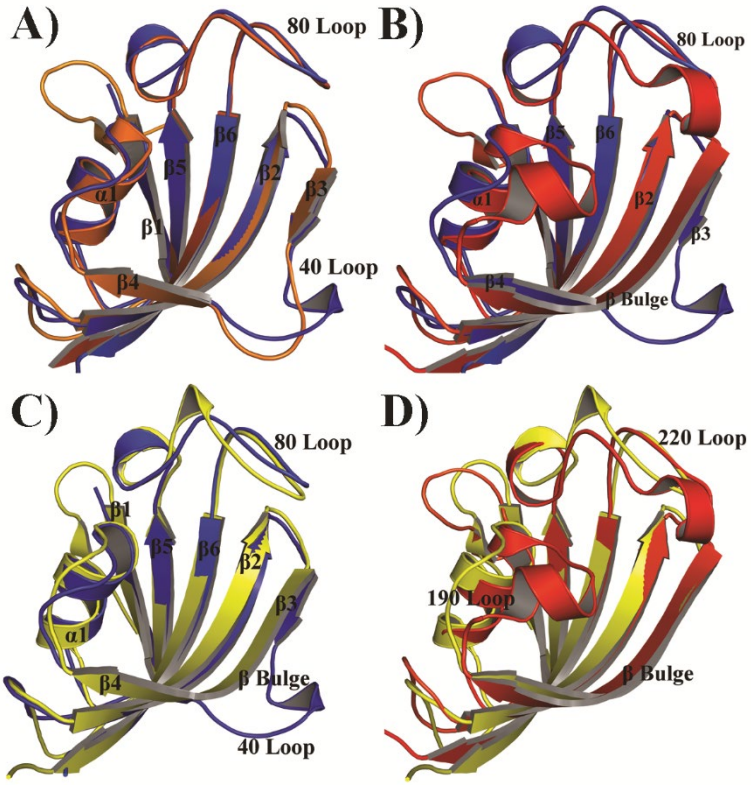

Figure 9: Comparison of active and inactive PPIase domains of FKBP52 and FKBP38 with archetypical FKBP12. A) Superimposition of active FK1 domain of FKBP52 (orange) with FKBP12 (blue) reveals small changes at the 40-loop. B) Overlay of inactive FK2 domain (red) of FKBP52 with FKBP12 shows lack of 40-loop and insertion of extra helix between β4-α1-loop. C) Overlay of FKBP38 (yellow) and FKBP12 (blue) shows the presence of β-bulge (lacking 40-loop). D) Overlay of FKBP38 (yellow) and FK2 domain (red) of FKBP52 reveals the presence of extended α-helix in FKBP52 in comparison to FKBP38.

The FK1 domain binds to its substrates and is catalytically active; conversely FK2 is inactive. Insertion in the loops flanking the FK2 ligand binding pocket K234 (in the 221-242 loop) and G195, E196, M197, L198, D199 (in the 192-199 loop) pushes the loops

into the binding pocket thereby interfering with FK506 binding (Fig. 9D). FK1 and FK2 domains are joined by an inflexible, hydrophilic hinge. The inflexibility of the hinge plays an important role in regulating FKBP52-Hsp90 interaction. Phosphorylation of T143 on the hinge of FKBP52 by casein kinase II abrogates binding to Hsp90 but does not alter ligand binding [69]. Though FKBP52 shares 75% sequence similarity to FKBP51, it displays contrasting Hsp90 binding characteristics and opposing effects on hormone binding to the GR receptor, tau interactions and microtubule polymerization.

Within the TPR domain, residues at the FKBP52/Hsp90 binding interface are strictly conserved in both FKBP51 and -52 with the exception of Q333, F335 and A365 that correspond to R331, Y333, and L363 in FKBP51. These substitutions result in a varied interaction interface and could account for the differential binding of these FKBP52 and FKBP51 to Hsp90. Additionally, the C-terminal end of FKBP51 is more compact than FKBP52 as the $\alpha 7$ helix of FKBP52 shifts by >30° from the Hsp90 interface relative to FKBP51. This, in turn may also contribute to tighter FKBP51-Hsp90 interaction.

I.7 FKBP5/FKBP51

Structurally, FKBP51 is composed of three domains - two consecutive PPIase or FK506 binding domains (FKBDs), termed FK1 and FK2, and a three-unit repeat of the tetratricopeptide repeat (TPR) domain. FK1 has the typical FKBP fold having six anti-parallel β-sheets converging around a central α-helix. Notably, the loops between $\alpha 1$ – $\beta 4$ (50-loop) and $\beta 4$ – $\beta 5$ loops (40-loop) are disordered. The FK1 domain has a 60% similarity to FKBP12 with major differences at the “80-loop” (residue 110-125). This region shows the highest variation among the FKBP domains [70]. The FK2 domain

lacks the “40-loop” and the insertion of D195, H196 and D197 residues between β5 and α-1 helix protrudes into the FK506 binding pocket obstructing the FK506 or substrate binding and therefore FK2 domain lacks PPIase activity. Though the presence of the insertion loop has no apparent effect on FKBP51 binding to Hsp90 but its deletion decreases FKBP51 association in progesterone receptor (PR) complexes.

TPR domains are helical hairpins consisting of 2-16 units of a 34 amino acid motif and bind the MEEVD motif of Hsp90 C-terminal domain (CTD) [71]. The FKBP51 TPR domain has 3 such units plus an additional helix. Each unit has two α-helices of 12-15 residues crossing at an angle of ~ 20° to each other. Structurally, the TPR domain is similar to Hsp90-binding domains of co-chaperones like Hsp90-organising protein (Hop), protein phosphatase 5 (PP5) and cyclophilin 40 (Cyp40). Superimposition of TPR domains from Cyp40 and Hop with FKBP51 showed that a conserved alanine in Hop (A46, A267) and Cyp40 (A281) are changed to methionine (M325) in FKBP51. The mechanism for antagonistic effects of FKBP51 versus FKBP52 is not clearly known; probably the differential binding mode of the TPR domain of these proteins to Hsp90 could explain their opposing roles.

FKBP51 functions as reciprocal modulator of androgen and glucocorticoid signaling. FKBP51 serves as a negative regulator of glucocorticoid, progesterone, and mineral corticoid receptors and as a positive regulator for androgen receptor signaling [62, 72-76]. In the absence of dexamethasone, GR forms a super-chaperone complex by associating with Hsp90 dimer, p23 (a co-chaperone molecule) and FKBP51 forming an inactive stable state. Apart from FKBP51, other chaperones like FKBP52,

cyclophilin 40 (CyP40) and serine-threonine protein phosphatase 5 (PP5) also associate with the Hsp90 dimer and form alternative super-chaperone complexes.

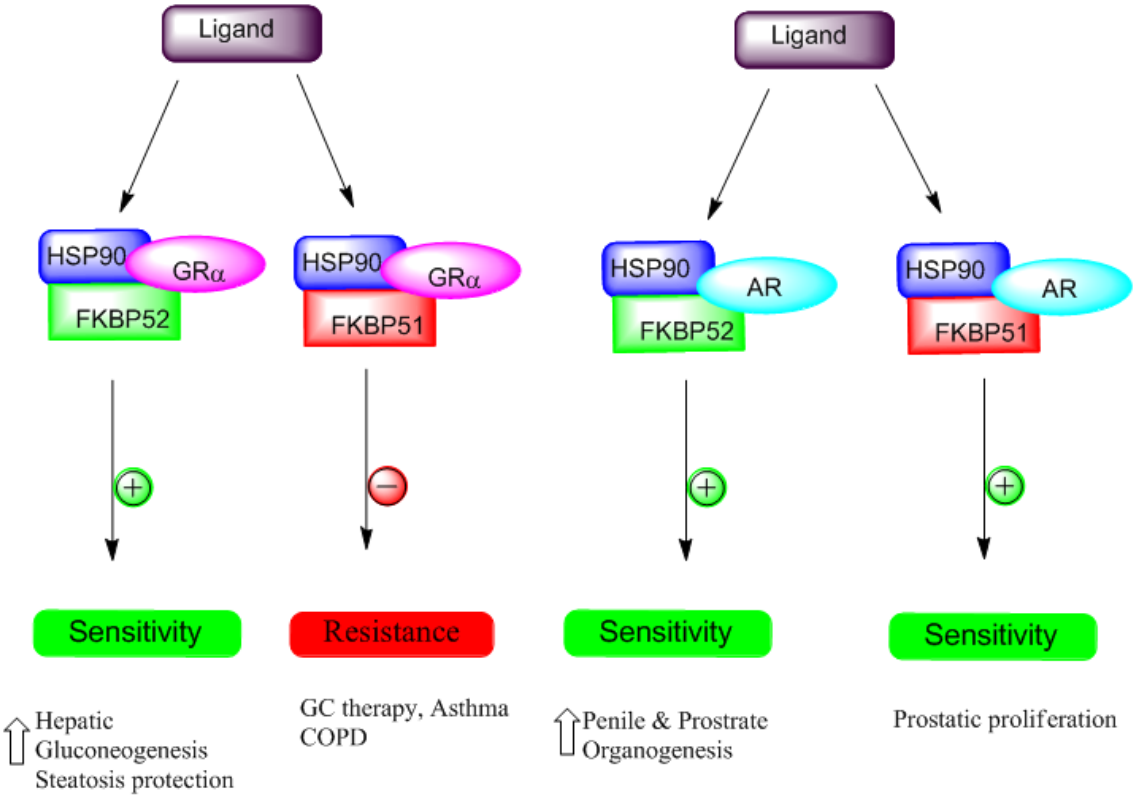

Figure 10: Pathway specific antagonistic roles of FKBP51 and FKBP52 on glucocorticoid and androgen receptor activities and emerging roles of these proteins in modulating specific physiological responses such as chronic obstructive pulmonary disease (COPD), prostatic proliferation, penile and prostrate organogenesis, hepatic gluconeogenesis and protection from steatosis. Ligand (FK506) binding to FKBP52 mediates glucocorticoid signaling and sensitizes chemoresistance while ligand binding to FKBP51-gluocorticoid-Hsp90 enhances chemoresistance. On the contrary, ligand (FK506) binding to either of FKBP51-AR-Hsp90 complex or FKBP52-AR-Hsp90 complex potentiates chemosensitivity.

Jaaskelainen and colleagues suggest that the binding of glucocorticoid to the GR shifts the equilibrium of super-chaperone complexes towards the FKBP52, facilitating dimerization and nuclear transport of the GR. The GR-enhanced expression of FKBP51 in turn moves the equilibrium back towards the FKBP51-containing

complexes, resulting in attenuation of the glucocorticoid action [77]. FKBP51 serves to counteract the actions of FKBP52 on the glucocorticoid receptor, nuclear translocation and responses induced by cortisol. Westberry and colleagues have shown that squirrel monkeys exhibit cortisol resistance in comparison to Old World Primates. This was due to the mutations in the glucocorticoid receptor gene or/and over-expression of FKB51 leading to high levels of FKBP51. High levels of FKBP51 result in a decreased ligand-binding affinity of glucocorticoid receptors and may mediate glucocorticoid resistance by disrupting microtubular transport [75, 78, 79]. Single-nucleotide polymorphisms in the human FKBP51 gene are shown to be genetically associated with various stress-related psychiatric disorders and with altered expression of FKBP51 [80]. Taken together, these evidences suggest an emerging role of FKBP51 as a relevant pharmacological target for treatment of psychiatric disorders. The molecular mechanisms of steroid hormone receptor modulation are beginning to unravel. It is now clarified that the FK506-binding domain plays a prominent role in modulating these actions. Though PPIase activity is not key for steroid hormone receptor modulation, a single amino-acid mutation L119P at the periphery (80-loop) of the FK506-binding site was sufficient to abrogate and partially reverse the inhibitory or stimulatory effects of FKBP51 and FKBP52 respectively [81]. Thus overlapping sites of the FK506-binding region appears to be critical for interaction of FKBP51 with the Hsp90-GR complex [82].

FKBP51 regulates important signaling pathways involved in cell survival or tumorigenesis and chemoresistance (Fig. 10). FKBP51 acts as a scaffolding protein in the regulation of AKT activation and AKT phosphorylation and in turn affects the chemoresistance of tumor cells. Scaffolding protein FKBP51 bridges the interaction between PH domain leucine-rich repeat protein phosphatase (PHLLP) and AKT.

FKBP51 with its TPR domain binds to the PHLLP, whereas the N-terminal domain of FKBP51 binds to the AKT and enhances PHLPP mediated phosphorylation at AKT-Ser473. Wang *et al.* model proposed that the high levels of FKBP51 inhibit the AKT activity and lead to chemosensitivity. Conversely, the decrease in FKBP51 levels enhances AKT activity promoting tumorigenesis and thus resistance. These observations implicate FKBP51 in mediating chemoresistance [83]. Very recently, Jinwal and colleagues have shown that FKBP51 enhances tau association with Hsp90 prevents tau clearance and controls tau phosphorylation activity via its isomerase activity and stabilizes microtubules [84].

I.8 FKBP8/FKBP38

FKBP38 contains a glutamate rich domain (ERD), FKBP domain, TPR domain interspersed by a consensus leucine-zipper (LZ) repeat region followed by a calmodulin binding motif and a transmembrane (TM) anchor. FKBP38 through its multiple domains interacts with itself or other leucine-zipper / coiled-coil containing proteins and can form multimers [85]. Human FKBP38 mRNA is highly expressed in the brain regions; moderately in the heart, lung, skeletal muscle and pancreas; lowly in placenta and liver. In mice, FKBP38 is widely expressed in brain tissues including neurons of the forebrain, striatum and thalamus and cells of Purkinje cell layer of the cerebellum [86].

Unlike the other FKBP family members, FKBP38 shows Ca^{2+}-calmodulin regulated PPIase activity and binds to FK506 only upon activation by Ca^{2+}-calmodulin. Presence of a TM domain enables FKBP38 to interact with membrane proteins located in mitochondria and ER membranes apart from its interaction with proteins in the cytoplasm [87]. Even though the FKBP domain of FKBP38 adopts the typical “half β-barrel” fold similar to that of FKBP12, the apo-protein is catalytically inactive and

doesn't bind to FK506 (Fig. 11). Residues required for FK506 binding and PPIase activities are loosely conserved (Fig. 11E); the lack of catalytic activity and ligand binding is attributed to the several amino acid substitutions in FKBP38. Not only the size of the active pocket is constricted by convergence of R184 (with its long flexible side chain) onto Q138 and closing the access to FK506 but also the conserved aromatic hydrophobic residues such as W59, F99 and F36 in FKBP12 are all replaced by aliphatic hydrophobic leucine residue (Fig. 11E) and the catalytically active residues such as Y26, D36, R42 in FKBP12 are changed to L127, Q138 and E140 respectively.

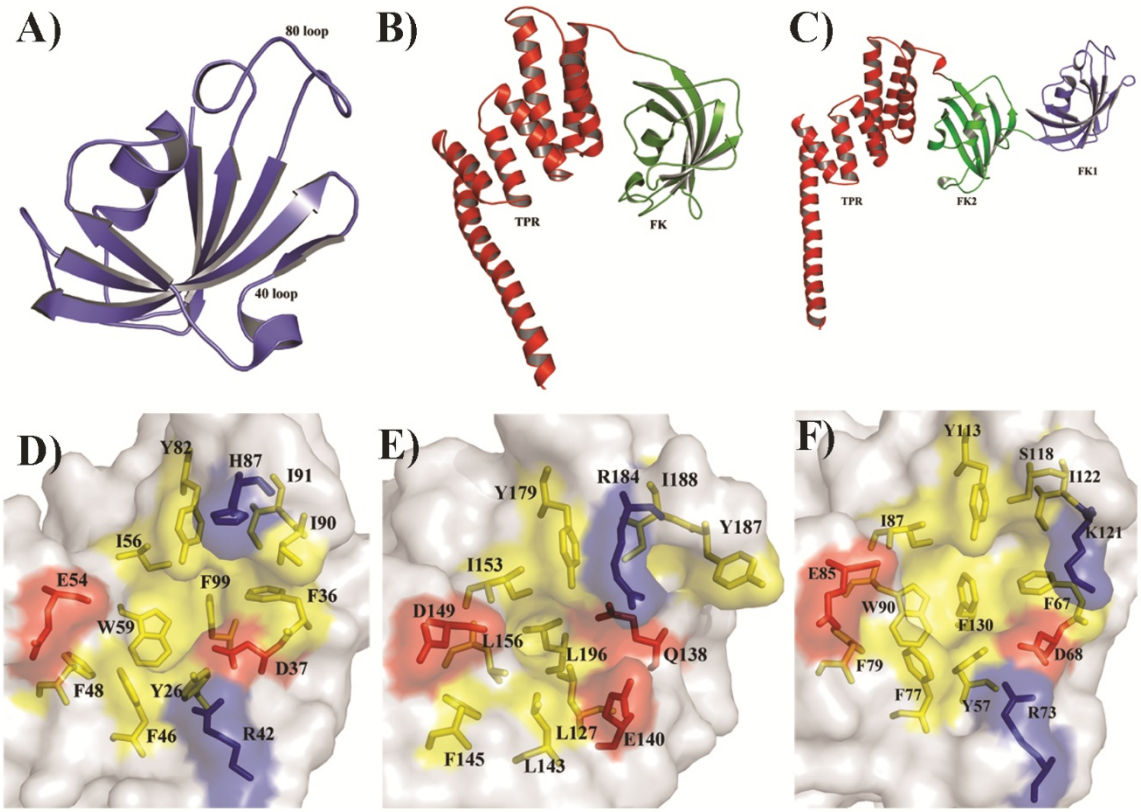

Figure 11: Comparison of FKBP family members. A, B, C): Cartoon models depicting the FKBP domain (blue), inactive FKBP domain (green) and TPR region (red) of FKBP12, FKBP38, and FKBP52; D, E, F): Surface view of FKBP domains highlighting the differences at the active sites of FKBP38 when compared to canonical members FKBP12 and FKBP52. The yellow colored region shows the hydrophobic residues; blue & red colored residues highlight the differences at the active site.

Additional features that further alter ligand binding to the active site pocket of FKBP38 include (1) lack of "40-loop" that introduces a bulge in the β4 strand [88]; and (2)

multiple amino acid changes in the V137-F143, G148-I153 and Y179-I188 regions that result in a net negatively charged rim of the active site.

The PPIase activity of FKBP38 is positively regulated by Ca^{2+}-calmodulin-dependent manner making it the first co-factor regulated FKBP [89]. The complex formation between Ca^{2+}-calmodulin and FKBP38 involves both the N-terminal and C-terminal regions binding to calmodulin with their corresponding termini and are thought to activate the enzymatic activity [90]. Lücke and colleagues have mapped a Ca^{2+} interaction site on the β4-α1 loop (L147-I153) containing acidic D149, D151 residues [91]. Interaction of FKBP38 with its partner proteins like Bcl-2 and Hsp90 is heavily dependent on prior formation of Ca^{2+}-calmodulin/FKBP38 complex.

I.8.1 Apoptosis

FKBP38 protects Bcl-2 from caspase dependent degradation by interacting with the flexible loop domain of Bcl-2 and thereby prevents apoptosis [92, 93]. FKBP38 by enhancing the stability of Bcl-2 levels promotes cell survival and thus contributes to chemoresistance [94]. On the other hand, presenilins PS1/2, which are multi-pass membrane proteins, increase the susceptibility to apoptosis by antagonizing the actions of FKBP38 in a γ-secretase independent manner [95]. Interestingly, Hsp90 also negatively regulates FKBP38/Ca^{+2}-calmodulin complex and abrogates the effects of FKBP38 on Bcl-2 and prevents cell death of neuroblastoma SH-SY5Y cells [96]. Inhibition of FKBP38, an anti-apoptotic molecule, by Hsp90 was able to rescue cell death in neuroblastoma SH-SY5Y cell lines suggesting pro-apoptotic roles of FKBP38 in a neuronal context (Fig. 12A).

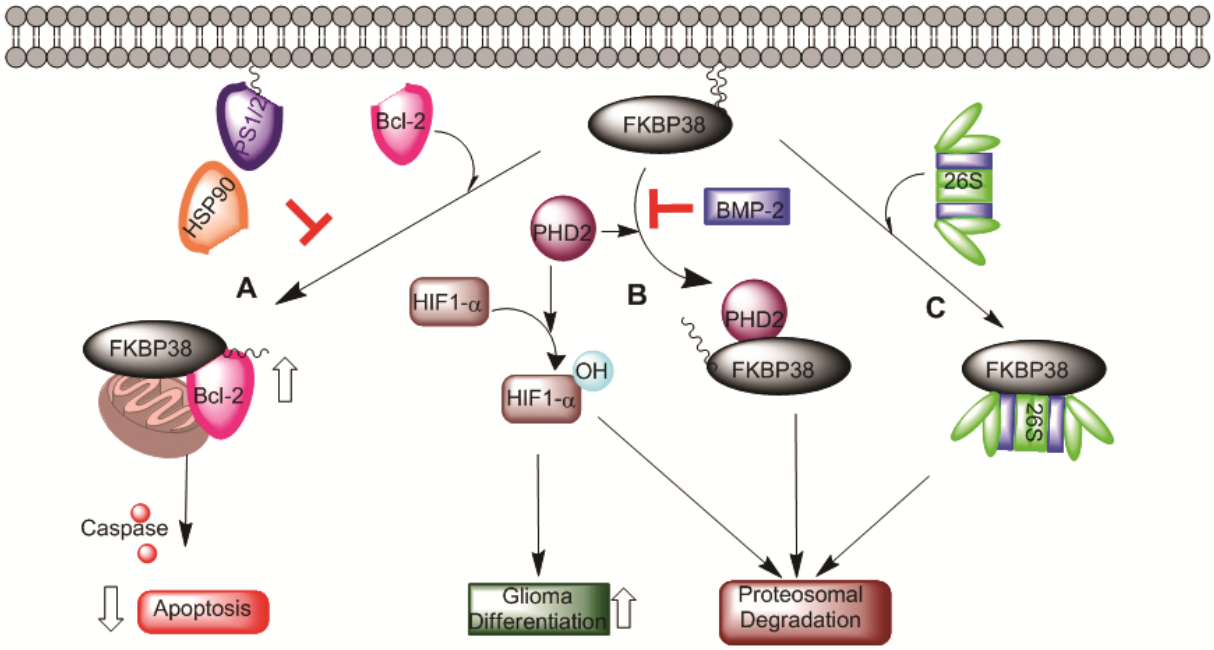

Figure 12: FKBP38 influences the stability of substrate proteins. (A) FKBP38 protects Bcl-2 by targeting it to mitochondria and prevents its caspase mediated degradation. (B) FKBP38 promotes proteasomal degradation of PHD2 and thereby enhances stability and transcriptional activity of HIF-1α. Growth factors like bone morphogenetic protein-2 (BMP-2) counteracts this FKBP8-mediated proteasomal degradation of PHD2 thereby decreasing HIF-1α levels and commits the differentiation of glioma cells. (C) FKBP38 regulates proteasomal degradation by interacting with the 26S proteasome.

I.8.2 Proteasomal degradation

FKBP38 serves to modulate protein degradation via its three tandem TPRs by directly interacting with the 26S proteasome (Fig. 12C) [97]. Yeast two-hybrid assays & biochemical studies have shown that FKBP38 specifically binds to prolyl-4-hydroxylase domain containing protein-2 (PHD-2) and modulates its stability. Hypoxia inducible transcription factors play a central role in regulating the responses to low oxygenation levels. PHD-2 hydroxylation activity promotes proteasomal degradation of hypoxia inducible transcription factor 1α (HIF-1α). FKBP38 modulates the PHD2 and HIF-1 α interactions in a PPIase independent manner. Depletion of FKBP38 did

not affect PHD2 mRNA levels but prolonged the stability of PHD2. As a result, PHD2 hydroxylation activity is enhanced and leads to reduction in transcriptional activity of HIF-1 α (Fig. 12B) [98]. The specific binding motifs for FKBP38-PHD2 complex (K_d 1 μM) were mapped to the ERD of FKBP38 and the MYND (myeloid, Nervy, and DEAF-1) type Zn^{2+} finger domains at N-terminal end of PHD-2. Furthermore, co-location of both FKBP38 & PHD-2 in both mitochondrial and ER membranes also suggests the critical role of membrane anchoring of FKBP38 for in vivo regulation of PHD-2 levels. Thus FKBP38 controls the stability of PHD-2 as an adaptor protein by modulating its degradation via proteasomal interactions [99]. Another yeast two-hybrid assay by Choi *et al.* has shown that FKBP38 interacts with phosphatase of regenerating liver 3 (PRL-3) in vivo and modulates the stability of PRL-3 by promoting the degradation of PRL-3 via the proteasomal pathway and thereby suppresses PRL-3 mediated p53 activity and cell proliferation [100].

I.8.3 Cell Size regulation

FKBP38 functions as a positive regulator of cell size and cell cycle mediated by Tuberous sclerosis complex (TSC) genes. Micro-array studies on TSC1 or TSC2 ectopically overexpressed HeLa cells have shown high levels of FKBP38 expression. Selective inhibition of FKBP38 by specific antisense oligonucleotide treatment showed the loss of TSC gene ability to control cell size (Fig. 13A). Similarly, over-expression of the dominant-negative mutant TSC2ΔRL down regulates FKBP38 levels and thereby up-regulates cell size and cell cycle [101]. These studies underscore the importance of FKBP38 in TSC1 or TSC2-mediated cell size regulation.

I.8.4 mTOR signaling

FKBP38 functions as an endogenous inhibitor of mTOR via the mTORC1 pathway. GTP-bound Rheb, in response to growth factor stimulation and nutrient availability, antagonizes the FKBP38 mediated mTOR inhibition and activates mTOR signaling (Fig. 13B) [102].

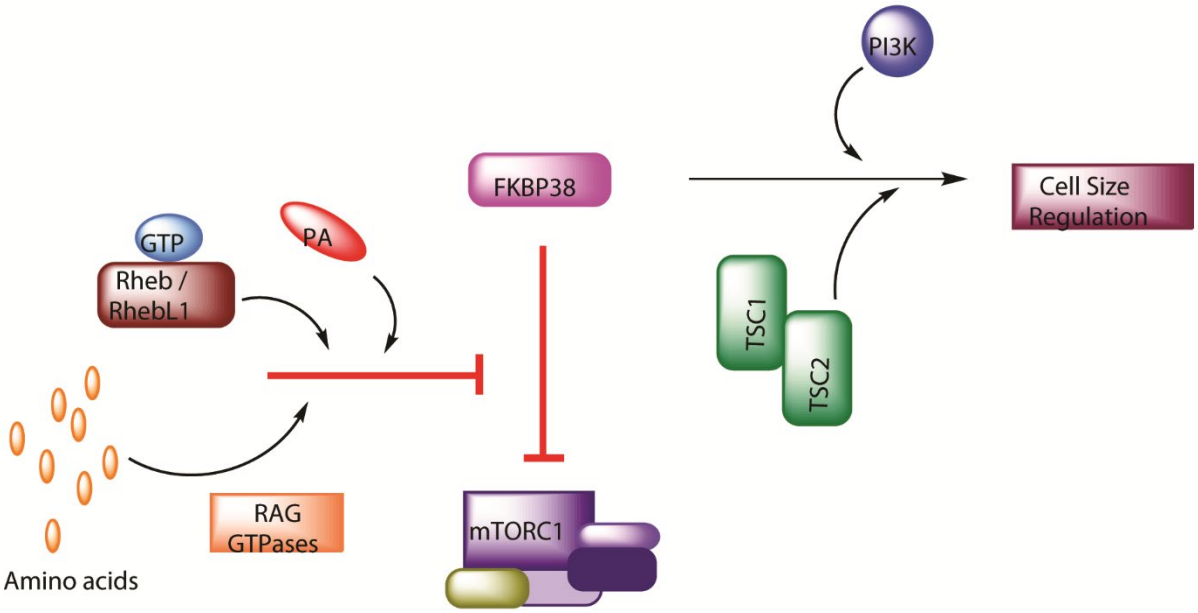

Figure 13: Importance of FKBP38 in cell size regulation and mTOR signaling. (A) FKBP38 together with PI3K maintains the integrity of TSC-mediated regulation of cell size. (B) FKBP38 functions as an endogenous mTORC1 inhibitor. (C) Excess amino acids, phosphatidic acid and GTP bound Rheb/RhebL1 protein complex (-es) antagonize FKBP38-mediated mTOR inhibition.

Though FKBP38's ability to antagonize GTP bound Rheb was questioned by other groups [103, 104], recently Dunlop *et al*. have shown that not only does FKBP38 antagonize the GTP-bound Rheb/RhebL1 mediated activation of mTOR activity but it also inhibits mTORC1 activity both *in vitro* and *in vivo*. FKBP38 can inhibit the activity of the L1460P mutant of mTOR (which responds to insulin treatment even in an amino acid-deprived state) but not that of E2419K mutant of mTOR which requires the presence of amino acids to respond to insulin stimulation. These data from Dunlop *et al.* suggest that the presence of amino acids stimulates the FRAP/TOR, ATM, TRRAP

(FAT) domain in mTOR and antagonizes the FKBP38 mediated inhibition of mTOR via a Rag dependent mechanism (Fig. 13C) [105]. Phosphatidic acid modulates the antagonistic effect of FKBP38 and activates mTORC1 signaling, but not mTORC2 [106].

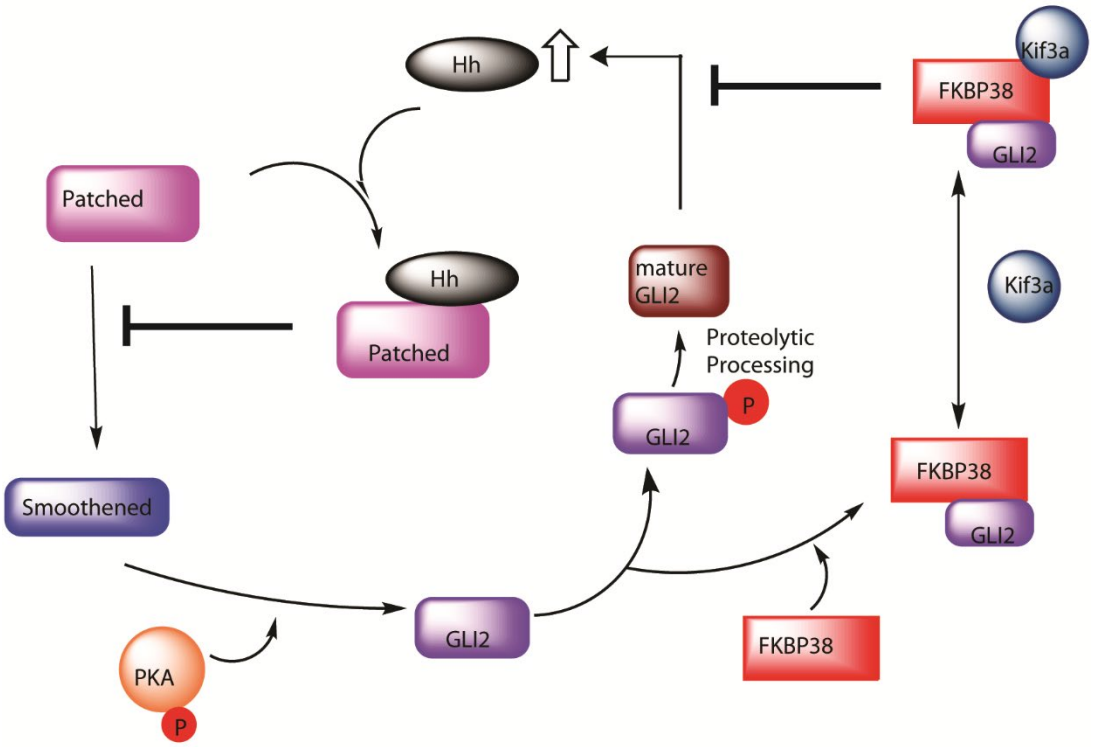

Figure 14: FKBP38 antagonizes Shh signaling independent of ligand (Shh) binding to Patched. FKBP38 binds to GLI2 transcription factors and in conjunction with Kif3a (intra-ciliary factor) inhibits the hedgehog secretions by preventing proteolytic processing of GLI2 transcription factor.

I.8.5 Negative regulation of Shh signaling & role in neural tube defects

Sonic hedgehog (Shh) signaling regulates neural patterning of the central nervous system by altering the genes that mediate dorso-lateral fates and ventral fates [107]. FKBP38 gene knock out studies have revealed that it functions as a negative regulator of Shh signaling. Hedgehog signal transduction occurs mainly by modulating the

activities of GLI2 protein family transcriptional factors. FKBP38 primarily acts in a cell autonomous fashion and modulates hedgehog pathway independent of upstream activator *smoothened* but dependent on kinesin-2 motor subunit kif3a (which mediates in intra flagellar transport (IFT) and cilia assembly (Fig. 14). FKBP8 depletion modifies the signaling of neural progenitors such bone morphogenetic protein (BMP) signaling causing non-autonomous effects on neural patterning [87, 108].

I.8.6 Developmental and Neuroprotective roles

FKBP38 null mice manifest developmental defects in neural tube closure (at the thoraco-lumbar-sacral region), skeletal, dorsal root ganglion development and organization of neural epithelium. FKBP38 null mice show an abnormal extension of nerve fibers in the spinal cord in embryos. Yeast two-hybrid assay screens identified that protrudin, a protein that regulates process formation and membrane trafficking, gets hyper phosphorylated leading to abnormal nerve extension. FKBP38, in part, by regulating protein folding, could alter the phosphorylation state of protrudin and ensure normal neurite formation [109, 110].

Selective inhibition of FKBP38 by specific inhibitor N-(N', N'-dimethylcarboxamidomethyl) cycloheximide (DM-CHX) has shown efficacy in achieving neuronal protection in a rat model of transient focal cerebral ischemia. DM-CHX not only protected neurons from ischemic challenge but also induced neural stem cell proliferation and neuronal differentiation signifying the role of FKBP38 in neurodegenerative disorders [111].

I.8.7 Chaperonic role on biogenesis of membrane proteins

FKBP38 functions as co-chaperone assisting the full maturation and trafficking of human ether-a-gogo-related gene (HERG), a voltage dependent potassium channel. Defects or mutations in HERG such as ΔF805C HERG affects its maturation and trafficking leading to disorders such as cardiac disorder long QT syndrome (which is characterized by a prolonged QT interval and increased susceptibility to cardiac arrhythmia). *si*RNA knock down of FKBP38 showed a reduction in HERG trafficking, while overexpression of wild type FKBP38 rescued the mutant F805C HERG trafficking. Thus, FKBP38 plays a limiting role as co-chaperone of Hsc70/Hsp90 chaperone network [112, 113].

Similarly, mutations such as ΔF508 in the cystic fibrosis transmembrane conductance regulator (CFTR, a chloride ion channel) alters the biogenesis, trafficking or stability of CFTR and disrupts the functioning of chloride ion channel. Using proteomic approach Wang *et al.,* have identified FKBP8 as one of the co-chaperones of Hsc70/Hsp90 chaperone machinery involved in the trafficking of ΔF508 and WT-CFTR proteins. Both *si*RNA knockdown as well as overexpression of FKBP38 has reduced both the ER and Golgi levels of CFTR-ΔF508 suggesting that FKBP38 tends to influence the stability of CFT-ΔF508 by maintaining steady state levels of Hsp90 for optimal functioning of a CFTR-centric Hsp90-client folding pathway [114]. FKBP38 is also shown to exert a role in regulation of CFTR synthesis, maturation and maintenance of steady state levels of CFTR and its post-translational folding. FKBP38 through its multiple domains modulates these actions and plays a crucial role in regulating CFTR protein synthesis. ERD enhances CFTR synthesis whereas TPR and transmembrane domains inhibit the CFTR synthesis; ERD and TPR domains of FKBP38 assist in maturation of CFTR. PPIase activity is implicated in post-

translational folding during biogenesis of CFTR on the cytoplasmic side of the ER membrane [115].

I.8.8 Invasion & adhesion - cancer cell progression

Single systemic administration of FKBP38/FKBP1a in the form of cationic liposome: DNA complexes (CLDC) have markedly reduced the metastatic progression of 4T1 or B16-F10 tumors in mice. In contrast rapamycin (administered i.p., daily for 18 days) failed to elicit a similar response indicating that FKBP8/FKBP1a gene overexpression acts by a different mechanism. cDNA microarray analysis using B16-F10 cells treated with rapamycin or FKBP8/1a overexpression has highlighted key roles of FKBP38 in modulating adhesion or invasion related processes during tumor cell invasion. FKBP38/FKBP12 overexpression (but not rapamycin treatment) not only up-regulated the anti-invasive Syndecan (Sdc1) levels (which maintains cell adhesion to extra-cellular matrix (ECM)) but also suppressed the pro-invasive MMP9 levels (which degrades ECM substrates) and thus decreased tumor invasion [116]. In contrast, global transcriptome profiling of curcumin treated lung adenocarcinoma cell lines revealed a down regulation of FKBP38 mRNA levels suggesting its role in invasion and metastasis processes [117]. As these observations are made on two different model systems, this could explain the discrepancy in observations; however, further studies are awaited for detailing the pathway through which FKBP38 plays a role in invasion and metastasis depending on cellular context.

I.8.9 Viral Replication

Hepatitis C virus (HCV) nonstructural protein 5A (NS5A) plays an essential role of viral replication by modulating the functions of several host proteins. A yeast two-hybrid assay screen identified FKBP38 as binding partner for HCV NS5 both in vitro and in

vivo. In vitro studies have shown that HCV NS5 with its BH-domain (Bcl-2- homology domain) binds tightly to TPR domain region of FKBP38 with an affinity of 82 nM. Immunoprecipitation studies have shown that FKBP38 forms a heteromeric complex with NS5 and Hsp90. Mutational analyses of NS5A revealed that a Val or Ile at position 121 is critical for the specific interaction between FKBP38 and HCV NS5. Furthermore, fluorescence and electron microscopy have revealed that FKBP38 partially colocalizes with NS5 into web like cytoplasmic structures, which are probable sites of viral replication and might play an important role in HCV replication [118-120].

I.9.0 *Plasmodium falciparum* FKBP35 (PfFKBP35)

P. falciparum FKBP35 (PfFKBP35) is a canonical form of FKBP which shows PPIase and chaperone activities. FK506 and rapamycin bind to PfFKBP35 and inhibits its enzymatic activities as well as in *vitro* growth of Plasmodium falciparum in 3D7 cell culture [121]. As discussed in introduction chapter I, FK506 and rapamycin interacts with FKBP12 and form binary complexes, which then interact with their cognate secondary targets - calcineurin or mTOR respectively and inhibits T-cell activation or proliferation respectively resulting in immunosuppression [2, 122, 123]. Efforts to find the FK506 binding protein in *Plasmodium* species - *falciparum* and *vivax* have led to identification and characterization of an FKBP with a molecular mass of 35-kDa [122, 124-126]. *Plasmodium* FKBP35 shows a high similarity to human FKBP12 at the catalytic domain whereas the overall structural arrangement resembles the TPR containing FKBP family members - FKBP38, FKBP51, and FKBP52 [122, 125]. Monaghan and colleagues have shown that PfFKBP35 displays potent PPIase enzymatic activity and chaperonic activity suggesting that it could function as parasitic chaperone. PfFKBP35 exhibits a stage-specific nucleocytoplasmic shuttling and does

not co-localize with calcineurin. PfFKBP35 is expressed in all the intra-erythrocytic life forms and indirect immunostaining studies have revealed that PfFKBP35 is predominantly in the cytoplasm during ring stage and as the ring form matures to trophozoite and schizont forms, PfFKBP35 translocates to the nucleus [126]. Furthermore it was also shown that PfFKBP35 associates with Plasmodium heat shock protein 90 (Hsp90), another member of the chaperone super family via the TPR domain [127].

Monaghan *et al*., have shown that both the PPIase and chaperone activities are selectively inhibited by FK520 and its non-immunosuppressive analogues [128]. This study has inevitably brought the attention back to FKBP proteins and their role in mediating anti-malarial activities. In this study, macrolide lactone analogs of FK520 such as 18-ene-20-oxa-FK520 and 13-Me-18-ene-20-oxa-FK520 which inhibit the chaperone activity but not PPIase activity have also been shown to inhibit growth of 3D7 culture and suggested that the TPR domain could also play a role in mediating these actions. For these reasons, the authors have emphasized the need to design and develop specific ligands that can inhibit either the chaperone or PPIase activities, unlike the macrolide lactone structures of FK520 analogs which inhibit both the activities.

Our lab has elucidated the 3D-structures of both the apo-form and FK506 bound form of FK506 binding domain from *falciparum* and *vivax* species of *Plasmodium* FKBP35 by NMR and X-ray crystallography. FK506 bound *Plasmodium* FKBD35 X-ray crystals solved from Plasmodium species have clearly shown that FK506 binds to the PPIase or FKBP domain and inhibit its PPIase activity. These studies suggest that the FK506

binding domain is important for imparting its anti-malarial activities [129-131]. Recently, our group has also shown that the FKBP35-TPR region modulates the chaperone activity and binding to the C-terminal MEEVD region of Hsp90. PfFKBP35-TPR has all conserved residues (K148, N152, N199, K229, and K233) that are required for carboxylate clamping interactions with C-terminal pentapeptide MEEVD of the heat shock protein. Surface plasmon resonance studies on wild type FKBP35 TPR and the alanine mutants of the aforesaid residues on the PfFKBP35-TPR domain have resulted in loss of affinity for the MEEVD pentapeptide [132]. This study shows that carboxyl terminal “MEEVD” residues are important for PfFKBP35 interaction with Hsp90 and could play crucial roles as a co-chaperone in regulating chaperone activity.

Lack of cellular toxicity of FKBP12 ligands has allowed researchers to exploit the ubiquitous nature of FKBP12 and ligand binding to it to improve the bioavailability of ligands targeting HIV protease using FKBP ligands as a presenter protein strategy. These studies showed that despite high affinity binding to FKBP12, the therapeutic efficacy of HIV inhibitors was improved due to increased in vivo half life time of HIV protease inhibitors and that FKBP12 ligands could evade cytochrome P(450) metabolism [133, 134]. These studies show that ligands binding to FKBP12 do not cause cellular toxicity in preclinical models. Further, the study by Braun *et al.* suggested the physiological levels of parasite FKBP35 are about 50 nM – 100 nM whereas the human FKBP12 levels is around 3-5 μM and therefore could present an avenue to selectively inhibit the Plasmodium FKBP35 than human FKBP12 [124].

I.10 Drug Design & Discovery Approaches

I.10.1 Structure-Based Drug Design

Over the years, structure-based drug discovery has become a complementary tool in drug design and discovery process serving as an alternative to experimental high throughput screening. Together with the advent of higher computational resources, a simultaneous increase in the number of public and commercial synthetic small molecule libraries and the increase in deposition of high resolution crystal structures for a number of protein targets have brought structure-based drug design (SBDD) methods to the forefront of drug discovery process [135, 136].

Drug discovery methods can be broadly categorized into 1) ligand-based and 2) structure-based methods. Ligand-based methods mainly emphasize comparative analysis of the structural shape and common or diverse pharmacophore features of known ligands. As this method does not rely on the structural information of the protein target, the knowledge of experimentally characterized active compounds is paramount to the success of ligand-based methods [137]. On the contrary, the structure-based methods do not entirely rely on experimentally active compounds but rather identify new molecules that are complementary to the protein active site. In particular, structure-based methods have increased the prospects of identifying truly novel scaffolds by inclining the search towards the active site or binding pocket itself. In these methods, the interaction of a given compound with a target receptor and its binding mode are estimated and predicted. Molecular docking, which mainly utilizes computers to predict the binding mode and the affinity of a given compound towards a target receptor forms the basic framework in receptor-based virtual screening procedures [138] and in lead discovery strategies [139, 140].

Molecular docking or virtual screening offers the advantage of docking of small molecule library into the active site and predicting the interaction energy. Alternatively,

the search for better binding fragments can also be done in a much more focused way by ensuring complementary to binding site of the protein. This is achieved by appropriate positioning or docking of fragments such as methyl or benzene, carbonyl and amino groups onto the active site residues. Better binding groups are identified by scoring and ranking based on their interaction energies, and these fragments are linked in-silico to obtain a new molecule. However, these early methods suffered from problems of synthetic feasibility. To overcome the synthetic tractability of molecules, the search was biased towards synthesizable or synthesized fragments. Recent progress in combinatorial chemistry has led to development of synthetic libraries of molecules in a short period of time. Taking advantage of progress in combinatorial chemistry, structure-based methods are improvised to make use of synthetic libraries by means of virtual screening the databases of synthesized combinatorial chemistry libraries. Initial docking methods are adopted in such a way as to blindly dock all the molecules in the synthetic libraries in a high through put way; scoring and ranking the hit list based on their affinity of protein-ligand interactions. Though blind docking method possesses inherent pitfalls, it enables a quick identification of tight binders to weak binders. Thus, virtual high-throughput screening (vHTS) helps researchers to quickly identify most probable binders thereby reducing the data set of molecules from millions to thousands and then proceed to standard docking to further filter the better binders. These methods were popular, though it is time consuming and cumbersome to handle large volumes of datasets [141].

In order to fish or screen ligands that are complementary to protein active site, programs such as Ludi [142] have been modified to convert the interaction hot spots (on particular residues of the receptor) into a pharmacophore model which can effectively screen the millions of chemical space in short time and provide a focused

library. Hits from such library can be further prioritized by a routine docking, scoring and consensus scoring methods to identify the potential hits that could bind to the protein in question.

Failures of SBDD methods are mainly attributed to the inherent lapses in scoring and ranking algorithms. Simplified assumptions or terms used to evaluate the complex protein-ligand interactions and their ability to predict the putative binding mode and its affinity. Despite these challenging problems structure-based drug discovery (SBDD) methods, in most cases, are very successful in enriching hit rates, though they sometimes fail in providing enrichment of hit rate. Some researchers concur that the current software programs are more effective at eliminating bad leads than identifying good ones [143]. As summarized by Warren *et al.* SBDD has its own pros and cons, though many docking and scoring procedures do well at predicting binding mode, reproducing ligand poses within 2 Å, but none could rank the ligands by affinity. In general, it is still not possible to identify “activity cliffs” meaning that nM-level affinity inhibitors or binders cannot be consistently ranked over those with μM-level binders (Molecules with small variations in the structure which result in significant variation in affinity) [143]. However, despite significant efforts to advance the methodology, it is still generally recognized that the performance of most docking and scoring algorithms are adequate to reliably impact industrial drug discovery productivity [144-146].

Numerous studies done for improving docking and scoring, and in particular pose prediction, have shown that combining results from multiple scoring functions and evolving consensus yielded better results than the use of a single scoring function [137, 139, 140, 146]. Consensus scoring has been shown to increase the chances of identifying the true hits and provide enrichments better than single scoring functions. Though the fusion procedures improve the performance of structure-based methods

retrospectively, it is still difficult to predict *a priori* what data fusion or other approach will work for a given system [145].

In most of the molecular docking algorithms, the target protein is kept rigid in a single low-energy conformation and only conformational flexibility of a ligand is explored. When one considers the flexible nature of protein conformation, together with the conformational changes induced by ligand binding, this exponentially increases the computational costs [147]. Some argue that using a single receptor conformation in docking experiments could lead to errors in identification of binding modes and errors in prediction of binding affinities. This can significantly hamper the chances of finding new ligands [148]. Various groups have attempted to include protein flexibility in the virtual molecular docking procedure. Schrödinger's Induced Fit docking used an iterative docking protocol that accounts for both ligand and receptor flexibility [149, 150]. This is done by docking the ligand into a rigid receptor using reduced van der Waals radii and then the receptor side-chain conformations are sampled for each receptor-ligand binding pose followed by an energy minimization and a second round of docking.

Knegtel *et al.* used an ensemble of experimental receptor conformations (crystal and solution NMR structures) in ligand docking, to generate combined interaction grids by averaging with respect to energy and geometry [151]. Alternatively, a large ensemble of receptor conformations generated from molecular dynamics simulation (MD) is also used to select a minimal subset of receptor conformations based on a correlation between the experimental binding affinity and the docking scores obtained from a preliminary docking experiment on a small number of known active compounds for virtual screening [150].

The Internal Coordinate Mechanics (ICM) flexible receptor-docking algorithm (IFREDA) samples the conformational space of the receptor by generating a discrete set of receptor conformations through seeding, soft van der Waals structure relaxation and energy optimization processes. Thus de novo generated structures and the native structures are used for the virtual screening and then the docking results are condensed with a merging and shrinking step [152].

Despite these efforts, the receptor-based virtual screening methods that accommodate structural flexibility of both the ligand and receptor are still too computationally expensive for a large library of compounds. In such a flexible system, there might be no clear relationship between docking and ranking [153]. Thus, the additional receptor conformations may actually increase the “false positive” rate instead of improving or enriching the hit rate.

I.10.2 Analog-Based Drug Design

Ligand-based methods such as 3D quantitative structure activity relationship (QSAR) Pharmacophore methods have been much more reliable methods than receptor based ones as they were able to predict the affinity or the activity of the compound based on the knowledge of known subset of inhibitors. This helps to quickly make decisions regarding the suitability of a selected hit and its purchase for further studies. Recently, Hawkins *et al.* have shown that a ligand-based shape-based virtual screening approach was often superior to a typical single-receptor docking procedures. However, the authors do show that efficient docking program’s such as GOLD or GLIDE show an equivalent consistent performance on par with the ligand-based methods.

Ligand-based methods are of much utility for diseases with no known protein target information and mainly consists of either developing a 3D QSAR pharmacophore model based on a data set of active and inactive compounds or identifying the common pharmacophore features that are important for activity among the active and inactive dataset. Furthermore, the inclusion of shape feature of the most active ligand is used to simulate hypothetical or pseudo receptor shape of the protein active site and is critical to recall hits that could bind with the protein in a manner similar to known actives.

3D quantitative structure activity or property relationship studies are more popular methods in identifying hidden knowledge of properties of ligands that are critical for activity. A known data set of molecules with diverse structural features with varied activity is used to train a model which can identify the underlying hidden patterns relating the structural descriptor to activity and predicting the activity of the molecule. These methods are important as they not only identify the statistically significant descriptors that define the activity but can also predict the activity of similar scaffold like molecules with good precision. These methods are highly useful in the lead optimization process where one has a promising lead and these methods actually highlight the optimization points which could improve the activity of the initial hit. These methods actually enrich the decision making as to which substitutions can be taken up for improving activity. 3D QSAR methods thus enrich the synthetic outcome to more active compounds. However, the early 3D-QSAR models can only predict the activity of unknown compounds with accuracy based on the 2D and 3D descriptors incorporated into their QSAR equation of descriptors that influence biological activity. But these models are not useful to search and retrieve novel molecules from combinatorial-chemistry libraries. To overcome this problem, pharmacophore

modeling was devised to develop a model weighted with good statistical significance from a training set data with structural diversity and good activity spread (4-fold). This feature model or hypothesis or pharmacophore model is useful to search the virtual combinatorial library or database and prioritize the screen by predicting the activity with good statistical significance.

Given the experiences with structure based and ligand based drug design approaches, I have tried to use the synthesis of both structure of the protein and pharmacophore modeling (usually employed for ligand based method) as exemplified previously [154] to generate novel hit for the proteins under my thesis study.

I.10.3 FKBPs as Drug Targets and Immunophilin inhibitors

FKBPs play important roles in various cellular processes such as apoptosis [86], receptor signaling [18, 20], calcium homeostasis [17], spermatogenesis [155], neuroprotective or neurotrophic [4] and malaria [128]. These physiological activities are in part modulated by binding of canonical ligands such as FK506 & rapamycin to FKBP proteins. These ligands can mediate protein-protein interactions as well as disrupt protein-protein interactions. FK506 or rapamycin binding inhibits protein-protein interactions such as TGF-β-FKBP12, FKBP12-YY1 and FKBP12-mTOR-PGC-1α interactions and thereby regulate the cell cycle and repress transcription. FK506 and rapamycin also mediate important protein-protein interactions such calcineurin and mTOR binding and regulate T-cell proliferation and immunosuppressive actions. Though FK506 and rapamycin are approved FDA approved drugs for preventing graft rejection, they have also attracted much attention for their neuroprotective and neurotrophic actions. Its immunosuppressive properties limited its clinical utility for these clinical indications.

FK506 and rapamycin owing to their macrolide lactone structure are thought to directly act on sarco/endoplasmic reticulum Ca^{2+}-ATPase (SERCA) channels and modulate the calcium levels [156, 157]. Recent efforts are to develop ligands that bind selectively to members of this degenerate FKBP family wherein rapamycin analogs such as ILS-920, WYE-592 (3rd generation FKBP ligands) are shown to bind specifically to FKBP52. However, these rapamycin analogs are also shown to bind to voltage gated calcium channels and exert their neuroprotective activities without immunosuppressive effects [158]. The binding of either FK506 or rapamycin to multiple proteins makes it difficult to elucidate the mechanism of FK506 or rapamycin analogs.

Most of the efforts in the last decade were spent on developing non-immunosuppressive (non-calcineurin binding) ligands such as 18-OH-FK520 or GPI-1046 that are able to afford neuroprotective, neuroregenerative and neurotrophic activities in different cell based and animal models [159]. Ab initio efforts have identified small molecule ligands that such as V-10367 and GPI-1046 (second generation FKBP ligands) that bind only to FKBPs showing nanomolar efficacy in cell based models. However lack of consistency in different animal models and the findings that V-13670 which does not bind to FKBP12 but shows efficacy similar to FKBP12 ligands has questioned the role of FKBP12 in mediating the neuroprotective / neurotrophic activities [160-163]. Later studies from Gold *et al.* and Tanaka *et al.* have shown that these ligands mediate their action via FKBP52 and not FKBP12 [55, 162, 164] GPI-1046 was shown to be neuroprotective by preventing progressive dopaminergic axonal degeneration and neuronal cell death in a mouse model [165]. V-10367, an FK506 analog, was shown to have neuroprotective activity on different

cell lines like PC12 and Neuro2A cells but not on SHSY-5Y cells [166]. GPI-1046 also protects the neuroblastoma SH-SY5Y cell lines from cell death, upon induction with cell-death inducers like etoposide, camptothecin and ionomycin. Fischer *et al.* have reported N-(N', N'-dimethylcarboxamidomethyl) derivative of cycloheximide, as specific inhibitor for FKBP38, provides neural protection and neural stem proliferation in an acute focal cerebral ischemic rat model [111]. These studies have demonstrated that small molecule inhibitors of FKBP38 helps in combating a variety of neurological disorders like Alzheimer's disease, Parkinson's disease, cerebral ischemia and stroke. The following tables give a glimpse of three generations of immunophilin ligands that were developed over the years.

TABLE II:

A: First Generation of Neuroimmunophilin Ligands:

FK506	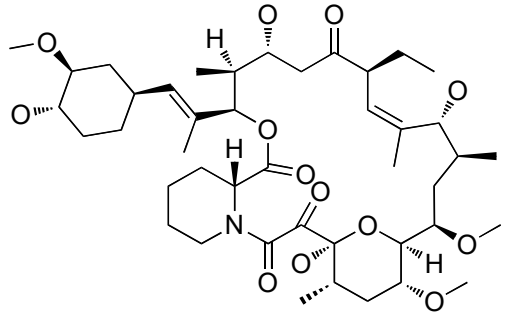	*Hs*FKBP12: K_d 0.4 nM [111] *Hs*FKBP52: K_d .72 nM [111]
FK520 (L-683,590)	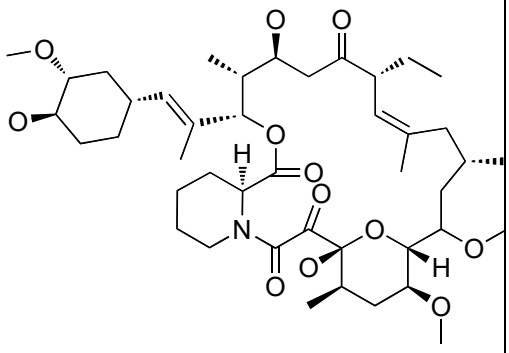	*Hs*FKBP12: K_d 0.5 nM [159]
18-OH-FK520 (L-685,818)	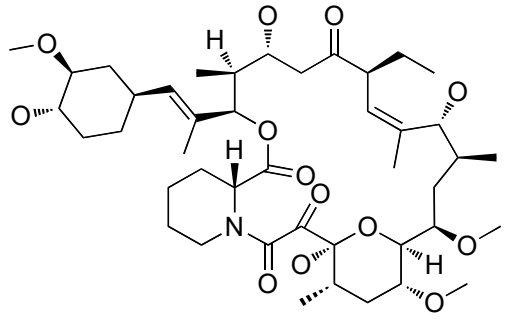	*Hs*FKBP12: K_d 0.7 nM [167]
Rapamycin	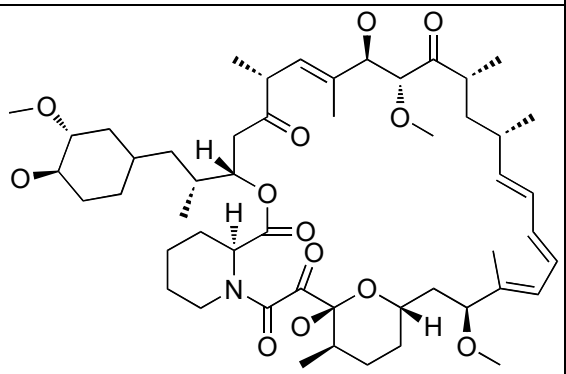	*Hs*FKBP12: K_d 0.3 nM [158] *Hs*FKBP52:K_d 1.4 nM [158]

13Me-FK520	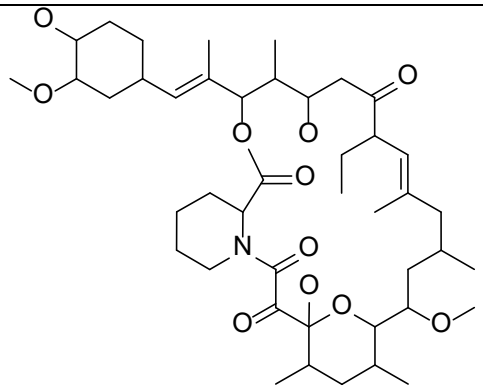	PfFKBP35: IC_{50} 0.63 μM [128]
18-OH-13-Me-FK520	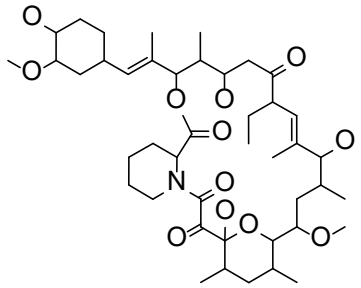	PfFKBP35: IC_{50} 0.8 μM [128]
18-ene-20-oxa-FK520	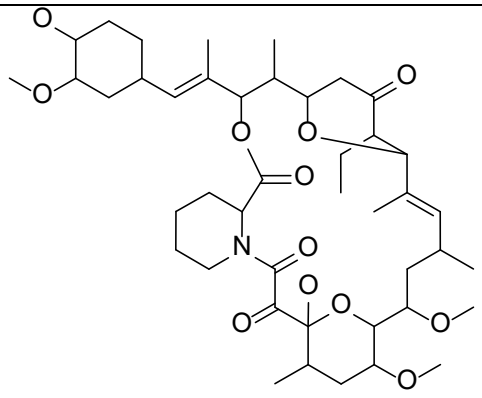	PfFKBP35: IC_{50} >5 μM [128]
13-Me-18-ene-20-oxa-FK520	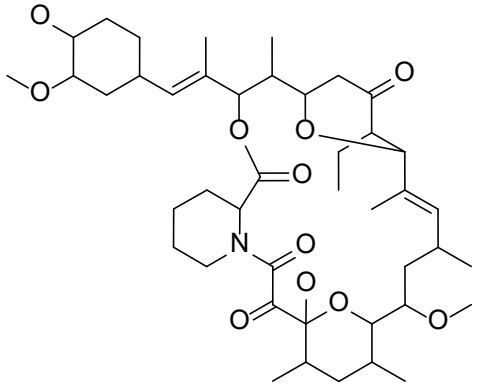	PfFKBP35: IC_{50} >5 μM [128]

B: Second Generation of Neuroimmunophilin Ligands

V-10,367	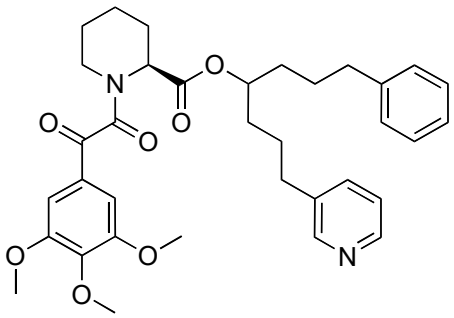	*Hs*FKBP12: K_i 0.5 nM [168]
GPI-1046	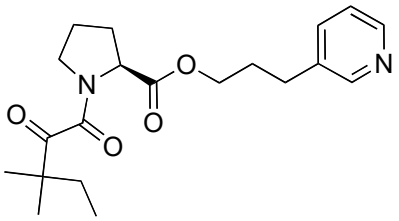	*Hs*FKBP12:K_i 306 nM [111] IC_{50} 7.5 nM [169] *Hs*FKBP52:K_i 936 nM [111]
SB3	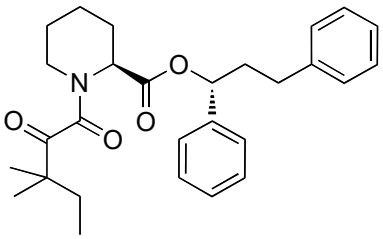	*Hs*FKBP12: K_i 10 nM [170]
4	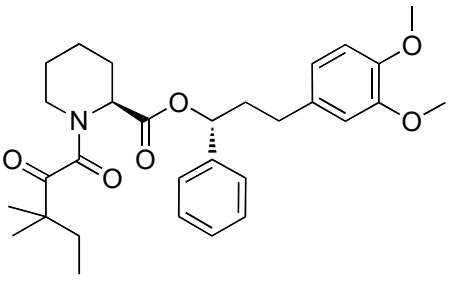	*Hs*FKBP12: K_i 2-6 nM [170]

C: Third Generation of Neuroimmunophilin Ligands

DM-CHX	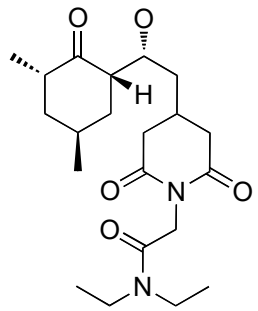	*Hs*FKBP12: K_i 29500 nM [111] *Hs*FKBP38: K_i 85 nM [111] *Hs*FKBP51: *K*i 958 nM [111] *Hs*FKBP52: K_i 155 μM [111]
WYE-592	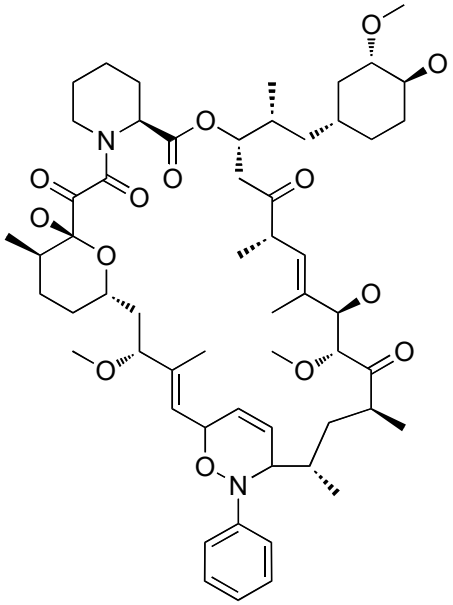	*Hs*FKBP12: K_d 4.7 nM [158] *Hs*FKBP52: K_d 0.55 nM [158]
ILS-920	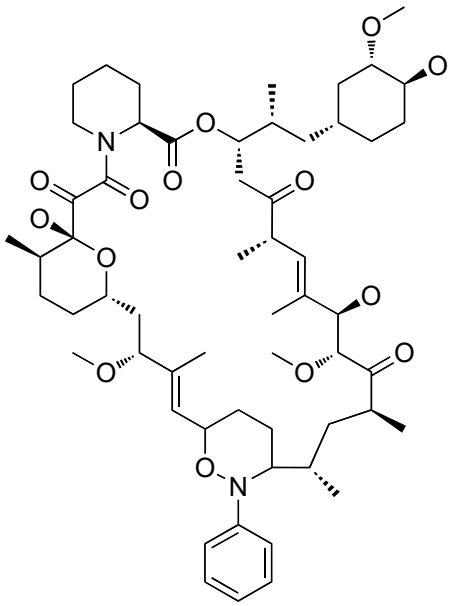	*Hs*FKBP12: K_d 110 nM [158] *Hs*FKBP52: K_d 0.72 nM [158]

II. Materials & Methods

II.1 Molecular Modeling.

II.1.1 Ligand Preparation: Chemdiv's [171] database, a highly diverse non-redundant library comprising about one million molecules, was used for virtual screening. 3D-coordinates and molecular properties were generated for all the molecules in the Chemdiv's library by using the *prepare ligands and molecular property calculation* modules in Discovery Studio. This module allows one to filter the molecules by Lipinski's rule of five (*Ro5)* [172]. Lipinski's rule of five suggests that ligands having 1) a molecular mass not more 500 Daltons, 2) not more than five hydrogen bond donors, 3) not more than 10 hydrogen bond acceptors, 4) LogP of less than five have the probability of being drug-like molecules. During later years, *Ro5* was further improved by Veber [173] who proposed that molecules must also meet the following criteria of i) 10 or less rotatable bonds and ii) a polar surface area of less than or equal to 140 $Å^2$. Together with Ro5 and veber's rules, calculation of absorption, distribution, metabolism, excretion (ADME) and toxicity (T) properties via ADMET and TOPKAT (software to calculate the toxicity properties such as LD50, carcinogenicity, mutagenicity, skin and ocular sensitivities or irritation based on chemical structure) [174] modules helps to predict the solubility, LogP, absorption, distribution and toxicities associated with the molecules and helps in the selection of molecules with desired ADMET properties. Such property filtering enables one to exclude molecules that do not obey the Lipinski and Veber rule and are likely to have unfavorable Ames mutagenicity, carcinogenicity, skin and ocular irritant toxicity parameters. Thus, filtered database is further processed for energy minimization to obtain lowest energy conformation for the each of the ligands in the database.

II.1.2 Energy minimization

Energy minimization for the property filtered library was carried out by using the **Ligand minimization** module. This module has different algorithm options to carry out energy minimization. Smart minimizer, a hybrid method that utilizes a cascade of steepest descent and a conjugate gradients algorithm for faster convergence towards the local minimum was employed for energy minimization. Maximum number of minimization iterations was set to 2000 steps. Minimization routine is exited (by the program) when the tolerances such as i) RMS gradient is less than or equal to 0.001Å and ii) the energy change is less than or equal to zero kcal / mol from one iterative to another iterative cycle of minimization.

II.1.3 Diverse conformation generation

FKBP12 dataset – pharmacophore modeling:

For all the structures, partial atomic charges were calculated using the CHARMm force field and minimized using the smart minimizer algorithm with a convergence gradient value of 0.001 kcal / mol. Multiple confirmations are generated by “Best search” method which utilizes a poling algorithm to sample the conformation space [175-177]. A maximum of 250 conformations were generated for each compound to ensure maximum conformational sampling with an energy threshold of 20.0 kcal / mol above the global energy conformation.

II.1.4 Construction of 3D Database

The development of a virtual 3D-database is prerequisite to the pharmacophore screening. Based on the uniqueness and synthetic volume of chemical libraries as shown in table III, Chemdiv’s Discovery collection [171] (single vendor database) was

chosen for building the 3D Database. Depending on the size of the library either a single conformation database or multiple conformations for molecules in the library may be opted for. As our lab has legacy license system for Cerius^2 version as well as Discovery studio, I have developed the 3D-virtual libraries that can be used from either of the modeling environments - Cerius^2 legacy version or Discovery Studio version. A single confirmation database was generated for seven chunks of Chemdiv library each with 100,000 molecules. Similarly, the Clean-Leads section of the Zinc database with 17 chunks with ~ 28,000 molecules each [136] (4,76,000) was used to build a single conformer database. Apart from these two databases, I have also employed a synthetic natural product database from the Interbioscreen [178] vendor and generated a multi-conformational database for database search with Cerius^2 modeling environment.

Later, we have updated our modeling environment to Discovery studio and accordingly the multi-conformer databases of Maybridge, Chemdiv discovery, NCI and InterBioscreen natural product collections were built by using the Caesar algorithm to generate multiple conformers. Thus, built libraries of Chemdiv, InterBioscreen natural product [178], Maybridge and NCI databases are installed on our modeling server (wabbit.sbs.ntu.edu.sg) and can be used for database searching with a pharmacophore model based on protein structure or by analogy to lead structures by using the SEARCH 3D DATABASE module of the Structure based focusing module of Cerius^2 and Discovery Studio 2.5 or higher versions.

Table III. Chemical diversity among the commercial vendor fragment databases.

	Timtec	SPECS	Selcia	Pyxis	Prestwick	Otava	Maybridge	LifeChemicals	Keyorganics	InFarmatik3D	**Enamine**	**Chembridge**	**ChemDiv**	**Asinex**
Timtec	3164	61	45	0	38	106	19	3	65	0	13	123	119	22
SPECS	61	4407	101	0	104	198	84	2	113	1	38	141	197	7
Selcia	45	101	1301	0	105	0	155	0	58	0	17	22	30	2
Pyxis	0	0	0	312	0	0	0	0	0	0	0	0	0	0
Prestwick	38	105	104	0	2786	65	67	1	71	0	13	26	52	16
Otava	106	198	59	1	65	4837	44	9	167	3	68	202	527	35
Maybridge	19	84	162	0	67	44	1500	0	88	0	12	32	33	3
LifeChemicals	3	2	0	0	1	9	0	8087	5	0	3	8	62	8
KeyOrganics	65	113	58	0	71	167	88	5	7025	0	39	73	153	19
InFarmatik3D	0	1	0	0	0	3	0	0	0	270	2	0	2	0
Enamine	13	38	17	0	13	68	12	3	39	2	1190	34	62	0
Chembridge	123	141	22	0	26	26	202	8	73	0	34	4570	298	1
ChemDiv	119	197	30	0	52	527	33	62	153	0	62	298	10455	17
Asinex	22	7	2	0	16	35	3	8	19	0	0	1	17	5142

Adapted from http://homepage.mac.com/swain/CMC/DDResources/Hit_iden/frag_coll_profiles.html

The red letters indicate the fragments that are unique to a particular vendor. Black letters indicate the amount overlapping fragments that are also available with other vendors.

II.1.5 Database Search

In the Cerius^2 modeling environment, clicking 'structure based focusing deck of cards' will pop up the 3D database search module. After opening the program, one has to locate the directories of 3D-virtual libraries and define the search type (best / flexible) and proceed for 3D-searching. Depending on the number of features involved in pharmacophore query, the program recalls/retrieves the compounds fitting to the pharmacophore and output is given in structure document (SD) format. Similarly, in Discovery Studio (DS) environment, clicking Pharmacophore tab provides options such as ***Search 3D database, Screen library***, and ***Ligand Pharmacophore mapping*** protocols which will perform a database search job. A Shape constraints license is available in DS and can also be used during search to filter hits by shape constraints.

II.1.6 Protein Preparation

Crystal structures of PfFKBP35-FK506 complex (2VN1) [131] and human FKBP38 (2AWG) were used for protein preparation. Both the proteins PfFKBP35 and HsFKBP38 were optimized by deletion of hetero-atoms, addition of hydrogen atoms at pH 7.0, correction of charges and potentials, and energy minimization (of relative positions of added hydrogen atoms) with heavy atoms fixed using consistent valence force field by the conjugate gradient method for 2500 steps in InsightII [174]. Thus minimized protein was used for generating a pharmacophore model and for docking the molecules retrieved by the pharmacophore model.

II.2 Drug Design Approaches

II.2.1 Receptor Based Pharmacophore modeling

Structure based focusing module in Cerius^2 [174] was used for generation of receptor based pharmacophore model. The geometric centre of the co-crystallized ligand or a region around 5 Å radius of the active site residues were used to define the binding site. A Ludi [142, 179] interaction model utilizes hydrogen bond donor (HBD), hydrogen bond acceptor (HBA) and lipophilic features to identify possible interactions that a ligand could probably make with at the active site residues.

Discrete clusters of vector site points are generated from the defined active site. One needs to customize or optimize the features targeting the important residues that are required for binding / inhibition from these clusters of vector site points. This is achieved by hierarchical clustering of cluster vector site points based on the feature type and RMS distance of 0.7 Å (default option) (or it can be varied, depending on the number of features that are required at the targeted residues). A size exclusion model is also incorporated during development of the receptor based pharmacophore model [154]. This exclusion model helps to avoid bumps with other protein atoms and is also a key factor in the retrieval of hits (that could be selective to the protein in question) during database search. Structure based pharmacophore modeling generates numerous pharmacophore queries/models based on the number of features that are defined during generation. These queries can be prioritized based on their ability to identify a known set of ligands (whenever such control data is available) which target the same binding site.

II.2.2 Virtual Screening / Molecular docking

Molecular docking simulations were performed using the GOLD v3.3 program [180] which utilizes genetic algorithm (GA) to explore the possible binding modes by effectively placing the ligand by fitting points to the hydrogen bonding groups (acceptor or donor) on the protein as well as on the ligand and by mapping hydrophobic points of the ligand (CH groups) into the protein cavity.

Whenever there is protein - ligand information available in the pdb, the docking parameters are optimized by simulating the crystal ligand conformation. For the PfFKBP35 protein, most of the parameters were default GA settings, except for PfFKBP35 where the planar R–NR_1-NR_2 flexibility option is kept fixed. Annealing parameters for van der Waals interactions and hydrogen bond interactions within 4.0 and 2.5 Å respectively and solutions within a RMSD of 1.5 Å were considered for analysis.

II.2.3 Consensus Scoring

The docking solutions obtained from the GOLD search engine are further evaluated by rescoring with different scoring functions such as PLP [181], Jain [182], PMF [183, 184], Ludi [185, 186] and Ligscore scoring functions [187] available with the Accelrys modeling environment and consensus was evolved among these scoring functions. Together with the filter of consensus scoring, all the ligands were visually inspected and ligands which had a better fitting into the active site and interactions with select residues like Tyr44, Asp56, Trp78, Tyr101, Cys106, and Ser109 were selected for purchase. The hits that were readily available from the vendor were chosen for purchase and further experimental screening. A similar approach was also adopted for selecting hits for FKBP38.

II.2.4 Fragment Based de novo ligand Design

To apply this method, at least one known or well characterized compound is a prerequisite as this method doesn't rely on 3D structural information of the protein. The following are key steps involved in this method. The first step is to identify the important pharmacophore features (HBA, HBD, hydrophobic, ring aromatic, positive ionisable, negative ionisable features) and to create a reference pharmacophore. Second step is to create the fragments of the reference pharmacophore. When dividing the parent molecule into fragments depending upon the size of the ligand, the program manual advises not to define more than three link or query atom(s). Once the fragments to be made are decided, all the atoms, features and query atom(s) involved in each of the fragment are copied into new workspace, added with shape constraint and saved as fragment pharmacophore(s). The third step is to search the 3D fragment databases (Maybridge or fragment library from Chemdiv built previously) with each of fragment query and the resulting fragment libraries are enumerated for all combinations [$F1_x$ $F2_x$ N (no. of link atoms)] and finally the de novo compounds are verified by mapping to the reference pharmacophore and best fitting de novo compounds could be selected directly for synthesis or sub-structure search of best fitting fragments on a commercially available database. This can provide a focused library for experimental studies.

II.3 Expression and Purification of *Plasmodium falciparum* FK506 binding domain 35 (FKBD35).

For biochemical studies, the PfFKBD35 (hereafter referred to as FKBP35) gene (which was cloned into *E. coli* expression vector pET29b by our earlier colleagues) was over expressed and purified by a Ni^{2+}–NTA (nickel-nitrilotriacetic acid) affinity and gel

filtration column chromatography as described by Kang *et al.,* [125]. The plasmids pET29-PfFKBP35, pSumo-PfFKBP35 & pSumo-PvFKBP35 [129, 131] were transformed into *E. coli* BL21 DE3 cells and transformed cells were grown in LB medium containing 30 mg/ml of kanamycin at 37 °C. The protein was induced by adding the isopropyl β-D-1-thiogalactopyranoside (IPTG) to 1mM final concentration when the cell culture absorbance (A600) reached 0.6–0.8, and the culture was induced and further incubated for additional 3 h at 25 °C. The cells were harvested by centrifugation at 10000 g for 8 min, re-suspended in the re-suspension buffer (20 mM $NaPO_4$, 500 mM NaCl, pH 7.8), and lysed by sonication with 3 sec pulser with an interval of 1 sec for 20 min on ice bath using a 23% amplitude sonicator . The cell lysate was cleared by centrifugation at 20,000 g for 20 min and purified by Ni^{+2}–NTA resin as described before [131]. In case of the pSumo constructs of Plasmodium falciparum and vivax, the purified proteins are buffer exchanged to remove high concentrations of imidazole from the buffer and the sumo tag was cleaved by sumo protease (50 mM Tris-Cl, 150 mM NaCl, pH 7.5, 2-5 µg/10 mg of recombinant protein) overnight at 4°C and the cleaved protein was collected in the flow through [129]. Gel filtration analysis was performed on HiPrep 26/60 Sephacryl S-200 column (Amersham BioScience) with the buffer containing 20 mM $NaPO_4$, pH 6.8, 150 mM NaCl, 1 mM dithiothreitol (DTT), 0.01 % NaN_3 at a flow rate of 1 ml/min. The purified proteins were analyzed by a SDS 12% polyacrylamide gel. Similarly, ^{15}N-labelled samples of PfFKBP35 were prepared in minimal media [188] with 0.2% glucose as the carbon source and 0.2% ^{15}N ammoniumchloride as the nitrogen source. The media was also supplemented with 10 mg / L thiamine. The recombinant PfFKBP35 was purified to near homogeneity. The purified proteins were stable after storage for one

month at 4 °C. The concentration of the purified protein was determined by Bio-Rad laboratories protein assay kit.

II.4 Crystallization, X-ray Data Collection, Structure Determination

Purified PfFKBP35 was used for crystallization at a concentration of 15 mg/ml. Initially, a series of ligands were screened for crystallization as a cocktail containing two or three ligands; the cocktail approach makes screening for initial crystal hits efficient and unlimited [189]. These cocktail of ligands were incubated overnight with the protein at a molar ratio of 1:1. The protein-cocktail complexes were screened using an ammonium sulphate-buffer grid. After 2 weeks, rod shaped crystals appeared in 3.5 M ammonium sulphate and 0.1 M citrate buffer, pH 5.5 with cocktail containing D42 and D44 inhibitors. Further optimization with individual inhibitors, D44 alone yielded bigger crystals in 3.5 M ammonium sulphate and 0.1 M citrate buffer, pH 5.75. Crystals were cryo-protected with 20% v/v glycerol, and data from a single crystal to a resolution 2.75 Å was collected at 100 K on beamline 13B1 at the National Synchrotron Radiation Research Center (Hsinchu, Taiwan) using an ADSC-Quantum 315 detector. The diffraction data were indexed, integrated and scaled using the HKL2000 [190] suite of programs. The crystal belonged to the tetragonal space group $P4_32_12$, similar to the previously solved PfFKBP35-FK506 complex [131] (PDB ID 2VN1). The Mathews co-efficient indicated the presence of three monomers in the asymmetric unit, due to an enlarged unit cell. Therefore, a molecular replacement search was employed using the program PHASER [191], with a monomer unit of the PfFKBP35-FK506 (PDB ID 2VN1). PHASER identified the three monomers in the asymmetric unit. After initial refinement using REFMAC [192], the electron density was observed for D44 in the Fo-Fc difference Fourier map at 3 σ cut-off. Further cycles of map fitting

using the program COOT [193] followed by refinement resulted in the final structure with good geometry and stereochemistry. A few missing residues were observed at the terminal ends of the protein. The program MOLPROBITY [194] showed none of the residues outside the Ramachandran plot [195]. The data collection and refinement statistics are given in Appendices (iii).

Similarly, PvFKBP35 protein expression and purification was carried out as described previously [129] and was used for crystallization at a concentration of 15 mg/ml. The ligand D5 was incubated overnight with the protein at a molar ratio of 1:1.5. This protein-ligand complex was screened using an ammonium sulphate-buffer screen from Hampton Research. Needle shaped clusters appeared in 3.0 M ammonium sulphate and 0.1 M bicine, pH 9.0. Then after trying the additive screen from Hampton Research bigger crystals appeared in the presence of 30 mM Glycl-Glycl-Glycine as additive. A similar protocol was also adopted for the PfFKBP35-D5 complex, but the crystals could not be improved as they remained as thin needles. The PvFKBP35-D5 crystals were cryo-protected with 25 % v/v glycerol added to their corresponding mother liquors and flash-frozen at 100 K during data collection. Data up to 1.72 Å were collected from a single crystal of PvFKBP35-D5 using a Rigaku R-Axis IV image plate mounted on an in house Rigaku Micromax-007 HF X-ray generator.

The diffraction data were indexed, integrated and scaled using the program iMOSFLM [196]. The PfFKBP35-D5 crystal belonged to the body centered monoclinic space group I 2. The Mathews co-efficient indicated the presence of one molecule in the asymmetric unit located using the program PHASER [191] with a monomer unit of PvFKBP35-FK506 (PDB ID 3IHZ) as the search model. After initial refinement using REFMAC [192], the electron density was observed for D5 in the Fo-Fc difference Fourier map at 3 σ cut-off. Further cycles of map fitting using the program COOT [193]

followed by refinement gave a final structure with good geometry and stereochemistry. A few missing residues were observed at the terminal ends of the protein. The program MOLPROBITY [194] showed none of the residues outside the Ramachandran plot [195]. Appendices (iv).

II.5 PPIase assay

PPIase activity of the PfFKBP35 domain in presence and absence of inhibitors was measured by protease coupled assay method described by Fischer *et al.,* [5]. Succ-Ala-Leu-Pro-Phe-*p*nitroaniline was used as substrate (Peptide Institute, Osaka, Japan) for measuring the enzymatic activity. All the reagents were pre-equilibrated at 0º C. The final reaction mixture contained PfFKBP35 (100 nM), compounds (1 nM-1 µM) incubated for an appropriate period of time (10 min) at 4º C, substrate - succinyl-Ala-Leu-Pro-Phe-p-nitroaniline (100 µM), bovine α-chymotrypsin (300 µg) (sigma aldrich) in a assay buffer [50 mM HEPES, 100 mM NaCl, pH 8.0] The reaction was initiated with the simultaneous addition of substrate and α-chymotrypsin and subsequent cleavage of and release of chromophore (pNa) from *trans* form of substrate by α-chymotrypsin. Increase in absorbance as a consequence of isomerization of Leu-Pro bond and release of pNA by α-chymotrypsin was measured at 390 nM. IC50 values of PPIase activity were determined from the respective dose-response curves using GraphPad Prism Software [197]. All reactions were done in duplicate and results were corrected by subtraction of the corresponding values from a no-enzyme reaction.

II.6 Calcineurin Assay

Calcineurin assay was carried out using human calcineurin (CaN) as described [198] with some modifications as follows. Reactions (50 ml) contained 50 mM Tris-Cl (pH

7.5), 100 mM NaCl, 6 mM Mg^{2+}-acetate, 0.5 mM $CaCl_2$, 0.1 mg/ml bovine serum albumin (BSA), 0.5 mM DTT, 0.025% NP- 40, 40 nM *human* CaN, 12.5 μM *human* CaM, 5 μM *h*FKBP12, 5 μM PfFKBP35 (all the four proteins prepared in-house), 10 μM drugs (FK506, D5 and D44), 0.5 μM RII phosphopeptide (a specific CN substrate). Reaction mixtures were incubated for 10-30 min at 30 ºC prior to the addition of the substrate. Reactions were then initiated by the addition of the substrate peptide, and dephosphorylation was allowed to proceed at 30 ºC. The liberated inorganic phosphate was measured by a Malachite Green color assay using the Calbiochem kit (San Diego, CA). All reactions were followed with time to ensure linearity and results were corrected by subtraction of the corresponding values from a no-enzyme reaction.

II.7 Time Course Assay of Parasite Growth Inhibition

P. falciparum parasites (5% parasitemia, 2% hematocrit) were incubated at the mid ring stage (~6-10 hours post-invasion, hpi) with 250 nM of FK506 or 1 μM of D44 inhibitor (corresponding to concentrations achieving maximal inhibition ($2xIC_{90}$) determined by standard growth inhibition assay or in absence of treatment (control). Parasites maturation was monitored every 8h for an entire intraerythrocytic developmental cycle (IDC) by giemsa staining of fixed smears for comparison of parasitemia and parasite morphology at each time point.

II.8 Parasite Stage-Specific Growth Inhibition Assays

Highly synchronized ring, trophozoite and schizont stages of 3D7 *P. falciparum* culture were separately treated with FK506 (250 μM), D44 (1 μM), 500 nM of SRA or SRA-1 and SRA-2 without inhibitor (control). Parasite maturation was monitored by

microscopic examination of giemsa–stained smears at 4, 8 and 16 h after addition of the inhibitor.

II.9 2D HSQC Chemical Shift Perturbation analysis

All NMR spectra were obtained at 298 K using a Bruker 700-MHz spectrometer equipped with a 1H/13C/15N cryoprobe and z-axis gradients. Data were acquired and processed using Bruker TopSpin 2.1, NMRPipe [199], NMRDraw and the Sparky [200] software packages. 0.1 mM ^{15}N- labeled protein sample in 20 mM sodium phosphate, pH 6.5 was used and chemical shift perturbations were analyzed upon addition of increasing concentrations of ligand D44.

III. Results & Discussion

Part I – PfFKBP35

III.I PfFKBP35

III.I.1 *De novo* approach: Ludi & receptor based pharmacophore modeling

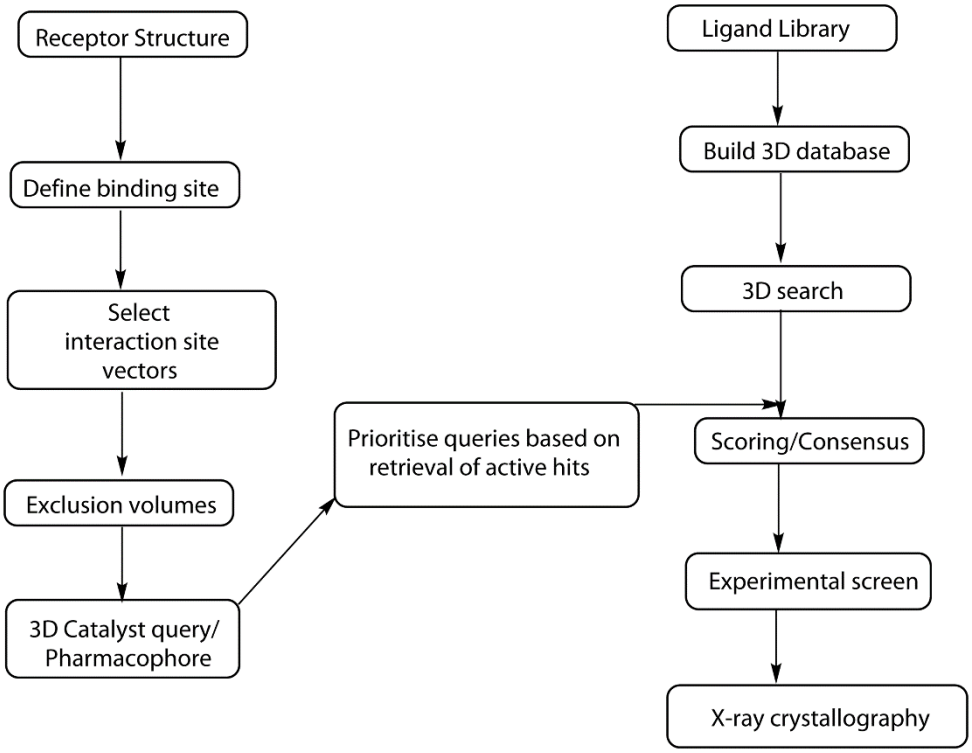

Figure 15: Scheme of work flow that led to identification of novel chemical entities. Molecular modeling methods have identified potential hits and these hits are validated by experimental screens and their binding mode by X-ray crystallography.

Virtual screening requires two important inputs 1) a 3D database and 2) a model or query representing the protein pharmacophore, which can search the 3D-database and return complementary hits in the form of library in SD format (Fig. 15). The first step is to build a structure (receptor) based pharmacophore that encodes the active site information and then to screen the 3D database and obtain a focused library complementary to the protein active site. Together with predictive consensus scoring and in vitro experimental screens can identify leads that are further are validated by X-ray crystallography.

Previously, our lab has solved the crystal structure of *Plasmodium FKBP35* bound to FK506, which revealed a similar binding mode to that of human FKBP12. Further, most of the mutagenic studies on FKBP12 [9, 12, 201-203] have shown that Trp59, Asp37 and His87 occurring at the active site of FKBP12 are very critical for FK506 binding and inhibition of PPIase activity.

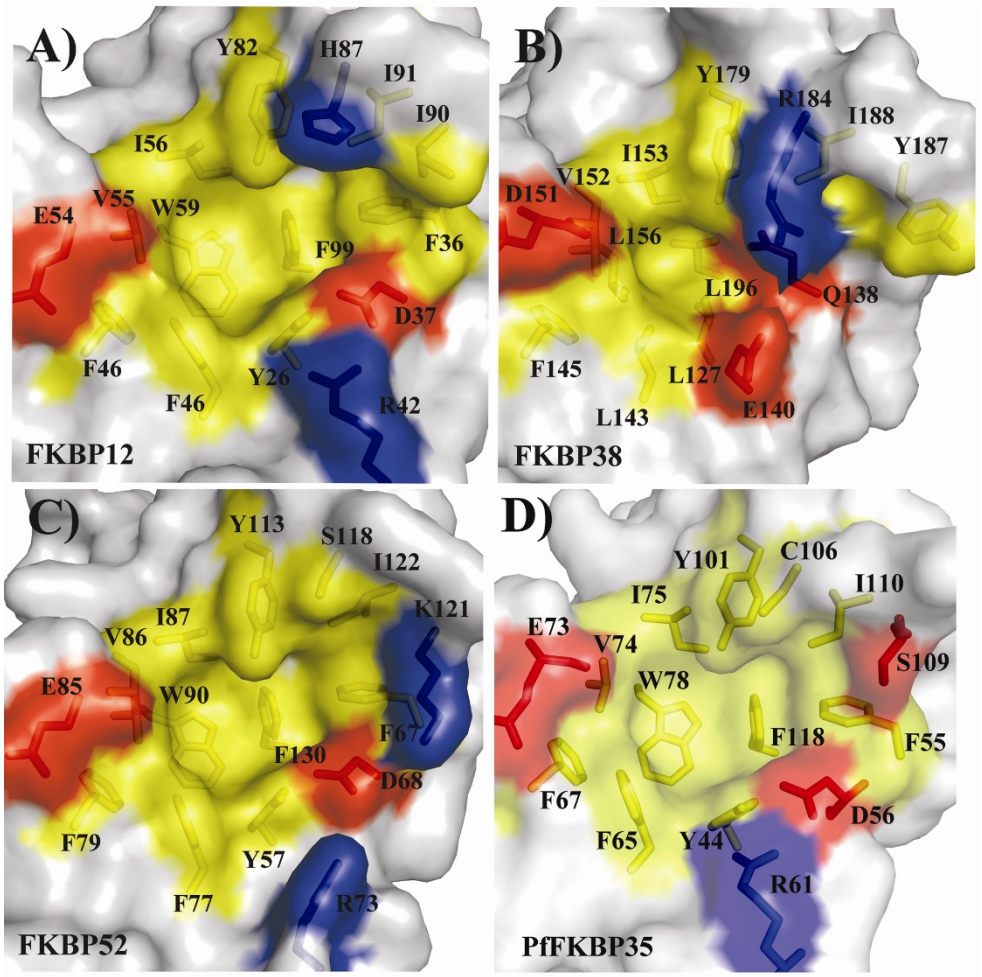

Figure 16: Surface representation of active sites highlights the subtle difference among the FKBP family members. The yellow region highlights the conserved hydrophobic residues. Red colored highlights the conserved negatively charged Glu and Asp residues, of which aspartate residue is important for catalytic activity. Blue colored residues highlight the difference among the FKBP family members. Mainly, residues such as H87, R42, D37 (FKBP12) are varied in FKBP38 and most of the conserved hydrophobic residues are changed to leucine, accounting for the non-canonical nature of FKBP38.

Though PfFKBP35 is well conserved at the active site, it shows subtle variations in possessing Cys106 and Ser109 in place of His87 and Ile90 in human FKBP12 (Ser118 and Lys121 in human FKBP51, -52) at corresponding positions occurring in the β5-β6 loop (Fig. 16) [131]. Careful observation of the surface views of the human FKBP homologs and Plasmodium FKBP35 clearly highlights that the cavity surrounding these variations (Fig. 16) (highlighted in blue color) at the β5-β6 loop can effectively be targeted apart from the canonical binding site.

As mentioned in materials and methods, the Ludi interaction model [142, 154, 179] gives interaction vector site points from the defined active site region with which the ligand can form favorable interactions that could be vital for activity. The vector sites generated at the active site are hierarchically clustered according to the feature types using a RMS distance of 0.7 Å. The user should specify the number of features to be included during development of a structure-based pharmacophore. Based on the number of hydrogen bond acceptor (HBA), hydrogen donor (HBD) and hydrophobic (Hy) features specified, the program generates different possible pharmacophore(s) at the active site. For PfFKBP35, initially we included one feature group for HBA, HBD and hydrophobic feature in the pharmacophore development. Thus, the program generated 35 different possible pharmacophore queries targeting different residues. Upon screening the control ligand – FK506 only a few pharmacophores were able to return the control ligand.

Alternatively, I have attempted to build a receptor based pharmacophore by targeting specific residues. For convenience, I have considered the active site as two regions – site S1 and site S2. Site S1 consisted of residues such as Trp78, Ile 75 and Tyr44 which form the platform for pipecolinyl binding and the site S2 comprises of Asp56,

Tyr101, Cys106, Phe55 and Ile110. This region is also important for FK506 binding as the C10-hydroxyl group on FK506 forms bonding with Asp56 and the C13 methyl group gets positioned into the hydrophobic pocket formed of Phe55, and the Ile110 residues. Therefore, the receptor based pharmacophore model [154] was generated in accordance with these important active site residues Tyr44, Ile75 and Trp78 from the canonical site 1 and Asp56, Phe55, Tyr101 Cys106 and Ser109 from the site 2 (Fig. 17).

A three feature pharmacophore model was evolved with two hydrophobic features targeting Tyr44 and Trp78; an HBA targeting Ile75 at site 1 (Fig. 17B). Another three feature model consisted of a hydrophobic feature extending into another hydrophobic pocket composed of Phe65, Ile110, Ser109, Cys106 and a HBA at Tyr101 and a HBD at Asp56. These two models were merged to produce a six feature protein pharmacophore model. A size exclusion model was added for the active site residues (Fig. 17). Addition of size exclusion volume filters non-specific hits and serves as active site shape type filter and excludes hits that could bump with these protein atoms. In the final model, a hydrophobic group from site 1 is manually removed and a five feature model is used to screen the Chemdiv database, biasing the search towards the site 2 (Fig. 17 D). A control data set of FK506 served to validate this pharmacophore and on screening retrieved FK506. Thus the validated receptor based pharmacophore is used for screening the processed Chemdiv virtual library.

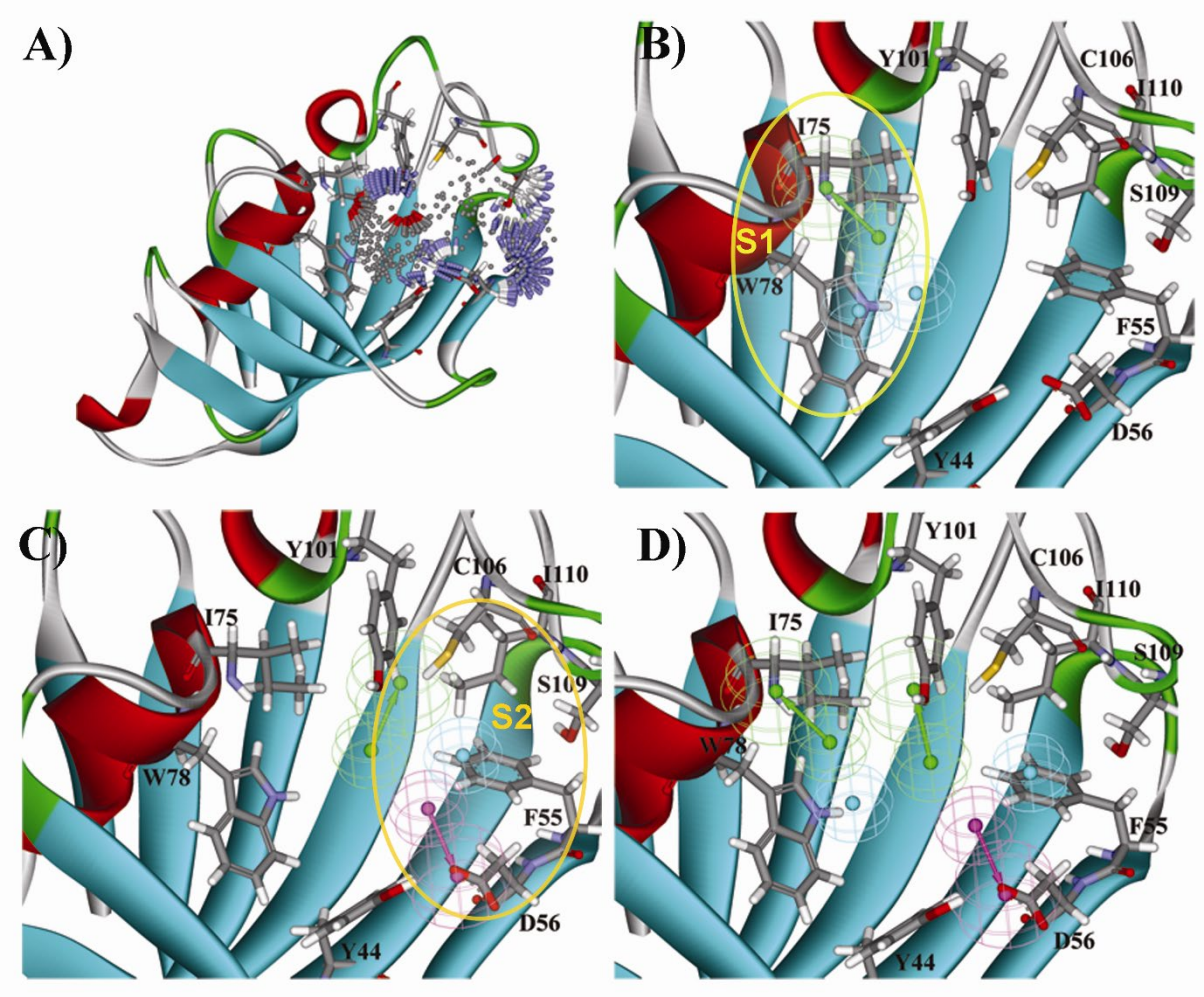

Figure 17: Ludi interaction model of the PfFKBP35 active site. A) Ludi program identifies discrete acceptor (red rods (OH)), donor (purple rods (NH) and hydrophobic (black spheres) vector sites with which a ligand can form efficient interaction with the protein; B& C) Hierarchical clustering of acceptor, donor, and hydrophobic vector site points enables one to select features targeting select residues as depicted at site S1 (B) and at site S2 (C). D) Five features were selected targeting specific residues such as F55, D56, I75, W78, and Y101 residues that were included in the structure or receptor based pharmacophore.

III.I.1.1 Virtual screening

Pharmacophore screening with this five feature pharmacophore model returned a ~18000 molecule library (Fig 18 A, B, C, D) that could potentially bind to the defined active site residues. This library was further refined by applying the ADMET filters and

ligands with good or optimum solubility, distribution and hepatic toxicity parameters and this reduced the library size to ~3000. The GOLD molecular program was employed to dock these molecules by using the default scoring function to predict binding pose and score its affinity with the protein.

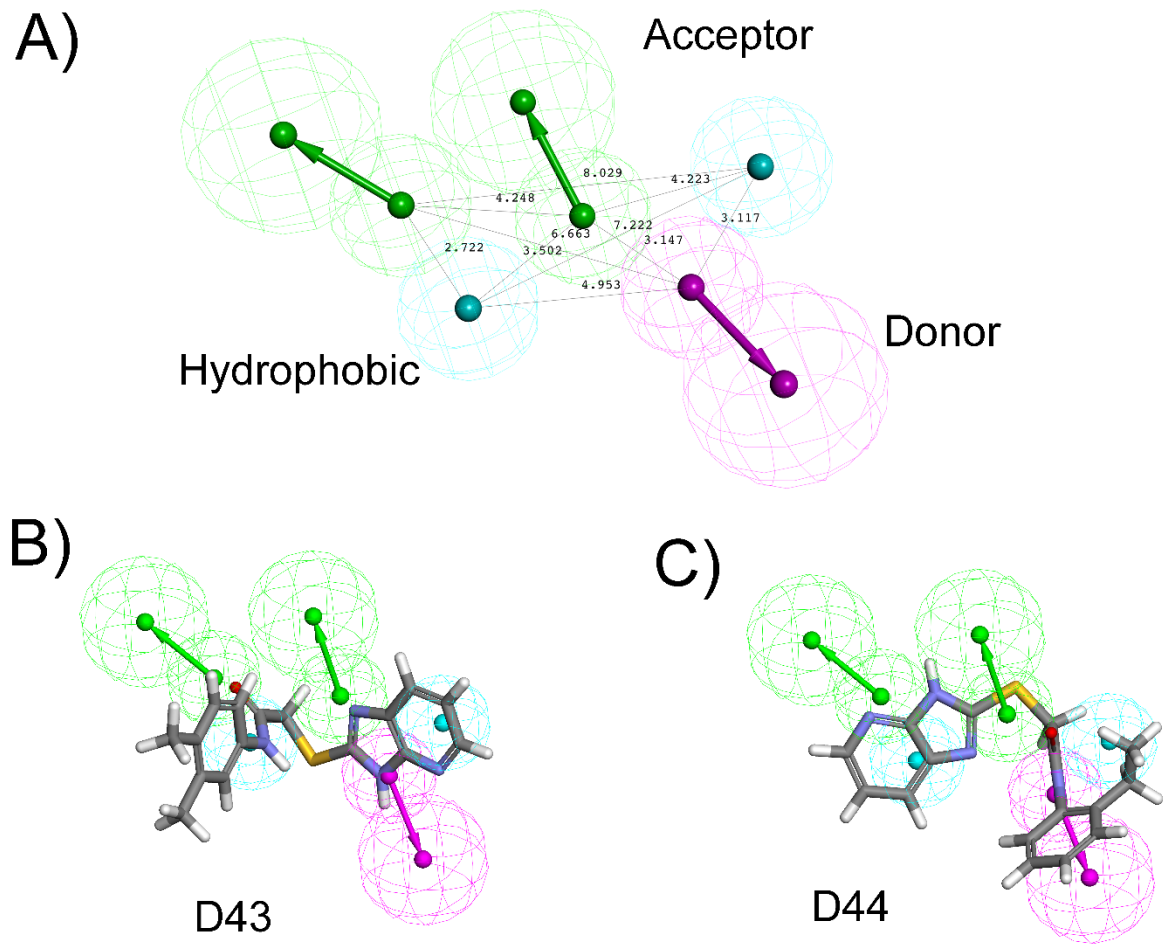

Figure 18: Structure based pharmacophore model. A) Structure based pharmacophore model with interfeature distance between the 5 pharmacophore features, B& C) Alignment with one of the best fitting hit D43 and D44

Rescoring prioritizes the best binding fragments from a huge sample of predicted binders. The dock solutions (Fig. 19A) from the GOLD search engine are further rescored with the glide scoring function (do not dock option) and with other scoring

functions - different versions of Ligscore, PLP1, PLP2, PMF, JAIN and Ludi scoring functions available with the Accelrys suite.

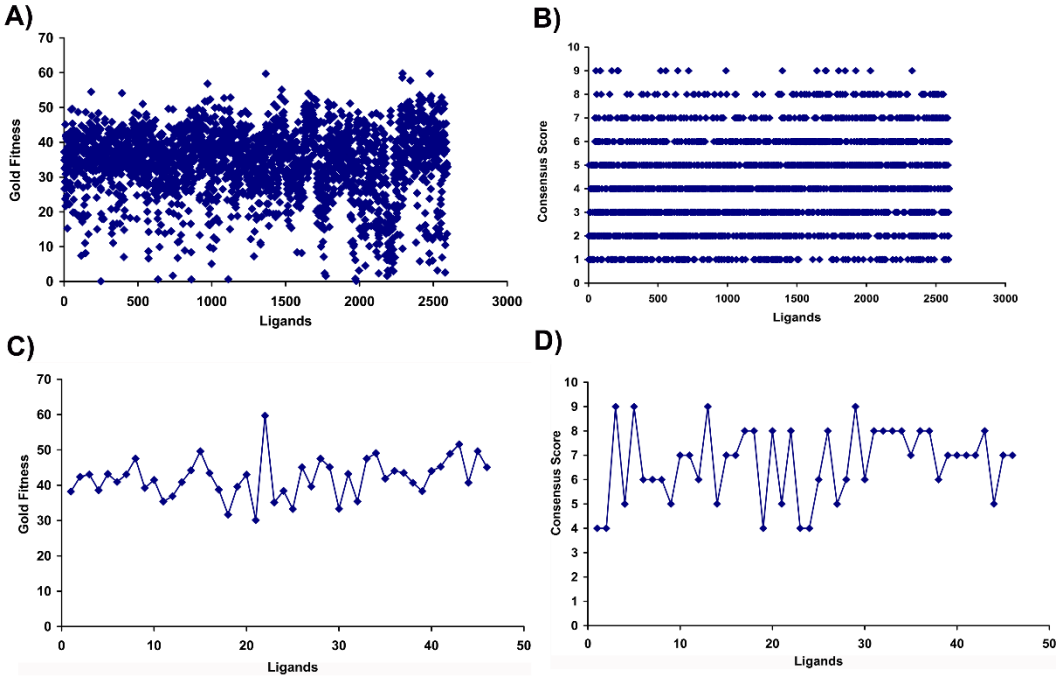

Figure 19: Scatter plots of molecular docking results using GOLD scoring & consensus scoring. A) Scatter plot of GOLD docking scores for 2620 molecules. B) Consensus scoring results showing the number of ligands which are in agreement with different scoring functions employed in this study. C, D) represents the scatter plots of GOLD scoring and consensus scoring of 46 molecules respectively chosen for experimental study.

Consensus scoring highlights the ligands that are in agreement with most of the scoring functions (Fig. 19B). Top ranking ligands with each of the scoring functions are identifying by evolving a consensus and by providing the consensus score indicating as to how many scoring function(s) agree that a particular ligand is the top ranking one and avoids any bias that may be involved with the use of a single scoring function during selection of hits. Among the employed of GOLD, LigScore, PLP1, PLP2, PMF, JAIN, Ludi, GLIDE scoring functions ligands which are in agreement with more than three scoring are further considered for visual analysis. After careful

interaction pattern analysis, ligands with favorable interactions are selected from this pool. (Fig. 19 C, D).

For example, as shown in Fig. 20A, the bulky bicyclic ring of D3 occupies the site S1 and the side chain “thio-amide” interacts with Ser 109 whereas the azide linker interacts with Asp56. Similarly in D13, the bicyclic ring occupies the S1 site whereas the carboxyl side chain interacts with Asp56 (Fig. 20B). In D20, benzothiophene occupies the site S1 while the piperazine ring extends into site S2. The 3-carboxy-methyl substitution on benzothiophene interacts with Asp56 (Fig. 20C). In the D25 and D35 molecules (Fig. 20D, E), the interactions not only extend into site S2 but also form good hydrophobic contacts with Trp78 and hydrogen bonding interactions Glu77 and Tyr101 at site 1. In D40, the pipercoline moiety sits into site S1 and the purine ring nicely projects into site 2 forming hydrogen bonding interactions with Asp56 and is able to have close van der Waals contacts with Cys106 and Ser109 (Fig. 20E, F). These hydrogen bonding interactions at Asp56, Tyr101 and van der Waals contacts with Cys106 and Phe55 were taken as a basis for selection of 46 molecules that showed better binding computationally (Appendix (i)) for further experimental studies.

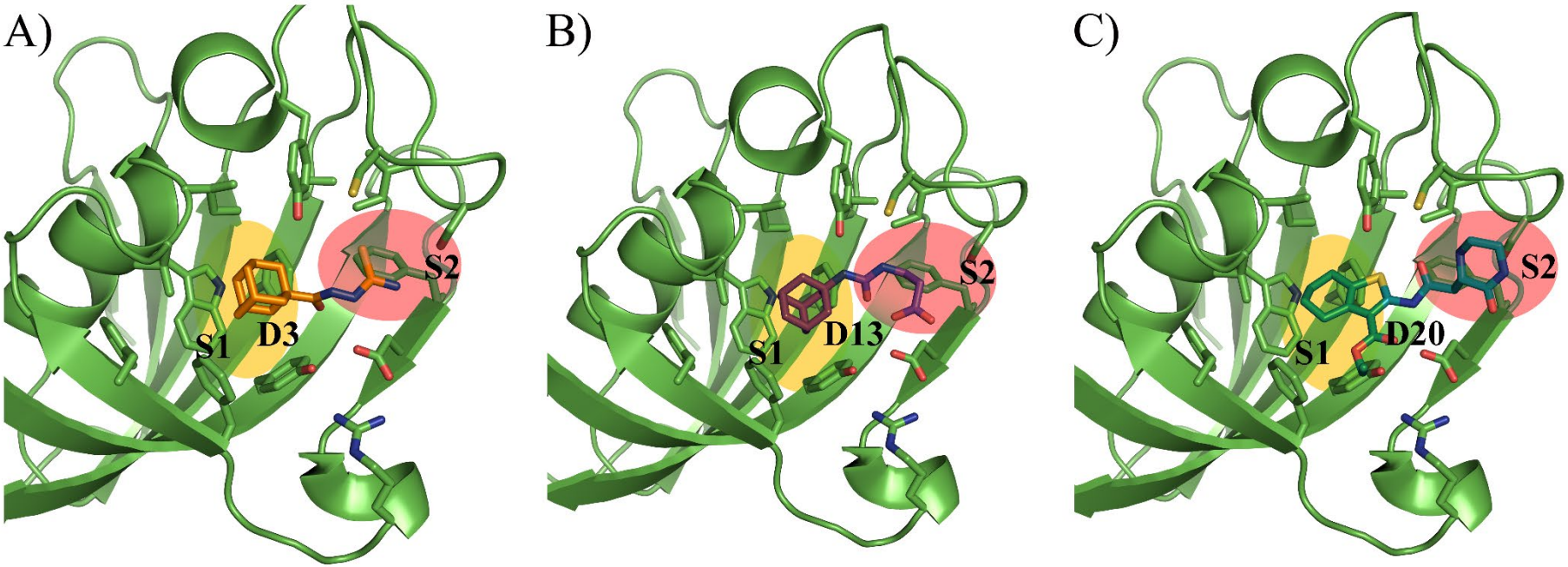

Figure 20:Predictive binding pose for the best hits selected for experimental studies from virtual screening protocols. A & B) Predictive binding poses of D3 & D13 with a bicyclic adamantyl ring sitting at the base of FKBP binding platform (S1) highlighted in yellow and targeted site (S2) highlighted in light pink color. B & C) D20 bearing an benzothiophene moiety sitting at the S1 pocket while the piperazine side chain is extending into the S2 pocket. D) Predictive binding pose of D25 which anchors the FKBP binding platform (S1) highlighted in yellow and targeted site (S2) highlighted in light pink color. E & F) Other hits D35 & D40 bearing an pipecolic moiety sit nicely into the S1 pocket and the side chain (pyridinyl (D35) and purinyl (D40) rings extending into the S2 pocket.

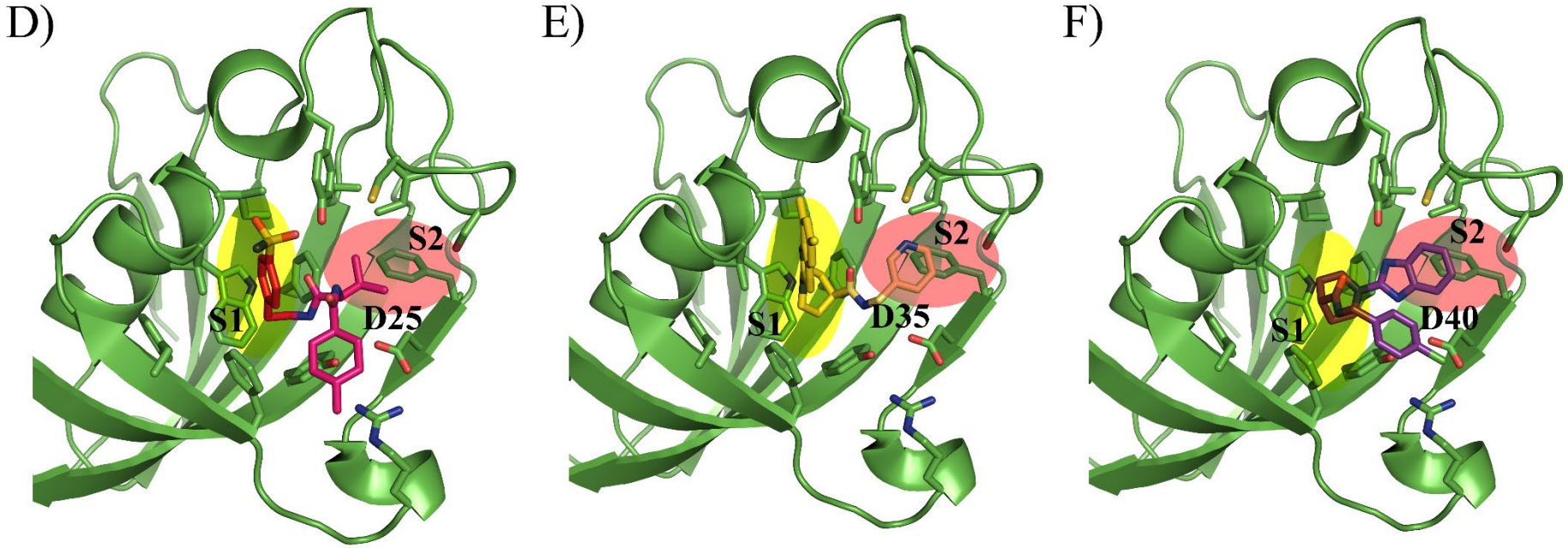
D)
S2
S1
D25
E)
S2
S1
D35
F)
S2
S1
D40

In summary, as shown in Figure 21, our molecular modeling efforts in designing the 3D-libraries, structure based pharmacophore modeling, ADMET prediction, virtual screening, scoring and consensus themes have successfully identified a pool of ligands that are computationally predicted to bind selectively to *Plasmodium* FKBPs.

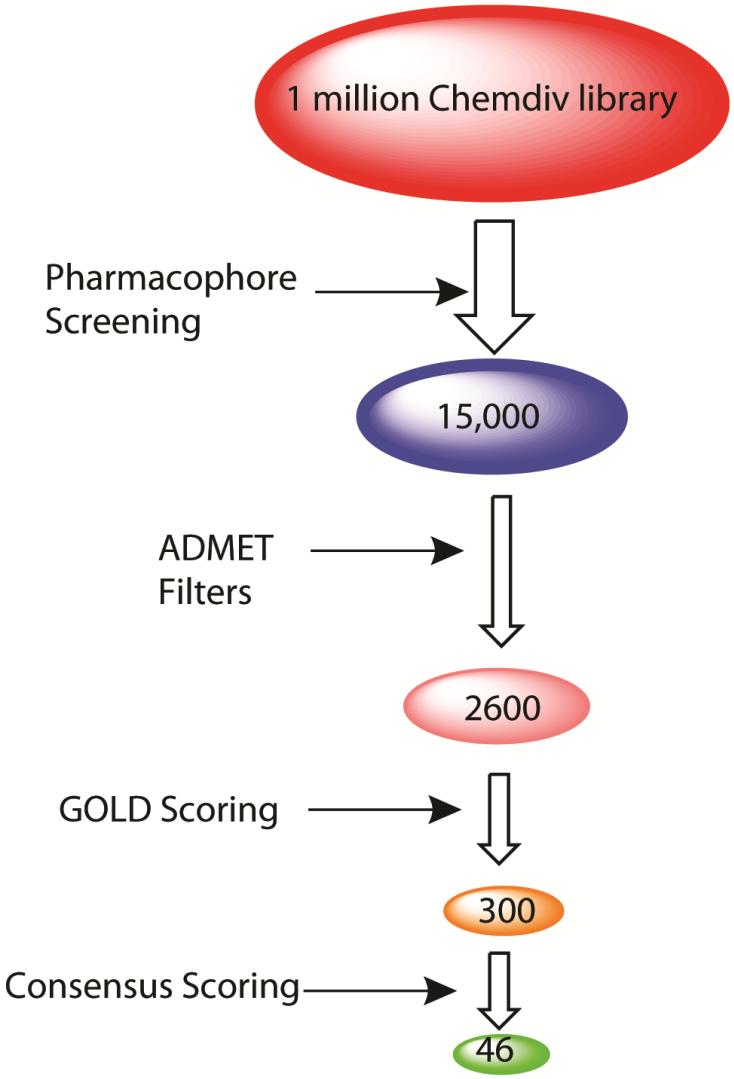

Figure 21: Schematic diagram showing the steps in identification of hits from structure based drug design. Structure based pharmacophore screening retrieves hits that are complementary to the protein active site and provides a focused library. This focused library is further refined by filters such as ADMET, GOLD scoring and consensus scoring to 'cherry pick' 46 ligands for experimental assays.

III.I.2 Biochemical & Biophysical Characterization of ligands that modulate the PfFKBP35 enzymatic activity

III.I.2.1 Expression and purification of *P.falciparum* FKBP35

P. falciparum FKBP35 (PfFKBP35) protein was purified as described in materials & methods. The purified protein obtained from Ni^{+2}-NTA affinity purification was analyzed on a SDS 12% polyacrylamide gel (Fig. 22A). The protein obtained was further purified to a near homogeneity by using gel filtration chromatography (Fig. 22B). The purified proteins were stable after storage for one month at 4 °C.

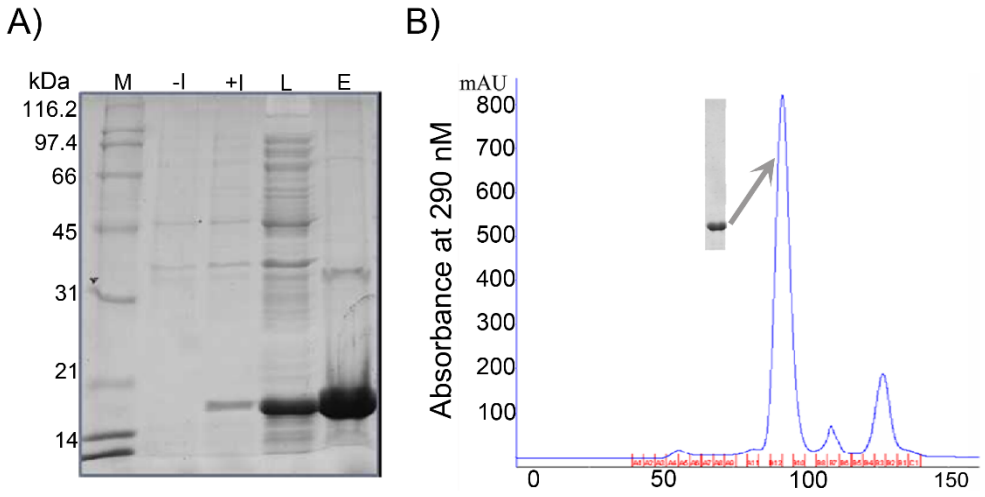

Figure 22: Purification of PfFKBP35 (FKBD domain alone). PfFKBP35 was expressed and induced as described in Material and methods. A) The over expressed protein was first purified by Ni^{+2}-NTA affinity purification. Samples of PfFKBP35 from various steps (Before induction (-I), after induction (+I), load (L), eluate (E); M-Protein marker) were analyzed by SDS 12% PAGE. B) Gel filtration chromatogram of PfFKBP35 and eluted sample (first peak) analyzed by SDS 12% PAGE. Shown in inset is the purified protein obtained from gel filtration, analyzed on SDS 12% PAGE. (Red marked lines in panel B indicate the collection fractions of eluate).

III.I.2 2 PPIase & Calcineurin Phosphatase activity

PPIase assay was employed to screen the compounds that were purchased after computational design. This assay provided a convenient way to assess whether the compounds are able to inhibit the enzymatic isomerisation of the substrate Succ-ALPF-pNA. The enzyme isomerises the *cis* form of the substrate to *trans* form. The *trans* form is specifically cleaved by the a-chymostrypsin that is coupled during the initiation of the reaction and releases p-nitroaniline (pNA). The amount of pNA released is proportional to the enzymatic activity and is measured at 390 nM and provides the read out of amount of enzymatic isomerisation of substrate (Fig. 23).

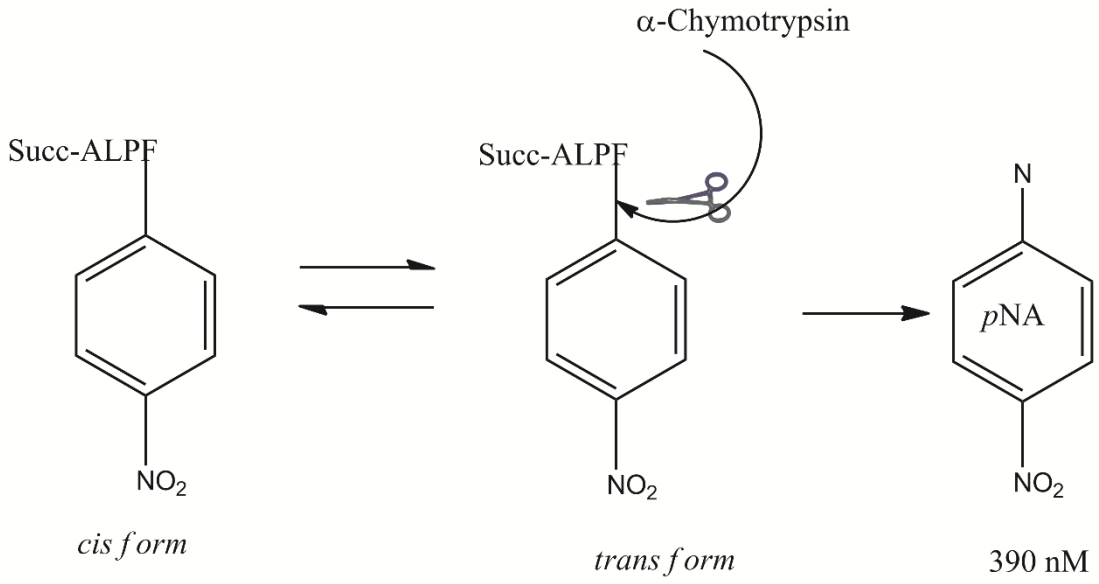

Figure 23: PPIase isomerizes the proline residue in substrate ALPF-pNA to its *trans* form. The *trans* form of the substrate is specifically cleaved by α-chymotrypsin to release pNA from the *trans*-substrate. The amount of pNA released is proportional to the isomerase activity and is read at 390 nM.

P. falciparum FKBP enzymatic activity was tested both in the presence and absence of the compounds by using the *in vitro* PPIase assay. The effect of the compounds (10 μM) was monitored by their ability to inhibit the *cis* - *trans* isomerization of the substrate

Succ-ALPF-pNA and was calculated by comparison to untreated control. The substrate hydrolysis curve of PfFKBP35 in presence or absence of inhibitors was as shown in Fig. 24. In contrast to substrate hydrolysis by the enzyme, the presence of a potent inhibitor such as FK506 (IC50 100 nM) significantly inhibited the substrate hydrolysis. No enzyme (background) reaction was subtracted from the each of the enzyme (catalyzed) and inhibitor titrations. The untreated and the FK506 inhibition responses were used as controls.

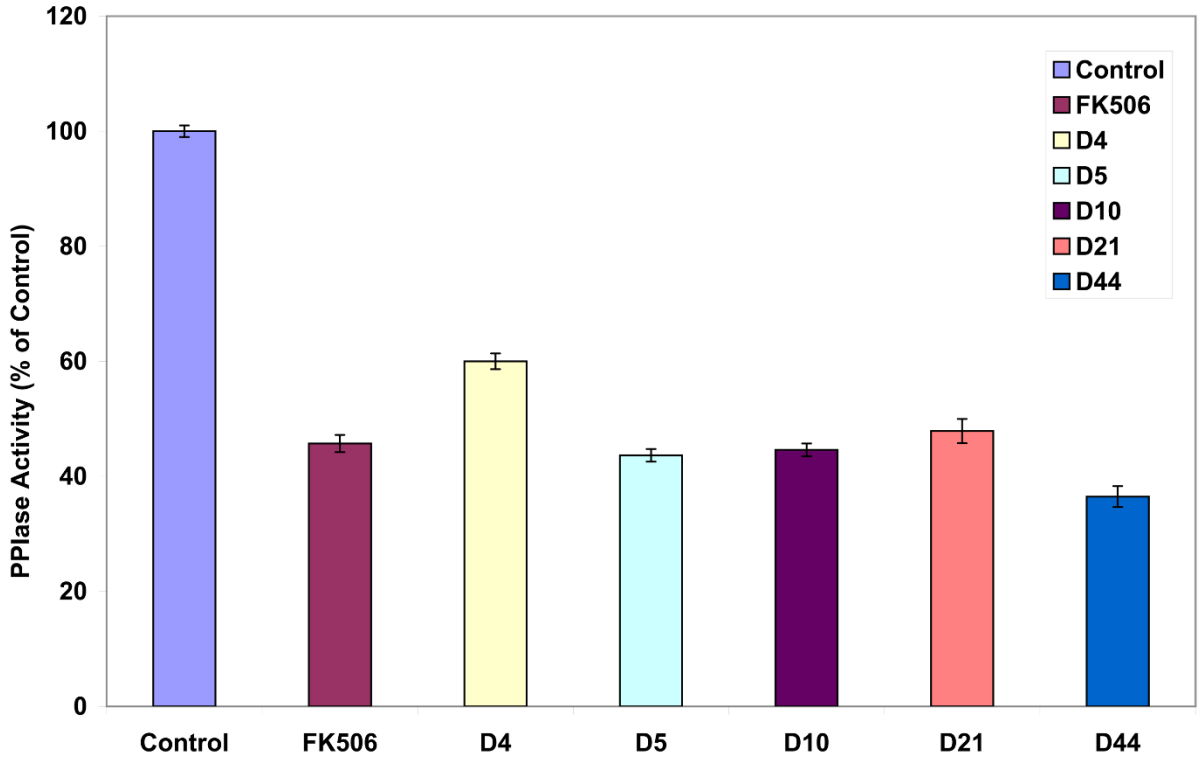

Figure 24: Effect of hit compounds on PfFKBP35 PPIase activity. Histogram depicts the effect of lead compounds (10 µM) & FK506 (100 nM) on PPIase activity of PfFKBP35 (100nM). Percent PPIase activity in presence of compound was calculated as percent of control (without inhibitor). Error bars represent the standard deviation from two independent titrations

The inhibitory effect of novel ligands (10 µM) was determined by the amount of PPIase activity as percent of control. In this way, 15 compounds were identified having notable inhibitory activity at 10 µM concentration. Among these compounds 4, 5, 10, 15, 21,

44, and 46 were found to be the most potent ones (Fig. 24). Dose dependent inhibitory activity of the most active compound D44 was determined as percent inhibition of PPIase activity. D44 significantly inhibited the enzymatic activity of both the P. falciparum and P. vivax FKBP35 with IC_{50} of 132 nM (Fig. 25A) & 127 nM respectively. As anticipated in our design of these ligands, D44 was unable to inhibit the PPIase activity of either FKBP12 or FKBP52 even at high concentrations of 10 μM (Fig. 25C). Further, our in vitro calcineurin assay results demonstrate that unlike HsFKBP12-FK506 complex, D44 complex with HsFKBP12 do not inhibit the calcineurin phosphatase activity and do not possess the ability to interfere with immune response system (Fig. 25B).

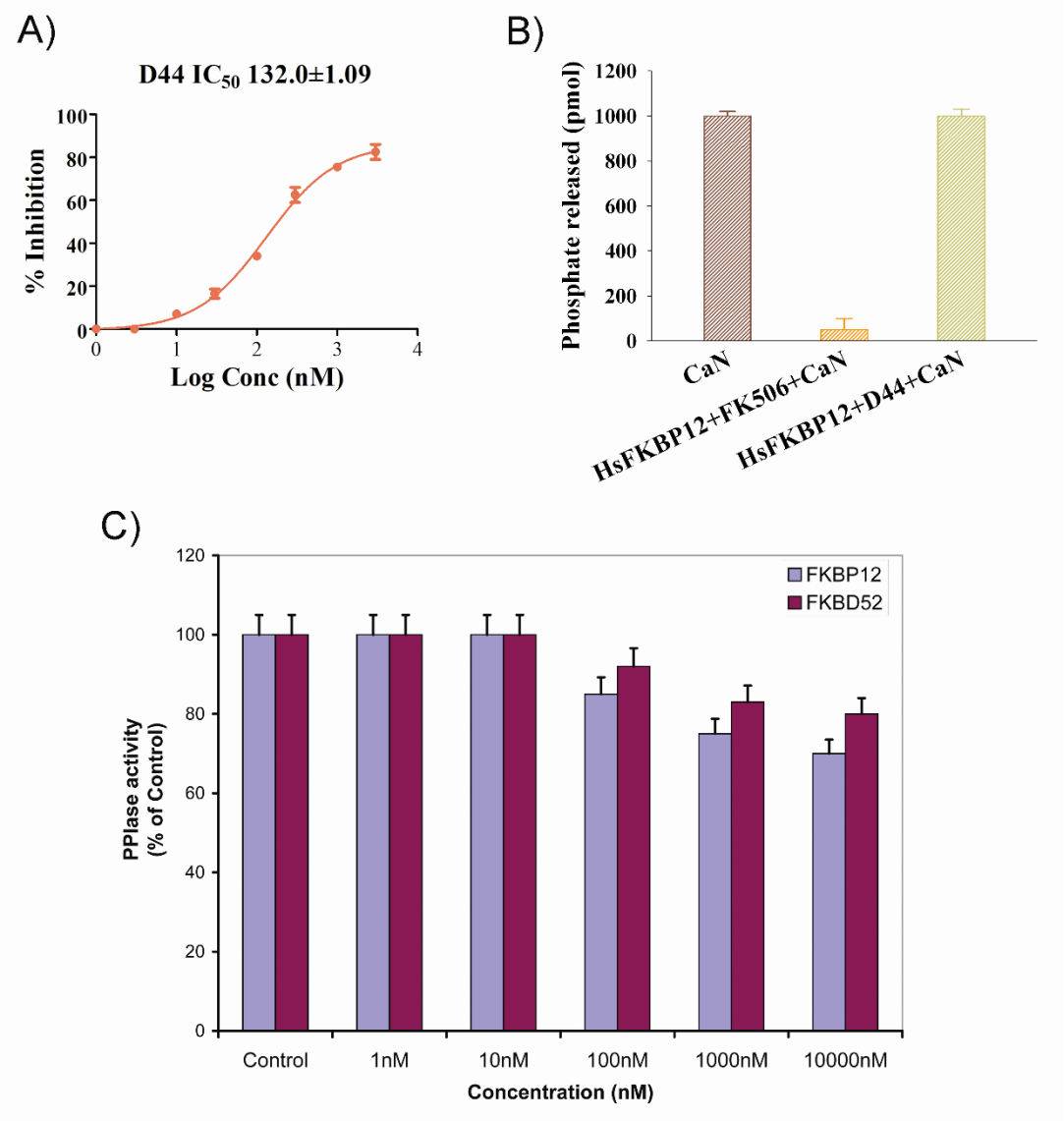

Figure 25: Effect of D44 on PPIase activity and calcineurin phosphatase activity.

A). Percent inhibition of P. falciparum (100 nM) and P. vivax (100 nM) PPIase activity in presence of compound D44 (1 nM-1 µM) was estimated by fitting the data with standard dose response inhibition model using graphpad prism software. Error bars represent the SEM values obtained from two independent titrations. B). Calcineurin phosphatase assay measures the amount of phosphate released from RII phospho-substrate upon addition of malachite green. FK506 (10 µM)-FKBP12 (5 µM) complex of human inhibit the calcineurin phosphatase (40 nM) activity whereas the compound D44 (10 µM) did not inhibit the calcineurin phosphatase activity. Error bars represent the standard deviation from two independent duplicate reactions. C) Histogram showing the lack of inhibition of enzymatic activity of human FKBP12 and FKBD domain of FKBP52 by D44

III.I.2.3 2D HSQC Chemical Shift Perturbation analysis

Our 2D HSQC NMR experiments revealed that most of the active site residues including W78, F65, D56 and F118 show chemical shift perturbation upon titrating with D44 (Fig. 26) indicating that the D44 binds to FKBP35.

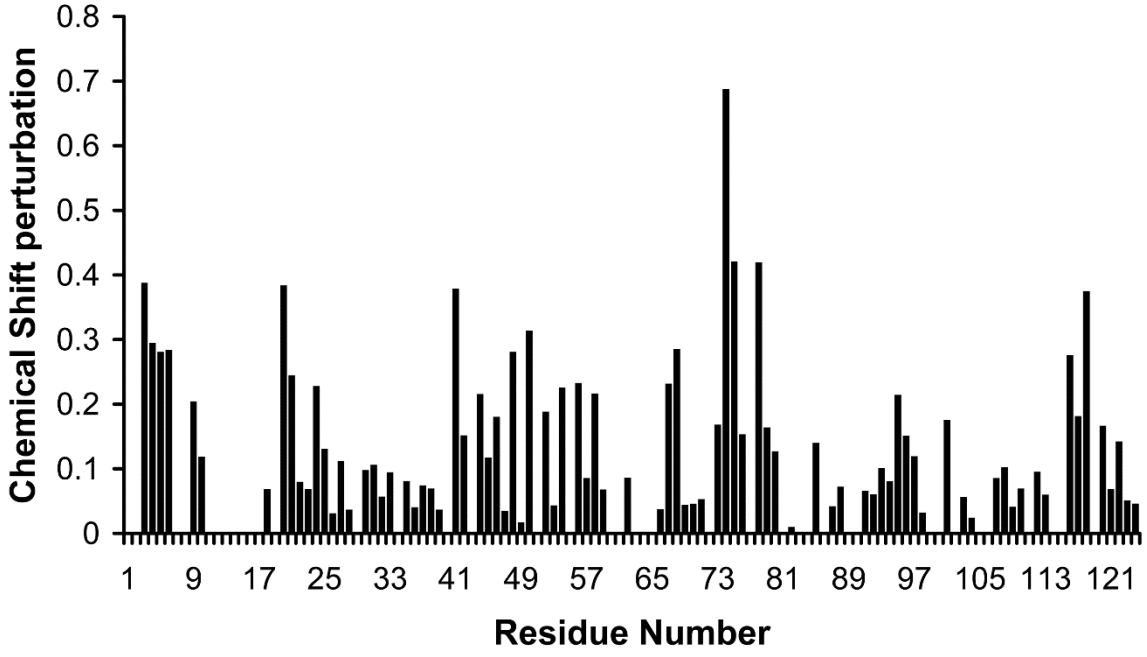

Figure 26: NMR chemical shift perturbation analysis of PfFKBP35 upon titration with D44 in 1:2 molar ratio reveals that the ligand D44 mainly interacts with 40-loop and 80-loop residues and more prominently with I75 residue.

III.I.2.4 Effect of D44 on Plasmodium IDC

To study the effect of our lead compounds, our lab has collaborated with Prof. Peter Preiser's lab at Nanyang Technological University and Dr. Makhtar Niang was helping us to evaluate the efficacy of the lead compounds. The effects of D44 treatment on the *in vitro P. falciparum* intraerythrocytic developmental cycle (IDC) were examined by growth inhibition assay.

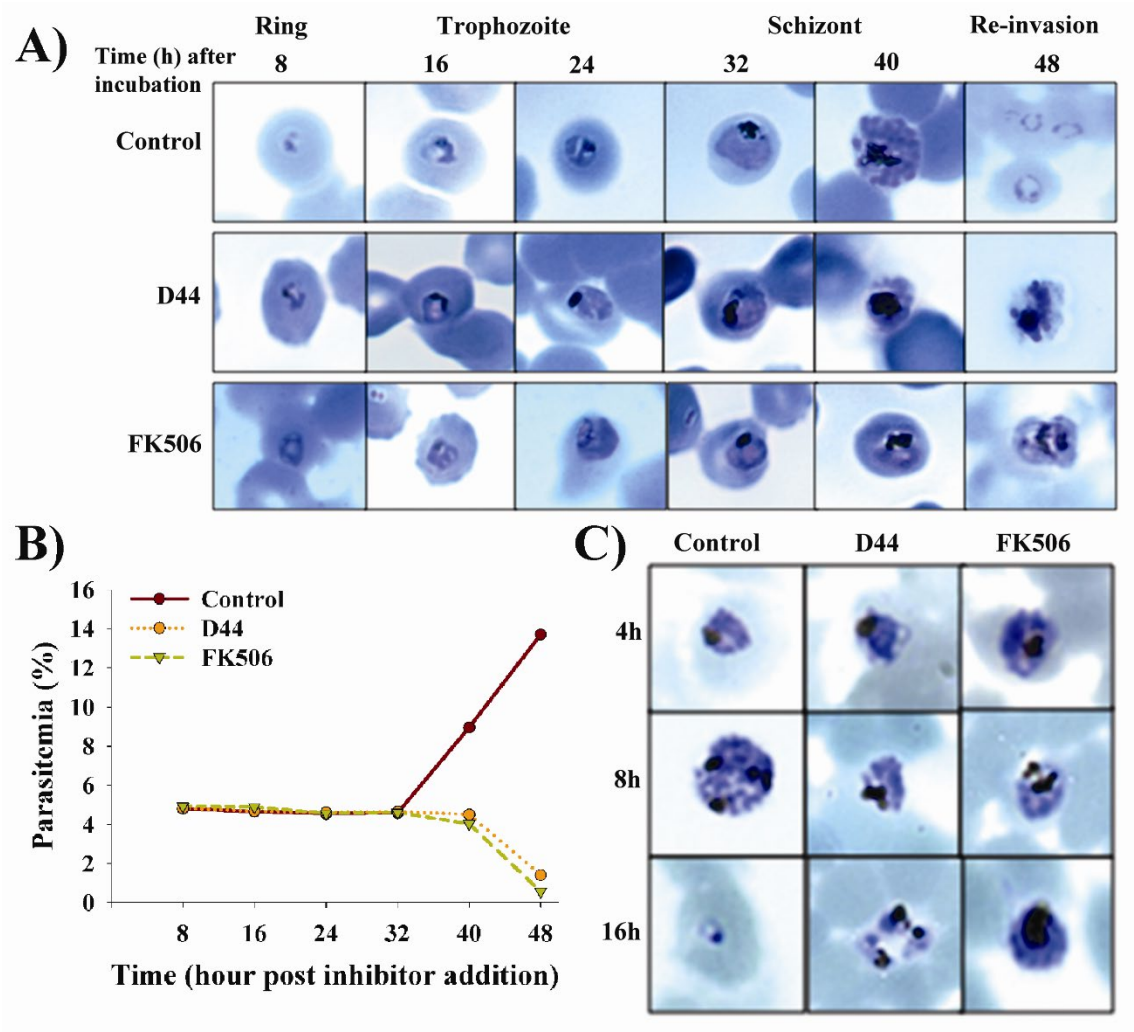

Figure 27: Effects of D44 on *Plasmodium falciparum* IDC

(A) Effects of FK506 and D44 inhibitors on *P. falciparum* IDC (synchronized ring stage) was monitored every 8h upon addition of inhibitor and were compared to untreated control parasites. (B) Effect of D44 (1 µM) and FK506 (250 nM) on parasitemia (%) was monitored every 8 h time point upon addition of inhibitors. (C) Effects of FK506 and D44 on schizont stage development. Parasite (schizont) morphology was monitored by Giemsa stain at 4, 8 and 16 h after addition of inhibitor. Illustrations of schizont morphology at 4, 8 and 16h after addition of inhibitor were as shown. During the first 4 h, no significant morphological differences were observed between the treated and control parasites. During the subsequent development, the control parasites progress to the next generation (formation of mature schizont and ring) while the treated cells remain arrested at the late schizont stage. The results show that D44 mainly interferes with schizont stage development.

Synchronized ring stage parasite culture prepared as described in materials and methods was added with the D44 and the morphological changes were observed by Giemsa-stained thin smear slides under the microscope at 8h time point interval and were compared to FK506 treated and untreated controls.

Dose response assays of D44 estimated the IC_{50} as 300 nM (data not shown). D44 and FK506 were used at 1 µM and 250 nM respectively corresponding to ~ 2X IC_{90} which has been determined by standard growth inhibition assays. Both parasitemia and parasite morphology was monitored on giemsa-stained smears. From the ring to early schizont maturation, there was no change in parasitemia or parasite morphology (Fig. 27A, B) between the D44, FK506-treated and the untreated control parasites. During subsequent development, the untreated control parasites successively matured into late schizont and ring stages (Fig. 27A) resulting in an increased parasitemia (Fig. 27B) whereas both D44 and FK506 treated parasites remained arrested at the schizont stage. This suggested that D44 could interfere with the schizont stage development similarly to FK506 [129].

To validate this finding, we closely monitored the maturation of early schizont stage parasites (~36-40 hours post invasion) treated with D44 and FK506 and in absence of treatment (control). During the first 4 hours, no significant morphological difference was observed between the treated and untreated parasites (Fig. 27C). However, during their subsequent development, the untreated control progressed to the next generations (formation of late schizont and ring stages) whereas both D44 and FK506 treated parasites remained arrested at the late schizont stage (Fig. 27C) confirming the findings that D44 directly interferes with the schizont stage maturation.

III.I.2.5 Crystallographic characterization of D44 in complex with Pf FKBP35

To gain better structural insights into the mode of action of D44, the crystal structures of PfFKBP35 and PvFKBP35 in complex with D44 (PD IDs: 3v37, 3v3A) were determined to a resolution of 2.75 Å and 1.73 Å respectively. The refined crystallographic structure revealed a topology consisting of seven β-stranded sheets and a short α-helix similar to the previous *Plasmodium* FKBP35-FK506 structures from P. *falciparum* (PDB ID 2VN1) [131] and P. *vivax* (PDB ID 3IHZ) [129]. The PfFKBP35-D44 complex consisted of three monomers in the asymmetric unit (Fig. 28A) with chains A and B forming a covalent dimer via an intermolecular disulphide bond between Cys106 from both the chains. Similarly the third monomer (chain C) also forms an identical dimer with the neighboring chain, which is generated by crystal packing. On the other hand, the PvFKBP35-D44 complex consisted of one monomer in the asymmetric unit (Fig. 28B) forming a dimer with the neighboring chain, generated by crystal packing, with the help of a disulphide bond through Cys105. The P. *falciparum* and P. *vivax* FKBP35 structures superposed well with an RMSD of 0.314 Å. The electron density for D44 (Fig. 28C) was traced unequivocally in the electron density difference map in the hydrophobic binding site. One ligand per monomer was observed sitting in the dimer interface facing each other separated by a distance of 3.6-4.2 Å.

Comparison with their corresponding apo forms (PDB ID 2OFN, 2KI3) determined by NMR [130, 204] indicates that the overall fold is similar with a backbone root-mean-square deviation (RMSD) of 2.28 Å and 1.37 Å for PfFKBP35 and PvFKBP35 respectively. Mainly, the three loops, which flank the binding site, namely β3 - β4, β4 - α1, and β5 - β6 undergo small structural changes with an increase of accessible surface area. In PfFKBP35, the psi angle of Phe55 undergoes a change from 124º (in

the apoenzyme) to -21º, which is 6º more than the FK506 complex; whereas for the corresponding Phe54 in PvFKBP35, there is an increase of 2.6º. These changes could well be attributed to the non-bonded contacts made by D44 with Phe55/54, unlike the hydrogen-bonded contacts of FK506, which gives the residue more flexibility.

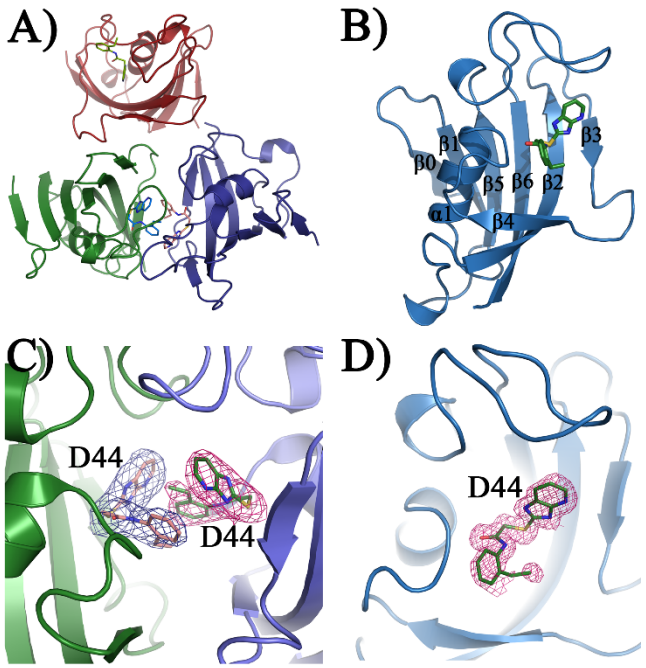

Figure 28: The crystal structures of *Plasmodium* FKBP35- D44 complex. The cartoon representation of the asymmetric units of *Pf*FKBP35 (A) and *PvFKBP*35 (B) in complex with ligand D44 (in stick mode), showing the three chains and a single chain respectively. The 2Fo-Fc difference Fourier map contoured at 1 σ cut-off of ligand D44 in complex with *Pf*FKBP35 (C) and *PvFKBP*35 (D).

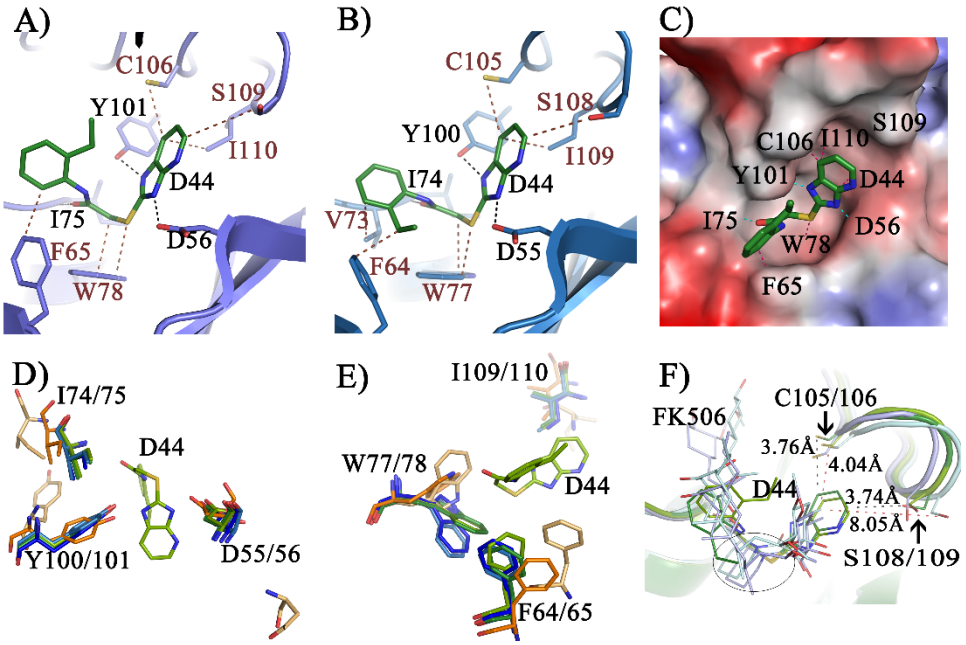

Figure 29: Comparison of binding site interactions of D44 with *Plasmodium* FKBPs (A & B) The stick representation of residues making hydrogen bonds (black) and the non-bonded contacts (brown) with ligand D44 in *Pf*FKBP35 (A) and *Pv*FKBP35 (B). Ser 109/108, one of the highly conserved residues is also shown for clarity; (C) Electrostatic surface representation of *PfFKBP*35 in complex with D44 (in stick model), showing the docking of the ligand into the hydrophobic active site cleft; (D & E) Superposition of interacting residues of apo (*Pf* - light orange ; *Pv* - orange) FKBP35 with their corresponding FK506 (*Pf* – light green ; *Pv* –green) and D44 (*Pf* – light blue ; *Pv* – dark blue) complexes. Large deviations in hydrogen bonded residues can be observed for *PfFKBP*35 compared to its *P. vivax* counterpart (D). The residues involved in non-bonded contacts (E) clearly show a movement away from the active site as the size of ligand involved in binding gets bigger, compared to the apo form; (F) Specificity of ligand D44 towards the highly conserved Cys 106/105 and Ser 109/108 can be observed when superposed with the corresponding FK506 structures. D44 (*Pf* – light green; *Pv* – dark green) clearly moves closer to Cys 109/108 than FK506 (*Pf* – light blue; *Pv* – cyan). The distances are shown for the *PvFKBP*35, with D44 at 3.76 and 3.74 Å from Cys 105 and Ser 108 respectively, compared to 4.04 and 8.05 Å in FK506. In addition, the hydroxyl group of Ser108 flips towards the ligand (B & E) in the *PvFKBP*35 structure enhancing the selectivity towards the ligand. It could also be noticed that the thio-acetamide linker in D44 compensates for the pipecolinyl moiety (shown within the

black open circle) of FK506, a unique feature pertaining to D44. These results were generated using the program *PyMOL [205]*

Table IV: Interactions between D44 and PfFKBP35 and PvFKBP35.

Non-Polar contacts [a]			
D44 Atoms	*Pf*FKBP35 residues		*Pv*FKBP35 residues
	Chain A	Chain B	Chain A
C5		Phe65	Phe64,Val73
C6		Phe65	Phe64,Val73
C9	Phe65		
C10		Phe65	Phe64,Trp77
C11		Phe65	Phe64
C12	Trp78	Ile75, Trp78	Trp77
S13	Trp78	Trp78	Trp77
C16			Tyr100, Ile109
C17		Phe55	
C19	Tyr101, Cys106, Ile110	Tyr101, Cys106, Ile110	Tyr100, Cys105, Ile109
C20	Cys106	Ile110	Cys105, Ile109

Hydrogen Bonds [b]					
D44 Atoms	*Pf*FKBP35 Atoms	*Pv*FKBP35 Atoms	Donor-Acceptor Distance (Å)		
			Pf Chain A	*Pf* Chain B	*Pv* Chain A
N15	Tyr101 OH	Tyr100 OH	2.65	2.53	2.66
N18	Asp56 OD2	Asp55 OD2	2.69	2.60	2.57
O1	Ile75 N	Ile74 N	3.29	3.22	3.02

[a]Non-polar contacts and [b]hydrogen bonding residues / atoms shown here are identified using the program LIGPLOT [206]. Standard hydrogen bond between the donor and the acceptor – 2.5-3.5 Å, was used to represent the hydrogen bonding distances.

The Crystallographic ligand complexes show that the purine like ring of D44 makes critical hydrogen bonding contacts with the catalytic residues Asp56/55 and Tyr101/100 (Fig. 29A, B) and the thio-acetamide linker of D44 through its keto group interacts with Ile75/74 locking the ligand in the active site pocket (Fig. 29A, B & C). Further non-bonded contacts (Fig. 29A, B) with residues like Phe55/54, Phe65/64, Trp78/77, and Ile110/109 stabilize the ligand complex. Comparison to the NMR structure (apo form) [126, 195] not only reveals a translation of ~2-6.8 Å (Fig. 29D) on

residues involved in hydrogen bonded interactions, but also noticeable changes in the local conformations of Phe65/64 and Trp78/77 side chains (Fig. 29E). Quantitatively, in the crystal structures Phe65/64 moves by ~4/2.8 Å and ~5.5/3.5 Å in complex with D44 and FK506, respectively, while Trp78/77 sways by ~6/5.7 Å and ~7.5/5.9 Å (Fig. 29E). In addition, directionality can be conferred as these two residues approximate towards the thio-acetamide owing to the strong hydrophobic interactions of sulphur with the hydrophobic residues. Furthermore, earlier structure activity relationship studies on FKBP12 inhibitors [10, 198] have shown the presence of pipecolinyl or proline moiety being prerequisite for the binding and inhibition of enzymatic activity. Here we present a unique scaffold which possesses a thio-acetamide linker compensating the lack of bulky pipecolinyl group and through its strong hydrophobic interactions induce local conformational changes (Fig. 29E, F) at the active site. Overall, though D44 (MW of 312) is much smaller in size compared to FK506 (MW of 804), it interacts with specific residues as predicted in modeling, confirming that these interactions between the protein and ligand are critical for the inhibition of the enzyme. Our molecular modeling was mainly aimed to target the two highly conserved Cys106/105 and Ser109/108 residues within the *Plasmodium* FKBP to achieve selectivity towards *Plasmodium* FKBP35. Our crystallographic structure of *Plasmodium* FKBP35 in complex with D44 validates our GOLD genetic approximation (GA) settings and the predicted docking solutions were consistent within a RMSD of 2.0 Å. In the PfFKBP35-D44 complex, the ligand D44 is much closer (Fig. 29F) with the nearest atom, from the purine like ring, located at a distance of 3.6 Å and 4.3 Å from Cys106 and Ser109 respectively, compared to 3.9 Å and 5.4 Å in the corresponding FK506 complex. Similarly in the PvFKBP35, Cys105 and Ser108 are at a distance of 3.76 Å and 3.74 Å from D44, compared to 4.04 and 8.05 Å in its FK506

(Fig. 29F) complex. The hydroxyl group of Ser108 in PvFKBP35 flips towards the purine like ring of D44 (Fig. 29B, F) owing to close van der Waals contacts with this residue which is well conserved among the *Plasmodium* species, thereby enhancing its selectivity towards *Plasmodium* FKBPs. In addition, the thio-acetamide moiety in D44 makes up for the conventional pipecoline ring (Fig. 29F) for the canonical FKBP binding. The above observations corroborate that D44 could be pivotal towards selective *Plasmodium* FKBP35 inhibition with non-immunosuppressive properties.

III.I 3 Analog based modeling on FKBP12 inhibitors

Previous study by Braun *et al.,* has shown that the synthetic ligand of FK506 (SLF) binds to human FKBP12 very tightly (K_d 3 nM) but does not cause any deleterious/toxic effects in vivo or in cellular models. This could probably be due to ubiquitous nature of human FKBP12 [124]. On the contrary, SLF binds tightly to *Plasmodium* FKBP35 activity (K_d 43 nM) and inhibits the growth of parasite *in vitro*. Braun *et al.,* have reasoned that this context dependent activity could be due to the different physiological levels of parasite FKBP35 and human FKBP12. *Plasmodium* FKBP35 levels are much smaller (50-100 nM) than human FKBP12 levels (3-5 µM) and this could provide a window to achieve selectivity towards *Plasmodium* FKBP35.

Non-toxicity in cellular models and tight binding of SLF to FKBP12 has been further exploited to enhance the bioavailability (by increasing the in-vivo life time) of HIV protease inhibitors using FKBP ligands as presenter protein strategy [124, 133, 134]. Therefore, FKBP12 ligands serve as good startup scaffolds for achieving malaria parasite FKBP35 inhibition selectively without affecting human FKBP activity.

III.I 3.1 Compound collection.

For the generation of a valid FKBP12 pharmacophore model, compounds with K_i values for FKBP12 inhibitory activity were selected from the literature [170, 207-210] and 3D coordinates of molecules were built by using the 'Prepare ligands' module of Discovery Studio 2.5.

III.I 3.2 Training set selection.

To achieve a good-quality pharmacophore model, a training set should ideally represent structurally diverse representatives (at least 16 molecules) covering an activity range of at least four orders of magnitude [211, 212]. Accordingly, 19 compounds (Fig. 30) with K_i values ranging from 0.2 to 30,000 nM were selected as training set, while a set of 61 compounds, ranging in activity from 2.8 to 50,000 nM, served a test set to validate the hypotheses generated from the training set. The activities (K_i) against FKBP12 reported are broadly classified as: *** - Most active (<100 nM), ** - active (100 - 1000 nM), * - inactive (>1000 nM).

III.I 3.3 Pharmacophore generation.

A pharmacophore model is a spatial arrangement of an ensemble of chemical features that are required for the biological activity. Function mapping helps to identify the chemical features like hydrogen bond acceptor (HBA), hydrogen bond donor (HBD), hydrophobic (Hy) and ring aromatic (RA), positive ionizable (PI) and negatively ionizable (NI) that are available with the most active compounds.

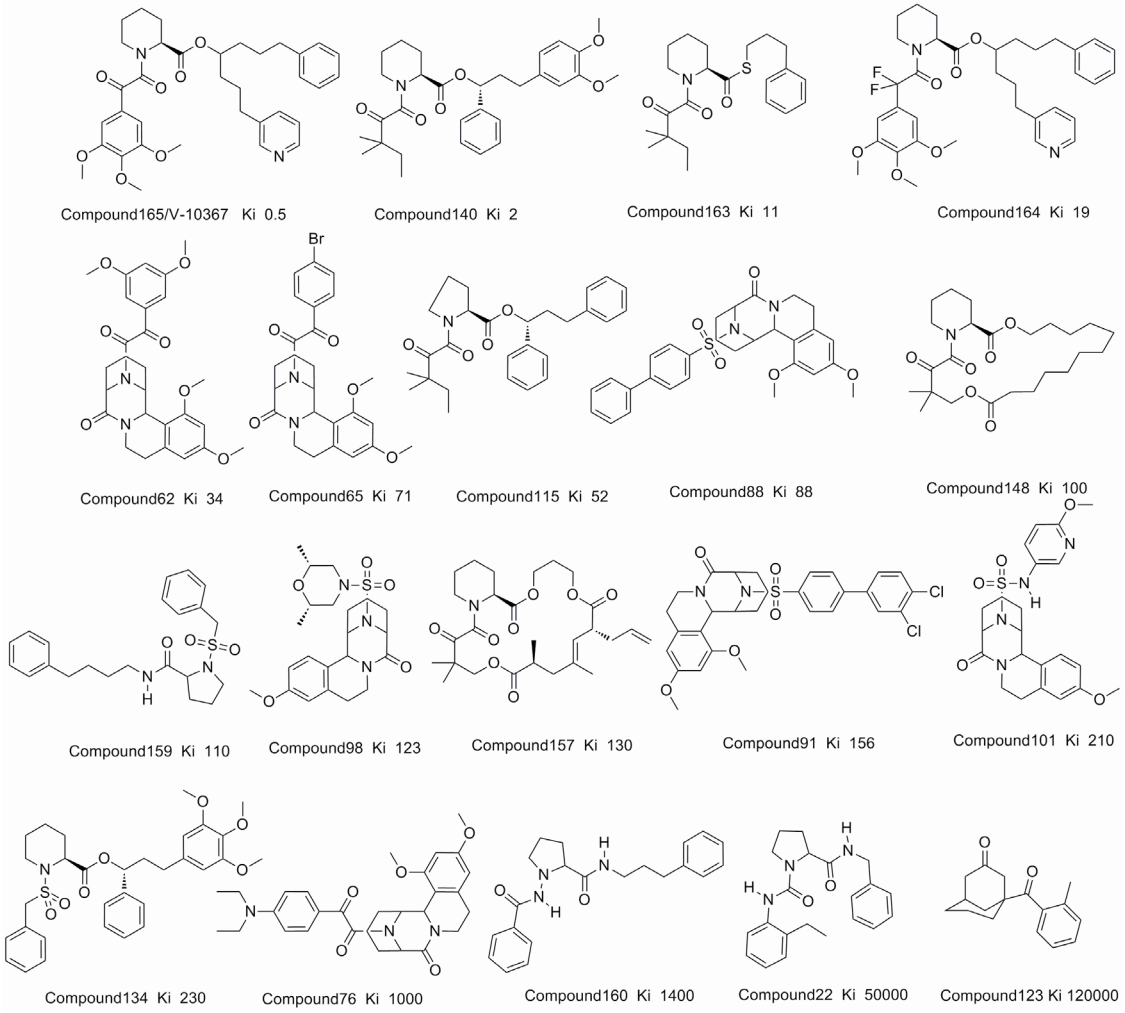

Figure 30: Chemical structures of 19 molecules (K_i – nM) used as training set. Molecules were selected based on structural diversity and 4-fold spread in activity K_i values.

The HYPOGEN program encodes the features that are important for activity in the pharmacophore model depending on the (minimum to maximum) number of each feature included, interfeature distance and uncertainty value for the activity in the training dataset.

3D QSAR (HYPOGEN) uses the given data i.e., training set, conformational models, chemical features, parameters, etc., to generate top ten pharmacophore models. HYPOGEN builds the simplest model that can correlate the estimated activities with measured activities. The pharmacophore model is generated in three phases. 1) a

constructive phase – which identifies the most active compounds and builds hypotheses that are common among the most active compounds, 2) subtractive phase – where the hypotheses that are common among the inactive compounds are removed, and 3) optimization phase – where an attempt is made to improve the initial model. The final models contain a set of generalized chemical features in three dimensional space as well as regression information that helps to predict the measured activity [212]. One of the greatest advantages of these pharmacophore models is that they can be used as searchable queries to mine for potential leads and also predict the activity of a potential lead like compounds [213].

III.I 3.4 Validation of pharmacophore model

The generated pharmacophore model is evaluated by its ability to identify active compounds from a known database and to estimate the activity of the molecules in a statistically significant manner. The following metrics like (i) cost analysis, (ii) randomization test, (iii) test set prediction and (iv) GH (goodness of hit) score are usually used to validate the derived pharmacophore models.

i) Cost analysis

HYPOGEN provides important theoretical cost parameters – (i) Fixed cost & (ii) Null cost to decide the quality of the generated pharmacophore model. Fixed cost is the minimal cost of the pharmacophore that fits all data perfectly whereas null cost is the highest cost (as it lacks the structure data) and estimates the activity to be the average of all the activities in the training set. (iii) The total cost of optimized pharmacophore should ideally lie between the fixed & null costs and should be closer to the fixed cost than the null cost. Further, randomized studies have found that the meaningful pharmacophore model can only be obtained when the total cost differs from null cost

by 40-60 bits, which indicates that there would be a 75-90 % chance of a true correlation in the data. If the difference is less than 40 bits then the model is a chance correlation and one has to reconsider the training set before proceeding any further with the model. Another useful parameter that decides the utility of the model is the entropy of pharmacophore space. In general, if a run generates an entropy value greater than 17 then one should seriously consider modifying the training set before proceeding. Hypogen works well for training sets with entropy up to 17 which corresponds to 2^{17}=131,072 starting hypotheses. For training sets, entropy higher than 17 suggests that the training set molecules are highly flexible to allow proper sampling in space during conformational analysis.

Other parameters that influence the quality of hypotheses are error cost which depends on the root mean square difference between the experimental and the predicted activities of the training set molecules. RMS represents the quality of the correlation between the experimental and the predicted activity data. The best pharmacophore model has the highest cost difference, the lowest RMSD, and the best correlation coefficient.

As the pharmacophore model is built from most active compounds, it is obvious that the active molecules should map most of the features in the model. Conversely, an inactive molecule misses the important features or the features are not oriented properly in space. The geometric fit points out exactly how the function is localized in the center of a feature sphere. The pharmacophore model estimates the activity values by a simple regression of geometric fit values versus the activity of the training set compounds. The greater the geometric fit, the greater the activity of the compound.

Predictive ability of the model depends on how well the model estimates the activities for the compounds in the training or test compounds by their fitting to the model. The

best pharmacophore model obtained after cost analysis and randomization tests was then used to predict the biological activities of those compounds in the test set by correlating the values that are obtained by linear regression of the geometric fit index. Fit function checks mapping of chemical substructures into feature constraints, as well as distance deviations of chemical functions from the center of the feature, followed by the evaluations of the correlation coefficient (r) and root-mean square deviation (RMSD), maximum residual, average residual, and standard deviation of residual between the observed and predicted K_i values.

ii) Randomization test: The Catscramble test arbitrarily randomizes the affinity data for the training set compounds and generates random pharmacophore models. These randomized models should not yield hypotheses with statistical significance; otherwise the generated model is a chance correlation. To obtain 95% confidence levels, 19 random hypotheses were generated by the catscramble module. None of the randomized models gave hypotheses with lower total cost or better correlation (r) than the best hypotheses. These results indicate that best model is statistically significant and can be used to screen and predict the activity of unknown datasets with high confidence levels (Fig. 31, 32).

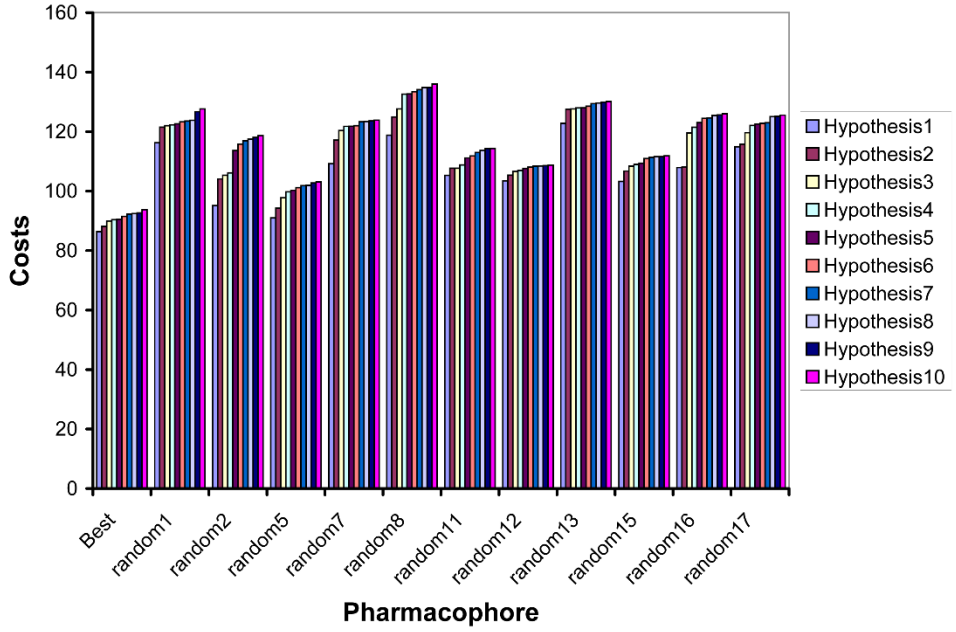

Figure 31: Randomization test showing cost values. The best hypothesis 1 had the lower cost values (86.34) than the randomized hypothesis 1-17.

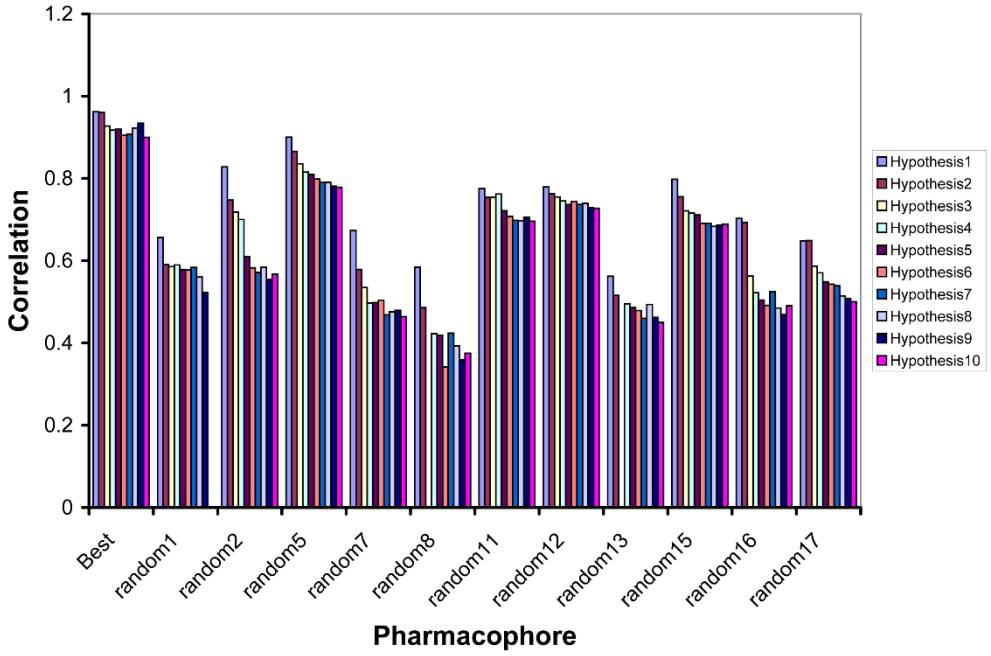

Figure 32: Randomization test showing correlation values. The best hypothesis 1 had the best correlation (0.96) than the randomized hypothesis 1-17 verifying that the model is not a chance correlation

III.I 3.5 FKBP12 Pharmacophore model

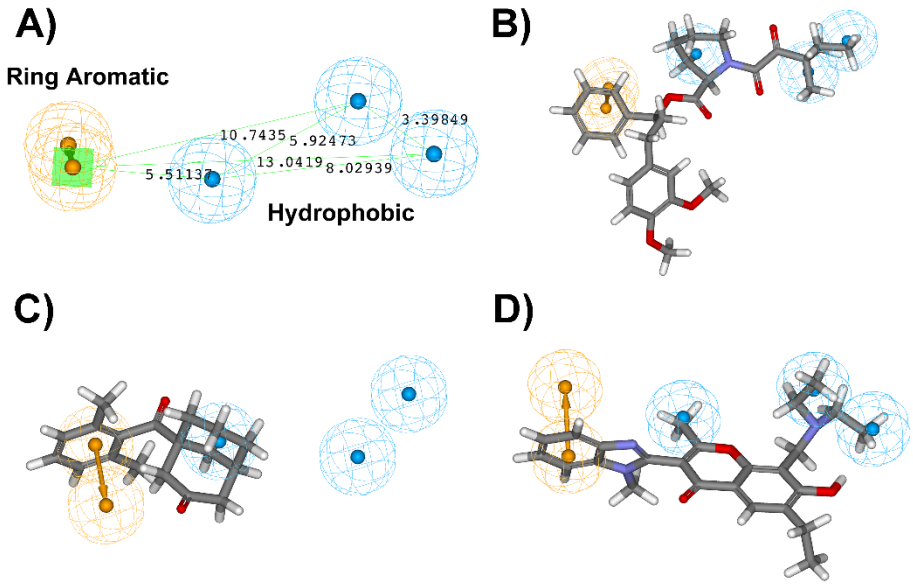

Figure 33: FKBP12 Pharmacophore model and alignment with known actives/inactive and novel hits in the screen. A) Three hydrophobic (blue) features and ring aromatic groups spaced at specific geometric distance from each other represents the pharmacophore that is required for FKBP12 binding. B) Alignment of the most active ligand in the training set maps all the features with the FKBP12 pharmacophore. C) Alignment of least active ligand misses the key hydrophobic features in the pharmacophore resulting in low FKBP12 activity. D) Alignment of one of the best virtual hit compound possessing a coumarin scaffold showed better fitting with the FKBP12 pharmacophore.

A HYPOGEN run results in generation of 10 best pharmacophore models. The geometric fit values of the top pharmacophore model and each of the FKBP12 ligands on the training set correlated well with the activity values. The best pharmacophore model has a correlation coefficient (r) of 0.96 and root mean square (*rms*) error of regression of 0.72. The null cost, fixed cost, pharmacophore cost and configuration costs were 127.6, 79.76, 86.3 and 14.73 respectively. The pharmacophore cost was well below the null cost and closer to the fixed cost which indicates that correlation is not obtained by chance. The Pharmacophore model consisted of 4 features: 3

hydrophobic aliphatic features, and one ring aromatic group. The best hypothesis 1 (Fig. 33A) had a high correlation coefficient between experimental and predicted K_i values on a test set of molecules of 0.94 and a cost difference of more than 40 bits which indicates that the hypothesis 1 is having more than 75% of true correlation. The inter-feature distance among the features of the best pharmacophore model is as shown in Fig 33A. As expected, the most active compound 140 is mapped nicely to the pharmacophore model (Fig 33B) whereas the least active compound 123 missed certain features (Fig 33C).

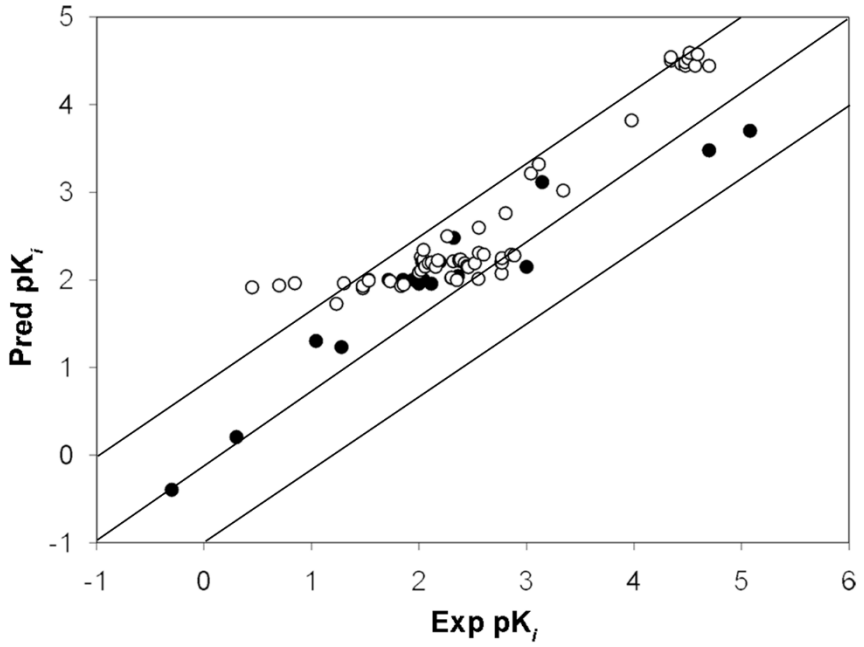

Figure 34: Graph showing the correlation between experimental K_i. to the predictive K_i of test set molecules.

Robustness of a pharmacophore model mainly depends on its ability to i) predict the activity of external data and the (ii) Güner-Henry (GH) score [153]. Hypothesis 1 had a good correlation of 0.96 for training set and 0.94 for test set (61 molecules) (Fig. 34) as tabulated in Table V. GH score refers to the quality of pharmacophore models by its ability to recall the known inhibitors from a known library (containing 100 molecules)

spiked with known FKBP inhibitors. Hypothesis 1 is rated with excellent GH score of 0.89 and is the best model for predicting the FKBP12 activity of new molecules obtained by database search these validation tests, suggesting that there is at least 95% probability that this hypothesis represents true correlation in the data [211]. This validated pharmacophore can be used either to screen our library to find FKBP binding fragments or can also be used as counter pharmacophore filter for virtual screening studies. Database screening has provided with hits that could have nanomolar activity and shown in Fig. 33D is one such ligand with a chromone nucleus with a predicted K_i in the nanomolar range.

Table V. Predicted activities of the FKBP12 ligands by the best hypothesis 1

Sl.No	Compound	fitness	Actual k_i (nM)	Predicted k_i (nM)	Actual Scale	Predicted Scale
1	Compound165	9.924	0.5	0.4	***	***
2	Compound140	9.319	2	1.6	***	***
3	Compound163	7.95	11	20	***	***
4	Compound164	8.29	19	17	***	***
5	Compound62	7.47	34	100	***	***
6	Compound115	7.452	52	100	***	***
7	Compound65	7.521	71	100	***	***
8	Compound88	7.263	88	100	***	***
9	Compound148	7.582	100	90	***	***
10	Compound159	7.169	110	100	**	***
11	Compound98	7.266	123	150	**	**
12	Compound157	7.57	130	90	**	***
13	Compound91	7.316	156	160	**	**
14	Compound101	7.037	210	300	**	**
15	Compound134	7.468	230	110	**	**

16	Compound76	7.379	1000	140	*	**
17	Compound160	6.41	1400	1300	*	**
18	Compound22	5.08	50000	3000	*	**
19	Compound123	5.079	120000	5000	*	**
20	Compound145	7.607	2.8	82	***	***
21	Compound154	7.583	5	86	***	***
22	Compound142	7.562	7	91	***	***
23	Compound112	7.797	17	53	***	***
24	Compound141	7.559	20	91	***	***
25	Compound162	7.616	30	80	***	***
26	Compound146	7.592	30	85	***	***
27	Compound61	7.53	34	98	***	***
28	Compound85	7.538	54	96	***	***
29	Compound144	7.592	68	85	***	***
30	Compound66	7.574	72	88	***	***
31	Compound67	7.438	100	121	***	**
32	Compound90	7.263	104	181	**	**
33	Compound53	7.409	105	129	**	**
34	Compound82	7.314	107	161	**	**
35	Compound83	7.31	110	162	**	**
36	Compound68	7.292	110	169	**	**
37	Compound48	7.179	110	219	**	**
38	Compound84	7.37	114	141	**	**
39	Compound69	7.329	123	155	**	**
40	Compound70	7.324	131	157	**	**
41	Compound55	7.374	143	140	**	**
42	Compound99	7.3	150	166	**	**
43	Compound100	7.025	183	313	**	**
44	Compound132	7.498	200	105	**	**
45	Compound58	7.494	201	106	**	**

46	Compound78	7.309	208	162	**	**
47	Compound60	7.526	225	99	**	***
48	Compound102	7.291	236	169	**	**
49	Compound72	7.305	238	164	**	**
50	Compound92	7.291	244	170	**	**
51	Compound93	7.333	266	154	**	**
52	Compound108	7.365	279	143	**	**
53	Compound94	7.376	288	139	**	**
54	Compound95	7.331	330	154	**	**
55	Compound96	7.511	357	102	**	**
56	Compound103	7.215	360	202	**	**
57	Compound104	6.925	360	393	**	**
58	Compound158	7.232	400	194	**	**
59	Compound74	7.323	583	157	**	**
60	Compound75	7.448	586	118	**	**
61	Compound105	7.328	590	156	**	**
62	Compound107	7.274	591	176	**	**
63	Compound39	6.761	640	574	**	**
64	Compound36	7.234	720	193	**	**
65	Compound97	7.244	772	189	**	**
66	Compound43	6.307	1100	1634	*	*
67	Compound10	6.202	1300	2079	*	*
68	Compound47	6.503	2200	1040	*	*
69	Compound3	5.701	9500	6589	*	*
70	Compound12	5.019	22000	31691	*	*
71	Compound9	4.981	22000	34598	*	*
72	Compound118	5.057	27500	29031	*	*
73	Compound27	5.078	30000	27668	*	*
74	Compound19	5.039	30000	30285	*	*
75	Compound13	4.994	32000	33545	*	*

76	Compound18	4.931	33000	38781	*	*
77	Compound2	5.079	37000	27631	*	*
78	Compound45	4.948	39000	37285	*	*
79	Compound23	5.08	50000	27549	*	*

Fitness measures the fitness of compounds with the pharmacophore, greater the fitness greater would be the predicted activity. Compounds are divided into three bins based on their activity. 1) Activity Scale: * - Most active (<100 nM), 2) ** - active (100 - 1000 nM), 3) * - inactive (>1000 nM). The ability of the model to predict the activity is shown in predicted scale and is compared with actual scale.**

Table VI. Correlation and cost difference of the best hypothesis 1 in comparison to other hypotheses between the training and test set.

Hypothesis	Total Cost	Cost-difference	RMSD	r² (Train Set)	r² (Test Set)
1	86.3467	41.2883	0.726065	0.962	0.94
2	88.0914	39.5436	0.764159	0.960	0.63
3	89.918	37.717	0.978789	0.927	0.78
4	90.3882	37.2468	1.03524	0.917	0.25
5	90.5181	37.1169	1.024	0.920	0.67
6	91.496	36.139	1.10429	0.905	0.35
7	92.2777	35.3573	1.09946	0.907	0.65
8	92.4471	35.1879	1.03183	0.922	0.54
9	92.672	34.963	0.978655	0.934	0.5
10	93.7381	33.8969	1.14353	0.900	0.76

III.I 4.0 Adamantyl derivatives as a lead candidate to evaluate PfFKBP35 activity

As mentioned earlier, the interaction pattern of FK506 with *Plasmodium* FKBP35 is very much similar to that of human FKBP12-FK506 with a few variations at β4-β5 loop [129, 131]. These similar interaction patterns of FK506 suggest that similar FKBP12 binding ligands could also be useful in inhibiting the parasite FKBP.

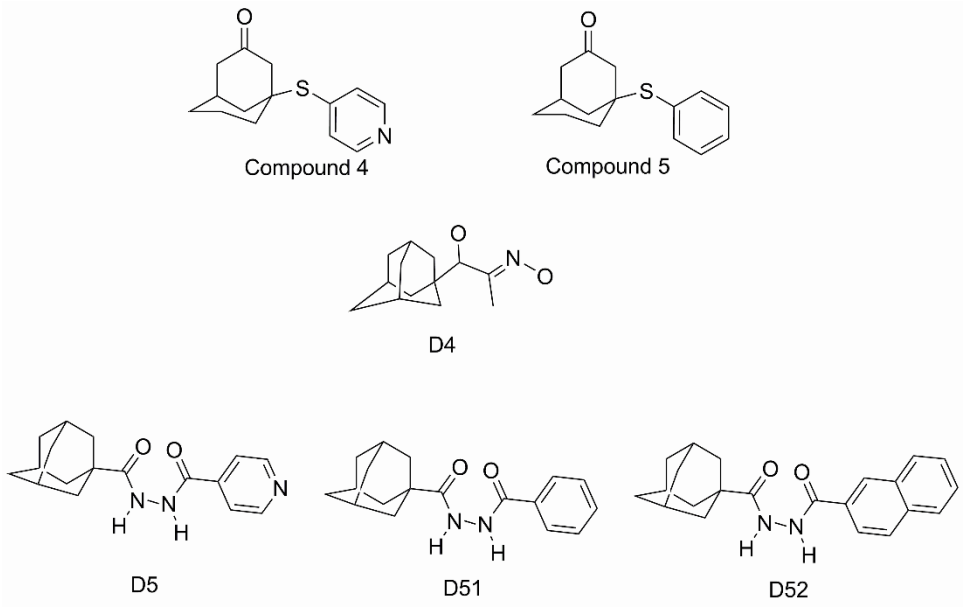

Figure 35: FKBP12 ligands having adamantyl like scaffolds (compounds 4 and 5) and SRA/D5, D4, D51, D52 derivatives ligands designed with 4-atom linker length.

Previous studies from Babine *et al.,* have shown that an adamantyl like fragment binds to FKBP12 and the crystallographic complex of compound 5 [214] with FKBP12 showed that the adamantyl like fragment sits on the base of Trp58 whereas the distal pyridine ring interacts with His87 residue at β4-β5 loop. The inhibition constant of compound 5 on human FKBP activity is in the low micromolar range. As shown in Fig. 35, both the compounds (4, 5) have the adamantyl like fragment bonded to pyridine via sulphur atom. We reasoned to keep the adamantane ring as such and to increase the linker length in order to induce steric clashes with His87 of human FKBP12 and in particular to enhance the probability of binding to *Plasmodium* FKBP35. Our molecular

modeling studies on the adamantane derivatives predicted that adamantane fragment sits at the canonical binding site Trp78 (S1) and linker forms strong hydrogen bonding with Ile75 and Tyr101 and hydrophobic contacts with Tyr101 favored the S3 site between the α1- β5 loop and oriented away from this β4-β5 loop (S2) which is involved in a number protein-protein interaction such as those including calcineurin, the IP3 receptor, TGF-β signaling as shown in Fig. 36.

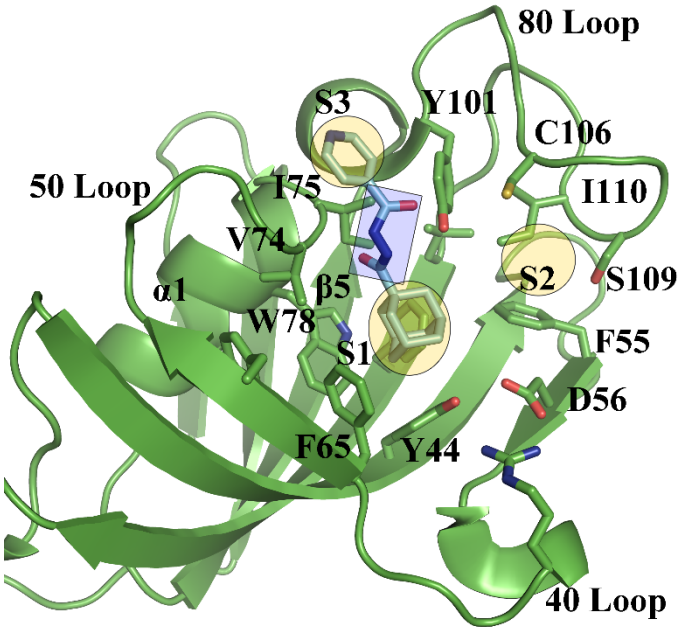

Figure 36: Predicted binding mode of D5 or SRA with *Plasmodium* FKBP35. As shown in the figure, the bulky adamantyl group binds to the ligand binding platform (S1) while the pyridine ring is solvent exposed and orients to site S3. The linker highlighted in blue forms hydrogen bonding with Ile75 and Tyr101. As the length of the linker increases, it could move away from S2 site and re-orients into the S3 region. This kind of re-orientation into S3 site by ligand SRA is very much similar to other ligands co-crystallized with FKBP12.

Dr. Kalyan Kumar P from Asst/Prof Liu Xuewei lab at School of Physical and Mathematical Sciences, Nanyang Technological University has synthesized these

molecules for carrying out biochemical, biophysical assays and in vitro growth inhibition assays.

III.I 4.1 PPIase activity and Calcineurin assay

SRA and its derivatives SRA-1, SRA-2 inhibits PfFKBP35 activity significantly in the nanomolar range. Percent inhibition of PPIase activity at concentrations ranging from 1 nM-1000 nM were used to calculate IC_{50} values by non-linear regression of dose responses from GraphPad Prism software version 5.0 [205]. More importantly, SRA and its analogs do not inhibit calcineurin phosphatase activity (Fig. 37) signifying that these novel ligands do not affect the immune response pathway, unlike FK506 which inhibits the phosphatase activity of calcineurin leading to immunosuppression. The IC_{50} values of SRA, SRA-1, and SRA-2 (Table VI) were determined by a standard growth inhibition assay on *in-vitro P. falciparum* development.

Table V1I: *in-vitro PPIase* assay *and in-vitro* growth inhibition assay results.

	IC_{50}, nM	
	*In-vitro Pf*FKP35 PPIase assay	*In-vitro Growth inhibition assay*
SRA (D5)	**83**	**100**
SRA-1	**95**	**90**
SRA-2	**50**	**105**

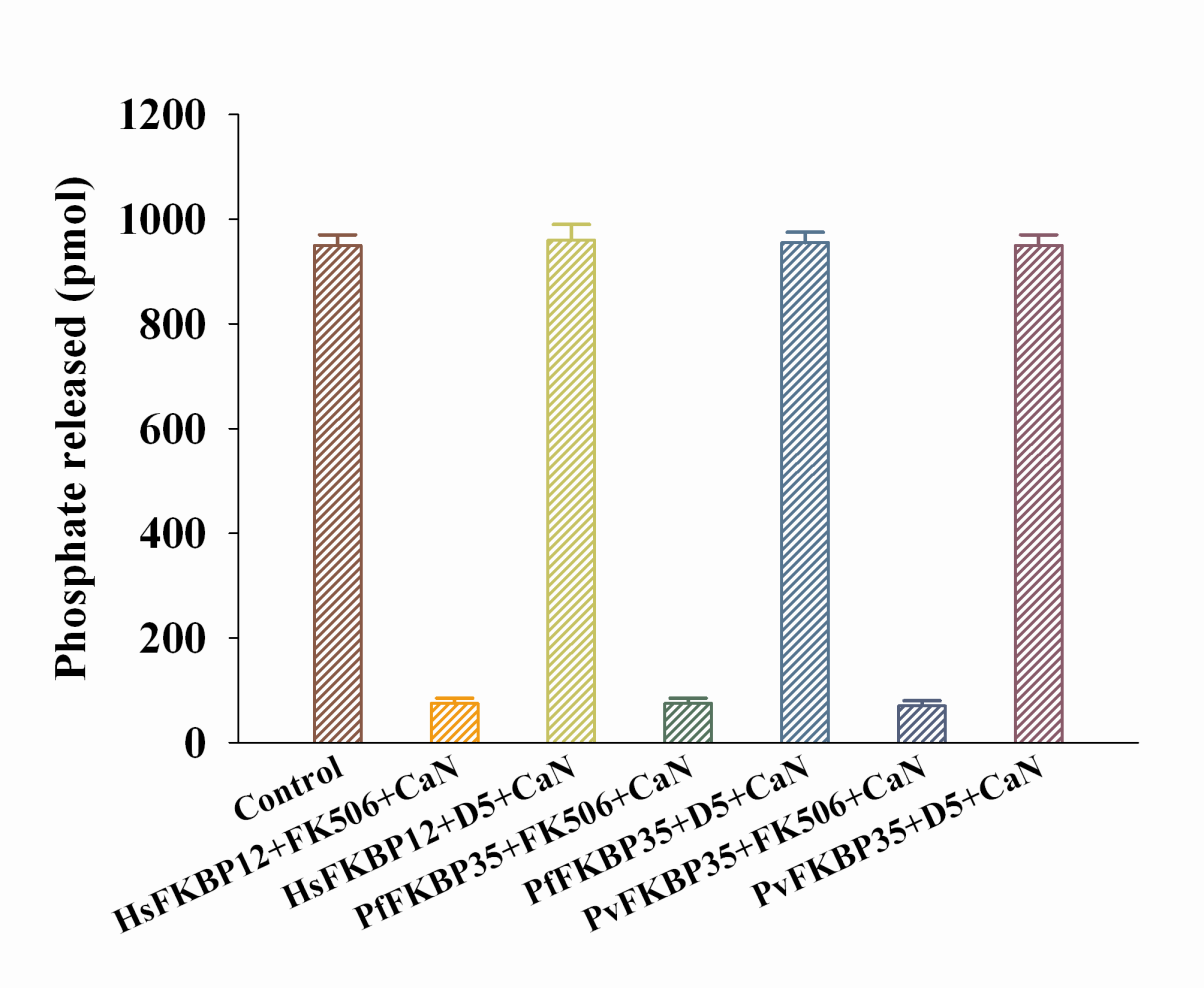

Figure 37: Calcineurin Phosphatase assay. The Compounds D5 complexes with human & *Plasmodium* FKBP had no effect on calcineurin phosphatase activity while the FK506 complex with human & plasmodium FKBP inhibited calcineurin phosphatase activity. Calcineurin alone served as control. Error bars represent the standard deviation of two independent duplicate titrations.

III.I 4.2 Growth inhibition assay

SRA was more effective with more than 50% inhibition at 100 nM respectively. We examined the effects of these inhibitors on *P. falciparum* IDC by monitoring parasitemia and parasite morphology on giemsa-stain smears at 8 h time points for an entire IDC from ring to schizont stages. During the first 8 h (ring-trophozoite

development), no morphological and parasitemia changes were observed between the SRA-treated and untreated parasites (Fig. 38B).

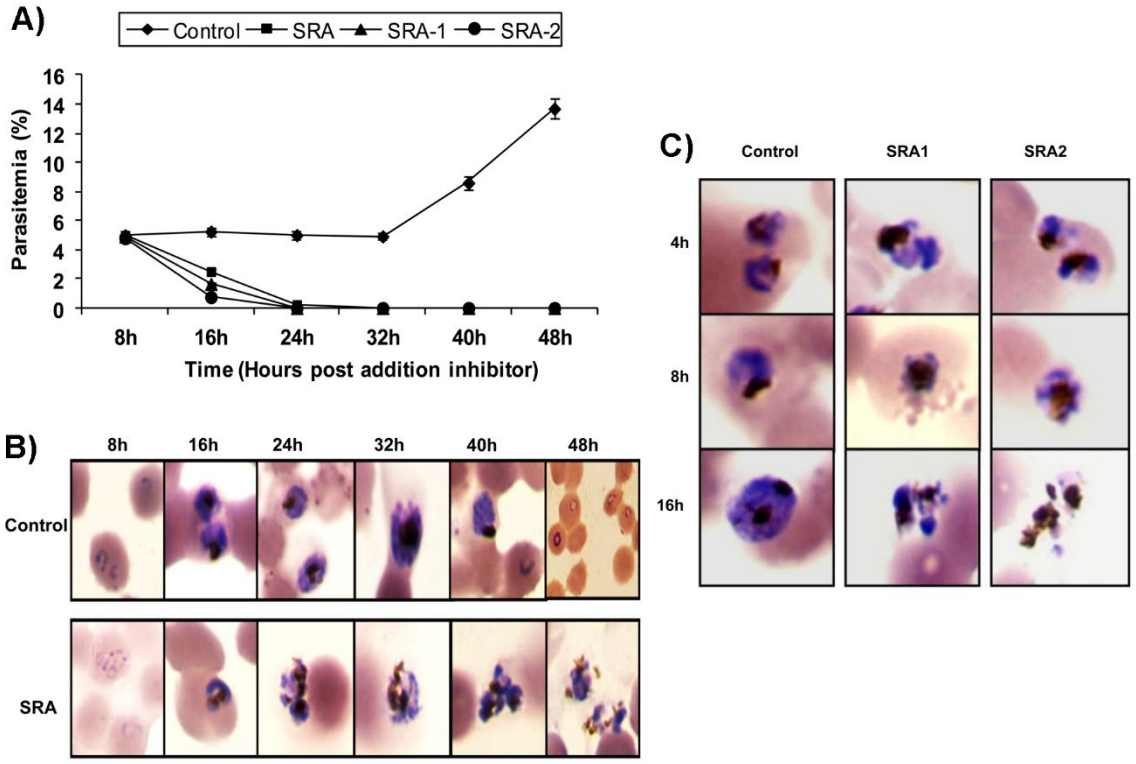

Figure 38: Effects of SRA analogs on *Plasmodium falciparum* IDC. (A) Effect of SRA (500 nM) on parasitemia (%) of synchronized ring stage was monitored every 8 h upon addition of inhibitor compared to untreated control parasites. (B) Parasite morphology was monitored by Giemsa stain at each time point. Illustrations of parasite morphology at 8, 16, 24, 32, 40 and 48h after addition of inhibitor are shown; (C) Effects of D5/SRA1 and SRA2 on trophozoite development. Parasite morphology was monitored by Giemsa stain at 4, 8 and 16 h after addition of inhibitor. During the first 4 h, no significant morphological differences were observed between the treated and control parasites. During the subsequent development, the control parasites progress to the next generation (formation of mature schizont and ring) while the SRA treated cells remain arrested at the trophozoite stage. The results show that SRA and its derivatives mainly interfere with trophozoite stage development.

During their subsequent development, control parasite mature into trophozoite and schizont whereas in SRA-treated parasites high parasite death with total growth arrested at 24 h post drug treatment (Fig. 38A) suggesting interference of these inhibitors with the trophozoite stage.

To validate this finding, we investigated the direct effect of SRA, SRA-1 and SRA-2 on trophozoite maturation by incubating synchronized trophozoites (~24-28 hpi) with 500 nM of each inhibitor. During the first 4 h, no significant morphological differences were observed between the treated and untreated parasites (Fig. 38C). During their subsequent development the untreated control progress to the next generation (formation of schizont) whereas the SRA-treated cells remain arrested at the late trophozoite stage (Fig. 38C).

III.I 4.3 Crystal structure of Plasmodium vivax FKBP35 with D5

To understand the structural basis of the mode of action of D5, the crystal structure of PvFKBP35 in complex with D5 was determined to a resolution of 1.72 Å. Though we could not obtain crystals for the PfFKBP35-D5 complex, the conclusions from the present PvFKBP35-D5 holds good for both species, as observed from the previous structures [126, 128, 129, 189, 206] which indicates that the structures from both the species are identical, especially at their active site residues. The refined crystallographic structure revealed a topology consisting of seven b-stranded sheets and a short α-helix (Fig. 39A) similar to the previous FKBP35 structures. The PvFKBP35-D5 complex consists of a monomer in the asymmetric unit forming a dimer with the neighboring chain generated by crystal packing with the help of a disulphide bond through Cys105.

The crystal structure was compared to their corresponding apo (NMR – PDB ID 2KI3) form and other ligand complexes (FK506 – PDB ID 3IHZ; D44 – PDB ID 3V3A). The crystal structures were almost identical with each other, with an rmsd of 0.29 (0.09), whereas the NMR apo form had a maximum deviation of 1.25 Å. As expected, the three loops which flank the binding site, namely β3 - β4, β4 - α1, and β5 - β6, undergo small structural changes. When compared with the NMR structure, the psi angle of Phe54 undergoes a change from 146º to -17.9º (D5 complex), where the β3 - β4 loop nucleates.

The electron density for D5 (Fig. 39B), corresponding to one ligand per monomer, was traced unequivocally in the electron density difference map in the hydrophobic binding site. The dimeric molecule could be generated using crystal symmetry, where two ligands are found to cross over each other in the dimer interface stabilized by a hydrogen bond at a distance of 2.78 Å. Crystallographic ligand complex show that the atoms in carbonyl hydrazide linker region make critical hydrogen bonding contacts with the catalytic residues Tyr100 and Ile74 (Fig. 39B) which holds the ligand in the active site pocket. Further non-bonded contacts are formed predominantly by the adamantyl ring of D5 with residues like Tyr43, Asp55, Phe64, Val73, Trp77, Tyr100, and Phe117 which lock the ligand deep inside the pocket where Trp77 forms a platform-like architecture (Fig. 39B). Further the superimposition of the D44 and D5 in the active site pocket (Fig. 39C, D) lead to few interesting observations. The purine like ring of D44 docks deep inside the pocket towards the β5 - β6 loop region (Fig. 39D) whereas the adamantyl ring sits on the Trp77 and pyridine ring of D5 orients itself towards the pocket facing the surface. Importantly, in D5 the adamantyl ring has stronger bonds with the active site residues in comparison with the thio-acetamide of D44.

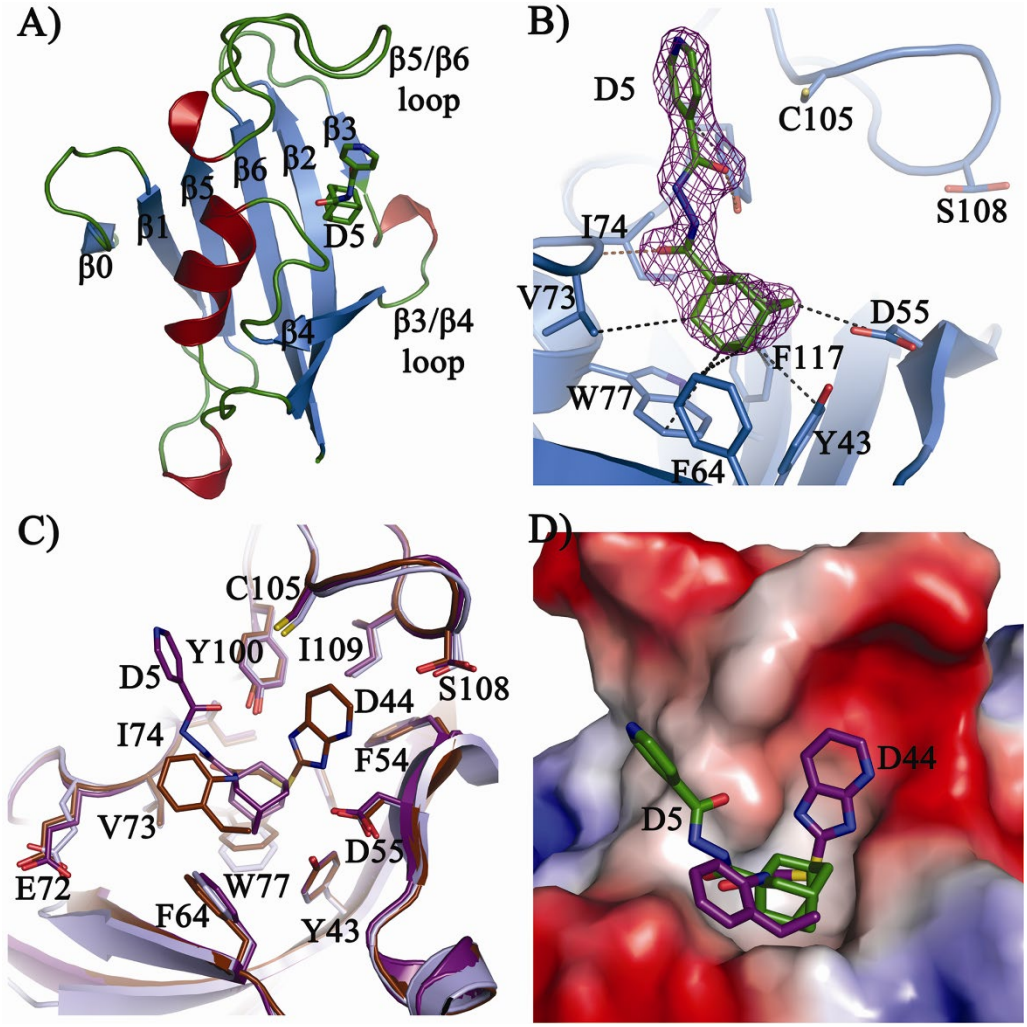

Fig 39: Plasmodium vivax FKBP35 crystal structure and D5 interactions. (A) Cartoon representation of the monomeric unit observed in the asymmetric unit of *PvFKBP*35-D5 complex. The secondary structure regions and the ligand are labeled for clarity. (B) The 2Fo-Fc electron density map contoured at 1.0 σ for ligand D5 showing the critical hydrogen bonded interactions with residues Ile74 and Tyr100 (brown colored dashes) and the non-bonded contacts (black dashes) made predominantly by the adamantyl ring. (C) The comparison of the active site residues of the crystal structure of the apo (blue white), D44 complex (brown) and the D5 complex (violet). Though most of the residues remain unperturbed, Trp77 can be seen moving away due to the thrust made by the adamantyl ring. (D) The electrostatic surface diagram of the *PvFKBP*35, comparing the orientation of the ligand D5 and D44, clearly showing the purine like ring of D44 occupying the larger pocket while the pyridine ring of D5 facing the pocket towards the surface.

Part II: FKBP38

III II Computer Assisted Drug Design of FKBP38 inhibitors

As described previously in introductory chapter I. 7.0, FKBP38 is a non-canonical FKBP family member which interacts with multiple proteins through its multiple domains (ERD, FKBD, leucine zipper motif, TPR, calmodulin binding domain and transmembrane (TM) domain). It mediates important and divergent physiological roles such as modulating the stability of its substrate proteins, apoptosis, neural tube development, hypoxia, cystic fibrosis, long QT and neurodegenerative disorders.

III.II.1 Approaches employed for identification of FKBP38 binding ligands

III.II.1.1 Fragment based de novo lead design

A literature survey on FKBP38 inhibitors showed two distinct inhibitors: i) DM-CHX which inhibits the PPIase activity of FKBP38 and ii) curcumin which was shown to inhibit FKBP38 mRNA levels by more than three fold in a lung adenocarcinoma -based micro-array study. I have attempted de novo ligand based design by utilizing the previously characterized specific FKBP38 inhibitor DM-CHX structure as a starting point to evolve fragments that bear no resemblance to DM-CHX and are entirely new in chemical space. In this direction, I have generated a common feature model from predicted bioactive conformations of DM-CHX in FKBP38 and proceeded with fragment based pharmacophore modeling. The common feature model showed 6 key pharmacophore groups - a hydrophobic feature, an acceptor, and a donor features on one side of the molecule and similarly one hydrophobic feature, two acceptors on the other side of the molecule. This 6 feature model is divided in to two fragments with three features each with a predefined link atom at C11 position for both the fragments (highlighted in red circle Fig.40).

A shape constraint was included on both the pharmacophore fragments A, B (Fig. 41A, B) to mimic the active site region of the molecule and to filter the non-specific fragments. These two fragment pharmacophores with shape constraint are screened against the Maybridge library and the fragment 1 query returned 290 hits while fragment 2 returned 88 hits that are fitting to these models. These fragments were joined at the predefined site to create whole molecules by using the ENUMERATE FROM FRAGMENTS protocol.

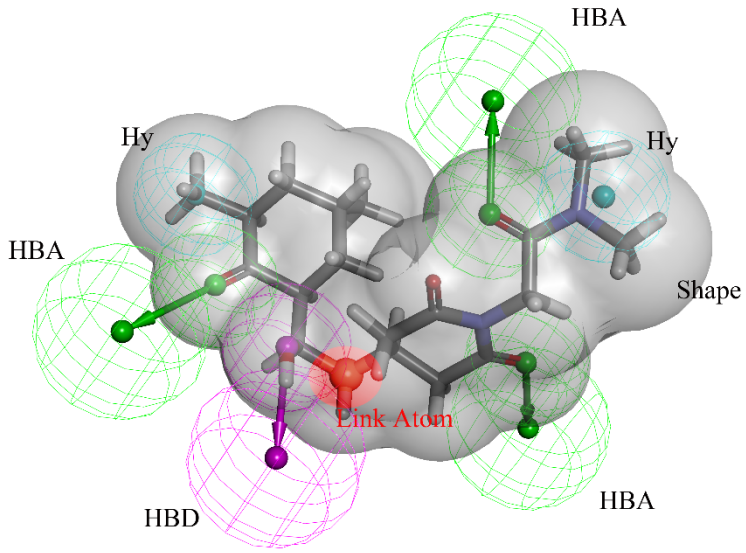

Figure 40: Reference pharmacophore of DM-CHX (N-(N', N'-dimethylcarboxamidomethyl) cycloheximide) **showing the important pharmacophore features of DM-CHX that were identified from common feature pharmacophore modeling and supplemented with a shape constraint to simulate the protein active surface. This reference pharmacophore is split into two fragments by defining C10 atom as the link atom (red circle).**

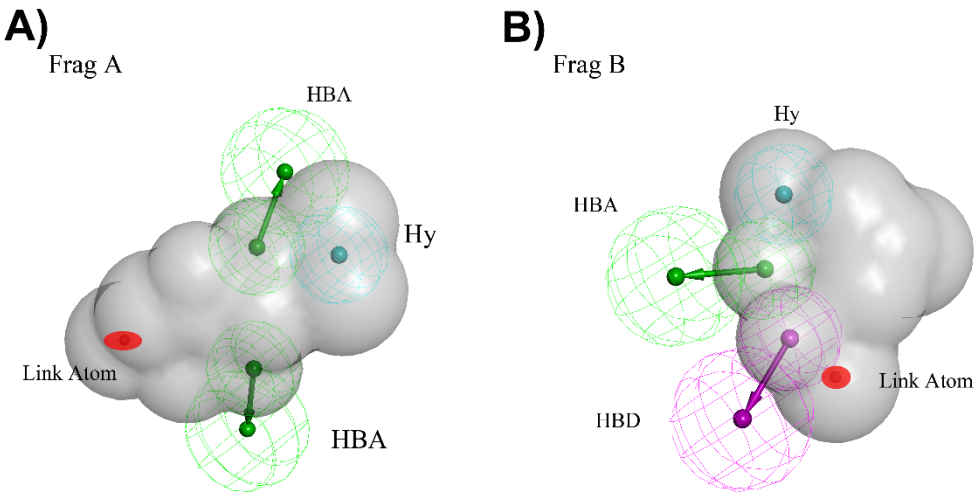

Figure 41: Fragment based de novo ligand design. A) The fragment (Frag A) which possesses the N, N-dimethylacetamide fragment in DM-CHX confers selectivity to FKBP38. An acceptor feature and hydrophobic feature targeting the N, N,-dimethylacetamide fragment are incorporated along with another acceptor feature targeting the keto group on the cycloheximide fragment. These features along with the C10 atom defined as link atom and a shape constraint included were employed to screen the Maybridge 3D library. B) The fragment (Frag B) comprises of a 2, 6,-dimethyl-cyclohexane fragment in DM-CHX. An acceptor feature, a donor feature and hydrophobic feature are included in the Frag B pharmacophore. These features along with the C10 atom defined as link atom and a shape constraint were employed to screen the Maybridge 3D library.

This generated a de novo combinatorial library from the hits obtained from the respective fragment queries. In the present situation as only one link atom is defined, closest atoms between the fragments from each source are fused by linking the fragments together.

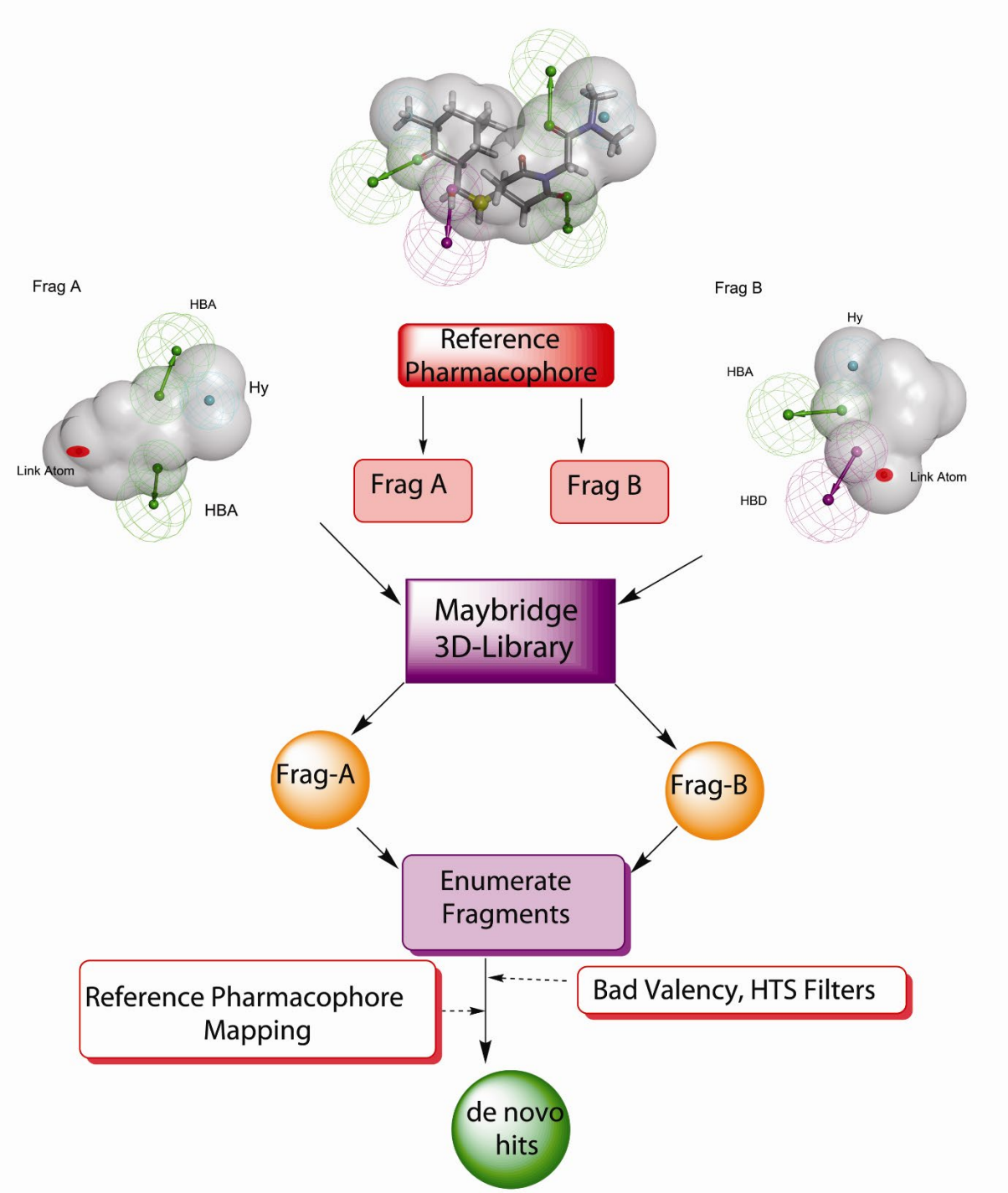

Figure 42: Scheme showing the fragment based de novo ligand design by pharmacophore enumeration. This protocol helps to generate de novo ligands even in the absence of protein information using the ligands surface pocket as a complementary filter to screen selective hits possessing similar pharmacophore features but yet structurally diverse molecules.

As shown in Fig. 42, ENUMERATE FROM FRAGMENTS protocol option produces a library containing all the combination of assembled fragments and link variation. The resulting ligands are standardized by neutralizing the molecules, hydrogens are adjusted accordingly, ligands with bad valency are filtered and finally energy minimized by using CHARMM force field to provide a de novo library. The generated de novo library is further filtered by mapping to the original common feature model and the ligands with fit values comparable to the reference compound can evaluated for consideration to synthesis feasibility. Shown in table VIII and in Fig. 43 and 44 are the best fitting compound that are generated de novo and can be sent to chemist for advice on synthetic possibility.

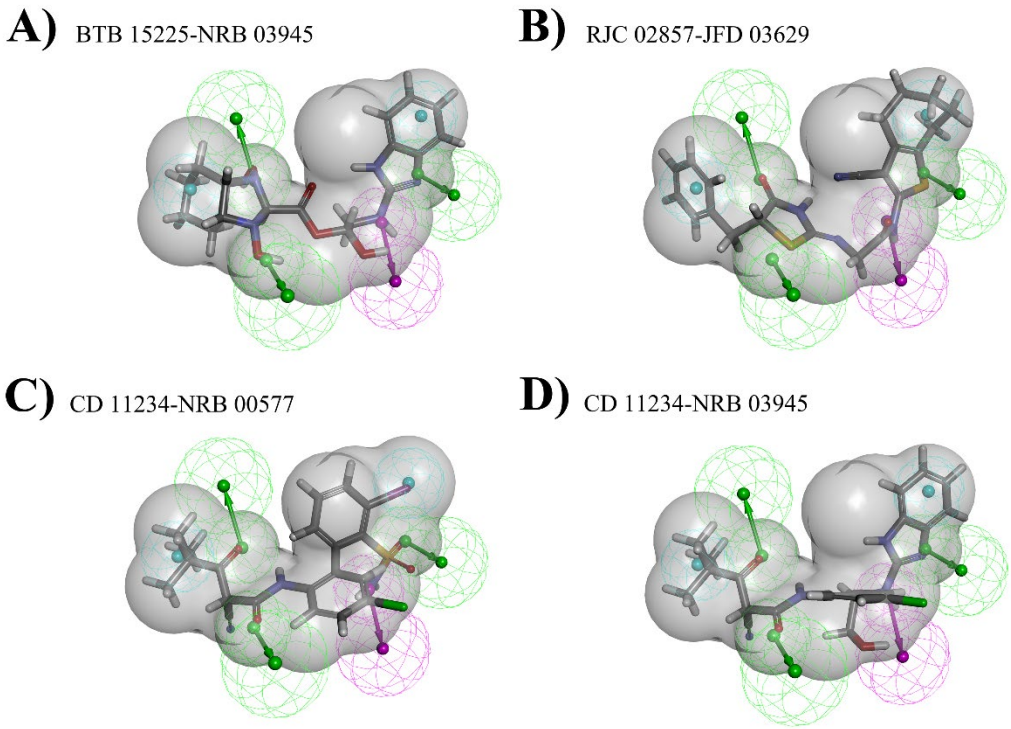

Figure 43: Enumerated whole molecules returned from the fragment pharmacophore; A, B, C and D show the best mapping of hits with the reference pharmacophore with shape constraint. These fragments hits can be assessed for synthesis or alternative substructure search with synthesized libraries and could yield hits that could be tried for experimental purposes.

Table VIII. Best twenty hits identified from the enumerated fragment library showing the mapping and their respective identification numbers in Maybridge library.

Sl.No	Enumerated library*	Fitness*	Frag-A	Frag-B
1	CD 11234-NRB 03945	5.57621	CD 11234	NRB 03945
2	CD 11234-NRB 00577	5.38108	CD 11234	NRB 00577
3	CD 11234-SPB 05877	5.37558	CD 11234	SPB 05877
4	CD11234-MWP 00830	5.34629	CD 11234	MWP 00830
5	KM00134-DSHS 0740	5.2501	KM 00134	DSHS 00740
6	CD 11234-CD 11531	5.24755	CD 11234	CD 11531
7	CD 11234-RJC 01093	5.22675	CD 11234	RJC 01093
8	BTB15225-NRB03945	5.20903	BTB 15225	NRB 03945
9	CD 00916-JFD 03629	5.20593	CD 00916	JFD 03629
10	JFD03391-NRB 00577	5.16904	JFD 03391	NRB 00577
11	BTB 15225-RF 02685	5.16512	BTB 15225	RF 02685
12	S 14255-RJC 01093	5.13665	S 14255	RJC 01093
13	S 09710-NRB 00667	5.13361	S 09710	NRB 00667
14	RJC02857-JFD 03629	5.12788	RJC 02857	JFD 03629
15	KM02168-MWP 00830	5.12162	KM 02168	MWP 00830
16	JFD 03391-JFD 03629	5.12161	JFD 03391	JFD 03629
17	BTB15225-WP01105	5.11634	BTB 15225	MWP 01105
18	CD 00397-JFD 03629	5.11496	CD 00397	JFD 03629
19	BTB 05702-CD 00397	5.11425	BTB 05702	CD 00397
20	CD 00861-JFD 03629	5.11264	CD 00861	JFD 03629

***Codes mentioned in enumerated library column as well as Frag A, B columns refer to the identifiers of the molecules in Maybridge library; Fitness refers to how best the compounds fit to the reference pharmacophore. Greater the fitness to the pharmacophore, greater would be the chance to being a true hit.**

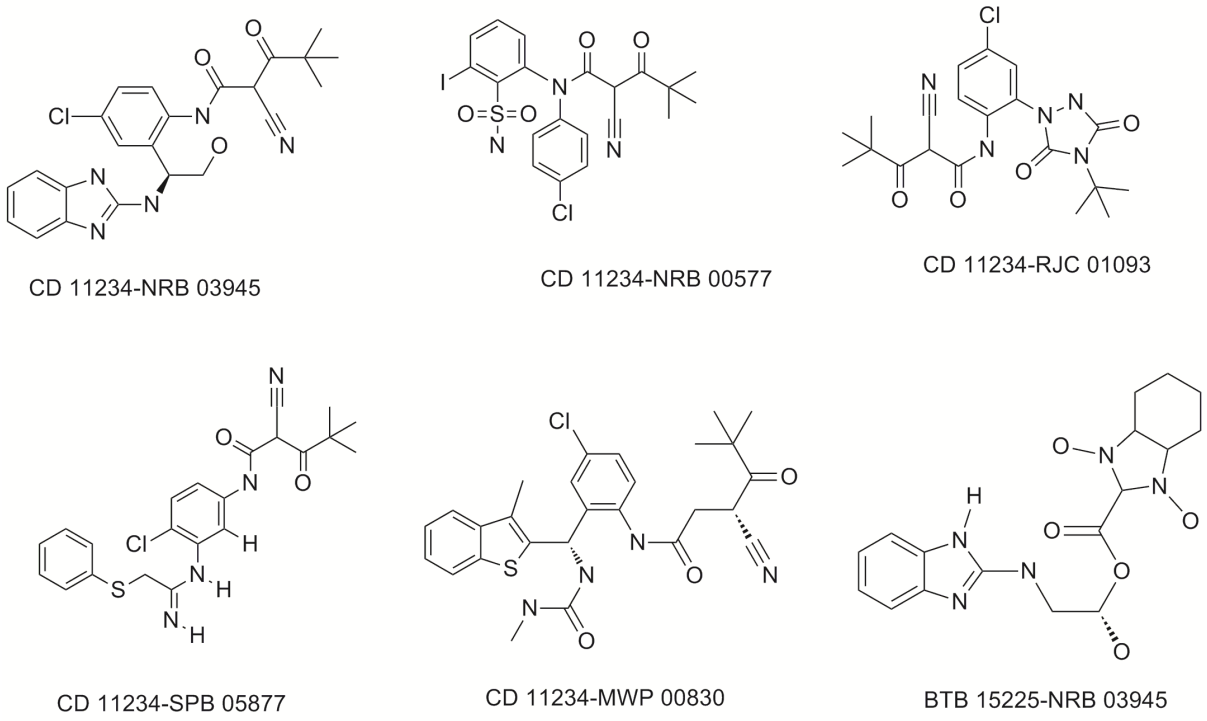

Figure 44: 2D structures of hits that had best mapping to the reference pharmacophore.

III.II.1.2 Structure based focused modeling on FKBP38.

Though fragment based method generates completely de novo compounds that fit to the reference pharmacophore but the main problem is their synthetic feasibility and has to be synthesized to proceed for experimental studies. Because of this limitation, we have proceeded with structure based pharmacophore screening on commercially available libraries.

As discussed previously in chapter II.2 and III.I.1, structure based focusing module in the Cerius^2 modeling environment was utilized to find novel ligands that could probably bind to the FKBP38. Though FKBP38 exhibits a typical “half β-barrel” fold similar to FKBP12, it lacks the 40-loop (Fig. 45) and most of the active site aromatic residues such as W59, and F36, F46 and F99 are changed to leucine. Furthermore, the residues (D36 and Y26 in FKBP12) involved in salt triad interaction are varied to Q138

and L127 respectively. Moreover, the H86 (FKBP12) or C106 in *Plasmodium* species is varied to a basic R184 (Fig. 46).

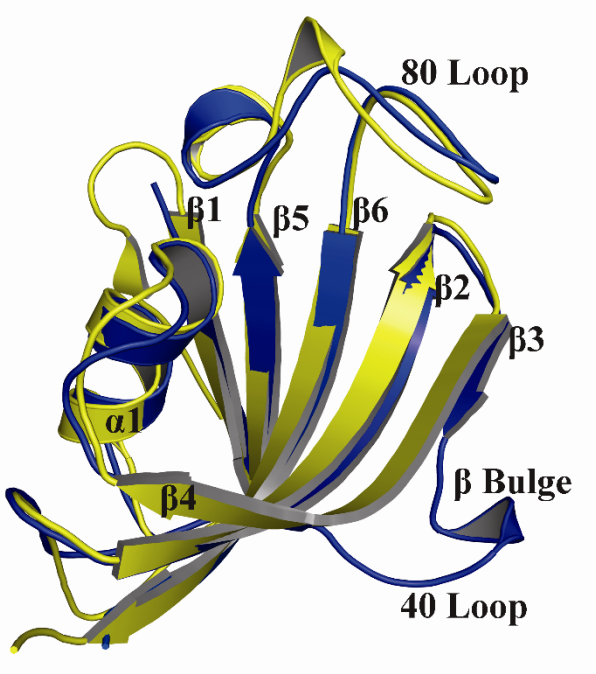

Figure 45: FKBP38 adopts a half β-barrel shape, it forms a β-bulge showing the lack of 40-loop which is known to play a key role in ligand binding. Yellow color cartoon represents the FKBP38 and the blue color cartoon depicts the FKBP12.

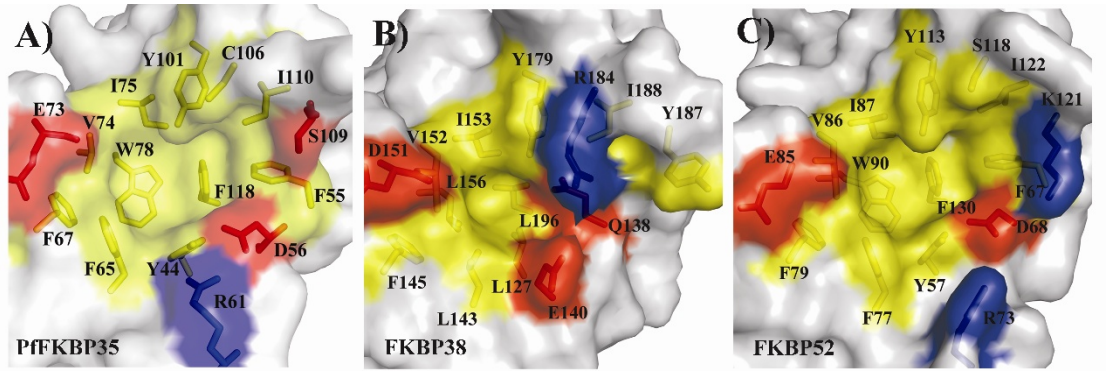

Figure 46: Comparison of Surface view of FKBP domain family members PfFKBP35, HSFKBP38 and HsFKBP52. The yellow regions are conserved hydrophobic regions, the blue color depicts the positively charged residues and the red color shows the negatively charged residues. Visual comparison of A and C with B shows the loss of residues such as tryptophan, phenylalanine, and aspartate result in a shallow and constricted active pocket. Further, R184 and Q138 substitutions further constrict the size of the ligand binding pocket.

As a consequence of these multiple changes, the active pocket is shallow in FKBP38 and neither accommodates FK506 nor shows PPIase activity. Therefore, using the varied residues of FKBP38 active site, I have chosen to build a three feature model targeting Ile153, Y179 and Q138 residues for hydrogen bonding interactions and L156, L127 and L196 residues for hydrophobic interactions as described previously (Fig. 47).

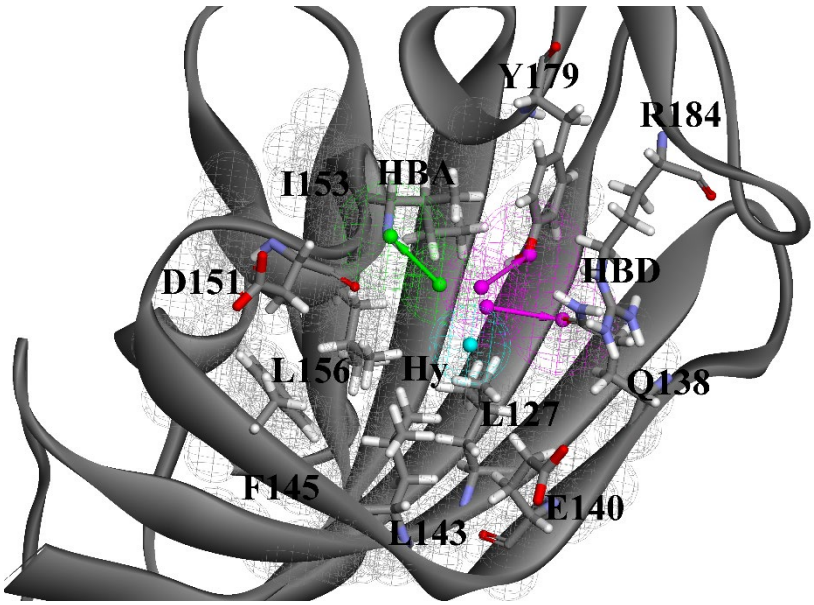

Figure 47: Receptor based pharmacophore model of FKBP38. Hierarchical clustering of interaction vector site points leads to four features with an HBA targeting Ile153, two HBD features targeting Tyr179 and Gln138 and a hydrophobic feature in vicinity of Leu127, Leu156 residues

After hierarchical clustering of these vector site points, an acceptor feature targeting isoleucine 153, two donor features targeting tyrosine 179 and glutamine 138 and a hydrophobic feature in the vicinity of the L156, L127, L196 residues were added with an exclusion model (black spheres) to prevent clashes of ligand atoms with proteins. Giving priority towards the most conserved such as I153, Y179, and aliphatic hydrophobic residues L127, L143 and L156, the donor feature targeting Q138 was manually removed from the model and a simplistic three feature model (Fig. 47) was employed for database screening of the Chemdiv 3D library. Database screening

yielded ~80, 000 ligands from this model. These ligands were further filtered by using ADMET filters and 5000 ligands with good predicted blood brain barrier penetration were selected for virtual screening. Molecular docking was carried out with default gold parameters as there is no bound ligand conformation to standardize the docking parameters. The GOLD docking solutions are further refined by rescoring with Ligscore versions 1 and 2, PLP - 1 and 2 versions, Chemscore, Jain, PMF, Ludi - 1, 2 and 3 versions, GLIDE SCORING and consensus scoring was applied to identify the ligands that are in consensus with all the scoring functions and 42 ligands possessing favorable interactions at the active site were manually selected for purchase from Chemdiv [Docking scores - Appendix (ii)].

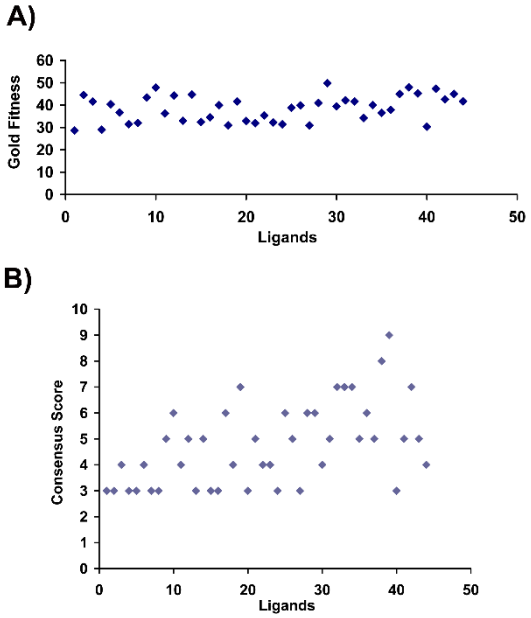

Figure 48: Sampling of FKBP38 focused library by GOLD scoring and consensus. A) Scatter plot of Gold Fitness showing the spread of docking score for the selected 42 molecules. B) Distribution of the selected 42 molecules and the number of scoring functions which are in agreement that the ligands would be the best hit that can be selected for experimental screening.

The scatter plots of gold fitness and consensus scoring of the purchased hits was as shown in Fig. 48A, B. Ligands were selected on the basis of interactions at the targeted residues together with their interaction energies and consensus scores.

Our in-silico virtual screening results suggest that hit D39, which is in agreement with most of the scoring functions possesses a quinoxaline scaffold sitting at the shallow cavity and makes extensive hydrogen bonding interactions with I153, Y179, Q138, and R184 residues (Fig. 49). Another hit having a similar scaffold, D19, having consensus with seven scoring functions and is predicted to sit into the shallow cavity making contacts van der Waals contacts with F145, L143, L196, and hydrogen bonding interactions with I153, R184 and D151 (Fig. 50). Similarly, hit 42 which possess an isoxazo[5,4-d]-pyrimidyl-piperidine scaffold was predicted to sit into the shallow cavity making contacts van der Waals contacts with L196, L127 and L156 and hydrogen bonding interactions with I153, D151 and R184 (Fig. 51). The 2D structures of best 10 hits are as depicted in Fig. 52. Further studies are awaited for characterization of activity with biochemical and cell based models.

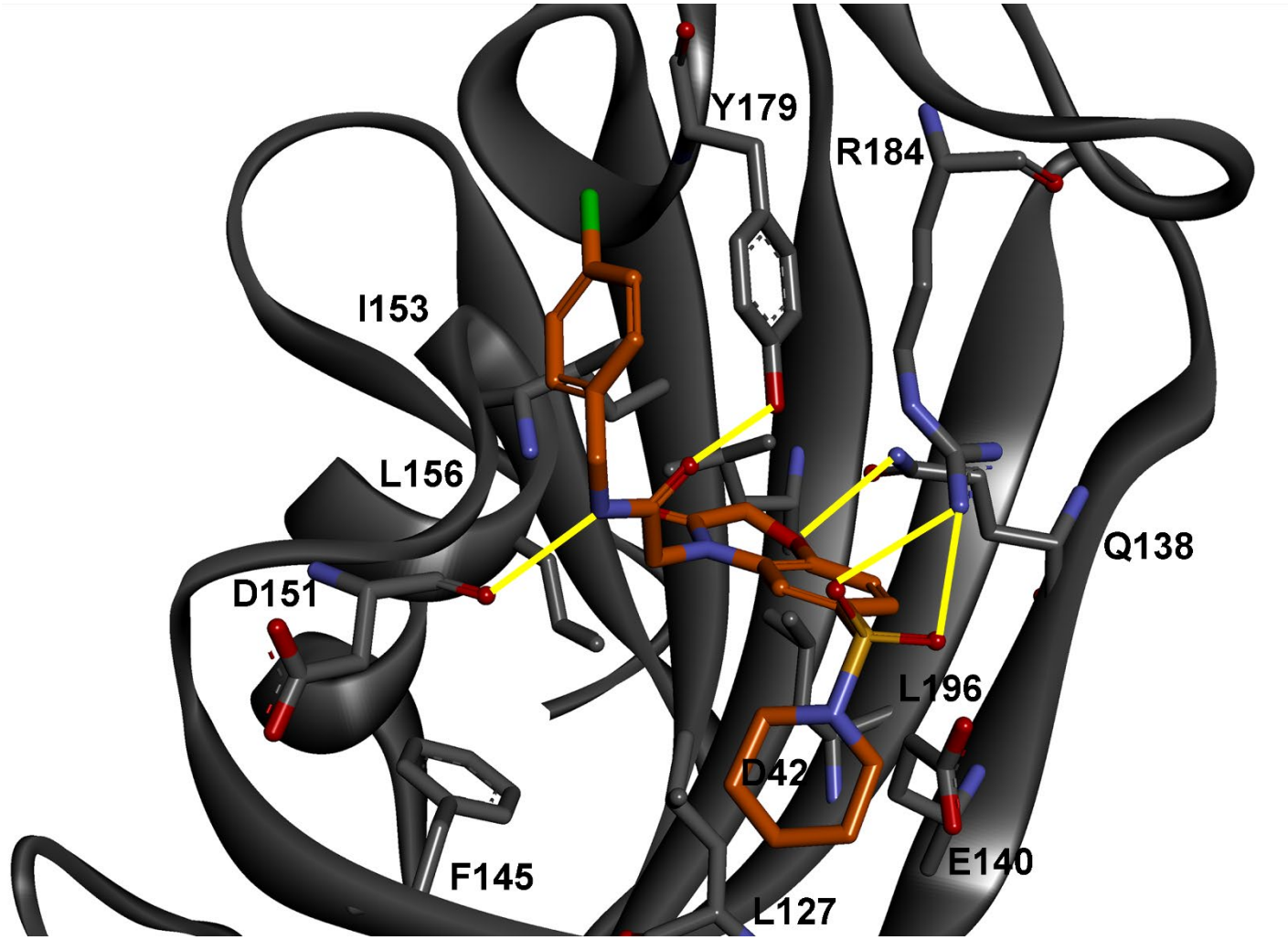

Figure 49: Predicted binding mode of the selected hit D39 which possesses a quinoxaline scaffold and is predicted to sit into the shallow cavity making hydrogen bonding interactions with I153, Y179, Q138 and R184.

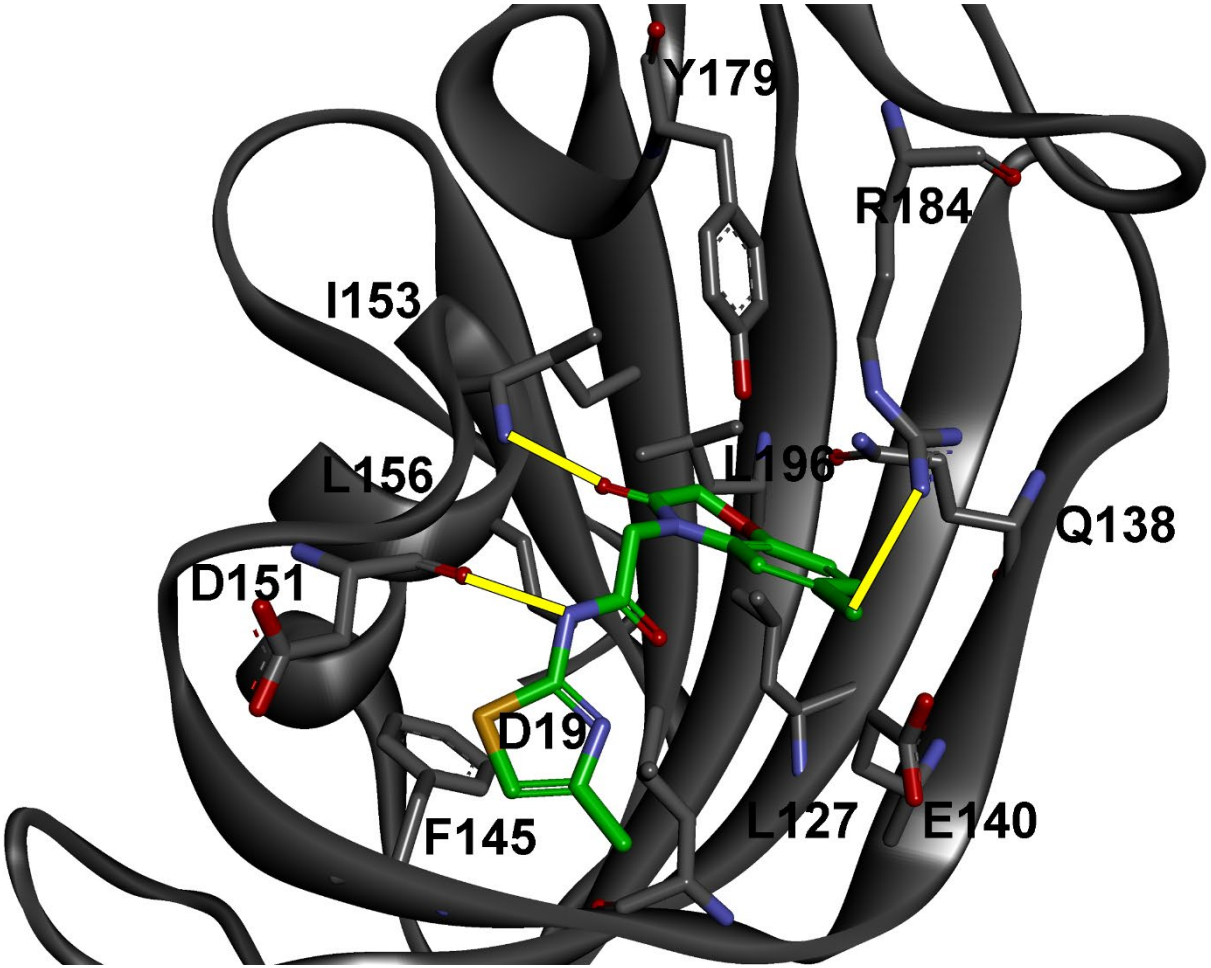

Figure 50: Predicted binding mode of the hit D19 which possesses quinoxaline scaffold and is predicted to sit into the shallow cavity making van der Waals contacts with F145, L143, L196, and hydrogen bonding interactions with I153, R184 and D151.

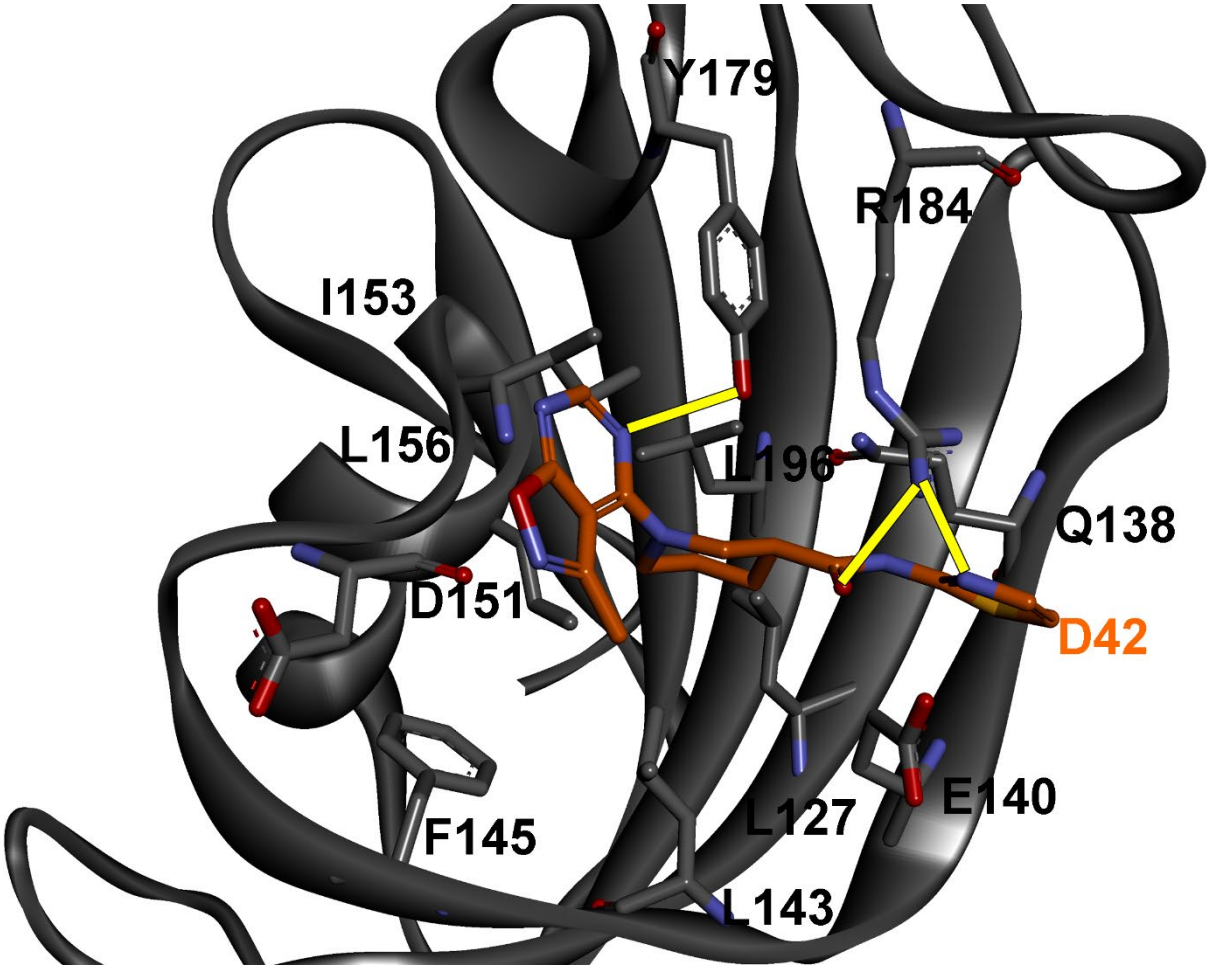

Figure 51: Predicted binding mode of D42 which possess an isoxazo[5,4-d]-pyrimidyl-piperidine scaffold and is predicted to sit into the shallow cavity making van der Waals contacts with L196, L127, L156 and hydrogen bonding interactions with I153, D151 and R184.

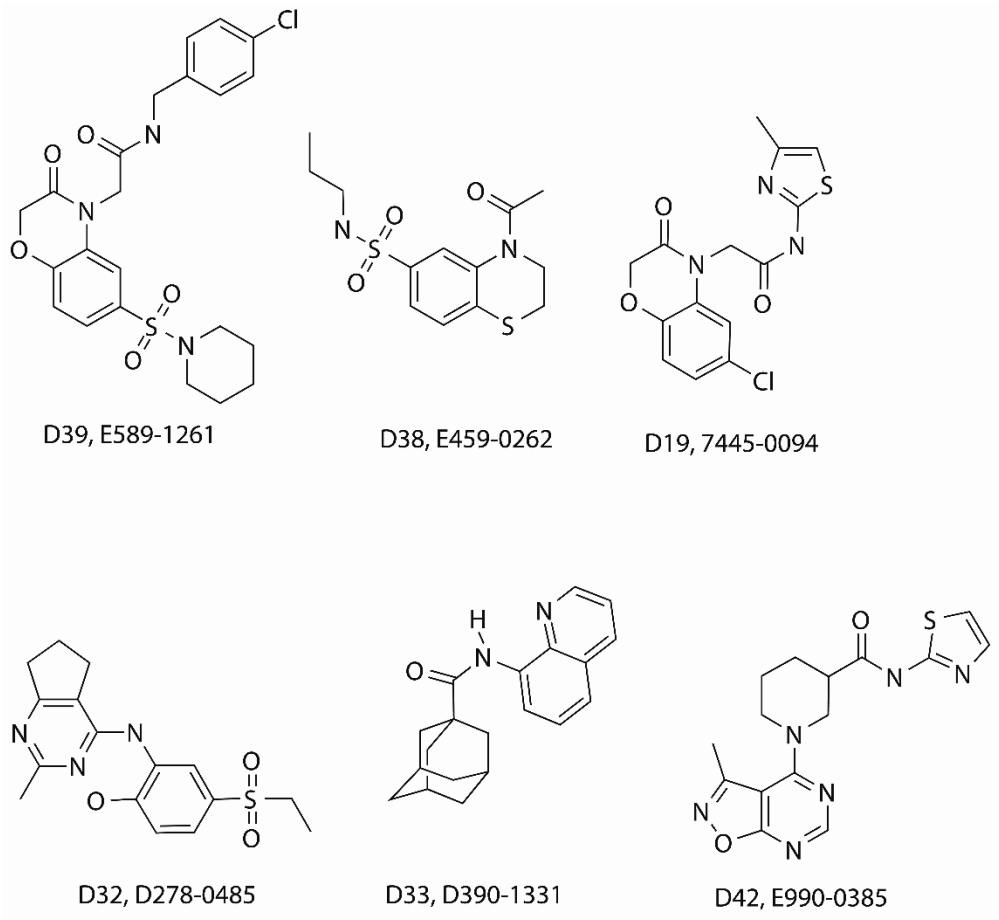

Figure 52: 2D structures of top hits from consensus scoring selected for purchase

IV. Conclusions

1) Our de novo approach has identified a novel small molecule antagonist (D44) of *Plasmodium* FKBP35 and demonstrated its activity at sub-micromolar concentration on both the growth inhibition of P. falciparum as well as PfFKBP35 enzyme inhibition. Crystal structures of *Plasmodium* FKBP35 in complex with D44 further confirmed the selectivity of ligand to *P. falciparum* and *P. vivax* FKBP35. D44 did not show appreciable inhibition of either FKBP12 or FKBP52 enzymatic activity even at concentration as high as 10 μM. The ability of D44 and D5 to bind to *Plasmodium* vivax FKBP35 and inhibits its enzymatic activity could open up avenues to prevent the relapsing form of malaria infection caused by *P. vivax.* Thus the information obtained from this study could be used to design selective small molecule inhibitors that bind to the parasite FKBP and potentially antagonize its function in the parasite life cycle.

2) Our analog - based drug design helped us to identify potential hits that could bind selectively to *Plasmodium* FKBP35. This study has identified chromone and adamantyl derivatives that are predicted to have inhibition constant (K_i) in the nanomolar range. From these hits, adamantyl derivatives - supradamal (SRA / D5), SRA51, and SRA52 have shown sub-micromolar efficacy in in vitro *Plasmodium* growth inhibition and enzyme inhibition studies. Crystallographic complex of SRA or D5 clearly shows that the adamantyl derivative D5/SRA binds to the canonical FKBP 'S1' site and orients away from the S2 site which is critical for many protein-protein interactions such as calcineurin, IP_3 receptor and TGF-β signaling. Therefore the smaller ligands D5 binding to FKBPs doesn’t affect the crucial protein-protein interaction.

3) Fragment-based approaches and structure-based drug design on FKBP38 suggested new de novo ligands that might have a high probability of binding to FKBP38 and achieving neuronal protection and regeneration in cell culture and animal studies.

V Future Prospects of hits identified in this thesis.

A) The leads identified in this thesis D44 and SRA targeting *Plasmodium* FKBP35 are initial leads and these have to be further optimized to improve their efficacy in parasite growth inhibition and a comprehensive structure activity relationship study has to be done to clearly identify the key groups that are essential for the activity. D44 with its purine like ring is nicely sits into S2 site of Plasmodium FKBP35 whereas adamantine ring in D5 fits into the S1 site Therefore, further improvements can be done on adamantyl ring by extending substitutions to the purine ring of D44 (S2 site). Biosteric groups or groups resembling purine like ring such as indole, indazole, napthyl or benzo-pyrimidine rings might improve the activity.

B) Hits identified in the FKBP38 project have to be experimentally characterized to identify potential lead-like compounds and their utility in variety of neurodegenerative disease models like Parkinson's disease, Alzheimer disease and Tau related neurodegenerative diseases.

VI Glossary

AKT: A serine/threonine protein kinase that regulates apoptosis, cell migration, transcription, proliferation and glucose metabolism.

Chemical Shift: The chemical shift is the resonant frequency of a nucleus relative to a standard. Often the position and number of chemical shifts are diagnostic of the structure of a molecule by nuclear magnetic resonance (NMR) spectroscopy.

E-C coupling: Excitation–contraction (EC) coupling is a term used to describe the physiological process of converting an electrical stimulus to a mechanical response.

FKBP51: 51-kDa FK506 binding protein that binds the immunosuppressive drug FK506 but does not interact with calcineurin and does not suppress the immune system.

FKBP52: 52-kDa FK506 binding protein that binds the immunosuppressive drug FK506 but does not interact with calcineurin and does not suppress the immune system.

FK1 domain: FKBP12-like domain 1 of FKBP51 and FKPB52, responsible for binding to FK506, for PPIase activity and for steroid hormone receptor regulation.

FK2 domain: FKBP12-like domain 2, present in FKBP51 and FKBP52; differs slightly from the FK1 and lacks PPIase and FK506 binding ability.

FK506: also called tacrolimus, a macrolide drug that complexes with FKBP12 and inhibits calcineurin phosphatase activity. This leads to immune suppression by blocking T-cell signal transduction cascades and interleukin-2 transcription.

Hsp90: The 90-kDa heat shock protein is a molecular chaperone involved in protein folding, tumor repression and cell signaling. Steroid hormone receptors require association with Hsp90 to fold to a conformation capable of binding to a ligand.

Hypothalamus pituitary adrenal (HPA) axis: interactions between the hypothalamus, the pituitary gland and the adrenal glands are crucial parts of the neuroendocrine system. This pathway is responsible for the regulation of stress reactions, energy storage and output, emotion and affect, sexuality, digestion and the immune system.

NF-AT: Nuclear factor of activated T-cells refers to a family of transcription factors that are important for mediating immune responses.

PPIase activity: Peptidyl-prolyl *cis-trans* isomerase activity catalyzes cis–trans isomerization reactions of peptide bonds involving the amino acid proline. PPIase activity is required for the proper folding of several, but not all, proteins.

Tau: Tau proteins are found primarily in neurons of the central nervous system and normally help in microtubule stabilization. Defective folding of tau and the resultant agglomeration are associated with neurodegenerative diseases such as Alzheimer's and Parkinson's diseases.

TPR domain: The tetratricopeptide repeat is a structural motif used in protein-protein interactions. The TPR domains on FKBP51 and FKBP52 bind specifically to the extreme C terminus of Hsp90.

VII Abbreviations & Symbols

3D	Three-dimensional
CaM	Calmodulin
CaN	Calcineurin
CFTR	Cystic fibrosis transmembrane conductance regulator
Cyp	Cyclophilin
DM-CHX	(N-(N', N'-dimethylcarboxamidomethyl) cycloheximide)
DTT	Dithiothreitol
FAT	FRAP/TOR, ATM, TRRAP
FKBD	FK506 Binding Domain
FKBP	FK506 Binding Protein
FPLC	Fast Performance Liquid Chromatography
HDAC	Histone deacetylase
HEPES	4-(2-hydroxyethyl)-1-piperazineethanesulfonic acid
HERG	human ether-a-gogo-related gene -
HIF-a	Hypoxia inducible factor alpha
HPA	hypothalamus pituitary adrenal axis
HSQC	Heteronuclear single quantum coherence sspectroscopy
IPTG	Isopropyl-β-D-thio galactoside
LB	Luria Bertani

PAGE	Poly Acrylamide Gel Electrophoresis
PGC-1 α	Peroxisome proliferator-activated receptor gamma co-activator 1-alpha
PHD-2	Prolyl hydroxylase-2
PHLLP	PH domain leucine-rich repeat protein phosphatase
pNA	para-nitroaniline
PPIase	Peptidyl-prolyl cis-trans isomerase
Sdc1	Syndecan1
SDS	Sodium dodecyl sulphate
SERCA	Sarco/endoplasmic reticulum Ca^{2+}-channels
TGF-β	Transforming growth factor β
TPR	Tetratricopeptide repeat
TSC	Tuberous sclerosis complex
YY1	Yin-Yang1

VIII. Tables

IX Figures

X Appendix (i): Scoring of PfFKBP35 virtual Screening solutions

Among the employed of GOLD, GLIDE SCORE, Ludi, PLP1, PLP2, PMF, JAIN, scoring functions ligands which are in agreement with more than three scoring are further considered for visual analysis. After careful interaction pattern analysis, ligands with favorable interactions are selected from this pool.

Index	IDNUMBER	Consensus	GoldFitness	LUDI_ 1	LUDI _2	LUDI_3	LS1	LS2	(-PLP1)	(-PLP2)	JAIN	(-PMF)
4	C796-0230	**9**	59.7456	494	464	877	1.89	3.87	77.31	82.68	5.13	167.47
8	C153-0563	**9**	55.362	328	327	797	1.59	4	66.14	68.11	5.11	170.57
16	**C797-1158**	**9**	52.4886	380	361	723	1.79	3.89	55.58	60.04	5.05	155.31
21	C797-1113	**9**	51.5845	386	336	761	1.63	3.75	56.21	61.77	4.54	156.11
22	7380-0028	**9**	51.4355	487	399	814	2.2	4.69	76.06	78.3	3.63	167.14
31	C153-0580	**9**	50.5616	367	363	822	1.92	4.26	71.13	75.12	4.51	197.17
32	C791-0405	**9**	50.3118	300	287	817	1.88	4.58	61.38	64.47	3.79	180.33
47	C794-0026	**9**	48.9934	461	429	630	2.37	3.87	66.39	64.62	4.25	160.02
80	C163-0167	**9**	47.3068	344	356	504	3.04	3.98	79.19	72.05	4.04	182.35
113	7388-0008	**9**	45.5152	423	414	658	2.92	4.09	64.79	64.04	4.48	156.68
137	7846-1092	**9**	44.2491	467	423	671	2.32	4.2	56.86	68.39	3.96	182.43
138	0832-2903	**9**	44.242	301	352	469	2.31	4.42	64.55	67.89	4.17	176.6
140	0KPI-0112	**9**	44.2204	332	337	302	1.87	4.37	56.1	56.5	4.17	172.67
158	1000-0653	**9**	43.7231	405	387	584	1.82	3.89	64.68	66.68	4.46	153.25
170	5348-0112	**9**	43.4456	384	337	870	1.73	4.12	61.13	62.71	4.28	154.99
185	0111-0171	**9**	43.0539	453	427	402	2.71	4.51	61.14	62.3	4.44	174.46
196	0167-0239	**9**	42.7381	393	351	831	2.6	4.69	65.52	63.73	3.58	153.67
197	0417-1813	**9**	42.727	452	411	378	2.26	4.35	68.92	67.87	3.82	183.87
208	0488-0160	**9**	42.2556	481	412	705	1.5	3.72	61.1	62.8	3.82	182.62
253	0214-0027	**9**	41.2797	388	361	782	1.79	3.92	53.46	59.66	4.59	165.61
254	0KPI-0095	**9**	41.2648	401	365	336	3.07	4.54	59.73	59.72	3.9	175.26
263	0111-0179	**9**	40.9281	309	333	297	1.74	4.26	56.07	58.54	3.92	174.47
264	C155-0196	**9**	40.8922	348	343	392	3.03	4.02	64.67	58.55	3.55	157.47
270	0334-0093	**9**	40.7145	444	438	408	1.95	4.23	65.14	66.42	5.97	170.57
2	C782-0473	**8**	59.8065	361	411	918	1.4	4.61	90.21	89.1	4.78	184.08
3	C796-0227	**8**	59.7778	405	405	704	1.58	4.67	76.22	78.64	5.39	174.22
5	C156-[1]0038	**8**	55.7523	310	309	720	3.19	4.91	64.31	67.54	3.74	158.85

6	7213-0290	**8**	55.5807	399	391	855	3.36	3.75	55.27	67.42	4.15	171.2
10	C174-1209	**8**	55.0472	374	372	827	2.02	3.92	54.05	63.22	4.62	180.65
11	C796-0235	**8**	55.0138	423	402	591	2.44	4.71	80.6	83.82	4.73	173.77
15	C163-0059	**8**	53.9929	374	392	640	2.96	3.78	64.28	58.6	4.14	165.68
17	C153-0647	**8**	52.4261	369	398	862	1.67	3.95	70.58	78.97	5.8	177.74
18	C166-0079	**8**	52.159	266	300	660	2.04	4.53	61.78	62.27	4.1	186.84
28	7213-0282	**8**	50.7529	299	296	561	1.9	4.43	63.5	61.29	0.92	153.64
30	C173-0577	**8**	50.7013	479	440	665	2.8	4.49	75.12	72.46	4.13	163.34
33	C782-0037	**8**	50.2662	445	433	1,003	1.19	4.59	88.91	88.48	4.99	181.37
34	C791-0484	**8**	50.2488	319	332	862	1.74	4.27	59.46	61.77	4.01	163.46
36	0106-0155	**8**	50.0865	332	359	495	1.66	3.96	71.07	70.74	4.4	168.1
38	C166-0172	**8**	49.5867	393	390	422	1.99	5.21	63.78	65.11	3.83	163.88
41	C785-1499	**8**	49.3896	394	388	679	1.92	4.42	69.7	65.52	3.42	184.74
42	C782-0017	**8**	49.3288	394	404	923	1.47	4.99	86.8	84.58	4.34	175.46
43	C782-0018	**8**	49.1398	451	441	846	1.42	4.06	82.25	83.55	5.48	181.38
44	C776-3405	**8**	49.0759	441	407	869	1.76	3.64	68.08	75.5	6.36	175.43
46	C791-0329	**8**	49.0423	373	347	879	1.96	3.67	75.66	78.99	4.57	178.03
50	C791-0402	**8**	48.758	374	353	940	1.64	4	72.12	71.51	4.59	156.02
51	C797-0209	**8**	48.5737	374	350	878	1.94	3.92	59.35	59.01	4.54	210.65
52	0934-0574	**8**	48.5203	467	418	434	3.29	4.8	66.18	66.62	4.19	199.6
56	C791-0359	**8**	48.2822	406	373	965	1.65	3.9	66.88	73	5.29	156.26
58	0685-0080	**8**	48.2594	371	361	568	2.89	3.72	50.32	57.01	3.85	160.67
60	C172-0541	**8**	48.1927	368	361	479	2.98	5.28	65.57	66.96	4.02	157.92
61	C797-0041	**8**	48.1808	425	424	828	0.91	3.8	70.06	71.55	5.01	164.87
62	C188-0323	**8**	48.1625	489	429	951	2.3	4.59	69.04	68.78	4.53	160.11
63	C797-0047	**8**	48.1037	378	409	929	1.54	5.01	68.79	71.57	4.55	182.75
64	1030-0093	**8**	48.0902	314	341	318	2.51	4.59	76.69	75.27	4.19	175.81
65	C796-0232	**8**	48.0058	457	434	682	2.53	4.46	69.37	72.56	6.2	181.18
66	C785-0999	**8**	47.9544	270	310	260	1.52	4.09	55.93	59.82	3.56	148
68	C782-0029	**8**	47.9014	409	416	991	1.1	4.31	77.42	79.19	5.52	171.41
72	8001-0257	**8**	47.7091	262	287	535	1.73	3.61	59.03	61.47	4.86	171.99
73	C782-0101	**8**	47.6632	374	393	817	2.22	5.17	54.06	68.27	4.35	184.66
75	7287-0188	**8**	47.5912	396	342	816	1.57	4.04	54.56	55.61	3.55	127.36
76	C163-0286	**8**	47.5871	382	405	598	2.28	4.02	74.48	68.96	3.39	157.2
77	C776-3278	**8**	47.5419	329	337	695	1.65	4.18	64.67	63.57	4.69	186.64

78	C797-1621	**8**	47.4732	341	356	939	3	4.62	56.23	55.39	3.56	115.7
81	7388-0005	**8**	47.2934	435	431	575	2.33	4.32	70.66	64.31	4.06	157.72
84	C166-0164	**8**	46.8359	236	282	538	1.56	4.16	64.73	64.7	3.2	184.41
86	C156-0092	**8**	46.8075	342	340	739	2.3	4.16	61.79	57.45	2.52	181.79
89	C794-0024	**8**	46.6225	390	366	559	2.21	4.21	61.68	60.9	2.91	156.47
91	7571-0844	**8**	46.5677	420	369	627	1.54	1.77	55.73	60.87	4.04	168.28
94	7571-0843	**8**	46.4793	507	454	700	1.52	2.48	57.49	63.45	3.7	171.12
95	C795-0382	**8**	46.4547	537	477	837	1.93	3.49	52.15	57.51	5.43	156.38
99	C798-0013	**8**	46.2292	365	350	710	1.75	3.95	60.46	59.51	3.7	154.45
100	C174-0236	**8**	46.1287	344	340	598	1.85	3.94	63.53	62.69	4.94	131.8
102	C797-0031	**8**	46.0544	315	322	795	1.93	4.42	67.03	59.17	2.82	153.11
107	C776-3394	**8**	45.8913	335	376	787	2.42	4.46	69.35	69.86	4.76	187.9
109	5928-0059	**8**	45.8291	464	404	671	2.07	3.69	64.43	68.86	5.62	185.18
110	C163-0285	**8**	45.7334	415	402	587	2.29	3	58.6	63.62	3.54	160.77
115	7591-0713	**8**	45.3972	417	390	678	2.46	3.98	59.47	60.67	5.34	174.66
118	C782-0062	**8**	45.3452	427	395	812	1.69	5.42	85.28	82.61	4.21	177.95
120	0945-0267	**8**	45.3085	439	397	651	1.54	3.78	54.14	56.76	3.48	138.04
121	4130-5852	**8**	45.279	426	369	665	1.77	3.86	59.98	62.19	4.02	170.16
123	7599-0949	**8**	45.03	420	359	1,172	1.98	4	62.92	63.46	3.86	110.05
124	7954-4278	**8**	44.9992	434	406	431	2.34	4.57	75.42	75.25	3.25	170.35
126	C156-0188	**8**	44.9603	368	367	625	2.03	4.3	72.45	71.82	5.52	136.33
128	0848-0061	**8**	44.9263	486	411	661	1.64	3.95	54.93	61.08	5.08	136.93
129	C187-0123	**8**	44.7877	346	343	819	1.83	3.65	62.64	64.4	4.36	157.58
134	1000-0654	**8**	44.3811	378	374	581	1.67	3.71	53.89	59.61	3.57	153.86
139	C190-0420	**8**	44.2266	230	263	449	2.9	4.49	61.5	66.22	4.36	165.24
141	C797-0070	**8**	44.2202	348	356	882	2.17	3.9	71.18	66.27	3.39	75.23
142	C791-0328	**8**	44.0653	415	384	906	1.93	3.73	74.95	75.98	4.12	178.6
143	4883-0040	**8**	44.0411	374	356	828	1.95	3.99	60.24	63.11	3.46	171.3
147	C174-1038	**8**	43.9014	408	373	572	2.27	4.13	60.68	62.23	4.84	137.35
151	0272-0175	**8**	43.8181	411	377	616	1.61	3.84	55.04	62.6	3.56	165.92
154	C174-0238	**8**	43.7926	344	305	559	1.9	4.13	63.87	64.56	4.89	131.47
156	C191-0018	**8**	43.7443	335	337	865	1.97	3.71	61.9	66.22	4.93	156.55
160	C782-1462	**8**	43.6916	490	453	794	1.88	4.08	52.94	56.28	5.86	170.47
162	C153-0664	**8**	43.6336	343	321	726	1.57	4.21	69.2	70.64	3.24	185.57
165	C776-0109	**8**	43.6008	406	384	839	1.89	4.46	77.1	75.77	4.2	180.3

168	C166-0044	**8**	43.5447	367	366	667	1.83	4.03	62.14	62.36	4.15	168.42
169	C779-1383	**8**	43.4616	427	388	573	2.19	3.74	62.31	66	4.51	142.54
176	0342-0097	**8**	43.2696	531	450	930	2.39	4.49	54.4	55.68	3.26	134.08
178	C155-0390	**8**	43.2192	249	266	302	1.99	3.76	66.15	67.02	3.61	151.61
180	C156-0147	**8**	43.2094	333	340	467	1.87	4.07	70.86	65.4	3.74	130.27
181	C181-0902	**8**	43.2046	295	309	673	2.23	4.29	53.87	59.34	4.4	175.02
182	0889-0036	**8**	43.1547	418	390	745	1.99	3.99	57	60.53	5.07	166.44
191	0162-0062	**8**	42.8772	427	383	424	2.02	3.84	62.82	65.03	6.24	187.1
192	C797-0283	**8**	42.8769	424	400	1,040	1.75	4.78	86	86.44	5.75	167.75
198	C795-0467	**8**	42.7106	422	403	808	1.5	3.95	61.81	66.52	3.96	168.37
200	0418-0143	**8**	42.6964	327	343	322	1.95	4.22	55.72	57.46	3.34	173.27
201	C174-0172	**8**	42.611	337	361	493	2.33	5.01	60.78	63.28	3.43	137.75
203	C797-0184	**8**	42.465	411	393	799	0.89	3.78	68.06	69	4.49	180.18
206	C175-0098	**8**	42.3273	425	347	813	2.52	4.31	56.09	57.36	3.19	168.15
207	0417-1816	**8**	42.3118	329	322	295	1.91	4.22	55.81	56.56	2.64	168.65
212	0140-0002	**8**	42.2047	280	305	287	1.07	4.13	57.22	60.03	3.66	171.31
213	C175-0078	**8**	42.183	448	381	851	2.46	3.92	54.68	58.86	4.29	163.79
215	1000-0685	**8**	42.1237	334	335	580	2.3	3.9	58.87	59.07	3.37	160.79
221	1000-0658	**8**	42.0335	419	396	587	1.87	3.63	57.31	60.25	4.08	153.12
222	7591-0886	**8**	41.9725	395	364	449	1.69	3.65	63.77	64.82	3.9	168.93
223	C175-0139	**8**	41.9484	434	352	868	2.51	3.93	55.79	60.09	3.54	179.29
224	C174-0534	**8**	41.939	366	353	582	1.59	3.86	56.23	57.75	3.44	136.14
227	0242-0461	**8**	41.9078	283	275	538	2	3.86	52.52	51.26	3.99	159.08
229	0291-0021	**8**	41.8344	405	380	577	2.2	4.19	53.28	54.44	3.19	157.24
232	C781-0261	**8**	41.8145	360	353	1,154	1.61	3.86	61.65	60.67	3.65	192.96
234	C791-0198	**8**	41.7964	528	488	802	1.79	4.09	64.63	63.6	3.96	119.44
235	C797-0294	**8**	41.7708	375	374	902	1.77	4.98	73.41	75.12	5.33	195.67
236	C153-0183	**8**	41.765	387	354	830	1.89	3.66	77.96	78.22	4.92	201.38
240	0418-0121	**8**	41.6167	408	368	352	1.78	3.52	52.66	59.51	4.19	179.21
243	7658-1728	**8**	41.5695	453	367	619	2.19	4.22	60.78	64.33	3.38	155.63
244	0255-0077	**8**	41.5674	281	291	776	1.88	4.25	62.87	60.27	3.79	145.59
245	C797-0158	**8**	41.4886	366	384	811	1.65	5.2	79.01	76.12	4.22	165.02
248	C168-0116	**8**	41.4207	399	364	504	2.36	4.46	85.79	85.15	3.47	157.27
251	0120-0009	**8**	41.373	366	339	822	2.06	4.49	61.38	61.12	4.15	148.26
255	0992-0060	**8**	41.2367	431	391	651	1.49	3.68	55.7	60.93	5.18	155.59

257	7472-0016	**8**	41.0791	470	418	584	2.42	4.47	69.13	69.5	3.59	153.03
258	0180-0339	**8**	41.0677	542	461	943	2.38	4.52	57.52	58.67	3.41	133.48
269	C782-0136	**8**	40.7887	405	417	764	1.33	4.8	87.34	83.18	4.57	183.95
278	C797-0361	**8**	40.5154	359	367	959	1.59	4.43	71.58	73.89	4.06	172.18
280	7445-0095	**8**	40.5034	351	345	825	1.74	3.85	56.86	60.11	3.1	152.67
281	0167-0131	**8**	40.4096	240	270	744	1.7	3.59	63.78	66.62	3.73	154.71
283	C191-0025	**8**	40.3266	377	344	870	1.66	3.69	50.17	55.21	3.66	173.95
286	C174-0237	**8**	40.2536	387	358	606	1.57	3.72	65.61	65.22	4.87	144.8
295	0KPI-0040	**8**	40.0738	281	313	297	2.1	4.24	53.09	53.92	4.1	159.82
296	C796-0417	**8**	40.0149	406	399	913	1.55	4.53	78.01	74.97	3.9	155.31
1	7839-0014	**7**	60.6107	388	386	628	2.03	4.2	60.16	64.8	4.38	131.08
7	C175-0038	**7**	55.4676	458	381	789	2.08	3.23	54.38	60.42	6.02	152.72
9	C153-0492	**7**	55.0711	283	318	853	1.39	3.87	65.28	68.56	4.85	183.96
12	7297-0005	**7**	54.7209	442	391	915	1.91	2.59	65.06	72.69	3.54	99.23
13	C796-0466	**7**	54.3215	520	458	702	2.13	4.4	79.51	84.58	5.62	168.63
14	0832-2790	**7**	54.1204	420	392	462	1.95	3.86	65.4	70.54	5.94	200.76
19	C796-0241	**7**	52.0181	382	391	804	1.02	3.77	58.27	59.8	5.05	166.84
20	C153-0658	**7**	51.7379	355	363	829	0.72	2.06	67.57	63.96	4.66	172.33
23	C153-0609	**7**	51.3159	375	369	731	1.7	3.74	80.83	85.03	5.35	189.95
24	C797-0324	**7**	51.1762	428	415	769	1.72	4.8	60.17	63.44	4.37	135.23
25	C797-1622	**7**	51.1605	223	264	1,063	2.17	3.72	50.98	58.9	2.79	158.9
26	C156-0176	**7**	51.1442	369	352	592	1.53	3.51	58.88	63.15	3.76	117.83
27	C791-0817	**7**	51.0168	450	383	964	1.47	3.81	63.4	63.47	4.71	147.82
29	C173-0499	**7**	50.7313	261	322	850	2.45	4.1	61.55	59.57	1.42	169.75
35	C796-0271	**7**	50.1951	361	375	506	2.07	4.24	69.76	68.23	2.84	158.04
37	C797-0316	**7**	49.932	387	399	921	1.04	3.94	67.2	68.9	2.92	182.23
39	4856-0075	**7**	49.5551	454	403	818	1.67	3.59	63.41	64.57	4.79	193.53
40	C797-0318	**7**	49.4141	410	398	926	2.16	4.02	61.12	66.28	4.19	145.07
45	C174-0471	**7**	49.0726	378	354	551	0.72	2.13	57.73	64.19	4.83	155.01
48	C797-1111	**7**	48.9054	397	366	846	1.2	2.66	56.95	63.16	4.86	153.16
49	C797-0201	**7**	48.7984	344	389	859	1.19	4.52	76.9	75.66	4.21	193.96
53	7656-0859	**7**	48.4454	494	448	641	2.24	3.96	66.67	62.7	5.32	131.4
54	7287-0225	**7**	48.4355	470	403	937	3.29	4.55	61.58	61.89	4.49	131.05
55	C785-0901	**7**	48.3029	390	355	647	2.34	4.65	63.61	59.24	2.67	180.55
57	0988-0093	**7**	48.2681	438	421	604	1.66	3.54	60.01	63.18	3.85	166.15

59	C163-0280	**7**	48.2237	334	319	687	3.28	3.54	59.6	53.61	4.35	193.81
67	C797-0222	**7**	47.9265	439	407	988	1.95	4.07	58.16	62.63	4.7	147.73
69	C156-0203	**7**	47.8833	363	340	866	2.3	3.67	63.57	62.92	3.82	175.74
70	C782-1500	**7**	47.8581	464	457	796	1.3	3.81	78.12	79.46	5.38	188.53
71	C163-0168	**7**	47.7908	397	415	591	1.97	3.04	61.81	63.33	3.97	156.31
74	7213-0313	**7**	47.6081	264	317	540	2.55	4.82	53.42	55.02	2.89	132.27
79	C795-0165	**7**	47.3258	431	424	948	1.23	4.37	74.89	77.11	5.78	174.08
82	C172-0414	**7**	47.2421	378	386	680	1.61	3.67	65.27	65.4	4.46	144.85
83	C174-0220	**7**	46.9721	357	345	469	1.9	4.43	51.04	55.38	3.9	129.32
85	7213-0477	**7**	46.8233	476	410	605	2	3.57	63.98	62.79	4.37	173.04
87	8001-3399	**7**	46.7527	359	337	653	1.55	4.57	67.9	62.82	3.96	172.68
88	0364-0024	**7**	46.72	264	297	321	0.99	3.73	66.3	66.22	5.51	161.82
90	C794-0286	**7**	46.5849	347	310	431	1.86	3.89	45.84	58.36	2.52	188.49
92	C187-0142	**7**	46.5438	337	355	930	2.08	4.48	68.89	68.97	3.26	179.65
93	C166-0050	**7**	46.5364	416	407	762	1.76	3.69	50.36	54.83	4.74	183.81
96	0573-2291	**7**	46.3594	437	392	412	1.86	3.76	65.33	64.73	4.19	191.88
97	C190-0383	**7**	46.3072	360	344	694	2.22	4.39	54.83	67.45	5.21	178.79
98	C791-0322	**7**	46.2604	333	290	768	1.53	3.58	60.58	59.01	2.74	179.43
101	C163-0149	**7**	46.0611	335	310	509	2.55	3.93	61.34	60.42	1.92	124.96
103	C781-0110	**7**	46.0465	414	409	483	2.22	3.5	58.32	63.42	4.97	180
104	C168-0498	**7**	46.0009	402	380	561	1.98	4.31	69.48	71.25	2.81	196.21
105	C156-0097	**7**	45.9485	278	325	772	1.61	3.92	55.14	57.72	1.95	178.56
106	C173-0523	**7**	45.9089	353	389	968	3.06	4.56	58.72	60.17	2.1	156.87
108	C191-0011	**7**	45.8864	278	288	577	1.93	3.85	58.27	62.75	1.91	163.41
111	C797-0226	**7**	45.719	511	506	841	1.88	4.87	67.61	72.56	3.84	151.38
112	C785-0971	**7**	45.6484	367	355	542	2.42	4.31	57.69	58.67	2.26	175.58
114	1000-0399	**7**	45.4936	427	407	659	1.53	3.93	63.02	61.52	3.64	131.68
116	C174-1205	**7**	45.3825	277	282	738	1.64	3.9	58.3	61.11	2.88	179.4
117	0111-0183	**7**	45.3741	314	342	313	1.57	3.61	57.69	57.46	3.8	171.67
119	C791-0382	**7**	45.3304	335	328	637	1.75	4.3	56.39	58.98	2.65	119.83
122	C797-0400	**7**	45.2527	466	431	1,060	1.55	4.42	75.09	77.8	5.62	163.93
125	C795-0596	**7**	44.9849	358	349	815	1.83	3.69	67.7	67.69	2.68	165.11
127	7472-0207	**7**	44.9499	430	396	583	2.04	4.63	57.14	58.41	3.57	127.73
130	7271-0132	**7**	44.7561	418	381	627	1.21	3.7	52.93	56.6	3.67	154.76
131	C163-0052	**7**	44.7036	374	382	587	2.11	3.96	64.54	61.57	2.58	114.85

132	C166-0059	**7**	44.6916	327	355	643	1.7	4.15	54.14	61.87	3.43	181.81
133	7682-0094	**7**	44.6178	428	366	561	2.56	3.81	52.75	55.57	4.93	148.27
135	0278-0048	**7**	44.3026	308	291	397	1.59	3.86	46.79	55.7	3.23	119.2
136	C782-1162	**7**	44.2602	488	449	910	1.19	3.92	78.12	79.69	5.13	159.12
144	C797-0300	**7**	44.0119	438	417	1,049	1.69	4.59	81.06	86.69	5.3	162.82
145	C174-0008	**7**	43.9747	320	302	658	1.73	4	46.97	56.82	3.9	152.96
146	C782-1638	**7**	43.9046	381	382	738	1.21	4.12	60.44	61.06	3.35	161.46
148	C200-1892	**7**	43.8964	293	333	587	1.94	4.28	62.23	65.75	3.25	154.1
149	0945-0415	**7**	43.8934	429	372	633	2.09	4.11	58.95	64.24	4.45	142.33
150	0977-3417	**7**	43.8292	361	360	398	2.39	4.92	69.24	65.78	4.19	199.65
152	0945-0263	**7**	43.8116	344	315	527	1.82	3.61	53	55.02	3.71	112.37
153	C795-1032	**7**	43.8113	380	391	792	1.32	4.65	70.94	73.4	4.43	170.12
155	C200-0497	**7**	43.7688	257	264	436	2.58	5.05	57.42	58.43	2.18	201.08
157	7472-0022	**7**	43.7372	346	378	1,020	1.82	4.04	72.74	70.82	3.2	156.58
159	C782-1144	**7**	43.715	461	434	716	2.11	4.66	68.59	69.04	3.26	144.96
161	C174-0173	**7**	43.6347	358	373	506	2.12	4.71	60.97	63.74	3.97	136.36
163	C190-0370	**7**	43.6127	278	321	493	1.82	3.97	54.57	62.2	3.02	159.1
164	7534-4640	**7**	43.6044	251	241	333	1.54	3.9	63.93	64.83	1.99	136.13
166	C168-0522	**7**	43.592	418	382	670	2.17	4.58	59.55	63.23	2.65	186.49
167	C191-0026	**7**	43.5488	261	315	841	1.86	3.46	54.71	59.51	3.74	160.2
171	0508-1913	**7**	43.4371	401	394	483	1.53	4.33	79.09	76.88	4.26	189.28
172	C153-0027	**7**	43.4207	346	329	571	1.24	3.55	72.33	69.23	3.88	156.54
173	7213-0286	**7**	43.3996	359	368	624	2.1	3.69	66.6	62.87	3.81	129.61
174	6319-3504	**7**	43.3597	407	362	669	1.69	3.44	64.08	69.98	3.61	158.55
175	C153-0535	**7**	43.2781	321	320	634	1.53	2.75	70.31	74.96	4.27	167.96
177	C782-1186	**7**	43.2529	425	399	681	1.14	4.09	54.95	58.65	4.47	165.02
179	C172-0696	**7**	43.2166	425	423	443	2.18	4.47	81.04	80.53	4.95	183.77
183	C782-1254	**7**	43.0871	307	352	558	1.06	3.49	66.1	69.59	4.37	170.61
184	4513-1296	**7**	43.0706	363	344	826	1.91	4.3	58.98	68.24	3.65	138.68
186	7602-0031	**7**	43.0407	318	333	416	1.69	4.66	67.86	69.9	3.89	187.32
187	5641-1636	**7**	43.0068	378	371	445	1.88	2.96	58.97	66.01	5.35	152.5
188	C187-0151	**7**	42.9502	442	398	926	1.71	3.77	67.12	66.14	2.94	161.19
189	7472-0148	**7**	42.9262	329	336	468	1.81	4.61	61.93	62.9	3.35	177.78
190	C174-0916	**7**	42.9261	280	287	573	1.88	4.5	58.63	59.95	2.84	182.39
193	C156-0048	**7**	42.8546	344	360	722	1.62	3.91	61.98	66.45	5.1	119.94

194	0831-1306	**7**	42.7511	376	342	582	1.85	3.98	57.38	58.41	3.42	111.03
195	C155-0340	**7**	42.7464	396	343	418	2.23	4.16	55.51	59.66	4.15	161.35
199	7213-0474	**7**	42.6982	411	384	679	2.38	3.65	61.2	58.7	2.47	165.46
202	7576-1281	**7**	42.5099	453	430	674	0.92	2.72	54.22	59.43	3.53	171.24
204	C200-1369	**7**	42.4234	384	375	617	2.32	3.74	57.08	60.43	2.76	153.76
205	1037-1126	**7**	42.372	399	370	504	1.57	4.29	70.12	65.83	3.25	138.49
209	C776-0103	**7**	42.2507	445	415	874	1.34	4.26	66.8	70.63	4.84	162.38
210	C156-0122	**7**	42.2166	353	343	638	1.85	4.36	56.9	59.84	2.64	162.25
211	7472-0094	**7**	42.208	412	380	731	2.08	4.04	54.81	56.43	3.6	165.27
214	C794-1050	**7**	42.1553	281	292	377	1.97	4.19	72.32	70.43	3.48	170.67
216	7582-1559	**7**	42.1193	281	319	565	2.08	4.43	57.74	58.43	1.59	176.83
217	C163-0284	**7**	42.086	417	403	814	1.73	2.76	54.88	58.94	4	158.41
218	5517-0059	**7**	42.0666	315	330	470	1.75	3.89	60.52	63.15	3.81	170.25
219	7828-0498	**7**	42.0408	392	367	448	1.57	4.27	59.18	66.95	4.45	193.78
220	0367-0984	**7**	42.0389	177	235	493	1.89	4.25	56.51	58.51	3.08	141.41
225	4490-1984	**7**	41.9126	515	441	961	2.01	4.36	76.93	63.67	3.51	179.98
226	C174-0436	**7**	41.9114	258	263	297	1.95	4.59	59.49	55.33	2.96	128.44
228	C155-0329	**7**	41.8559	321	329	397	1.52	4.22	66.12	63.17	3.23	181.12
230	0242-0679	**7**	41.832	356	331	647	2.27	4.34	57.76	58.12	3.22	126.57
231	0140-0335	**7**	41.8311	394	390	416	1.55	3.87	77.63	73.39	3.02	178.05
233	C156-0127	**7**	41.8104	425	372	770	1.79	3.2	62.21	66.28	2.2	156.68
237	6843-3204	**7**	41.6583	282	296	773	1.91	4.09	55.24	54.73	2.72	124.23
238	C155-0005	**7**	41.6343	372	357	429	2.28	3.68	47.78	55.38	3.1	162.52
239	C172-0214	**7**	41.6284	338	344	595	0.05	2.26	56.15	56.37	3.88	153.52
241	0774-1169	**7**	41.6066	364	346	445	1.52	3.69	51.34	57.22	3.52	142.81
242	4031-0974	**7**	41.6033	353	310	569	2.15	4.49	58.19	59.98	3.26	150.32
246	C782-0129	**7**	41.459	437	435	713	1.85	3.82	61.22	60.77	3.79	168.76
247	C174-0180	**7**	41.4367	361	371	549	1.52	3.86	61.93	63.6	3.63	142.73
249	7882-1423	**7**	41.4185	390	347	388	1.98	4.16	62.12	60.86	4.52	142.41
250	C155-0331	**7**	41.3923	309	346	419	2.89	4.58	60.9	59.76	3.7	174.15
252	C794-1049	**7**	41.3471	269	272	311	1.38	4.12	61.54	58.56	3.37	119.24
256	C797-0279	**7**	41.1025	428	386	570	2.08	4.66	77.7	71.45	3.9	159.38
259	0106-0153	**7**	41.0604	324	329	304	1.79	4.57	61.8	59.62	2.99	169.82
260	0644-0010	**7**	40.9929	462	405	1,034	2.28	4.5	59.88	60.59	1.78	167.98
261	C175-0120	**7**	40.9847	419	356	824	2.29	4.11	67.39	69.01	3.07	172.61

262	C172-0335	**7**	40.9386	335	321	565	2.25	3.92	66.06	76.59	4.4	157.7
265	0272-0154	**7**	40.8678	378	388	753	1.8	3.63	56.36	60.71	3.75	159.79
266	0334-0123	**7**	40.8537	391	364	347	1.5	3.91	51.9	52.97	3.63	171.29
267	C172-0681	**7**	40.8289	418	402	409	2.42	5.12	64.43	66.23	4.51	165.91
268	7610-2227	**7**	40.7937	393	369	792	2.24	4.62	62.17	59.53	2.75	156.49
271	6404-0218	**7**	40.685	375	381	572	2.45	4.88	61.64	70.03	4.63	163.43
272	C776-0128	**7**	40.6612	399	379	714	2.99	5.1	75.63	80.66	3.38	153.96
273	C172-0680	**7**	40.6453	309	320	332	2.2	4.81	52.06	59.5	3.62	167.29
274	C168-0222	**7**	40.6097	339	341	526	1.96	4.5	57.9	58.67	2.85	169.91
275	5325-0037	**7**	40.6064	374	369	607	1.06	3.9	66.22	62.89	3.49	166.53
276	C174-0713	**7**	40.5738	229	261	733	2.09	4.25	59.68	54.92	2.46	99.64
277	7747-0545	**7**	40.533	481	410	777	0.9	2.38	55.47	58.82	4.76	159.94
279	7567-0290	**7**	40.5083	415	408	711	1.98	3.14	61.02	59.51	4.8	126.94
282	C191-0081	**7**	40.3645	352	343	697	1.76	4.02	70.85	70.44	2.64	180.63
284	7954-2543	**7**	40.3232	476	438	454	2.71	4.91	56.68	63.35	3.4	197.52
285	C155-0472	**7**	40.2551	210	239	280	2.48	3.77	52.15	55.02	1.95	149.5
287	C163-0288	**7**	40.2254	392	373	685	2.77	4.46	61.63	59.71	2.48	159.93
288	0896-2903	**7**	40.2005	306	285	325	1.28	3.75	52.48	55.19	4.35	130.18
289	4951-0792	**7**	40.184	435	373	682	2.18	3.93	61.66	64.47	3.3	168.4
290	C797-1400	**7**	40.1779	414	385	836	1.55	3.88	56.68	54.91	2.57	155.12
291	C174-0176	**7**	40.171	340	337	359	1.94	4.59	62.16	61.41	3.7	134.94
292	C153-0484	**7**	40.163	385	364	775	2.11	4.06	46.53	61.96	4.67	153.77
293	0668-0096	**7**	40.1398	324	360	392	0.87	2.98	65.23	59.05	4.07	161.38
294	0134-0077	**7**	40.1302	308	304	336	2.17	3.95	55.55	62.28	2.48	149.18
484	C782-0298	**6**	59.8781	444	448	1,126	1.43	4.03	69.34	75.74	7.3	170.32
485	C153-0194	**6**	54.9466	384	386	905	0.08	1.34	52.15	58.48	6.15	186.1
486	C153-0021	**6**	53.9098	358	381	851	1.31	2.6	72.19	75.15	5.93	188.38
487	7616-0521	**6**	52.9052	423	396	481	1.28	2.68	54.29	58.04	4.63	116.21
488	C797-1159	**6**	52.8946	304	314	672	1.72	3.61	50.41	58.94	3.48	148.93
489	C785-1455	**6**	51.4671	299	303	598	1.63	4.25	59.07	52.72	2.43	156.03
490	C794-0273	**6**	51.3739	371	342	628	1.71	3.5	45.89	49.8	3.18	176.59
491	0111-0172	**6**	51.3199	318	356	396	1.26	2.46	48.67	59.82	5.44	168.15
492	C796-0987	**6**	50.777	316	313	715	1.35	4.13	61.37	64.96	2.37	196.92
493	6691-0355	**6**	50.3215	274	315	555	2.03	4.24	54.43	50.97	3.48	158.64
494	C163-0209	**6**	50.2634	356	351	684	3.17	5.03	69.68	72.45	2.05	160.99

495	C163-0061	**6**	50.0724	329	342	594	2.33	4.5	47.64	47.68	2.59	155.14
496	C163-0174	**6**	50.0452	374	369	566	2.31	4.09	52.11	50.17	3.95	143.27
497	7213-0321	**6**	49.8141	288	324	561	-999.9	-999.9	59.9	61.03	3.31	110.96
498	0272-0171	**6**	49.3896	576	507	808	1.51	3.39	64.18	67.76	3.41	145.15
499	6466-0053	**6**	49.1743	399	381	726	1.69	3.1	69.41	65.99	4.21	150.93
500	7472-0166	**6**	49.1684	491	439	689	1.35	2.72	52.77	63.19	5.95	153.64
501	C785-1169	**6**	49.0488	433	388	729	2.13	4.3	50.05	55.02	2.54	165.51
502	C785-1474	**6**	49.0156	359	353	646	2.2	4.57	52.18	45.83	2.84	170.14
503	7238-1208	**6**	48.8858	401	359	653	1.81	4.37	59.24	59.51	3.15	195.28
504	C797-1609	**6**	48.6408	337	292	549	2.5	3.63	61.97	61.36	3.13	129.79
505	C153-0025	**6**	48.5961	389	350	412	-999.9	-999.9	60.67	64.99	3.35	145.88
506	C200-1181	**6**	48.369	611	544	733	1.6	2.54	71.27	71.88	5.01	151.43
507	C794-0274	**6**	48.2567	321	291	611	1.6	3.69	24.48	38.73	3.29	170.01
508	7591-0752	**6**	48.1911	377	352	708	1.51	2.54	54.22	65.37	3.83	205.57
509	C163-0287	**6**	48.1695	350	362	551	3.46	4.28	46.83	37.23	3.64	150.49
510	7287-0226	**6**	47.9476	389	386	619	2.57	4.25	62.71	62.84	2.19	126.97
511	C197-0372	**6**	47.9294	393	347	815	1.69	2.31	50.6	54.83	4.36	164.28
512	1030-0092	**6**	47.8867	318	313	286	2.29	4.43	63.57	66.44	3.14	161.04
513	C191-0110	**6**	47.4278	391	391	802	1.37	2.5	73.65	75.56	6.3	163.29
514	C173-0278	**6**	47.3462	326	282	463	1.61	3.79	75.55	76.37	2.18	141.31
515	C153-0102	**6**	47.2336	378	390	901	0.78	1.93	68.07	75.72	6.18	194.2
516	C796-0582	**6**	47.1546	355	348	649	0.88	3.3	57.82	59.15	1.7	163.8
517	C794-0279	**6**	47.0682	369	344	765	0.16	1.71	41.45	56.75	3.71	178.28
518	C200-0665	**6**	47.003	490	438	676	2.22	3.48	52.99	58.05	3.52	153.36
519	C156-0162	**6**	46.9478	294	290	528	2.06	4.95	71.92	71.17	2.16	129.46
520	C163-0169	**6**	46.8336	318	341	483	3.12	4.05	70.26	61.66	3.61	128.2
521	C191-0100	**6**	46.822	386	368	880	1.38	3.53	60.85	68.56	4.43	185.54
522	7445-0116	**6**	46.7114	350	321	798	2.37	3.45	65.57	55.87	1.83	146.52
523	7238-1238	**6**	46.4961	371	365	672	1.12	3.17	57.11	61.02	4.11	168.29
524	C156-0110	**6**	46.3298	377	367	831	1.02	2.97	57.74	60	4.11	180.98
525	C163-0203	**6**	46.127	388	364	437	1.56	4.03	56.87	57.8	2.67	129.8
526	C785-2646	**6**	46.0863	252	278	562	1.69	5	59.63	64.33	2.41	184.61
527	C786-2694	**6**	45.9925	403	358	592	2.54	3.95	19.46	36.48	4.6	173.37
528	C187-0104	**6**	45.9372	398	369	958	1.25	3.71	65.69	67.07	3.59	157.4
529	C797-0194	**6**	45.8558	369	384	695	1.15	3.96	52.48	59.39	3.82	145.48

530	C776-3318	**6**	45.6212	306	359	749	1.6	3.74	68.57	71.37	3.12	164.72
531	0573-2289	**6**	45.6113	340	330	362	1.29	4.22	67.43	67.75	3.49	191.88
532	0918-1077	**6**	45.4304	226	227	808	2.05	3.99	42.26	46.07	1.99	161.37
533	C168-0099	**6**	45.4075	249	276	414	1.41	4.06	60.84	62.87	2.97	187.1
534	C790-0173	**6**	45.261	425	380	577	1.16	2.83	56.12	58.67	3.71	127.01
535	C156-0096	**6**	45.2382	359	354	707	2.38	3.8	61.11	61.05	1.89	172.08
536	7296-3326	**6**	45.188	360	341	809	1.6	4.44	64.45	65.94	2.63	138.97
537	C172-0437	**6**	45.1514	245	282	581	1.7	2.92	52.38	54.91	4.22	155.94
538	C795-1030	**6**	45.0806	454	435	894	1.25	4.55	85.42	83.63	4.51	150.14
539	0832-2865	**6**	44.9551	331	357	391	1.48	4.09	64.5	67.28	4.11	197.72
540	6969-0987	**6**	44.9497	423	359	774	2.77	3.84	64.71	56.07	1.85	147.06
541	0364-0004	**6**	44.918	291	319	296	1.13	4.6	64.47	62.77	3.31	144.11
542	C156-0148	**6**	44.9162	290	309	502	1.94	3.43	55.8	65.27	3.85	124.77
543	C174-0271	**6**	44.8919	349	352	606	0.96	3.79	65.48	66.06	4.03	159.17
544	7472-0031	**6**	44.8316	374	377	665	2.07	3.76	48.53	56.27	2.89	166.82
545	7591-0744	**6**	44.7606	324	287	478	2.38	4.02	55.02	53.18	1.66	154.16
546	C797-1613	**6**	44.7559	351	327	608	1.63	3.82	43.66	51.21	3.16	159.21
547	C797-0320	**6**	44.6913	383	393	958	0.8	2.82	66.13	69.6	4.51	165.71
548	C175-0056	**6**	44.6534	363	319	683	2.01	4.36	53.97	56.21	1.61	163.61
549	C191-0307	**6**	44.6388	234	291	535	1.29	2.4	76.25	80.25	3.34	185.93
550	C187-0134	**6**	44.5498	386	348	944	1.64	4.27	72.84	71.43	4.21	148.44
551	C797-0195	**6**	44.5282	461	432	672	-,999.9	-999.9	69.27	65.46	4.05	137.37
552	7706-0397	**6**	44.3114	418	367	729	3.34	4.47	52.02	54.16	4.04	168.81
553	C153-0600	**6**	44.2656	346	330	861	2.01	3.92	39.49	47.85	3.76	185.51
554	C795-1028	**6**	44.1569	429	400	905	1.28	3.87	87.89	83.62	4.11	140.16
555	C153-0586	**6**	44.1493	343	351	599	1.29	3.78	67.74	64.23	3.08	155.88
556	C156-0107	**6**	44.1423	404	399	923	-0.1	0.78	61.73	62.68	4.68	145.29
557	5555-0294	**6**	43.8737	218	237	335	1.71	3.74	53.92	54.02	2.44	135.55
558	7610-2184	**6**	43.8407	290	294	593	1.04	3.43	66.12	69.77	3.95	114.4
559	0848-0064	**6**	43.8263	373	369	619	1.49	3.67	52.7	54.86	3.38	124.91
560	C172-0411	**6**	43.7957	342	302	495	2.03	4.37	54.02	48.99	2.32	159.09
561	C153-0607	**6**	43.7733	259	279	580	0.67	2.35	61.59	63.93	3.3	158.66
562	0889-0046	**6**	43.6557	416	376	531	1.21	3.64	54.94	58.58	4.04	128.58
563	7407-0158	**6**	43.6389	386	357	894	0.25	2.05	46.66	54.96	3.99	177.69
564	C794-0237	**6**	43.5557	426	417	711	-2.65	-2.2	72.49	76.45	4.13	177.26

565	7882-1303	**6**	43.5084	362	347	597	1.73	3.88	51.53	54.95	3.91	144.34
566	7834-0097	**6**	43.3804	392	368	496	4.43	4.95	34.13	51.19	3.21	161.11
567	C155-0701	**6**	43.3803	349	343	418	1.84	3.96	43.81	48.26	3.46	159.71
568	C153-0203	**6**	43.3533	293	330	418	2.43	4.53	60.18	57.99	3.44	134.06
569	C174-0255	**6**	43.2757	351	349	717	2.01	4.35	57.99	60.97	2.81	165.32
570	0889-0037	**6**	43.2138	377	343	546	1.05	3.69	66.33	62.59	3.04	180.3
571	0106-0141	**6**	43.1884	371	373	467	1.29	4.02	75.14	73.87	4.3	192.59
572	C172-0485	**6**	43.1629	308	326	401	2.42	4.76	68.96	66.82	2.79	154.63
573	C174-0493	**6**	43.1544	411	382	791	1.32	4.13	63.74	65.31	2.56	161.76
574	C174-0433	**6**	43.0758	328	318	464	1.68	3.99	48.12	52.33	3.31	124.67
575	0663-0543	**6**	43.0324	369	327	677	1.6	3.5	61.72	70.32	3.44	161.16
576	C797-1623	**6**	43.0209	297	314	344	1.24	3.71	64.84	63.69	3.63	136.92
577	C166-0019	**6**	42.996	352	369	786	0.79	3.38	83.28	82.19	3.7	174.24
578	C181-0725	**6**	42.7175	461	386	916	1.75	3.69	54.17	68.41	4.36	142.92
579	C163-0317	**6**	42.6706	388	389	572	1.73	3.66	70.32	65.82	2.2	132.12
580	7213-0086	**6**	42.6101	195	257	557	2.16	4.95	57.75	52.9	0.03	150.98
581	0791-1318	**6**	42.5662	337	355	499	1.26	4.38	66.45	64.82	3.69	149.94
582	7472-0209	**6**	42.5649	396	351	584	1.58	4.43	73.68	66.97	2.4	147.74
583	000A-0618	**6**	42.5223	261	300	609	1.88	4.16	54.44	58.06	3.56	131.66
584	4965-0037	**6**	42.5066	267	298	651	2.23	4.04	39.76	43.87	3.25	154.39
585	0889-0030	**6**	42.4674	392	389	541	1.57	3.93	50.68	44.2	3.72	172.61
586	7407-0596	**6**	42.456	414	369	566	1.81	3.88	32.46	39.37	3.18	162.57
587	C794-0433	**6**	42.4182	369	371	497	1.5	3.73	62.29	55.97	1.57	154.65
588	4236-0429	**6**	42.4113	445	438	1,072	1.73	2.21	56.45	59.22	4.93	187.73
589	0242-0272	**6**	42.2409	176	250	282	2.01	4.62	45.67	62.43	2.51	117.26
590	0812-1018	**6**	42.1691	254	272	910	1.54	4.03	53.43	53.13	2.62	147.13
591	C153-0611	**6**	42.1531	281	305	612	0.91	3.01	58.1	59.35	2.79	163.97
592	7445-0074	**6**	42.0153	306	317	726	2.57	3.69	40.36	45.09	3.68	177.96
593	C785-3813	**6**	41.9792	281	278	593	1.71	4.29	58.27	57.41	2.18	169.53
594	C797-0048	**6**	41.9708	460	447	790	1.91	4.55	63.19	67.9	2.58	147.52
595	7543-0683	**6**	41.9502	321	293	539	1.89	3.99	61.66	59.1	2.38	130.45
596	7882-1550	**6**	41.8535	461	379	746	2.21	4.19	53.65	60.46	3	149.45
597	7563-5002	**6**	41.689	251	266	685	1.21	3.53	67.5	60.49	3.35	134.39
598	C174-0762	**6**	41.6675	336	367	549	0.72	2.85	58.66	61.84	3.53	140.86
599	C776-0138	**6**	41.5991	441	417	996	-999.9	-999.9	71.61	66.52	5.23	102.79

600	C172-0670	**6**	41.5663	279	299	816	2.18	4.14	58.25	55.75	2.49	133.56
601	C172-0683	**6**	41.5468	374	378	410	1.96	3.66	55.42	56.44	3.36	144.48
602	C176-0422	**6**	41.5046	265	316	340	2.75	3.86	58.05	67.96	3.58	117.15
603	7617-0116	**6**	41.467	347	383	460	1.2	3.72	70.22	69.71	2.14	186.16
604	7576-1335	**6**	41.4233	457	417	659	1.15	2.4	51.88	55.58	3.41	165.07
605	0968-0002	**6**	41.2609	331	309	457	1.62	3.91	49.45	52.91	3.98	136.31
606	C163-0501	**6**	41.1461	366	361	438	2.2	3.81	55.17	53.43	2.63	140.07
607	C153-0498	**6**	41.13	330	343	625	2.53	4.63	72.67	71.42	1.53	143.02
608	7445-0102	**6**	41.1203	357	310	725	1.62	3.16	54.48	58.6	3.92	145.3
609	C156-0178	**6**	41.0913	358	365	778	2.01	4.32	51.31	55.45	2.17	145.37
610	0622-0121	**6**	41.07	389	369	570	1.89	4.22	55.52	56.44	3.07	132.18
611	000A-0784	**6**	41.0364	287	300	393	0.98	3.78	55.01	55.33	3.81	144.9
612	7761-0005	**6**	40.9954	389	413	814	2.91	4.68	52.15	60.01	2.58	157.34
613	7213-0299	**6**	40.9807	215	260	387	1.67	4.38	57.76	51.8	1.05	127.65
614	7296-3315	**6**	40.9446	212	222	651	1.9	3.91	52.94	51.18	2.18	125.05
615	7202-4983	**6**	40.9362	210	249	374	0.86	3.82	53.97	57.22	1.15	160.44
616	5897-0081	**6**	40.9356	405	403	583	1.91	4.24	42.38	46.62	3.74	167.2
617	0242-0326	**6**	40.913	233	309	543	1.5	3.2	47.7	58.52	4.28	154.77
618	7668-0420	**6**	40.8049	326	309	514	1.9	3.87	51.07	55.63	3.41	146.5
619	C796-0449	**6**	40.7944	305	284	426	1.63	3.93	46.96	46.24	3.42	109.52
620	0568-0813	**6**	40.7243	292	286	603	1.65	3.83	49.45	52.63	4.74	134.2
621	C797-0233	**6**	40.6935	509	459	648	1.84	4.96	62.54	74.1	2.76	148.35
622	0688-1288	**6**	40.6683	269	272	532	0.78	3.15	52.21	55.64	3.42	141.39
623	0964-0015	**6**	40.6648	423	379	580	2.13	4.25	49.92	50.36	4.08	121.32
624	C797-0507	**6**	40.6408	470	445	904	0.67	3.2	56.17	61.9	4.21	153.26
625	C190-0376	**6**	40.5953	261	284	685	1.5	3.76	33.22	51.99	4.67	179.65
626	7472-0127	**6**	40.4564	442	380	896	1.73	3.76	58.08	58.52	3.13	152.65
627	C174-0171	**6**	40.4247	321	330	459	2.22	4.88	54.68	57.7	2.75	131.12
628	7407-0600	**6**	40.4231	328	312	558	2.02	4.06	36.59	43.11	1.6	179.99
629	C155-0197	**6**	40.3602	276	305	383	2.08	3.76	53.09	54.72	2.95	181.59
630	7706-0415	**6**	40.3512	246	255	566	2.57	4	54.66	55.76	0.61	172.59
631	C153-0504	**6**	40.3492	304	298	548	1.69	4.22	70.64	67.63	3.21	151.21
632	4110-0004	**6**	40.292	321	312	911	1.58	3.08	52.52	57.95	3.32	152.31
633	7213-0115	**6**	40.272	463	431	615	0.87	2.05	58.95	68.57	5.85	158.4
634	0964-0016	**6**	40.2683	340	323	583	1.93	4.24	53.29	54.27	3.29	117.93

635	C156-0126	**6**	40.148	313	336	683	0.93	3.11	57.32	63.94	3.24	162.75
636	C786-4026	**6**	40.1108	331	354	488	0.69	2.82	55.8	58.11	4.02	147.82
637	7576-1269	**6**	40.0512	320	339	532	1.09	3.07	55.19	58.64	2.44	171.13
638	0977-3231	**6**	40.0491	363	342	586	1.81	3.66	44.31	56.02	3.96	155.12
639	7202-2336	**6**	40.0106	367	379	458	2.19	3.79	57.09	53.73	3.29	135.02
931	C785-3284	**5**	57.7477	411	382	742	-0.05	2.13	62.11	61.84	4.36	181.35
932	C174-0687	**5**	52.4923	384	359	662	0.68	3.15	45.16	55.5	4.59	158.26
933	C794-0271	**5**	51.4369	325	353	650	0.66	2.36	16.49	32.92	3.79	155.29
934	7213-0289	**5**	51.1648	313	331	452	2.12	2.6	13.44	42.45	3.64	142.24
935	C785-1168	**5**	51.0045	379	367	704	1.94	3.97	43.47	49.14	2.19	159.3
936	C785-0908	**5**	50.7889	340	312	631	1.89	4.58	47.36	52.57	3.01	172.07
937	C153-0481	**5**	50.2073	324	343	811	1.16	3.1	59.32	66.44	4.38	175.42
938	C785-3428	**5**	49.9739	367	371	790	0.18	1.54	78.63	70.62	3.52	160.43
939	5293-0041	**5**	49.4807	197	222	592	1.83	2.63	22.14	32.31	4.91	107.79
940	C786-2966	**5**	49.2304	441	416	751	1.85	3.81	26.7	35.99	3.93	158
941	7259-6181	**5**	49.1369	449	413	892	1.29	3.49	57.93	64.66	4.1	177.88
942	C176-0239	**5**	49.1325	261	299	661	2.17	3.61	54.26	55	1.69	130.95
943	C172-0157	**5**	48.7237	378	383	625	0.31	1.43	60.05	59.28	4.26	193.56
944	0173-0041	**5**	48.6679	272	298	650	1.57	3.85	54.01	63.19	2.88	149.68
945	C785-1501	**5**	48.5938	267	305	549	0.77	3.46	57.64	56.98	4.71	153.32
946	C785-3794	**5**	48.5075	278	309	712	1.61	3.43	60.29	63.27	2.05	154
947	C155-0775	**5**	48.2578	396	380	508	2.62	4	42.8	54.38	3.62	148.26
948	7489-2091	**5**	48.1219	357	374	951	0.62	2.92	53.5	56.38	3.82	157.02
949	C795-0338	**5**	48.0376	424	394	699	1.26	2.55	18.12	37.38	5.01	162.97
950	C163-0170	**5**	47.8168	405	409	702	1.65	2.09	46.52	52.67	4.32	175.85
951	7213-0340	**5**	47.5766	299	318	559	1.71	3.95	69.97	74.9	2.14	93.48
952	7407-0455	**5**	47.3899	315	325	616	1.95	3.34	29.41	43.11	2.96	171.38
953	7213-0320	**5**	47.0619	251	292	686	2.78	4.02	47.7	58.8	1.96	167.61
954	7213-0308	**5**	46.7501	314	301	610	2.16	3.52	63.27	63.05	2.82	116.55
955	7617-0126	**5**	46.6357	352	349	419	2.02	2.79	55.56	57.99	3	109.65
956	0908-0031	**5**	46.5035	425	368	627	2.11	3.24	55.88	56.83	5.25	120.4
957	C786-2471	**5**	46.4369	363	338	534	2.34	4.37	29.07	39.66	3.68	176.04
958	C190-0437	**5**	46.4151	317	315	604	1.72	3.58	51.3	68.98	3.74	163.68
959	7472-0089	**5**	46.2146	446	409	702	0.45	2.51	69.6	71.37	4.64	155.93
960	C172-0533	**5**	46.1958	333	334	637	2.39	4.66	56.02	54.21	2.19	169.21

961	C153-0566	**5**	46.194	303	291	692	1.39	3.95	41.14	52.49	3.55	166.75
962	7407-0307	**5**	46.0607	347	321	793	1.86	3.37	46.36	53.66	3.85	171.05
963	C191-0101	**5**	46.0404	397	379	743	0.69	1.78	57.16	62.96	6.05	141.29
964	8001-3938	**5**	46.0288	358	348	874	1.05	1.83	61.37	63.15	3.9	134.17
965	7617-0135	**5**	45.9847	274	300	478	-999.9	-999.9	61.37	62.92	2.07	102.41
966	7472-0129	**5**	45.8521	320	312	330	0.91	3.89	56.35	58.63	3.35	110.38
967	C172-0671	**5**	45.6892	275	276	626	1.52	2.7	42.76	44.01	3.68	141.79
968	7534-4639	**5**	45.5951	347	330	523	1.2	2.69	47.55	58.08	3.87	122.51
969	0896-8794	**5**	45.5641	457	395	645	0.72	2.47	62.27	64.54	3.89	152.33
970	7213-0344	**5**	45.5272	267	318	551	-999.9	-999.9	54.26	52.86	3.78	104.1
971	C797-1596	**5**	45.2705	282	334	639	1.45	2.96	51.03	52.15	3.55	177.16
972	C156-0144	**5**	45.2026	344	344	658	1.19	3.92	55.03	54.96	2.63	157.21
973	7840-3325	**5**	45.0769	430	403	482	1.14	3.19	48.98	57.53	3.62	192.39
974	C785-3724	**5**	45.0333	326	301	549	0.65	3.22	61.3	63.12	1.76	154.46
975	5928-0068	**5**	44.8634	329	311	541	1.89	3.21	55.93	65.34	1.53	161.14
976	0359-0017	**5**	44.8607	396	414	867	1.59	4.13	57.79	64.14	3.01	121.51
977	C153-0237	**5**	44.849	312	337	691	0.07	2.31	38.05	60.17	3.26	159.76
978	6413-0259	**5**	44.7312	390	356	564	1.14	3.71	50.69	55.51	4.87	133.56
979	C176-0375	**5**	44.676	296	330	749	2.47	3.44	62.9	65.77	3.58	123.34
980	7202-4982	**5**	44.6423	219	248	388	1.69	4.07	21.01	34.27	2.48	161.52
981	C786-4387	**5**	44.5432	298	311	392	1.79	4.05	37.74	46.41	3.12	154.82
982	7591-0551	**5**	44.5415	364	373	676	1.93	4.62	65.54	61.87	1.73	150.26
983	C190-0406	**5**	44.4723	328	310	554	1.23	2.94	57.05	60.39	2.96	156.12
984	4013-0066	**5**	44.2405	359	328	692	0.22	1.35	54.89	59.26	3.75	142.17
985	0933-0082	**5**	44.1585	291	295	607	1.45	4.08	66.64	67.09	2.92	142.81
986	0342-0049	**5**	44.0753	217	225	428	1.29	2.99	53.75	54.7	1.69	164.78
987	7472-0149	**5**	43.9484	346	306	548	1.64	3.84	67.71	68.35	3.08	131.57
988	7287-0121	**5**	43.9465	277	291	433	0.79	3.28	62.56	60.22	4.17	143.15
989	C163-0090	**5**	43.875	311	315	513	1.47	3.69	60.69	56.2	2.15	169.92
990	C781-0115	**5**	43.8174	418	406	535	0.4	1.74	44.25	60.76	4.37	175.72
991	7954-2033	**5**	43.7895	257	274	471	1.65	3.82	47.93	43.92	3.38	120.88
992	0364-0001	**5**	43.7866	285	336	369	0.57	3.48	59.22	58.11	5.25	146.04
993	C797-0159	**5**	43.7788	428	465	878	0.44	3.17	62.16	68.75	4.82	145.18
994	C786-4147	**5**	43.7755	287	288	428	1.11	3.73	64.65	64.19	2.03	159.23
995	0974-0026	**5**	43.7688	427	414	824	1.5	3.26	48.44	48.39	3.28	171.5

996	C163-0165	**5**	43.7064	317	324	519	2.25	4.25	45.26	46.16	2.03	138.08
997	C190-0107	**5**	43.7053	309	293	714	1.59	2.89	40.91	53.05	4.98	142.01
998	0478-0684	**5**	43.6978	407	387	474	1.66	3.93	59.04	57.1	2.36	133.27
999	C797-0193	**5**	43.5585	386	377	799	0.11	2.41	53.58	57.49	3.76	129.77
1000	7472-0146	**5**	43.4265	402	375	604	1.57	3.55	57.89	61.02	3.51	145.52
1001	C176-0309	**5**	43.413	368	376	457	2.11	4.54	69.14	68.85	2.83	130.86
1002	C172-0504	**5**	43.3723	249	307	593	1.35	2.55	48.5	56.62	3.24	189.23
1003	0711-0306	**5**	43.3718	260	301	616	1.72	3.71	51.86	48.72	1.49	153.19
1004	7472-0199	**5**	43.2426	443	434	702	1.75	4.47	55.06	57.38	2.82	136.24
1005	C795-0598	**5**	43.1961	402	362	830	1.41	3	47.44	52.71	3.9	152.98
1006	C174-0926	**5**	42.845	346	337	534	1.02	2.49	50.13	56.68	4.97	130.05
1007	7514-0069	**5**	42.812	401	335	760	0.63	0.97	39.87	44.88	3.73	164.15
1008	C794-0173	**5**	42.8068	295	284	477	1.15	4.25	70.21	68.68	1.83	166.95
1009	C174-0204	**5**	42.757	310	308	381	1.87	4.52	52.14	52.92	2.58	123.09
1010	7407-0153	**5**	42.7415	422	378	859	1.02	2.74	44.51	53.4	3.92	166.56
1011	7916-1194	**5**	42.7247	289	334	815	1.67	3.91	53.77	40.74	1.9	126.05
1012	0933-0085	**5**	42.6416	318	305	563	1.89	3.09	34.09	33.94	3.58	94.3
1013	0868-0118	**5**	42.6117	316	320	403	0.49	3.09	62.81	60.66	3.44	135.02
1014	7752-0314	**5**	42.5582	343	319	853	1.22	3.66	55.41	55.05	1.98	119.22
1015	C163-0171	**5**	42.4359	262	299	473	1.64	3.7	45.28	48.14	0.61	159.42
1016	6404-0217	**5**	42.4322	257	291	363	2.15	4.28	37.74	45.43	3.74	149.35
1017	0896-8799	**5**	42.397	371	347	500	1.26	4.28	69.55	71.75	3.42	134.94
1018	0106-0146	**5**	42.3898	429	411	494	0.86	1.11	40.72	57.69	6	185.84
1019	0478-0704	**5**	42.3738	254	251	503	1.61	2.52	34.72	44.95	4.11	108.6
1020	3966-4838	**5**	42.3678	278	314	568	0.24	2.79	56.79	58.37	3.44	142.44
1021	C797-1595	**5**	42.3609	340	353	607	1.61	3.41	46.26	47.59	5.6	132.92
1022	0KPl-0058	**5**	42.331	316	338	362	1.18	3.56	53.11	59.16	3.84	196.51
1023	0567-1072	**5**	42.3297	311	298	603	1.31	4	63.34	64.63	4.95	145.05
1024	C786-2588	**5**	42.3289	353	336	592	0.75	2.57	26.41	41.19	3.55	188.06
1025	C153-0583	**5**	42.2675	306	314	662	1.45	4.5	53.32	59.49	2.34	173.92
1026	C174-0761	**5**	42.2229	332	320	655	1.45	4.52	58.82	62.92	2.6	180.78
1027	C190-0375	**5**	42.172	329	331	568	2.27	3.67	28.96	41.56	3.66	171.7
1028	0632-0877	**5**	42.1277	358	356	661	1.34	2.31	53.92	60.9	5.31	135.79
1029	C172-0194	**5**	42.1203	286	320	458	0.15	2.35	55.62	60.67	3.45	187.88
1030	C786-2431	**5**	42.1111	402	353	921	2.74	4	51.73	50.46	3.76	167.64

1031	C785-3001	**5**	42.0986	320	315	512	0.95	2.38	54.27	55.47	2.79	155.66
1032	C794-0256	**5**	42.0585	396	366	1,112	0.58	2.55	50.77	60.61	3.96	155.63
1033	6466-0035	**5**	41.8392	375	359	723	2.12	3.5	56.65	68.79	2.8	143.3
1034	7238-1496	**5**	41.8057	258	287	647	1.39	4.14	68.14	63.53	1.21	135.08
1035	0831-1308	**5**	41.7252	370	335	537	1.8	4.3	50.97	52.6	3.19	109.52
1036	0417-1666	**5**	41.631	337	338	303	2.65	4.8	46.88	59.09	1.99	192.64
1037	C163-0278	**5**	41.593	366	375	779	1.39	3.24	61.91	64.52	2.08	121.66
1038	C174-0219	**5**	41.5586	341	336	463	2.02	4.55	49.28	53.16	3.92	126.67
1039	C174-0003	**5**	41.5388	391	360	899	0.81	2.51	52.71	57.68	5.98	130.3
1040	C785-3838	**5**	41.5061	350	314	501	2.02	4.24	59.95	53.38	0.79	169.36
1041	5762-1311	**5**	41.4414	413	357	842	0.96	2.1	42.63	55.79	5.09	184.9
1042	0364-0055	**5**	41.3736	315	317	565	2.01	4.01	40.41	51.85	2.86	193.49
1043	C190-0394	**5**	41.3729	302	306	275	1.25	3	57.63	59.48	3.59	134.56
1044	C785-1523	**5**	41.312	302	312	278	1.76	3.99	50.25	42.02	2.1	120.07
1045	7684-2346	**5**	41.305	253	294	517	1.91	4.16	70.85	66.8	2.02	150.47
1046	7629-0056	**5**	41.2682	203	214	472	1.96	2.97	54.2	54.07	2.23	135.37
1047	7241-0522	**5**	41.2494	400	380	955	1.29	2.91	50.57	56.09	3.33	143.59
1048	0896-2219	**5**	41.2447	375	322	419	1.34	3.82	48.01	51.42	3.91	125.91
1049	C200-0757	**5**	41.2239	303	342	805	0.99	2.99	67.8	71.2	3.95	182.17
1050	7582-1731	**5**	41.2022	261	264	563	1.67	3.61	42.32	40.49	3.35	166.63
1051	C794-0384	**5**	41.1965	362	348	499	1.71	3.78	49.28	49.93	2.58	123.53
1052	C153-0488	**5**	41.1627	281	303	612	0.91	3.28	67.51	65.47	2.76	152.78
1053	7445-0107	**5**	41.1401	336	348	753	1.91	3.98	81.47	78.13	2.08	128.24
1054	7399-0145	**5**	41.099	267	253	633	1.76	3.31	68.78	57.79	1.88	139.16
1055	0717-0954	**5**	41.0911	289	291	772	1.46	3.97	55.23	54.62	2.26	121.14
1056	1021-0035	**5**	41.0877	348	317	622	2.33	4.11	40.06	29.9	1.95	113.67
1057	7840-5245	**5**	41.0707	417	395	708	1.82	3.82	48.79	48.12	3.61	149.32
1058	7491-0152	**5**	41.0426	329	350	604	0.97	3.95	55.43	55.56	2.62	123.43
1059	0167-0132	**5**	41.0387	338	303	456	1.74	4	50.02	50.38	2.49	130.1
1060	7834-0069	**5**	41.0298	282	279	576	2.62	4.34	54.33	58.95	2.26	151.97
1061	C797-0229	**5**	40.914	464	447	796	0.93	3.51	57.79	63.44	3.81	153.95
1062	5910-0313	**5**	40.8908	294	291	541	1.4	3.33	60.31	63.39	3.84	153.41
1063	0063-0004	**5**	40.8809	247	257	513	2.04	3.97	44.94	50.1	2.03	157.79
1064	7407-0264	**5**	40.876	364	330	679	1.47	3.69	46.36	49.05	2.97	175.62
1065	0550-0076	**5**	40.8256	468	382	560	2.18	3.85	43.15	46.36	4.14	113.18

1066	C172-0538	**5**	40.7939	332	350	378	2.31	4.55	45.7	53.66	4.59	156.29
1067	C153-0353	**5**	40.7352	329	337	805	1.78	3.35	51.01	57.55	4.84	195.94
1068	C155-0268	**5**	40.7258	475	444	392	4.63	5.99	69.57	65.12	2.71	148.76
1069	7752-0084	**5**	40.6725	358	325	744	1.35	3.23	71.51	74.19	3.37	149.18
1070	C797-1594	**5**	40.645	301	312	836	1.85	4.13	42.68	46.69	2.63	143.85
1071	0111-0120	**5**	40.63	319	326	290	1.38	3.81	49.36	51.5	3.66	168.33
1072	0140-0025	**5**	40.531	249	314	299	1.53	3.09	45.28	35.07	2.28	161.46
1073	0068-0009	**5**	40.4956	343	325	683	0.8	3.72	59.12	60.91	5.12	134.73
1074	7571-0910	**5**	40.4766	499	453	693	0.75	2.47	51.17	52.23	4.14	174.46
1075	C174-0657	**5**	40.4172	405	386	569	2.4	4.43	49.28	63.81	4.58	140.35
1076	7582-0257	**5**	40.4096	205	256	490	1.51	4.33	63.69	50.46	2.28	156.47
1077	0242-0327	**5**	40.3298	346	312	574	1.97	2.39	32.71	47.08	4.41	158.86
1078	1014-0012	**5**	40.3153	345	316	401	2.09	3.83	47.98	48.26	3.4	110.68
1079	0068-0008	**5**	40.3092	346	325	689	0.72	3.66	60.51	60.22	4.97	141.79
1080	7445-0094	**5**	40.2712	404	368	898	1.59	3.71	42.88	54.24	3.2	130.45
1081	7305-0073	**5**	40.0635	308	327	628	0.82	3.53	56.84	57.07	2.58	135.75
1082	C155-0475	**5**	40.0601	229	255	291	2.31	4.6	50.08	55.41	1.26	149.59
1083	7610-2196	**5**	40.0354	316	311	621	1.58	4.06	62.11	59.46	2.99	128.87
1084	7756-0056	**5**	40.0112	385	379	574	1.43	3.98	53.22	58.81	2.59	155.54

Appendix (ii): Scoring of HsFKBP38 virtual Screening solutions

Among the employed of GOLD, GLIDE SCORE, Ludi, PLP1, PLP2, PMF, JAIN, scoring functions ligands which are in agreement with more than three scoring are further considered for visual analysis. After careful interaction pattern analysis, ligands with favorable interactions are selected from this pool.

Structure Name	Cons	glidescore	GoldFitness	LUDI_EE1	LUDI_EE2	LUDIEE3	-PLP1	-PLP2	JAIN	-PMF
000A-0072	3	-5.1501	21.2062	318	339	358	50.01	52.66	1.75	82.91
0096-0264	2	-4.75939	33.5514	292	327	298	35.76	44.78	3.06	63.15
0140-0081	2	-4.76692	30.1933	278	297	267	42.13	42.38	3.7	63.5
0180-0339	0	-4.92867	37.132	261	257	279	40.31	33.36	2.58	39.07
0242-0679	0	-5.66774	37.8573	253	267	238	36.36	29.26	1.83	36.16
0242-0772	1	-4.93872	32.0712	236	251	230	43.96	45.68	2.23	60.43
0312-0030	0	-4.73653	34.8133	156	209	239	38.04	42.37	2.16	41.08
0342-0097	1	-4.6293	35.3669	267	253	220	42.33	35.38	2	39.49
0342-0165	3	-4.65022	28.6376	210	247	212	36.88	39.27	3.22	63.03
0342-0281	2	-4.56615	31.6901	270	298	326	42.62	47.48	2.55	63.33
0386-0495	1	-4.71791	30.1888	250	273	299	35.16	31.54	1.33	40.97
0386-0498	0	-4.79515	29.6082	240	273	295	20.21	23.58	1.53	35.24
0413-0259	1	-4.56344	29.8254	253	265	261	14.03	17.07	0.19	14.13
0413-0281	0	-5.0538	30.9872	344	331	306	27.15	28.91	1.3	34.11
0418-0109	3	-4.71283	27.324	234	272	245	43.91	44.13	3.63	61.53
0422-0126	3	-5.14165	27.6019	429	357	332	13.81	34	3.05	48.6
0475-0448	1	-4.6381	28.0728	250	284	253	25.43	15.5	0.83	42.62
0496-0020	2	-4.72225	30.4387	301	272	354	30.99	38.51	2.2	52.71
0496-0023	2	-5.35684	29.9237	351	311	339	23.57	40.31	3.1	50.44
0527-0216	4	-4.79158	27.4782	499	452	437	32.52	43.1	1.06	69.46
0555-0073	0	-5.31352	28.3881	265	261	280	31.1	37.45	2.41	50.08
0588-0028	2	-4.8103	31.7681	350	343	314	7.49	21.22	3.31	30.63
0591-5259	3	-4.65094	29.2753	266	296	313	53.19	52.6	1.78	43.77
0634-0074	0	-4.75716	37.2949	269	312	285	33.33	50.5	2.87	27.8
0634-0077	0	-4.73619	38.9181	330	338	366	36.3	45.32	1.18	36.11
0666-0814	4	-4.76665	43.2063	216	299	378	45.1	59.77	4.07	47.1
0787-0567	6	-5.6254	24.1328	415	411	479	53.15	58.57	4.69	45.22
0866-0010	1	-4.79255	7.2061	255	279	415	36.07	36.63	2.67	44.6
0866-0011	7	-4.68753	17.2628	398	378	399	62.36	54.66	3.91	46.54
0896-6245	1	-4.7616	13.1843	263	290	261	38.81	41.22	1.97	52.32

0964-0015	1	-4.67801	32.6264	262	263	289	45.18	38.62	1.69	46.72
0988-0229	0	-4.77137	32.1447	317	329	291	25.26	19.55	0.93	40.06
0992-0063	2	-4.84832	39.8115	329	352	300	32.27	47.51	3.49	21.42
0KPI-0011	1	-4.81107	22.9713	200	236	207	32.19	31.43	1.77	52.73
1030-0008	1	-5.1968	31.7257	330	346	302	37.69	37.22	1.86	55.37
1067-0457	4	-5.20962	46.3808	354	323	355	71.32	64.35	0.93	39.9
1153-0050	3	-4.56653	20.8703	235	260	239	51.64	48.79	0.79	74.31
1153-0139	3	-4.79258	37.306	376	328	288	48.39	52.46	1.4	45.08
1165-0527	1	-5.16043	27.7271	138	201	176	23.42	25.07	3.5	14.5
1189-0952	2	-4.5797	26.4535	243	271	240	38.7	37.08	1.48	61.34
1227-0187	4	-4.78715	38.6724	490	449	473	24.87	32.52	3.95	50.59
1269-4541	3	-4.98153	35.2011	318	330	456	52.98	53.44	2.55	51.66
1288-0128	3	-4.56588	30.3934	301	353	486	37.61	41.1	1.58	51.55
1288-0508	1	-4.89802	30.9814	268	308	273	29.84	40.11	2.62	52.34
1313-0763	1	-4.65735	32.7443	339	332	348	45.82	49.05	1.76	43.22
1313-0805	2	-5.35259	37.0993	424	399	372	8.24	17.57	0.92	33.87
1317-0302	5	-5.32875	40.4785	329	340	478	66.47	62.77	1.61	52.3
1473-0338	3	-4.79988	49.1872	313	314	334	29.49	38.69	3.98	80.73
1509-0035	2	-4.78546	30.2525	354	356	337	23.19	33.34	1.43	43.25
1575-0018	3	-4.57168	39.069	263	274	245	46.95	44.8	1.17	69.91
1586-0038	1	-4.76202	36.1016	197	249	326	36.81	39.13	3.06	36.71
1607-0221	0	-5.08766	29.3789	277	274	357	24.28	31.87	2.07	39.26
1611-0162	4	-5.23013	22.4938	406	412	428	28.17	36.26	2.19	85.4
1658-0120	0	-4.75826	27.9808	331	336	313	20.18	28.34	2.87	39.32
1682-4367	1	-4.70851	34.1173	320	304	345	38.8	50.41	1.77	45.07
1683-0651	6	-4.61766	40.5199	691	600	575	44.43	54.35	2.41	27.72
1683-2654	6	-4.57529	47.3511	341	347	426	68.29	60.37	2.47	70.96
1683-5307	2	-4.83429	35.3288	307	324	401	40.73	47.96	2.55	54.26
1716-1936	5	-4.56951	24.3497	397	353	440	43.15	44.08	1.67	59.71
1752-0023	3	-4.951	27.4647	386	348	336	43.01	56.98	4.63	43.17
1757-0101	0	-4.73159	29.8394	298	335	301	44.25	41.18	2.84	46.22
1762-0314	5	-4.83652	36.7626	449	441	511	46.91	44.01	1.91	74.82
1762-0334	4	-4.76458	36.642	397	391	413	39.81	49.03	0.86	66.6
1778-1607	1	-4.7359	29.8102	312	353	324	13.99	20.96	0.34	26.31
1890-1141	4	-4.8546	40.0727	511	472	498	29.95	37.3	1.22	51.46
1900-1465	5	-4.72714	44.8392	409	382	403	30.85	44.37	4.18	41.16
1956-0095	1	-4.77489	31.5566	271	281	263	29.43	32.67	3.96	31.29
1959-0262	2	-4.74115	34.4244	318	343	379	41.3	45.92	2.51	68.05
1988-0448	1	-5.15575	26.8445	318	344	374	18.83	32.32	4.75	35.15

1988-0450	1	-4.71587	28.1433	216	244	223	25.78	33.25	1.26	37.85
1988-0451	1	-5.45716	31.8891	273	305	271	19.9	25.39	3.34	17.3
1988-0453	1	-6.19519	28.2991	315	346	319	23.28	38.67	3.97	30.17
1988-0456	0	-4.9763	27.8618	308	332	315	19.07	21.27	0.88	26.9
1988-0460	1	-5.22546	33.242	336	332	301	21.39	24.47	3.28	23.38
1988-0471	3	-5.23004	39.8798	360	371	396	23.47	26.66	0.97	33.93
1988-0480	4	-4.56368	38.3865	353	358	386	26.03	29.75	0.85	46.58
1988-0482	0	-5.4575	30.6109	317	304	279	11.19	19.7	2.81	6.52
1988-0483	3	-5.08113	32.0496	335	359	394	17.93	27.75	4.1	30.36
2020-0001	1	-4.66022	28.0385	168	188	172	25.46	26.97	2.91	43.42
2054-0606	1	-4.74318	31.2602	299	315	290	16.59	23.42	1.66	55.16
2099-0114	1	-4.94975	37.3581	317	328	350	45.63	47.82	2.22	63.36
2141-0080	3	-4.6737	35.5255	310	314	289	38.37	37.26	3.14	56.75
2159-1021	2	-4.72059	27.4076	264	289	315	34.34	35.52	0.91	60.08
2159-3862	1	-5.28973	34.0845	331	328	290	19.02	24.81	3.49	27.33
2187-0777	5	-4.79597	45.0471	391	347	430	42.98	52.54	4.06	50.55
2191-2828	3	-4.92076	38.7655	343	369	491	36.96	45.03	3.64	37.45
2251-2896	4	-4.64242	28.3343	299	301	376	59.51	62.24	1.14	73.11
2322-1792	4	-4.8585	41.4253	349	324	360	47.07	47.7	1.64	54.29
2374-0068	5	-4.78137	36.2168	351	376	410	28.95	37.23	4.26	51.67
2449-0156	5	-4.84518	39.9295	368	374	375	53.64	55.93	3.2	37.35
2458-0006	2	-4.62398	32.4137	257	278	318	47.6	46.78	2.54	48.48
2657-0705	0	-5.07126	30.8543	276	300	264	45.7	45.13	2.64	43.17
2680-0469	5	-4.60291	43.4186	388	360	375	37.12	54.97	2.9	21.35
2683-0240	6	-4.66471	47.1679	379	385	405	50.67	48.44	2.73	49.59
2684-0991	2	-4.60657	33.4772	308	311	274	45.99	48.7	2.71	83.92
2766-0213	3	-4.58204	35.543	284	308	448	40.08	39.71	1.13	56.32
2798-1116	7	-4.78904	43.9967	478	412	427	56.1	59.71	5.43	50.67
2806-0100	6	-4.63641	45.2412	425	400	469	29.31	36.76	4.29	19.63
2895-0212	5	-4.6465	43.3062	363	359	368	26.94	36.22	2.43	71.47
2921-0055	3	-4.59787	32.8364	245	288	314	50.8	48.7	1.04	59.94
2922-0102	4	-5.01948	31.1558	163	212	198	59.36	59.98	3.76	72.88
2995-0032	3	-4.74002	37.4938	242	262	288	59.82	57.95	0.91	55.84
3000-1887	0	-4.99495	27.2986	170	205	224	22.26	25.02	1.17	37.66
3019-0081	7	-4.80688	40.2106	429	400	458	64.53	71.3	3.51	42.09
3030-5144	5	-4.59377	42.1119	417	386	461	45.21	41.12	2.87	17.34
3076-0094	0	-5.02838	28.6606	306	313	284	13.47	22.16	0.41	45.82
3161-0553	5	-4.91882	40.5119	440	422	440	49.2	48.42	2.44	20.38
3181-0100	3	-4.62739	30.2274	296	321	400	34.22	39.29	3.59	38.23

3232-1831	2	-4.59379	36.8117	259	295	368	42.95	45.08	1.88	62.29
3253-0341	5	-4.57871	31.7976	347	384	461	28.09	32.76	2.51	54.38
3253-0788	3	-5.08477	33.0131	362	344	376	26.69	32.95	3.19	53.18
3253-1719	0	-4.84237	30.9367	231	261	355	22.79	22.84	2.21	34.03
3253-1809	6	-4.70824	40.6125	426	356	389	41.95	49.48	2.97	54.2
3253-4636	8	-4.55666	43.3026	532	486	495	55.73	60.25	3.91	50.65
3254-2664	1	-4.59059	24.536	299	319	324	27.23	44.35	1.59	35.86
3286-0266	3	-4.72521	44.2466	396	392	361	38.15	38.05	1.04	46.08
3307-0780	2	-4.56914	34.7698	215	230	199	55.62	49.82	1.88	49.47
3342-1641	0	-4.83046	31.5311	294	296	332	36.06	34.24	0.61	45.06
3343-0130	6	-4.64497	43.2562	574	498	568	32.82	45.28	4.59	34.8
3365-1359	5	-5.06969	44.7473	407	382	424	39.94	45.9	4.13	42.46
3365-2357	8	-4.9219	43.6814	488	418	478	63.01	61.63	3.08	54.38
3365-4744	1	-4.69141	25.0446	225	271	237	36.33	34.68	0.97	38.14
3379-3181	8	-4.60852	38.0748	566	484	540	62.22	69.98	4.84	84.55
3379-3192	6	-4.85786	43.5743	485	412	480	34.22	42.05	3.7	79.63
3390-0036	4	-4.61997	31.3812	412	351	426	35.54	43.46	2.4	34.4
3428-1906	3	-5.49428	32.4803	392	344	439	28.44	41.43	5.16	42.16
3448-7635	6	-4.96512	35.4095	358	376	384	56.3	61.96	3.2	48.95
3454-1952	2	-4.72274	34.4598	283	310	393	44.28	46.11	4.38	45.43
3454-1960	1	-5.26615	30.821	356	326	344	45.47	44.24	1.98	47.6
3454-2283	0	-4.84239	28.3904	299	311	288	7.92	14.62	1.93	44.51
3454-3296	1	-5.13623	25.7736	271	276	240	31.31	34.32	2.33	62.36
3455-0729	1	-4.73822	34.0374	240	278	357	42.73	38.96	1.42	59.76
3461-1087	2	-5.13006	34.9687	288	314	346	37.03	54.47	1.58	76.09
3483-0163	2	-4.78077	34.633	309	328	349	50.25	54.01	2.5	49.83
3483-0166	2	-4.872	35.3728	303	326	350	49.56	52.06	2.9	39.23
3524-0048	2	-4.86639	34.9258	315	313	343	32.1	42.59	3.87	57.8
3529-0050	2	-4.58363	27.5052	291	307	280	13.74	31.65	3.28	26.78
3553-2133	3	-5.06994	37.2332	271	321	284	58.1	55.84	3.38	46.33
3558-0144	6	-5.0663	50.2429	438	427	448	28.13	43.24	4.45	61.13
3606-0468	4	-4.69327	36.1542	348	319	406	20.36	36.81	3.56	38.3
3653-0465	6	-4.76591	40.8765	389	373	386	44.36	55.85	3.27	26.53
3716-0340	8	-4.91081	48.4333	534	454	586	47.54	57.71	3.37	76.48
3785-0197	0	-4.82734	28.9354	283	256	238	27.43	29.93	1.01	51.63
3801-1356	0	-5.22486	29.8653	179	259	344	35.6	47.71	1.19	35.95
3902-0123	5	-4.66184	38.9714	327	330	356	47.43	59.67	3.61	52.93
3966-2654	5	-4.5808	38.4241	366	354	372	57.81	58.28	2.95	43.56
4031-0440	4	-5.72067	42.234	325	300	328	58.22	57.17	2.35	54.25

4031-0648	6	-5.52669	42.4339	400	362	314	47.66	54.32	3.13	24.53
4031-0652	3	-5.06043	42.6024	393	343	301	45.93	52.09	2.86	32.04
4031-0664	1	-5.54382	41.4571	318	309	275	33.66	42.94	2.94	34.54
4031-0925	7	-5.38332	43.2896	384	365	391	55.78	59.97	4.33	45.37
4031-0928	5	-5.29467	44.8957	388	338	363	60.52	64.22	3.42	43.13
4031-0973	0	-4.73058	33.7037	297	271	287	31.23	39.34	2.83	25.54
4031-1361	5	-5.28595	43.4592	421	377	344	60.58	60.1	2.4	41.94
4031-1995	4	-4.5883	26.8605	414	362	324	37.41	45.15	3.22	31.34
4161-2762	1	-4.97302	27.4814	302	310	278	46.34	40.18	1.34	72.11
4282-0022	1	-5.03161	34.1872	311	308	376	27.74	39.57	2.8	59.94
4286-0004	2	-5.22163	34.0261	225	271	409	45.32	40.61	1.65	55.31
4373-3092	1	-5.12403	38.8524	206	250	280	43.9	47.21	-0.06	77.34
4427-1198	1	-4.6026	32.9816	248	258	286	38.87	40.1	2.39	39.18
4476-3580	1	-4.58743	33.2328	275	260	226	22.45	29.87	1.98	40.6
4478-5322	1	-4.57034	23.7012	252	265	297	34.43	41.05	0.35	42.19
4483-3377	2	-4.64173	31.0169	313	287	325	32.88	44.07	2.37	60.02
4522-0096	2	-4.63819	36.3598	265	268	302	22.85	35.74	2.2	67.37
4567-0761	5	-4.56832	28.037	257	295	323	54.45	55.54	3.43	83.46
4607-0063	0	-4.73346	36.4265	309	324	360	38.76	41.33	2.46	50.16
4682-0017	7	-4.64852	48.8436	343	318	384	59.16	62.55	3.05	78.1
5008-0178	0	-4.98777	18.1418	233	254	276	16.8	26.12	2.95	42.24
5254-2281	3	-5.58333	34.8739	448	421	417	1.37	9.93	1.76	26.4
5321-4202	0	-4.936	13.0196	228	281	242	17.04	23.91	0.99	43.57
5458-1304	3	-5.02011	36.5094	359	330	345	48.98	50.19	3.62	33.25
5609-1436	2	-5.12774	30.764	288	323	393	52.32	51.21	2.34	35.55
5641-1679	8	-4.82667	41.2486	405	409	429	54.86	61.4	4.7	56.86
5910-0313	4	-4.70637	41.5279	288	311	329	57.03	48.65	2.24	65.34
5910-0314	3	-4.67752	43.5478	267	308	325	42.62	45.3	3	31.31
6025-6024	2	-5.49329	33.3235	411	370	363	-0.8	8.38	1.46	25.58
6036-1643	5	-4.73523	42.021	413	403	431	41.56	46.24	2.35	54.18
6049-1661	2	-4.71383	32.0702	313	305	377	42.13	49.81	2.98	45.48
6179-0051	2	-4.70714	28.3175	271	277	358	31.35	32.34	3	47.25
6228-0603	3	-4.60012	27.7189	207	254	278	29.15	34.74	3.37	59.16
6253-0647	6	-4.63883	40.0105	362	351	434	36.36	36.93	4.88	39.64
6466-0094	5	-5.56933	43.6383	335	381	384	48.51	59.93	2.55	12.44
6623-1015	5	-4.5995	29.1427	372	338	372	46.6	46.86	3.39	59.21
6623-1016	1	-5.26349	26.1209	323	276	306	44.38	50.64	2.69	54.48
6623-1017	1	-5.25767	27.629	279	282	295	46.41	47.98	1.56	54.92
6801-0196	4	-4.56539	42.3017	310	320	346	30.05	40.48	3.4	59.24

7213-0474	6	-4.69213	43.2253	462	406	414	36.43	47	6.14	47.07
7229-0672	2	-4.78909	25.9061	342	363	329	41.6	42.74	0.57	61.68
7229-0799	4	-4.83683	29.9274	345	351	428	45.75	46.98	3.31	52.76
7282-5703	5	-4.61722	40.1047	335	341	420	45.78	60.53	4.34	43.46
7287-0117	1	-4.92857	37.0385	172	206	183	45.65	56.54	1.5	46.15
7386-1001	4	-4.5785	33.0861	305	314	403	38.69	38.74	4.04	56.38
7386-1020	1	-4.79316	24.0305	247	271	285	40.29	46.04	3.05	49.67
7388-0009	2	-4.62088	32.5291	294	283	309	39.31	46.96	1.12	67.43
7399-0102	5	-4.9433	40.9516	370	373	438	31.89	42.12	4.53	43.5
7445-0094	7	-4.68043	41.7078	379	380	400	38.72	42.77	4.75	55.19
7445-0095	2	-4.60683	38.6228	322	316	344	35.23	43.5	2.85	57.86
7476-0330	1	-4.86645	28.1093	308	262	303	20.64	36.59	3.33	42.26
7489-2091	5	-5.83675	43.048	328	353	415	52.38	52.15	2.06	33.04
7599-1876	1	-4.84682	29.011	262	266	233	15.09	24.08	2.55	58.67
7610-2209	6	-5.10276	40.2977	367	317	453	62.16	61.79	2.75	53.37
7680-1114	3	-4.71526	37.9788	321	338	366	45.01	57.1	6.17	32.27
7682-0301	1	-4.90585	32.1107	338	305	280	23.42	32.83	1.36	51.8
7684-1460	5	-4.58984	26.2574	311	344	413	55.94	51.83	0.68	105
7747-0545	4	-4.56417	39.1145	400	371	386	40.16	45.77	2.23	43.26
7790-0729	3	-4.61043	32.9046	272	293	361	45.96	42.78	3.09	65.36
7790-1101	0	-4.83488	33.3028	263	300	374	17.2	27.54	2.11	35.94
7828-0498	5	-4.66866	35.4932	336	361	415	44.62	48.24	3.89	57.85
7834-0069	2	-5.09173	43.8035	299	289	358	44.21	55.28	1.74	33.97
7976-0008	3	-5.00202	25.7436	389	385	347	23.56	33.66	1.92	66.02
8001-8037	0	-4.81828	25.3265	261	243	282	40.09	42.55	2.77	50.17
8002-6761	2	-4.87049	38.0318	297	290	323	57.96	52.05	1.77	42.95
8002-8641	5	-5.00164	41.517	361	373	338	47.13	45.67	3.74	43.27
8003-2783	8	-4.62705	38.4774	389	358	384	50.96	54.96	3.74	57.78
8003-2963	2	-4.83929	37.103	345	348	305	36.14	47.81	3.47	58.66
8003-3379	4	-4.60001	41.0298	360	334	292	27.86	39.98	3	31.52
8003-4746	5	-5.1374	49.809	318	316	342	71.51	69.07	3.56	62.07
8003-4894	2	-5.10139	39.4934	315	305	261	48.17	51.75	2.38	38.41
8003-7273	2	-4.65313	28.5049	285	279	351	43.58	50.23	3.23	27.94
8004-0444	2	-4.89978	31.4963	342	322	285	49.91	47.87	3.18	46.68
8004-5579	7	-4.70271	40.8355	446	435	495	39.42	47.62	3.56	65.06
8005-1790	8	-4.61244	33.6769	633	563	625	63.4	80.64	6.16	74.19
8005-2024	6	-5.04833	31.9019	367	359	383	58.68	57.15	1.96	51.68
8005-2746	6	-4.63509	38.3513	404	359	389	40.31	47.49	3.03	56.96
8005-3895	4	-5.41518	41.759	348	337	293	56.56	58.14	2.44	28.73

8005-8292	2	-4.67726	31.4057	311	306	269	30.38	36.28	3.37	45.08
8005-8378	7	-4.56462	15.3477	394	372	392	56.87	53.56	2.46	58.4
8005-9052	1	-5.04916	33.3861	303	319	394	38.48	44.53	2.6	45.76
8006-0933	4	-4.64678	31.1364	360	350	315	40.82	44.73	1.98	56.82
8006-1073	0	-5.21548	28.6437	153	181	221	22.99	25.41	2.33	36.5
8006-5157	4	-4.90303	42.4601	332	350	363	56.5	61.95	2.85	32.28
8006-5775	1	-4.63113	29.3111	229	265	299	24.28	15.15	0.19	43.84
8006-6696	5	-4.67047	41.741	340	369	446	37.78	43.53	2.76	55.89
8006-7175	1	-5.60326	32.4901	268	268	241	45.62	46.06	1.93	64.68
8006-7176	1	-4.87027	31.051	308	305	388	37.92	42.48	2.29	44.44
8006-7183	1	-4.93907	27.3599	314	307	392	19.69	26.51	1.38	41.65
8006-9739	6	-4.82088	41.8036	407	400	422	35.93	46.54	3.58	56.66
8007-2396	3	-5.05991	32.7548	369	343	371	29.79	37.15	4.05	51.84
8007-3937	1	-5.1454	40.9781	249	294	320	43.37	49.81	2.91	30.74
8007-4032	4	-4.80999	27.7863	313	315	392	53.01	52.57	0.93	65.5
8007-5093	3	-4.60026	34.9744	308	339	351	51.48	54.22	2.35	45.82
8007-7978	2	-4.64593	39.1048	155	217	205	35.2	44.98	3.47	47.01
8007-8160	3	-4.55728	34.6116	293	298	260	58.94	57.27	2.76	33.98
8007-8760	6	-4.5921	55.5606	398	408	376	54.67	70.99	2.66	51.18
8008-0774	1	-5.69968	36.1187	240	289	268	27.63	34.37	3.97	29.47
8008-2612	3	-5.05148	-198.518	275	290	260	46.86	57.03	1.03	59.42
8008-4619	7	-4.95401	40.2165	392	342	380	58.69	61.01	3.8	80.4
8008-6724	2	-4.6132	37.2225	199	218	193	46.47	50.87	1.7	53.63
8008-6735	1	-4.73517	33.5453	200	264	275	40.37	37.77	0.68	57.38
8008-7356	2	-4.91619	33.5581	312	305	498	48.62	49.1	2.8	50.86
8008-9031	4	-4.58892	30.4253	308	335	412	32.81	44.97	3.06	55.61
8008-9495	2	-5.15606	29.8475	300	325	448	26.23	33.92	2.5	58.53
8008-9661	6	-4.93109	48.4204	423	401	529	66.48	65.61	2.44	50.45
8009-0880	2	-4.60366	21.9677	263	287	317	41.68	41.27	1.31	53.19
8009-2641	3	-5.16184	40.7483	301	286	361	40.54	50.21	4.89	58.08
8009-2666	3	-4.70819	33.733	179	227	314	52.14	52.42	2.57	31.55
8009-3676	1	-4.58372	39.1665	254	272	226	35.57	38.71	2.97	44.38
8009-7141	2	-5.09169	35.554	319	301	380	42.35	49.04	3.38	43.33
8009-9783	1	-4.86461	39.199	273	307	282	38.03	35.86	2.33	58.97
8009-9846	1	-4.82334	34.8212	333	342	303	30.03	27.37	1	64.69
8010-1146	4	-4.8312	35.6539	614	528	498	25.01	38.26	2.27	56.04
8010-3193	2	-4.63863	40.6957	316	323	298	28.34	29.91	0.64	50.82
8010-3699	7	-4.71807	38.1974	427	405	423	32.13	55.77	4.22	52.45
8010-4944	3	-4.79282	35.5498	245	283	307	57.12	56.57	2.27	60.14

8010-6526	0	-5.26514	25.5807	301	277	305	20.01	25.1	2.25	46.49
8010-8653	1	-4.90786	32.2132	280	321	372	43.12	42.33	0.52	69.33
8010-9393	3	-4.57734	27.6138	382	367	338	24.29	35.13	2.66	32.92
8011-1291	0	-4.75838	31.4331	223	266	245	23.63	30.61	2.04	37.77
8011-1481	1	-5.26862	30.2151	344	324	407	36.83	40.6	1.71	48.51
8011-4385	1	-4.60147	25.172	263	303	272	19.58	22.8	1.72	40.84
8011-7780	1	-4.60941	30.2245	249	271	244	35.97	39.65	1.77	47.53
8011-9745	9	-4.57185	45.2147	398	375	453	50.37	57.85	3.22	76.33
8011-9748	5	-4.96428	41.532	369	389	403	36.82	41.5	3.15	49.63
8011-9785	4	-4.57532	23.8541	322	319	355	54.86	53.3	2.88	56.67
8012-2209	4	-4.65577	32.6002	163	229	261	46.77	41.09	3.19	55.56
8012-4530	0	-5.06457	32.2258	250	245	275	36.63	42.22	2.65	39.35
8012-5165	1	-4.56305	20.2477	281	333	336	39.99	30.98	2.77	34.82
8012-5559	4	-4.77837	54.3408	489	426	397	36.61	36.15	1.99	50.59
8012-6946	8	-4.59481	38.5204	558	500	560	60.2	63.04	3.63	78.23
8012-8487	1	-4.57868	31.504	237	283	309	24.96	28.64	2.29	47.85
8012-9229	0	-4.84102	34.9276	225	223	212	21.57	28.92	2.85	38.49
8012-9240	6	-4.78155	47.0202	411	391	410	42.46	53.91	3.41	49.84
8013-0488	4	-5.08389	28.7386	306	311	329	53.32	55.44	3.17	51.86
8013-1615	3	-4.81468	50.396	176	247	375	47.91	51.95	2.64	37.39
8013-1744	5	-5.47966	47.7498	228	313	390	55.45	54.78	-0.04	69.38
8013-2144	6	-4.99708	48.4964	383	391	355	53.45	58.38	4.03	40.41
8013-2146	8	-4.58939	49.7984	437	410	430	52.58	62.44	4.23	38.59
8013-2310	6	-4.598	38.4427	452	445	414	20.88	41.58	4.27	60.25
8013-2412	1	-5.17163	33.3343	194	220	257	44.22	44.09	2.77	54.91
8013-6613	5	-4.57953	42.7617	305	340	415	44.07	60.15	2.42	54.99
8014-0488	5	-5.00131	37.6649	423	412	540	22.19	42.57	8.39	72.19
8014-1399	1	-4.91331	25.1489	238	229	266	25.41	30.08	2.8	60.73
8014-1556	2	-4.6521	32.4946	312	324	310	26.67	39.64	3.67	49.6
8014-1954	5	-5.09751	38.3496	330	352	415	50.78	54.06	2.61	76.51
8014-5665	6	-4.60403	43.4456	388	361	389	42.11	50.88	4.76	45.67
8015-0305	3	-4.87748	34.829	259	293	374	58.17	55.26	2.64	53.42
8015-0817	1	-4.55856	30.8492	289	274	353	41.11	39.36	1.74	51.54
8015-0997	1	-5.02885	26.1344	350	310	298	24.02	34.65	2.27	31.94
8015-1087	0	-4.85006	27.5156	161	196	178	41.84	39.84	1.72	51.12
8015-4159	4	-4.56305	43.544	248	310	336	48.57	54.76	2.95	45.48
8015-6484	2	-4.57044	28.5385	291	282	359	25.54	35.57	3.27	32.95
8015-6506	1	-4.66511	34.8538	220	284	251	12.61	24.09	1.29	46.89
8015-7063	2	-4.66774	34.4783	295	323	324	42.52	42.46	-0.21	65.48

8015-8433	2	-5.14307	32.5559	366	332	409	18.6	34.39	1.51	47.36
8015-9715	0	-4.72635	29.5345	257	258	335	39.65	41.24	2.98	35.34
8016-0681	0	-5.17046	29.429	342	319	287	23.47	35.17	2.8	50.05
8016-1802	0	-4.86163	31.266	321	295	268	24.88	30.47	2.8	35.26
8016-2906	3	-4.99337	25.7478	366	368	343	14.46	35.15	3.92	34.05
8016-3216	0	-4.89403	28.9199	232	228	263	26.48	30.55	1.25	38.49
8016-3361	5	-5.00603	40.3174	259	257	221	60.18	60.61	3.18	67.57
8016-3600	1	-4.75817	35.6318	308	319	298	26.23	35.92	4.41	23.37
8016-3877	2	-4.69693	34.1871	295	305	265	32.81	33.84	2.73	65.34
8016-5677	2	-4.90919	34.5729	245	294	411	28.16	32.39	1.05	56.77
8016-6433	4	-4.73968	39.8685	390	392	418	41.68	36.51	1.05	73.98
8016-6670	2	-5.00878	36.6006	237	254	225	50.67	50.02	2.39	52.2
8016-6733	3	-5.12338	43.6472	345	378	393	31.94	32.22	1.96	50.79
8016-6968	6	-5.09609	45.9513	424	385	354	50.44	48.83	3.85	76.16
8016-7328	1	-4.84213	35.1797	263	280	315	36.04	38.61	3.64	25.62
8016-8065	2	-5.17203	-18.7408	341	350	321	29.57	39.22	3.92	45.98
8016-8415	1	-4.90465	28.3954	190	220	193	39.78	36.55	2.7	62.85
8016-8433	5	-4.65927	40.6089	282	325	385	44.64	50.52	3.09	54.45
8016-8446	3	-4.6269	35.619	262	271	276	54.36	48.63	1.34	57.86
8016-8520	8	-4.55719	46.9659	410	401	398	71.42	70.37	2.23	75.44
8016-8521	3	-5.91245	50.799	343	335	414	39.2	51.59	4.3	47.97
8016-9130	1	-5.36258	27.6016	284	299	316	14.88	26.26	1.57	57.65
8017-0007	0	-4.86522	27.1856	194	185	227	10.05	16.16	1.56	29.94
8017-0163	5	-4.7329	41.7319	254	276	239	52.57	60.38	3.62	92.38
8017-1079	6	-4.56328	43.4056	298	326	401	61.9	60.77	3.14	31.72
8017-2169	9	-4.66118	42.1094	472	405	476	63.09	65.22	4.97	65.82
8017-2525	5	-4.76115	44.0611	399	386	341	61.85	63.12	2.33	31.26
8017-4049	1	-4.61222	24.2019	297	311	284	26.26	33.19	1.66	49.81
8017-4179	9	-4.66545	46.7065	457	421	538	69.37	71.54	4.11	68.53
8017-4495	7	-4.90145	43.3538	416	392	469	61.9	65.98	4.36	39.61
8017-4592	4	-5.4717	48.1411	325	366	386	58.3	47.15	2.91	43.88
8017-5520	2	-4.55887	34.2554	265	318	498	35.81	33.84	1.89	26.38
8017-8070	0	-4.88958	28.0863	332	330	307	32.35	35.05	2.29	45.53
8017-9350	3	-5.34082	40.3329	214	268	278	46.45	51.66	1.34	52.62
8017-9359	3	-4.70567	32.9885	373	329	349	23.59	37.47	2.11	52.06
8018-0388	0	-4.80955	30.7937	216	237	225	35.6	40.23	2.53	50.84
8104-00807	2	-4.57395	24.9243	281	318	289	16.42	24.36	1.19	56.53
8137-0524	6	-4.88991	33.12	364	352	439	65.47	67.76	3.09	38.61
8175-0085	1	-4.7985	34.7952	249	273	301	40.52	43.68	0.7	54.95

8211-0323	3	-4.95816	32.3864	331	333	393	55.05	50.02	2.27	73.74
8319-0173	2	-4.58541	19.4037	284	323	289	21.47	22.44	0.07	61.86
8377-0876	5	-4.82603	38.6388	352	348	408	58.38	57.04	1.41	59.18
8510-0382	5	-4.57784	36.3065	383	342	402	53.13	61.49	1.95	43.77
8538-0044	7	-4.78164	30.1654	388	354	420	54.51	59.37	3.09	71.06
8538-0075	3	-4.68969	35.502	299	290	375	49.24	43.76	2.45	58.04
8563-1175	1	-5.15058	33.9148	339	336	297	14.14	33.68	3.92	24.68
8603-0251	2	-4.57775	31.0238	333	321	357	21.34	32.17	2.87	67.71
8610-0307	7	-4.68809	42.4029	431	397	419	29.67	55.9	4.71	0.08
8640-0186	9	-4.57988	47.306	393	388	560	54.57	60.4	5.61	65.61
8645-0064	1	-4.68723	31.3694	250	312	336	28.02	31.58	1.19	40.19
8755-0072	4	-4.6369	35.4494	281	309	396	47.11	42.27	1.35	61.68
8755-0116	1	-5.05378	34.8447	173	223	247	45.4	53.92	1.33	41.12
A0012994	7	-4.66371	37.981	404	376	463	58.52	58.67	3	42.19
C066-2544	1	-4.83931	31.0453	302	292	319	14.57	21.89	3.09	26.01
C066-3578	5	-5.10949	32.5271	376	365	482	59.28	65.07	2.69	46.09
C066-4933	7	-4.88317	39.9989	444	363	509	52.6	68.18	4.4	32.53
C066-5640	4	-5.59862	34.5289	267	244	379	51.94	56.24	2.23	63.8
C067-0093	4	-4.61875	35.709	369	334	360	30.92	40.57	3.37	58.61
C082-0674	7	-4.80972	39.979	407	376	501	48.35	52.58	3.27	37.76
C085-1668	3	-4.57644	41.5623	309	356	334	18.45	20.35	1.32	24.21
C094-2422	3	-4.78783	32.4885	193	251	215	65.85	63.97	2.41	72.98
C102-0210	4	-4.68831	30.482	336	307	388	51.58	53.89	2.04	43.27
C113-0126	2	-5.18606	35.1662	261	274	348	21.5	34.23	3.07	54.2
C113-0251	2	-4.92001	31.27	254	277	316	51.04	54.11	1.73	32.14
C113-0510	3	-4.61442	39.055	209	296	370	53.9	54.73	2.53	42.33
C113-0548	2	-4.95272	41.9806	225	295	259	33.15	42.61	3.28	30.07
C125-0496	9	-4.7101	43.9293	486	448	616	71.88	71.12	4.69	105.43
C137-0519	5	-4.61077	52.0149	504	448	461	18.62	22.34	1.77	47.59
C155-0265	3	-4.95859	34.1314	317	306	277	52.11	56.68	0.89	51.72
C155-0266	3	-4.82981	31.6594	254	311	269	64.66	68.91	1.63	54.15
C155-0336	3	-4.70099	36.4132	291	291	255	46.13	52.38	2.06	52.23
C155-0722	2	-4.63154	28.7396	344	362	365	42.02	48.78	2.8	38.43
C166-0059	5	-5.16683	46.8684	225	287	309	63.89	64.96	2.99	55.79
C174-1038	3	-4.56637	36.9172	228	250	259	49.4	52.8	2.01	39.01
C200-1369	5	-4.71631	42.0923	326	357	293	64.24	68.19	2.22	46.43
C200-3151	0	-4.89939	34.4366	190	243	331	4.01	16	1.22	37.3
C201-0384	2	-4.56428	35.5949	250	241	279	20.28	37.16	4.88	26.82
C201-0608	7	-4.76755	42.2952	425	379	403	69.91	69.13	3.65	36.18

C202-3155	6	-4.80687	38.58	425	393	525	52.84	59.16	4.38	48.08
C205-0013	8	-4.95719	40.1512	418	391	461	52.69	62.3	4.8	62.92
C205-0142	3	-4.82131	29.9002	317	335	398	37.22	47.79	4.14	66.12
C206-0445	1	-4.91025	41.1894	281	303	333	37.4	50.87	2.79	42.15
C206-0803	0	-4.8547	32.8563	246	293	289	13.92	10.84	-0.68	15.24
C206-0850	0	-4.79307	34.2482	213	268	262	14.54	10.78	-0.64	10.37
C206-1136	1	-4.58865	35.298	183	281	256	33.34	33.64	0.52	31.06
C224-0058	3	-5.20895	41.2774	303	326	301	34.89	37.83	3	61.55
C224-0164	2	-5.37375	46.1331	195	263	283	41.89	43.44	2.2	64.24
C224-0247	3	-5.11745	43.3876	306	345	361	60.97	68.43	1.98	47.73
C224-1095	0	-4.82234	36.1589	233	270	298	19.81	31.27	2.73	45.8
C224-1182	1	-4.57313	35.3479	237	286	263	44.38	46.93	1.35	45.34
C224-3354	5	-4.64876	41.6524	378	406	428	39.32	40.2	1.83	45.86
C226-3307	4	-4.98851	42.1813	388	352	420	34.98	48.67	2.56	31.68
C226-3309	4	-4.9028	42.6432	339	335	360	53.77	50.01	3.5	55.3
C226-3441	7	-5.62029	41.596	377	366	386	54.38	60.69	4.86	25.61
C228-0432	5	-5.06055	48.439	486	444	419	26.9	47.13	6.01	20.57
C254-0021	7	-4.61061	42.4092	400	375	442	59.04	57.2	2.18	41.7
C255-0306	8	-4.67325	49.2448	410	389	460	49.35	49.54	4.73	67.98
C256-0834	4	-4.58935	41.362	327	346	310	9.15	26.5	4.83	58.74
C256-1383	2	-4.58957	43.1065	242	286	312	32.06	27.32	1.96	26.22
C259-0435	2	-4.67736	38.7006	263	282	255	43.74	35.79	3.22	40.89
C259-0486	2	-4.70797	38.091	331	329	351	39.03	37.69	3.98	34.07
C274-1829	3	-4.98549	41.3856	226	281	250	49.01	55.89	1.08	33.86
C274-1911	7	-4.56132	54.3354	433	426	395	50.59	47.22	2.23	55.09
C274-3160	6	-4.59861	44.4751	510	459	462	33.51	36.6	4.12	49.43
C274-8313	4	-4.77951	54.9924	336	352	378	31.56	38.92	3.63	28.49
C274-8350	4	-4.95788	38.6241	304	313	449	66.87	61.71	2.53	56.47
C274-8448	2	-5.13496	41.8221	304	337	338	7.1	31.41	3.12	37.59
C276-0073	3	-4.85897	29.8198	400	404	370	34.16	40.29	1.76	74.11
C276-0767	2	-4.57222	31.8135	322	321	275	34.1	34.46	1.47	62.02
C276-1646	6	-4.84911	29.637	431	394	411	48.07	51.75	2.93	71.22
C276-1680	4	-5.00431	31.2935	488	413	488	32.38	49.62	2.53	76.94
C276-1683	5	-4.65098	30.6961	394	371	332	41.75	38.66	3.12	54.65
C278-0019	3	-5.03153	39.6597	233	279	307	54.86	56.5	3.47	48.93
C278-0020	2	-5.83125	39.8339	325	326	356	57.67	57.73	2.78	49.16
C289-0449	3	-4.69947	39.7801	324	343	283	56.05	62.1	2.98	48.18
C289-0489	6	-4.64603	40.3229	375	374	338	54.73	57.84	2.07	34.64
C301-1417	5	-4.61194	44.4574	371	351	364	31.53	49.24	4.41	31.64

C301-1573	4	-5.30977	42.3115	351	353	311	39.51	51.3	3.19	36.48
C301-1870	0	-4.79677	30.6903	178	227	257	21.57	28.02	2.31	41.98
C301-2126	6	-4.70325	41.5777	437	396	432	48.19	51.22	2.84	17.5
C301-2177	5	-4.6799	43.8282	337	307	380	46.99	45	3.5	45.77
C301-2212	4	-4.7801	38.356	410	385	341	62.71	61.26	2.54	41.85
C301-3555	2	-4.72964	-68.081	351	333	348	30.37	33.17	1.01	74.77
C301-3622	3	-4.77796	-70.8393	336	342	516	64.07	65.89	2.16	47.69
C301-3678	6	-4.64732	41.4062	294	320	387	57.58	53.18	1.73	70.99
C301-3781	6	-4.63353	23.3881	351	358	414	69.6	64.97	1.66	35.39
C301-3825	0	-5.19466	37.1532	192	247	214	31.94	34.34	1.18	13.3
C301-4371	5	-4.59298	-71.7286	307	333	471	51.3	56.23	1.01	67.29
C301-8167	6	-4.85068	42.0277	398	359	421	81.44	74.49	2.03	45.29
C301-8273	2	-4.59337	40.2101	269	287	366	35.15	43.5	2.8	37.4
C301-9703	4	-4.62277	-1.4667	337	356	435	-0.7	20.54	1.57	67.28
C305-0598	3	-4.84282	47.1251	237	280	238	63.18	58.28	2.84	20.64
C324-1275	2	-5.02512	44.404	278	307	331	7.21	31.92	4.37	13.33
C324-2711	5	-4.71347	42.8703	460	465	438	23.88	25.77	1.93	44.79
C361-1812	3	-4.57467	50.6204	274	303	278	28.2	48.13	3.45	39.03
C361-2471	3	-4.91717	47.0191	171	282	240	55.39	49.98	3.66	39.41
C366-0266	5	-5.09618	53.6151	341	356	380	35.76	42.2	5.05	65.18
C444-0026	4	-4.80623	37.542	380	379	403	35.12	49.66	4.62	28.58
C444-0223	5	-4.62547	41.0196	317	339	403	70.45	66.76	2.61	31.23
C444-0432	1	-4.88867	36.5328	289	315	326	52.27	47.73	1.48	41.74
C464-3016	1	-4.73772	42.8348	229	270	254	31.77	44.38	1.27	45.12
C464-3031	7	-4.59353	45.0676	415	433	447	52.75	47.29	2.04	59.54
C467-0005	2	-4.55887	34.0501	290	334	349	40.91	46.11	3.15	7.31
C467-0015	0	-5.16729	32.7145	320	329	350	31.27	39.68	2.76	22.19
C467-0018	2	-4.64073	29.6275	288	327	350	33.24	38.91	3.16	18.65
C467-0031	5	-5.56245	31.6873	385	368	436	62.62	68.01	1.94	42.71
C467-0034	3	-5.05406	31.4293	347	337	355	42.8	53.75	3.25	37.65
C527-0309	9	-4.56049	55.9509	402	371	494	79.01	74.57	4.29	67.69
C527-1102	9	-4.65333	55.0288	382	392	509	74.82	72.39	3.96	56.97
C527-2038	7	-4.86805	55.7492	436	408	468	73.12	73.1	3.9	45.37
C533-1050	5	-5.19784	32.9445	419	389	402	53.54	58.31	2.93	35.17
C534-0239	7	-4.58369	44.5431	495	471	427	21.77	34.91	4.75	63.15
C548-2756	4	-5.31827	41.3339	169	271	354	49.05	53.71	0.73	53.88
C548-2823	4	-4.6441	42.3264	230	302	317	57.93	55.43	2.35	38.52
C548-2848	6	-4.58542	45.5394	272	353	430	80.19	74.77	1.45	41.84
C548-2982	1	-4.95893	44.9779	296	321	275	38.76	48.44	2.54	38.39

C548-2998	7	-4.62809	43.6351	400	405	531	83.14	83.46	2.93	33.69
C548-3033	4	-4.57935	45.8221	273	338	349	43.99	48.36	3.15	64.15
C548-3112	5	-5.21546	48.9739	313	353	368	52.52	55.63	3.02	38.87
C548-3710	6	-4.80021	48.6314	331	342	415	70.23	66.58	3.26	52.23
C548-3808	1	-5.33661	39.2634	283	345	314	20.09	36.43	4.38	27.7
C561-1863	6	-4.58382	41.6469	357	330	297	48.8	53.84	3.36	38.28
C562-1833	7	-5.2137	46.4641	481	477	491	38.37	51.94	4.92	69.14
C602-0445	0	-4.78082	36.7826	281	294	267	45.42	51.16	1.43	23.28
C607-0838	2	-4.60297	27.4067	232	270	334	24.37	31.99	1.5	53.73
C607-0928	6	-4.66707	38.7925	378	371	350	44.29	55.25	3.48	57.42
C607-0940	5	-4.62552	42.9502	299	327	345	55.83	60.43	3.16	31.06
C607-0945	3	-4.56607	35.5022	304	305	329	47.92	52.4	2.15	38.68
C607-0961	0	-4.72556	24.9804	239	264	237	35.7	33.84	1.91	40.75
C607-0971	6	-4.59392	42.3386	344	359	378	62.27	65.39	2.55	37.53
C607-0972	0	-5.18973	35.6263	264	289	260	41.98	37.69	1.16	35.8
C607-0985	2	-4.56624	28.9305	307	326	356	42.24	36.39	1.53	59.98
C614-0190	0	-4.92352	25.5095	287	295	329	28.43	33.11	1.85	44.5
C625-0100	5	-4.58172	37.5988	412	400	452	35.54	47.41	2.18	58.28
C646-0243	6	-4.55832	48.0943	392	405	420	40.96	48.13	3.27	42.7
C646-0281	3	-4.78862	49.1155	298	345	361	38.45	47.03	3.73	64.23
C648-0026	5	-4.89562	45.4226	324	343	377	48.33	59.43	2.53	67.05
C648-0253	1	-4.82799	41.1615	302	318	333	41.23	44.05	2.77	34.84
C651-0005	6	-4.66797	38.3205	415	364	494	57.92	56.69	2.4	50.79
C651-0089	0	-4.761	37.6939	311	309	288	34.01	47.85	2.78	31.21
C651-0090	5	-4.93	37.3804	408	351	369	59.98	65.76	3.44	31
C651-0341	3	-4.99498	38.7496	334	311	439	58.1	58.46	2.61	41.97
C700-1321	3	-4.79528	40.8901	272	297	369	49.86	55.84	2.39	39.29
C714-0007	2	-4.76286	36.5684	283	293	261	37.32	44.94	5.85	57.3
C714-0020	8	-4.59516	36.7054	396	363	391	55.54	55.1	4.12	60.64
C714-0021	6	-5.31918	36.7672	358	373	399	59.47	56.81	3.74	50.62
C714-0088	2	-4.88002	36.4706	277	278	306	28.21	34.35	3.18	57.99
C719-0097	6	-4.91939	35.0001	379	370	433	57.09	65.08	2.91	52.54
C730-0160	6	-4.89457	36.9361	432	383	401	48.67	57.51	3.91	30.97
C730-0429	8	-4.86481	49.2549	494	429	434	66.76	67.8	3.58	59.86
C734-0378	7	-4.67409	41.8342	426	394	412	40.61	51.51	4.08	66.98
C734-0393	3	-4.66198	30.9646	347	331	294	34.87	36.13	1.77	79.92
C734-0555	6	-5.17941	35.2049	388	360	413	53.62	60.79	3.79	37.43
C737-1673	7	-4.81205	37.6646	360	377	384	58.87	63.04	5.12	59.53
C737-1682	8	-4.67569	46.4348	420	415	481	61.45	59.8	2.28	79.7

C737-1790	6	-4.64298	44.0824	317	334	335	59.75	60.21	3.98	57.83
C741-1074	0	-4.82668	29.9866	345	349	354	29.76	40.06	1.43	26.86
C756-0057	2	-4.78817	42.4784	342	337	297	44	47.44	4.33	39.17
C756-0115	4	-5.43525	45.9902	341	359	319	47.46	44.77	4.68	37.94
C756-0134	4	-4.59893	23.8981	353	336	295	54.82	50.43	4.48	34.27
C759-0159	6	-4.83395	42.1022	275	311	392	53.31	55.15	3.47	65.34
C762-0220	6	-4.72325	40.3614	390	363	368	56.24	61.36	3.96	32.54
C785-3794	7	-4.57892	45.2679	372	347	521	64.25	65.28	2.73	86.02
C786-4125	3	-4.76046	45.4722	330	337	357	39.71	52.96	3.14	30.96
C791-0320	5	-4.68752	47.7333	333	346	360	54.46	61.15	3.99	45.97
C791-0449	6	-4.82195	44.7623	378	358	467	48.47	55.95	2.96	35.13
C794-0001	0	-5.02585	30.2574	213	255	323	26.01	26.67	1.27	34.83
C794-0028	0	-5.12024	29.9036	262	273	244	21.39	29	0.35	37.61
C794-0147	1	-4.97493	30.2514	283	272	266	19.31	31.67	3.25	27.02
C794-0330	1	-4.95168	29.6625	309	299	283	29.95	33.39	3.43	43.86
C794-0402	1	-4.85409	35.2564	321	337	319	6.56	14.01	1.78	53.14
C794-0445	0	-5.1173	26.7161	302	284	278	24.06	19.75	1.68	12.21
C795-0593	7	-5.53855	48.2529	423	412	474	57.63	62.92	5.08	45.03
C795-0609	7	-5.20217	41.5762	362	372	446	54.05	57.78	3.66	45.49
C795-0610	6	-5.17088	39.729	420	411	485	52.1	60.56	4.54	36.91
C798-0045	1	-4.83224	25.9047	286	278	306	21.44	28.42	3.48	35.53
C798-0067	3	-5.53124	34.1782	330	355	362	51.51	49.64	1.83	61.81
C798-0226	1	-4.70209	33.4432	241	256	331	6.99	17.88	1.06	48.3
C799-0155	7	-5.23051	45.1974	413	390	458	55.24	59.72	3.88	29.1
C799-0159	8	-4.67	45.3136	428	388	461	59.98	63.09	3.86	37.66
C800-0634	0	-4.74931	29.6107	250	284	257	46.35	37.72	1	46.59
C804-0122	5	-4.68439	41.484	266	291	368	59.55	59.51	1.84	90.48
C850-0006	7	-4.80527	31.6935	381	382	395	64.07	67.01	3.43	51.72
C852-0105	1	-4.72905	48.6858	270	327	296	32.53	43.43	2.95	33.14
C862-0071	1	-4.79284	29.2558	334	335	353	41.82	46.05	2.71	54.87
C867-0007	1	-5.30811	38.4774	275	304	340	21.57	37.83	4.77	48.01
C867-0020	0	-5.02183	35.2212	295	294	310	40.64	47.37	1.95	43.86
C867-0026	4	-5.04478	35.346	281	333	402	67.4	55.24	2.57	87.03
C867-0030	2	-5.11949	37.6857	295	325	335	51.38	50.85	3.22	39.5
C867-0082	3	-4.83327	40.5515	255	287	317	28.19	43.03	4.75	52.1
C867-0104	2	-4.84021	39.5628	330	302	373	55.53	56.96	2.72	33.3
C881-0362	6	-4.88684	44.5535	291	304	380	53.3	56.48	4.18	54.17
C887-0649	1	-4.74354	45.82	320	329	332	36.8	47.44	2.88	25.42
C924-1111	7	-4.7293	36.5148	444	403	480	52.35	56.12	3.07	57.18

C927-0019	0	-5.06611	39.5366	183	246	227	21.05	23.37	2.34	28.13
C927-0052	3	-4.5803	42.1129	286	305	316	42.52	36.28	3.92	29.14
C998-0605	5	-4.65774	44.4009	232	271	346	59.77	55	2.55	58.37
D003-1091	7	-5.23405	44.9163	413	389	470	59.64	57.23	4.91	47.21
D015-0083	3	-5.03975	29.4648	275	288	373	50.42	52.99	1.47	80.38
D030-0032	3	-4.67126	36.2155	193	268	293	60.92	65.49	2.37	39.92
D030-0116	1	-4.5837	33.2981	232	281	303	42.88	47.2	2.03	47.12
D030-0128	2	-4.64591	30.7827	267	266	284	46.77	47.85	2.25	48.07
D030-0142	3	-5.06541	38.0078	362	381	345	37.91	45.81	4.27	33.65
D030-0168	0	-4.87546	36.5952	223	285	288	38.45	45.56	2.74	47.49
D030-0175	4	-5.01717	36.237	341	370	393	21.25	31.48	4.26	56.17
D030-0737	1	-4.74287	-23.7385	208	260	284	36.55	38.7	2.05	66.88
D034-0287	7	-4.65896	45.1743	383	360	316	50.35	57.25	3.49	38.99
D042-0308	3	-5.51221	37.904	266	283	364	50.37	57.85	3.2	43.37
D043-0311	1	-4.81333	31.0123	243	223	191	38.49	31.77	1.28	56.2
D046-0022	1	-5.78175	29.7773	291	277	297	37.99	35.25	0.79	55.79
D060-0165	6	-4.56903	40.6565	318	344	311	48.31	56.43	4.76	61.33
D068-0028	7	-4.99828	46.4166	384	383	488	59.43	68.9	4.62	47.14
D087-0003	0	-4.72816	36.3993	168	228	199	40.17	41.41	2.07	34.27
D087-0007	1	-5.4143	40.485	222	282	255	37.9	38.84	1.87	29.77
D087-0009	2	-4.97388	45.3165	177	271	251	30.44	46.16	4.92	40.35
D087-0499	6	-4.57913	41.0351	189	270	239	51.37	55.17	4.23	72.22
D087-0539	1	-5.24373	36.257	223	290	256	35.78	39.41	2.66	59.88
D090-0053	1	-5.14546	37.1145	311	319	290	35.07	38.94	2.91	58.52
D107-0053	3	-4.67675	42.4653	306	313	388	24.97	40.86	2.66	20.94
D128-0008	4	-4.60576	39.438	238	300	387	47.16	38.16	1.35	54.86
D142-0032	5	-5.09488	41.7691	428	403	359	52.1	49.61	2.95	68.79
D174-0158	3	-4.86773	37.2598	295	310	321	54.54	56.11	2.93	58.12
D183-0015	1	-4.74081	1.1621	192	221	241	29.98	36.79	1.61	67.13
D216-0581	4	-4.67123	34.2232	359	316	394	41.45	49.49	3.39	46.9
D220-1094	6	-4.87408	30.0937	406	381	405	61.57	69.09	3.59	41.87
D247-0250	7	-4.91953	37.5925	491	444	443	47.24	57.82	5.14	65.56
D257-0682	5	-4.71191	36.2625	354	362	317	58.7	65.48	2.97	48.66
D265-0054	5	-4.62259	42.1688	425	391	424	30.82	38.37	2.18	46.46
D278-0485	7	-4.56667	41.6542	570	508	591	3.02	22.2	4.12	62.76
D283-0084	4	-4.59231	40.0791	272	298	373	47.58	54.44	2.44	48.94
D327-0029	9	-4.68237	45.1944	484	450	524	63.51	60.23	4.51	55.77
D355-0255	7	-4.70423	25.6246	355	355	417	58.55	61.11	2.68	85.29
D356-0316	4	-4.68303	46.9347	296	331	338	45.77	56.98	4.26	46

D356-0334	2	-4.75335	43.3111	295	314	279	37.52	47.03	3.3	32.21
D356-0370	4	-4.92978	42.8309	290	305	253	65.41	68.67	3.99	21.25
D365-0014	0	-4.76568	36.0546	224	272	355	39.24	40.63	1.54	44.73
D365-0053	3	-4.84198	43.2548	316	326	291	69.78	58.35	2.52	38
D365-0177	4	-4.64129	40.1781	296	320	282	67.91	58.43	2.55	37.19
D365-0185	9	-4.62144	44.4753	395	389	519	63.07	59.29	4.35	55.89
D390-1331	7	-4.96601	34.2042	373	385	396	55.09	61.73	3.78	53.57
D462-0117	3	-4.87946	28.5473	232	291	362	52.21	51.87	1.53	60.18
E002-0174	5	-5.27599	41.2865	345	341	414	55.08	61.39	4.11	34.17
E002-0226	7	-5.5468	47.5744	422	419	530	59.14	64.12	4	43.12
E002-0339	4	-4.75067	43.504	316	366	377	46.4	51.34	3.32	37.88
E002-0669	2	-4.59485	47.3509	341	318	342	32.8	35.44	2.15	48.14
E002-1567	2	-4.77285	31.6241	343	361	372	44.01	47.52	2.29	54.81
E002-2490	4	-4.60124	36.5749	385	358	411	44.25	48.58	1.14	50.37
E007-0113	6	-4.59118	32.8936	432	381	549	63.85	67.34	2.48	42.58
E022-0293	4	-4.66511	46.3382	357	363	370	40.71	49.58	2.13	44.25
E022-0758	5	-4.60295	47.9655	406	389	394	36.81	49.28	2.9	30.31
E022-0911	3	-4.58319	48.9002	348	347	359	37.91	38.98	2.65	36.33
E022-0983	1	-5.03836	46.1772	230	284	295	45.03	38.39	1.9	29.28
E022-1063	5	-4.85426	45.642	342	363	378	42	47.89	3.19	77.62
E135-0985	5	-4.67736	36.9312	279	315	390	59.93	56.45	2.69	71.63
E145-0093	2	-5.16657	38.2942	306	324	348	54.06	55.89	1.83	43.47
E155-0717	7	-4.76492	34.2419	407	378	388	54.23	62.73	3.28	52.34
E197-1071	6	-4.79727	38.9551	440	419	443	57.73	65.31	2.98	57.67
E207-0269	5	-4.61511	39.3533	332	302	379	54.43	55.25	3.73	33.82
E207-0308	2	-5.17719	44.6177	316	336	284	43.58	54.38	2.65	32.07
E207-0445	8	-5.44617	48.1676	388	362	430	61.18	64.2	4.63	71.68
E216-4847	5	-4.77441	35.0284	389	365	423	32.25	36.59	3.19	63.44
E216-4852	6	-4.55625	37.6423	377	372	389	55.98	55.08	2.64	41.43
E216-5172	4	-4.78312	30.7663	352	339	456	59	59.54	0.45	47.72
E216-5224	6	-4.61383	37.5065	418	394	441	52.34	60.81	1.55	43.77
E245-0072	2	-4.74275	39.9787	241	288	308	55.36	52.7	2.83	27.51
E245-0081	1	-4.65435	39.385	223	267	240	33.78	35.77	2.16	13.51
E245-0126	1	-4.8313	37.443	303	335	363	37.68	48.1	2.66	69.5
E245-0480	3	-4.77041	43.3386	352	371	330	36.81	49.87	2.21	30.37
E245-0483	4	-4.74822	43.1725	246	300	429	50.01	49.35	0.91	75.99
E245-0904	4	-4.87765	41.9027	341	336	366	57.37	61.91	4.28	30.36
E245-1317	3	-4.79879	36.242	366	345	420	27.1	27.95	4.21	30.17
E245-1460	5	-5.16326	37.3664	371	373	348	50.08	54.63	3.65	40.61

E459-0262	7	-4.76428	47.1724	395	413	495	47.73	48.7	5.11	53.54
E465-0050	4	-4.86348	43.7917	336	365	385	40.63	50.72	3.49	19.29
E465-0198	2	-4.89445	44.1499	320	371	325	28.8	31.48	2.85	41.24
E465-0647	6	-4.59767	44.4974	314	362	375	55.22	53.68	3.84	24.93
E511-0026	6	-4.78958	43.2527	392	359	314	53.21	61.02	3.49	49.03
E511-0632	2	-4.58668	29.0576	239	272	240	37.02	43.07	4.12	41.37
E511-1226	2	-4.6452	45.7098	264	280	357	45.05	49.93	2.39	32.25
E511-3273	2	-5.20092	38.6432	293	317	347	48.83	47.56	2.19	59.46
E511-3871	4	-4.63191	34.0059	319	331	357	44.46	57.49	3.5	72.49
E532-1515	7	-4.76831	43.9297	503	480	504	64.2	67.59	5.22	40.66
E557-0147	3	-5.96816	42.6515	305	320	337	43.44	42.91	3.33	52.57
E557-3255	4	-4.58682	49.3127	313	338	299	63.64	63.7	1.21	39.31
E559-0470	6	-4.61957	32.9077	395	395	513	52.49	52.83	1.62	44.56
E559-0703	0	-4.92554	28.7445	309	330	302	25.91	29.54	1.5	35.61
E559-0803	3	-5.57784	49.1565	298	341	316	48.9	51.58	3.15	38.66
E567-0050	4	-5.26851	44.8214	335	332	353	47.41	58.34	3.21	14.39
E567-0189	5	-4.88917	46.5775	359	344	362	60.05	59.94	4.6	33.6
E569-0183	3	-4.64276	47.3122	305	315	273	34.16	49.49	2.99	24.38
E569-0320	8	-4.61107	44.3008	433	382	455	52.85	57.04	4.27	48.59
E589-1261	9	-4.56041	44.8169	430	391	456	64.17	72.05	5.7	80.44
E589-1750	4	-4.59448	43.7291	341	341	357	65.29	63.18	2.48	25.89
E589-4547	2	-5.0559	37.8452	302	288	232	56.7	59.78	1.97	35.95
E589-4744	4	-4.82064	48.0187	452	444	411	37.92	36.61	1.66	46.5
E589-4884	3	-4.84504	43.8365	263	289	317	52.02	56.13	2.12	51.02
E589-4902	4	-4.99986	41.5682	255	298	368	52.68	54.87	2.21	54.16
E612-0638	3	-5.40195	38.5232	319	318	394	60.3	62.89	1.58	47.64
E612-0863	5	-5.31111	37.679	362	360	424	61.5	65.03	2.72	45.64
E612-1046	5	-4.93075	48.5894	276	297	433	58.83	62.61	3.87	50.2
E612-1047	2	-4.58638	45.2034	263	308	320	41	47.09	2.45	38.48
E612-1048	3	-4.732	47.9423	263	288	297	50.03	53.43	1.77	41.27
E612-1052	7	-5.03949	44.0287	375	394	466	54.28	56.82	2.29	59.26
E612-1136	2	-4.75303	42.4833	224	282	297	49.39	42.16	1.65	38.26
E612-2072	3	-4.55662	44.0025	255	291	296	47.53	49.2	2.8	26.15
E616-0628	7	-4.58746	31.1112	390	368	379	51.3	54.7	2.3	69.43
E616-0664	5	-4.6354	31.115	377	367	372	46.48	57.62	2.61	68.19
E616-0667	8	-4.65242	32.5193	380	370	388	65.39	61.35	3.27	88.77
E616-0737	2	-4.62587	33.1218	324	321	337	20.58	26.5	1.94	53.08
E643-0132	5	-4.68951	42.4613	350	349	312	31.48	41.63	3.28	56.99
E647-0001	7	-4.74018	44.465	477	416	377	47.04	56.3	5.75	39.44

E647-0019	0	-4.74078	37.9155	329	335	344	41.06	44.98	2.29	48.28
E647-0036	7	-5.1231	37.9878	375	357	383	65.53	65.37	3.74	69.9
E647-0038	3	-5.72274	41.1822	309	318	336	42.83	51.6	6.02	34.13
E647-0059	7	-4.74239	36.5222	366	360	385	60.21	60.3	4.86	65.79
E647-0061	3	-4.6821	42.462	322	327	340	17.36	33.67	6.01	24.01
E647-0088	5	-4.63211	35.4908	368	357	318	47.15	50.71	4.17	48.1
E647-0104	6	-5.50195	40.1776	377	354	321	47.03	54.44	4.54	44.66
E647-0224	4	-4.86791	44.2458	373	401	361	34.17	41.65	4.46	39.2
E667-1182	3	-4.59186	43.9311	285	288	325	36.19	42.13	1.31	57.92
E681-0423	2	-4.59221	34.4299	233	280	306	39.56	42.88	1.64	61.41
E686-0020	2	-4.62687	34.2611	323	340	354	48.09	49.13	2.85	48.61
E686-0140	2	-4.76414	35.4652	297	342	355	42.57	43.15	3.14	68.26
E734-0042	1	-5.16384	29.1889	258	269	294	9.99	25.77	1.92	60.95
E734-0058	3	-5.21804	43.2052	360	344	370	37.43	48.37	3	41.8
E734-0074	2	-4.63391	29.7488	259	260	282	11.28	26.95	1.44	58.84
E734-0087	3	-5.29629	30.7547	371	359	362	40.22	51.03	1.96	66.99
E734-0137	0	-4.92973	30.2179	306	298	307	-20.83	8.39	2.21	51.45
E734-0146	3	-4.95191	30.3819	399	357	366	35.26	47.15	1.16	55.99
E734-0156	4	-5.16667	27.801	354	332	344	47.54	53.35	0.94	66.56
E734-0179	1	-5.14836	28.114	269	268	291	12.39	26.81	1.22	61.75
E734-0222	1	-4.97631	34.6668	213	278	306	22.62	37.53	2.74	53.74
E734-1930	7	-4.65837	38.5603	415	410	476	70.22	68.24	2.64	101.43
E746-0788	3	-4.68773	38.3772	360	373	342	18.76	38.86	2.77	45.73
E756-0151	4	-4.61697	39.9108	359	354	369	27.04	40.25	3.8	51.21
E756-0705	3	-4.7037	39.4853	332	329	351	32.72	42.79	3.64	53.69
E851-1654	6	-4.87999	43.6288	460	412	427	43.22	47.67	3.31	80.37
E882-1088	1	-4.5723	39.0325	311	342	288	35.82	45	1.85	33.62
E882-1243	5	-5.14482	49.108	344	339	361	53.38	54.96	3.66	78.4
E959-1691	4	-5.7469	43.5567	377	350	391	37.67	41.86	0.21	49.88
E959-1702	2	-5.17478	43.9021	310	322	329	50.08	48.77	1.69	36.63
E959-1703	4	-4.6675	42.8731	349	337	357	38	31.05	0.41	62.75
E959-1705	6	-4.64226	44.3081	492	444	468	46.22	43	-0.14	59.58
E966-0516	5	-4.65588	30.2409	367	357	433	45.49	50.47	2.02	67.8
E966-0620	2	-4.61883	40.108	311	314	289	30.66	38.4	1.45	49.67
E966-1366	3	-4.68739	38.3966	278	301	308	50.85	54.05	1.21	17.71
E966-1421	4	-4.69123	35.5995	438	420	399	42.04	37.23	0.69	34.46
E966-1431	0	-5.25083	30.0944	316	338	347	41.12	47.85	1.77	25.81
E966-1438	2	-4.71696	36.5333	281	326	268	34.25	36.91	2.7	57.15
E971-0227	7	-4.57653	41.5354	395	390	446	47.08	52.35	2.69	42.61

E975-0513	4	-4.82677	49.1908	325	336	295	69.92	71.98	3.72	40.15
E975-1384	6	-4.6481	52.2788	447	466	476	42.18	49.27	6.08	34.32
E975-1472	6	-4.95247	52.8013	412	403	420	2.04	16.9	3.68	52.95
E975-1514	6	-4.57479	45.6912	494	443	408	18.79	29.19	2.61	55.95
E975-1561	7	-5.09769	41.0049	387	421	438	58.31	63.6	2.03	59.41
E975-1652	6	-5.40229	46.3575	397	405	437	9.86	22.27	3.13	60.33
E975-1688	7	-4.65797	40.1795	425	402	405	39.58	44.61	3.3	57.91
E975-1801	8	-4.70816	51.7535	392	389	403	66.23	77.31	4.49	45.36
E977-0038	4	-4.60459	36.9346	265	325	345	51.46	59.93	4.67	44.1
E977-0052	4	-4.63884	37.5632	343	386	395	36.48	52.56	2.94	36.75
E977-0059	1	-4.69987	39.0702	289	319	288	7.77	16.1	2.73	40.28
E977-0234	3	-5.15472	41.5439	365	413	374	31.04	34.25	2.77	46.77
E977-0253	8	-4.65992	40.6493	381	402	472	59.02	64.29	1.74	55.57
E977-0293	3	-5.24949	43.9114	288	302	325	64.47	63.34	1.99	42.45
E977-0335	4	-4.72539	40.944	250	298	312	53.26	58.55	2.41	54.96
E977-0362	8	-5.23601	50.2497	352	359	442	78.94	88.07	4.61	58.15
E977-0363	6	-4.98895	31.8706	348	376	451	56.62	62.32	2.41	57.19
E977-0473	6	-4.73022	37.8381	395	402	411	50.71	62.76	3.26	37.46
E977-0499	5	-4.56527	43.8274	289	341	297	62.07	67.06	3.84	38.21
E977-0655	5	-5.3231	45.4261	277	337	278	62.89	65.02	3.11	52.95
E977-0938	5	-4.89375	54.6188	242	298	372	85.55	87.14	4	59.32
E984-0063	3	-4.56999	38.8192	337	344	362	45.04	46.45	3.16	55.29
E984-0128	6	-4.6177	42.9402	457	434	432	45.39	49.8	3.11	46.32
E984-0485	2	-4.80818	38.6622	239	242	198	51.95	49	1.37	54.31
E990-0332	6	-4.73597	31.4595	443	395	355	70.75	60.79	3.69	59.9
E990-0385	7	-4.71943	42.2194	371	387	417	45.11	43.07	3.86	51.67
E990-0403	2	-4.98744	34.6029	366	348	362	46.02	46.73	1.46	67.05
E990-0419	7	-5.29865	34.9221	427	381	401	68.3	63.13	3.35	60.51
F019-1661	3	-4.86817	36.755	324	334	413	50.29	52.65	2.36	29.14
F044-0084	6	-4.69728	46.2572	344	295	378	54.02	56.39	2.94	60.66
F044-0095	8	-5.13082	50.5189	543	478	593	58.08	65.07	6.32	74.03
F063-0167	8	-4.75192	46.6129	594	482	616	52.4	55.11	6.72	52.68
F063-0244	7	-4.7912	42.9895	418	384	400	45.38	51.89	4.58	62.02
F281-0047	0	-5.28814	37.9943	218	285	368	27.5	34.05	2.57	37.86
F721-0092	3	-4.71169	2.5123	330	350	465	43.51	51.21	1.69	34.24
F721-0094	2	-4.65961	32.7969	262	294	318	22.44	27.43	3.43	26.89
F721-0129	0	-4.87559	-3.2816	185	227	353	34.66	35.22	0.33	48.08
F721-0142	2	-4.88173	24.2334	294	319	337	59.57	57.45	2.23	40.41
F743-0080	8	-4.6808	18.0509	407	393	510	53.3	54.18	3.38	80.21

F743-0098	5	-4.58655	42.5349	359	348	353	56.87	58.23	2.37	36.05
G008-1257	5	-5.04284	48.4089	380	365	448	32.1	45.04	4.21	44.64
G008-1259	8	-4.56493	43.103	429	400	536	55.65	61.55	3.67	47.23
G008-1475	4	-4.57961	38.5834	375	373	346	16.17	25.59	2.45	62.53
G008-1756	5	-4.66141	45.0004	471	478	449	31.95	38.7	2.55	45.12
G008-2168	5	-4.93505	35.2247	429	393	527	48.71	56.67	2.26	42.6
G008-2190	4	-5.67137	40.1168	301	334	349	46.93	54.32	1.5	58.58
G008-2200	3	-5.07008	37.036	282	319	334	48.36	55.13	1.63	66.08
G008-2528	2	-4.65617	42.3651	305	336	353	21.98	33.03	1.27	47.3
G008-2674	1	-4.78644	31.3535	271	309	392	16.57	41.62	1.1	-2.2
G008-2708	3	-5.17347	39.964	322	354	435	33.7	36.57	3.93	31.82
G008-2834	4	-4.61507	39.2401	321	313	388	64.5	58.2	1.98	10.45
G008-3306	3	-4.98172	41.8205	237	305	319	51.08	56.54	2.19	35.66
G008-3379	9	-4.67318	44.5695	392	384	454	47.39	53.67	4.5	52.3
G008-3681	5	-4.91764	48.2383	414	378	454	36.56	49.94	3.79	43.48
G008-5007	8	-4.59084	49.1947	404	402	474	42.38	57.17	4.38	66.38
G008-5085	7	-4.63183	41.2632	531	498	503	42.6	57.31	2.94	58.73
G008-5365	4	-4.86722	36.9798	431	410	475	22.9	33.97	0.79	77.31
G016-0503	6	-4.64737	38.6488	425	421	434	25.28	35.32	4.06	72.75
G017-0045	7	-4.9697	41.462	424	396	468	51.91	60.48	2.5	60.69
G017-0089	4	-5.26119	42.4318	347	344	353	55.09	64.14	2.67	29.72
G017-0177	2	-4.95007	41.9458	324	321	341	41.24	52.61	2.72	35.53
G017-1093	9	-4.7073	45.3204	365	366	384	59.32	67.38	3.43	58.92
G017-1102	9	-4.6703	43.9693	384	394	414	76.93	79.2	3.15	52.26
G017-1160	7	-5.36112	49.306	397	382	394	62.2	68.27	2.49	57.63
G017-2087	3	-4.67315	42.8099	337	346	368	37.83	49.68	4.92	17.45
G070-1123	6	-4.81325	43.3292	382	409	397	49.48	51.27	4.15	42.27
G114-0527	4	-4.89199	29.3625	489	482	449	24.99	31.69	1.48	52.99
G115-0527	3	-4.85611	41.692	303	339	350	46.75	53.36	2.41	34.61
G213-0210	7	-4.73826	49.0744	467	422	491	64.25	71.58	3.53	22.56
G242-0025	7	-4.62051	38.5327	428	392	462	50.35	55.49	2.55	64.74
G242-0026	7	-4.68724	40.3775	439	400	465	46.39	50.25	3.48	57.77
G242-0030	2	-4.58103	38.5161	312	330	335	45.01	54.21	1.48	27.23
G242-0032	4	-4.65203	43.7544	279	329	279	56.05	65.95	1.68	26.88
G242-0033	7	-5.58392	46.331	349	353	411	51.54	58.58	2.16	57.01
G242-0110	3	-4.67386	39.7605	315	342	353	51.29	59.1	2.57	26.08
G242-0144	8	-4.59919	45.6068	343	350	423	48.85	58.26	5.1	56.67
G242-0184	4	-6.04092	51.8982	473	450	495	44.5	49.76	2.07	42.2
G242-0222	8	-4.56135	40.2502	407	373	444	54.12	56.99	2.91	64.7

G242-0233	5	-4.83342	38.843	400	384	395	49.71	57.66	2.43	15.33
G242-0600	6	-4.59552	38.6576	419	397	457	44.22	49.34	4.19	58.41
G242-0650	3	-5.15801	42.6555	298	331	467	45.41	50.37	2.38	63.42
G243-0012	5	-4.85795	30.4378	348	378	383	48.69	45.7	1.33	86.08
G243-0015	4	-5.21182	42.5809	370	362	382	39.17	51.14	2.54	47.86
G243-0032	2	-5.03206	41.9928	327	356	304	34.48	38.36	2.69	33.07
G243-0035	1	-5.18282	35.2965	369	344	343	42.36	51.05	1.33	42.21
G243-0054	0	-5.02423	29.6737	301	320	319	39.48	46.73	0.77	36.29
G243-0061	1	-4.96519	37.3291	298	340	302	34.78	42.71	3.03	32.75
G243-0091	0	-4.7645	34.319	321	330	328	40.07	46.97	1.37	38.16
G243-0131	4	-4.68967	46.2687	343	332	346	43.62	53.77	3.4	13.76
G243-0145	2	-4.71359	40.3184	300	313	326	42.3	48.23	2.11	30.27
G243-0176	0	-4.78387	39.3668	328	327	341	37.47	49.29	1.81	30.65
G243-0232	2	-4.70807	40.0744	306	313	337	38.09	46.63	2.24	28.48
G243-0246	9	-4.62449	44.4435	384	360	420	63.11	62.64	3.01	55.04
G243-0435	4	-5.13501	35.7706	376	359	425	45.38	48.38	2.57	60.12
G243-0510	1	-4.79512	39.6261	339	363	366	36.04	42.43	2.7	36.67
G243-0548	3	-4.62563	36.3708	318	341	367	52.29	45.84	0.38	74.12
G243-0567	5	-4.87355	40.9726	439	400	403	45.89	55.71	2.42	43.4
G243-0592	5	-4.67372	32.7467	383	386	407	42.89	39.42	0.04	69.27
G243-0626	4	-4.63707	36.6229	351	363	374	41.3	48.58	3.17	45.79
G243-0868	2	-4.59899	43.3498	289	285	243	38.2	50.14	1.87	28.35
G243-0878	4	-4.99313	44.7945	295	305	269	50.52	58.95	3.3	28.91
G243-0913	5	-4.89685	39.7762	446	407	418	40.07	52.02	3.82	39.95
G243-1627	7	-4.55895	41.4236	398	375	439	49.93	47.43	1.29	67.07
G243-1798	4	-4.86327	39.7299	374	398	393	39.38	50.09	3.87	35
G261-0512	5	-5.27123	41.0339	466	435	400	17.86	28.17	1.71	55.9
G261-1230	5	-4.90224	43.5233	443	417	423	33.67	40.52	2.56	81.36
G261-1431	3	-4.77377	31.0079	313	328	435	60.78	57.48	2.19	43.84
G262-0030	5	-5.03585	38.412	437	397	472	43.09	54.35	5.39	47.4
G262-0032	0	-4.83016	37.7972	291	280	298	37.92	49.66	2.02	48.45
G262-0094	8	-4.57398	40.1089	457	400	471	47.27	61.41	3.93	48.91
G262-0104	2	-5.15986	35.4118	328	319	388	38.91	51.05	2.68	73.26
G262-0160	5	-4.63158	40.5663	290	310	385	40.08	47.07	2.99	55.69
G262-0165	6	-5.0752	38.4621	463	422	497	53.37	62.8	5.14	49.8
G262-0567	3	-4.63067	36.2632	340	322	331	53.68	55.5	1.31	44.15
G262-0841	1	-4.65754	35.3852	316	303	325	41.18	41.82	1.71	37.14
G262-0853	1	-4.79432	34.7183	301	307	264	43.94	48.83	3.08	38.34
G262-0913	8	-4.62039	38.5003	413	382	446	53.82	57.46	3.64	58.39

G262-0931	4	-4.86939	38.4062	347	354	359	50.8	54.23	2.18	30.18
G262-0970	7	-5.18224	38.6755	449	434	512	53.62	62.19	4.08	54.31
G262-0991	5	-4.62105	34.5115	307	332	394	57.87	60.2	1.71	53.87
G264-1364	9	-4.67734	53.1396	426	400	509	80.01	78.86	5.07	57.12
G305-0042	7	-4.86898	41.3974	392	353	320	53	55.89	3.47	53.45
G305-0137	1	-4.75434	39.3459	284	284	253	44.62	47.45	3.39	49.46
G305-1214	6	-4.61693	50.28	415	387	456	32.31	42.62	3.39	39.16
G305-1231	5	-5.28075	43.2814	437	421	445	32.46	42.72	3.37	28.17
G305-1268	3	-4.70289	44.1785	221	258	216	31.62	45.4	3.87	17.86
G305-1326	8	-5.18806	39.9966	379	363	440	47.42	59.22	4.75	64.34
G305-1398	2	-5.05893	40.0289	312	329	351	24.25	39.66	3.22	35.13
G305-1522	5	-4.58026	45.0439	382	392	378	10.52	26.09	0.1	38.23
G306-0101	1	-4.84831	31.7365	333	330	290	20.93	31.65	3.85	38.71
G319-0079	5	-4.78996	40.782	282	309	379	48.4	51.77	2.43	64.79
G319-0216	5	-4.63776	41.952	255	292	318	59.82	61.42	2.5	73.72
G321-0033	2	-5.17812	46.2507	244	302	245	43.5	51.28	1.81	53.97
G321-0213	7	-4.75785	44.5001	392	377	443	54.76	58.69	2.27	79.19
G328-0199	4	-4.88963	42.7724	287	302	309	58.76	62.4	2.69	54.32
G328-0289	3	-5.08848	39.5673	339	325	395	64.87	60.04	2.09	50.5
G328-0404	3	-4.92922	41.1815	295	314	330	55.63	58.74	2.35	49.57
G328-0406	3	-4.89726	40.7173	255	275	343	50.22	56.42	1.86	48.4
G328-0419	2	-4.71857	42.2377	209	240	199	38.78	38.8	1.53	40.66
G328-0548	4	-4.85002	44.323	294	326	335	61.12	65.39	2.99	43.97
G328-0607	3	-5.06085	47.7605	291	312	268	51.27	60.12	2.69	33.25
G333-0089	9	-4.60088	42.3512	434	426	450	50.44	57.31	5.29	54.29
G348-0421	6	-4.64327	28.8144	369	410	421	43.18	66.21	4.5	8.59
G357-1677	6	-4.63704	34.5345	376	364	484	76.44	76.88	2.72	32.28
G357-3175	6	-4.59998	36.4938	381	346	355	57.61	53.81	3.17	58.42
G366-0367	1	-4.75607	40.4504	304	275	347	30.05	39.58	2.41	48.68
G366-0381	2	-4.63574	38.944	359	346	301	44.16	48.89	2.95	45.46
G366-0416	4	-4.56251	43.7076	375	331	285	38.29	49.44	3.35	39.98
G373-0385	6	-5.16295	44.044	525	518	480	33.5	36.25	4.05	53.31
G373-0613	0	-4.83853	26.358	296	286	259	14.52	18.83	2.15	40.73
G373-1278	2	-5.09927	38.8106	393	378	353	11.48	19.58	1.08	39.9
G373-2620	0	-4.81517	31.4268	307	304	330	20.06	25.01	0.41	39.55
G384-0433	6	-4.9639	53.3459	503	475	493	25.79	45.7	6.13	53.74
G395-1206	8	-4.6197	25.6402	432	353	495	54.96	59.77	6.41	81.84
G400-0401	2	-5.00348	41.2698	289	327	286	8.63	35.44	3.96	-13.85
G400-0565	6	-4.71458	37.6973	515	457	456	57.11	58.53	2.37	42.46

G401-0036	8	-4.69747	46.2417	371	391	411	63.93	64.47	4.45	30.94
G401-0137	4	-4.82452	46.698	450	438	401	20.01	28.47	1.72	50.85
G408-0803	5	-4.87952	44.4226	452	399	422	37.05	47.76	3.35	47.95
G408-1238	1	-4.74155	36.3945	354	338	372	39.33	38.99	1.23	40.4
G434-0023	1	-5.32415	30.6772	232	272	253	24.91	34.2	3.49	33.06
G487-0052	3	-4.94819	33.8703	327	300	373	64.31	61.96	2.26	59.07
G498-0371	6	-5.39599	37.2035	421	393	403	56.4	61.4	3.2	49.9
G501-0017	1	-4.90235	31.0324	317	345	361	30.92	38.14	1.25	61.69
G514-0340	3	-4.7683	36.361	390	382	344	46.01	49.78	1.09	69.69
G514-0399	2	-4.81503	34.825	337	356	320	34.57	41.89	0.91	64.61
G529-0045	5	-4.75253	50.1367	327	330	399	55.96	63.61	4.17	41.48
G529-0207	5	-5.05467	48.9739	283	354	354	56.41	63.24	3.45	37.49
G533-0107	4	-5.09654	41.4949	357	353	428	40.88	44.78	2.68	38.3
G550-0001	4	-5.0822	39.9492	361	327	416	51.6	53.13	1.71	26.63
G550-0007	5	-5.411	39.6474	368	360	504	49.51	54.2	2.06	23.39
G550-0009	5	-4.57669	33.48	364	350	355	51.46	51.94	1.87	50.21
G550-0016	3	-5.19764	38.9255	341	331	420	58.69	60.16	1.73	31.02
G550-0020	0	-4.82176	37.4507	243	269	349	17.73	28.37	1.88	47.58
G551-0065	4	-4.77158	16.7603	367	362	377	20.54	33.26	4.09	23.4
G557-0049	7	-4.57191	39.9043	366	395	478	45.96	52.81	3.45	80.48
G557-0078	6	-4.57228	44.4303	334	385	411	35.02	44.91	5.06	53.95
G557-0095	4	-5.09846	38.9311	280	329	345	48.45	53.33	3.03	69.41
G557-0182	4	-4.57739	37.1212	320	351	417	46	46.9	1.02	61.93
G580-0090	1	-5.30897	44.8556	193	257	232	36.95	32.53	1.19	23.34
G587-0275	7	-4.61392	46.3506	372	382	489	50.91	55.24	2.89	39.22
G593-0005	5	-4.7435	44.6045	350	359	375	61.28	65.18	2.93	31.45
G593-0068	5	-4.83356	41.5198	386	406	482	38.66	45.18	3.73	13.09
G619-0186	5	-4.6385	26.5105	298	343	405	60.78	59.57	1.91	62.67
G632-2194	7	-4.67533	38.8777	367	366	384	61.84	69.81	4.91	46.75
G634-0398	4	-4.66695	37.551	303	328	411	59.22	62.01	1.73	30.79
G634-0417	4	-4.97914	32.97	335	365	374	48.47	47.81	3.16	54.16
G634-0608	1	-4.93653	36.8602	338	346	372	36.11	37.49	2.88	67.33
G640-0146	7	-4.57763	46.056	511	488	491	41.42	50.4	5.98	79.36
G658-0006	5	-4.63931	29.1692	242	289	247	55.97	56.44	3.63	53.6
G658-0107	3	-4.68069	38.8372	329	342	345	54.73	54.88	2.36	37.59
G660-0046	5	-4.64977	33.9241	545	538	545	31.36	52.17	2.65	41.81
G665-0002	3	-4.78757	38.2525	421	389	408	37.98	42.27	2.91	46.34
G668-0233	6	-4.63865	44.8226	357	345	418	60.55	59.46	2.65	38.57
G668-0276	2	-4.72346	40.5173	337	316	437	43.17	47.56	1.71	42.91

G745-1590	3	-4.82523	35.2886	403	383	454	27.68	44.46	2.58	37.54
G745-1626	1	-4.85138	42.7045	224	279	317	45.68	51.22	1.51	22.08
G765-0035	6	-4.66434	38.3053	437	390	456	50.44	53.85	2.06	39.97
G765-0052	7	-4.60858	33.4722	410	380	445	58.3	58.7	2.42	52.92
G765-0460	7	-4.70687	39.6132	462	374	387	63.74	63.08	3.48	46.25
G765-0514	7	-4.78191	41.0286	515	426	448	48.81	54.85	4.43	40.92
G786-0488	2	-4.57991	45.7365	199	307	274	42.94	50.78	1.53	45.84
G786-1486	3	-4.71953	50.051	280	329	359	31.4	51.14	3.17	21.51
G805-1078	5	-4.67261	49.7196	318	350	311	38.76	54.41	3.82	23.86
G806-0288	7	-4.77571	47.12	417	419	532	61.53	65.58	1.84	79.32
G835-0030	7	-4.88599	43.2212	385	368	383	69.21	68.9	3.95	38.69
G835-0052	7	-5.2044	41.4551	424	381	460	67.56	68.12	4.92	35.9
G839-0004	6	-4.62098	40.8298	310	314	383	49.81	55.4	4.3	40.95
G839-0143	6	-4.6606	45.5819	290	317	403	62.98	64	5.41	46.73
G848-0029	1	-4.58104	35.1904	267	303	257	30.23	24.71	0.39	36.2
G851-0296	8	-5.17633	43.6071	423	397	516	59.66	62.2	3.81	92.63
G852-0133	3	-4.97135	38.2942	476	445	428	16.24	23.76	1.29	42.6
G854-0039	5	-4.68172	41.1162	245	289	327	53.54	56.93	3.6	38.62
G855-2087	6	-4.62669	47.0015	404	421	388	37.02	42.12	2.3	71.55
G856-0515	6	-4.70433	47.8407	355	374	387	38.19	54.83	2.91	46.63
G856-0516	6	-5.24829	45.0549	364	360	376	51.48	59.97	1.87	64.79
G856-1489	8	-4.7336	42.839	460	432	444	57.86	64.28	4.96	52.59
G856-3115	1	-4.76481	42.783	296	326	344	33.09	41.85	1.38	28.12
G856-3121	3	-5.00448	44.6738	346	337	407	48.86	47.71	1.73	46.02
G856-3142	5	-4.82698	50.6048	285	357	372	49.02	55.69	2.9	66.34
G856-3729	0	-4.76694	33.7146	259	303	333	41.87	33.77	0.84	44.06
G856-4137	3	-4.74126	22.6234	176	226	308	53.02	48.69	3.07	61.19
G856-4583	4	-4.79736	49.6527	362	353	316	26.83	37.78	3.61	33.26
G856-4587	4	-4.74364	37.1994	366	359	313	45.37	49.48	3.11	52.72
G856-4606	5	-4.78759	37.6412	390	368	387	40.35	44.93	3.65	53.27
G856-4630	7	-4.614	41.4675	422	399	466	42.05	45.05	3.13	63.7
G856-5552	5	-5.6291	52.3049	534	496	461	42.52	50.74	3	45.04
G856-5561	6	-5.02664	47.5083	457	450	580	48.2	49.97	3.4	44.77
G856-5567	5	-5.21648	44.9785	454	440	457	41.3	41.22	2.73	70.49
G856-5678	2	-5.12845	46.3767	229	292	360	39.62	50.17	1.71	63.67
G856-5682	3	-5.20141	44.261	367	388	350	14.72	22.79	2.33	46.15
G856-7239	6	-4.69582	47.1566	369	361	440	45.57	46.89	2.7	52.1
G862-0293	6	-5.10502	38.6001	389	382	465	68.7	68.25	2.75	62.84
G877-0010	8	-4.5819	46.5187	412	396	397	55.7	62.57	3.19	23.19

G877-0048	7	-4.7234	44.5655	404	386	389	60.23	61.43	3.44	33.13
G886-0120	7	-4.61916	37.8036	417	402	474	47.48	55.12	4.16	34.5
G937-2878	7	-4.582	42.9188	532	488	443	48.42	50.25	1.61	58.05
J031-0421	3	-4.96946	30.1183	365	351	373	30.22	37.15	4.97	51.03
J043-0026	4	-4.77979	41.639	246	247	341	51.63	53.85	2.45	66.26
K061-0175	2	-4.72758	36.6307	312	324	344	66.56	63.29	2.26	39.47
K061-0179	1	-5.1503	40.7663	235	302	317	32.62	46.01	1.91	21.62
K061-0194	1	-4.87408	42.787	276	320	331	32.57	43.59	2.14	21.28
K085-0006	1	-4.63981	33.4434	292	287	311	44.69	45.5	1.34	25.23
K085-0018	1	-4.56047	38.7329	327	314	338	37.09	36.1	2.02	21.17
K216-0559	8	-4.65941	30.9184	471	416	441	51.29	59.6	6.06	58.63
K261-0975	0	-4.79923	34.3599	237	270	351	29.6	34.85	1.83	36.48
K261-1047	1	-4.56607	34.015	198	262	292	26.94	33.82	2.09	25.45
K261-1613	6	-4.56682	42.4296	342	374	508	59.35	63.65	2.84	46.73
K261-1770	0	-4.83976	36.9642	314	337	312	30.51	39.73	2.88	31.33
K261-1773	0	-4.72702	33.4685	249	317	279	22.2	29.41	2.89	25.24
K273-0164	7	-5.51143	34.4595	389	377	390	54.63	53.84	3.55	86.07
K280-0563	7	-4.85634	53.1466	426	406	495	63.28	73.52	8.03	45.1
K404-0816	4	-4.85797	33.9198	432	434	393	35.24	42.78	2.34	64.38
K504-2298	7	-4.71403	41.9257	423	398	532	33.18	53.26	3.86	30.66
K629-0014	1	-4.57909	34.1737	278	267	291	42.89	43.28	1.63	25
K666-0083	0	-5.17658	38.5588	172	225	310	45.58	45.7	2.53	41.61
K780-0947	3	-4.90186	32.7148	349	354	322	21.46	24.24	2.5	56.21
K780-0977	3	-4.70568	33.6968	316	350	316	22.35	30	2.57	55.71
K780-1301	3	-4.69751	27.41	364	325	345	20.86	31.81	3.57	37.88
K781-2691	0	-4.78151	30.1734	253	265	291	27.62	30.31	1.62	31.44
K781-4185	4	-4.71938	45.2689	144	239	257	60.1	66.16	2.64	42.69
K783-0396	4	-4.90215	47.0825	383	381	356	41.57	44.79	2.95	58.43
K783-0402	0	-4.83105	19.2766	272	320	333	16.29	28.17	2	42.34
K783-2936	2	-4.59801	30.9415	207	267	238	43.74	40.43	-0.84	68.35
K783-3883	0	-4.77698	29.282	283	304	269	21.91	26.44	1.01	36.31
K783-4388	0	-5.19705	30.5166	310	301	333	30.62	36.97	2.3	44.63
K783-4461	2	-4.66127	32.4454	309	313	343	39.55	44.17	3.09	47.63
K783-4502	1	-4.7937	27.8739	318	300	322	10.17	23.42	5.27	31.82
K783-4588	1	-5.0434	21.6727	347	335	297	4.53	21.53	2.37	32.68
K783-5492	0	-4.73186	32.5619	212	218	193	43.69	45.02	1.76	40.15
K783-5526	1	-4.56685	31.3706	300	316	285	16.36	26.33	2.65	36.68
K783-5554	6	-4.98109	45.2793	479	468	480	37.29	44.83	4.12	61.11
K784-3107	6	-4.62179	36.5082	493	422	389	39.55	45.78	4.99	56.96

K784-4049	8	-4.58204	40.4342	387	361	421	46.65	49.8	3.55	78.09
K786-0940	7	-4.78244	33.7488	507	454	466	60.84	61.91	3.33	73.01
K786-5898	4	-4.60051	43.436	323	339	291	52.9	62.96	2.85	35.35
K786-6473	3	-4.82692	17.1216	273	295	250	52.13	56.03	3.95	49.58
K786-6478	3	-4.96447	39.6578	333	358	314	29.03	34.47	3.12	68.97
K786-7229	3	-4.63349	48.199	259	297	302	8.51	24.32	3.87	27.79
K786-9164	6	-4.84833	45.2632	438	412	476	63.3	63.74	2.82	36.93
K786-9344	3	-5.1117	42.4124	242	290	244	60.56	61.25	2.25	39.88
K788-0950	2	-4.89835	39.1724	282	333	350	44.89	53.6	3.32	47.5
K788-8228	4	-4.69158	35.158	389	348	374	43.86	50.01	3.25	56.99
K831-0106	1	-4.95357	44.3955	252	293	370	41.28	44.98	2.33	37.53
K844-0623	5	-5.24755	25.6871	394	397	468	42.17	56.15	7.5	49.72
K893-0950	3	-4.84853	37.2545	230	320	398	37.58	35.15	3.24	54
K906-0571	1	-4.90676	34.6843	321	378	362	10.29	9.46	-0.4	9.78
K906-0751	6	-4.62136	43.0747	345	401	404	28.17	30.33	4.05	73.1
K906-1166	3	-4.56219	39.47	151	263	338	44.75	47.27	3.07	63.32
K906-1263	3	-5.09152	38.3865	439	421	404	33.21	36.7	0.61	36
K906-1270	3	-4.66111	37.1937	292	333	393	41.97	49.51	0.41	60.65
K906-1596	3	-4.58589	46.7646	271	330	305	42.45	40.44	3.26	50.12
K906-3373	2	-4.79258	38.3374	284	317	351	46.73	55.74	2.23	41.31
K906-4254	3	-4.58547	42.0283	301	270	250	34.78	44.36	4.46	46
K906-4503	2	-4.63845	30.5987	294	328	297	30.38	36.18	2.43	63.68
K915-0899	2	-4.56104	37.85	314	329	395	44.87	51.16	1.84	46.59
K915-1228	5	-5.09647	27.5684	480	443	393	17.8	33.18	3.44	66.3
K938-3199	1	-4.60675	38.1535	302	335	289	42.9	48.39	2.38	32.13
K940-1437	4	-5.77682	15.349	348	376	445	17.52	34.95	0.79	53.6
K978-1338	3	-4.66108	38.7068	325	343	361	45.84	53.38	3.12	16.88
L075-0713	8	-4.58807	32.0651	556	507	567	78.21	76.13	4.05	63.66
N010-0014	5	-5.66613	32.5422	366	357	432	34.29	40.48	4.78	55.77
N037-0025	2	-4.56879	28.3658	152	226	182	39.48	41.28	1.74	64.96
R052-2012	0	-4.72286	35.7099	192	228	256	27.84	40.13	2.93	44.54
R152-2017	0	-5.36464	31.2741	267	281	356	19.35	25.46	2.3	23.52
R382-0062	2	-4.59204	32.3561	238	268	338	39.94	41.94	2.48	64.82

Appendix (iii): PfFKBP35-D44 crystallographic data collection and refinement statistics

	PfFKBP35-D44	PvFKBP35-D44
Wavelength (Å)	0.9642	1.5418
Space Group	$P\ 4_3\ 2_1\ 2$	$P\ 3_2\ 2\ 1$
Unit Cell Parameters		
a=b (Å)	69.92	68.26
c (Å)	186.87	74.12
Resolution (Å)	30 – 2.75 (2.85 – 2.75) †	30 - 1.73 (1.79 -1.73) †
No. of Unique Reflections	12747 (1203)	21266 (2106)
R_{merge}	0.059 (0.569)	0.049 (0.187)
Mean [(I) / σ(I)]	27.31 (1.93)	22.3 (6.8)
Completeness (%)	99.6 (98.4)	99.8 (99.7)
Redundancy	6.8 (6.2)	10.32 (7.93)
Molecular Replacement Model	PDB ID 2VN1 - Chain A	PDB ID 3IHZ – Chain A
Refinement		
Number of Reflections	12002	20015
Resolution (Å)	20 - 2.75	20 - 1.73
R-Value	0.2269	0.1772
R-Free	0.2777	0.2148
No. of atoms		
Protein / Ligand / Water	2873 / 66 / 13	967 / 46 / 200
Mean Wilson *B* value ($Å^2$)	85.1	29.4
Mean *B* value ($Å^2$)	77.22	22.58
Protein / Ligand / Water ($Å^2$)	77.39 / 75.59 / 47.68	18.65 / 36.22 / 38.53
Rmsd (Å)		
Bond Lengths	0.010	0.014
Bond Angles	1.456	1.563
Torsion Angles	6.527	6.508
Ramachandran Statistics		
Preferred Regions (%)	94.71	98.28
Allowed Regions (%)	5.29	1.72
Outliers (%)	0.0	0.0

† Values in parentheses refer to the corresponding values of the highest-resolution shell

Appendix (iv): Crystallographic data-collection and refinement statistics of PvFKBP35-D5 complex

Wavelength (Å)	1.5418
Space Group	I 2
Unit Cell	
a ; b ; c (Å)	51.45 ; 46.01 ; 55.10
b (º)	117.37
Resolution (Å)	33.5 – 1.72 (1.81-1.72)†
R_{merge}	0.034 (0.162)
Unique Reflections	12119 (1662)
Mean [(I) / σ(I)]	18.3 (5.0)
Completeness (%)	99.0 (94.1)
Multiplicity	3.5 (2.9)
Molecular Replacement Model	PDB ID 3IHZ – Chain A
Refinement	
Number of Reflections	11028
Resolution (Å)	20 - 1.72
R-Value	0.1792
R-Free	0.2293
No. of atoms	
Protein / Ligand / Water	944 / 22 / 126
Mean B-Value (Wilson) ($Å^2$)	37.8
Mean B-Value ($Å^2$)	30.89
Protein / Ligand /Water ($Å^2$)	29.31 / 35.36 / 41.96
Rmsd (Å)	
Bond Lengths	0.014
Bond Angles	1.466
Torsion Angles	6.392
Ramachandran Statistics	
Preferred Regions (%)	96.67
Allowed Regions (%)	3.33
Outliers (%)	0.00

† Values in parentheses refer to the corresponding values of the highest-resolution shell

XI. Publications:

Harikishore A, Chakraborty G, Chattopadhaya S, Yoon HS. FKBP8 (FK506 binding protein 8, 38kDa). Atlas Genet Cytogenet Oncol Haematol. January 2012
URL: http://AtlasGeneticsOncology.org/Genes/FKBP8ID40579ch19p13.html

Chattopadhaya S, Harikishore A, Yoon HS. Role of FK506 binding proteins in neurodegenerative disorders. Current medicinal chemistry, 2011. **18**(35): p. 5380-97.

Alag R, Bharatham N, Dong A, Hills T, Harikishore A, Widjaja AA, Shochat SG, Hui R, Yoon HS. Crystallographic structure of the tetratricopeptide repeat domain of Plasmodium falciparum FKBP35 and its molecular interaction with Hsp90 C-terminal pentapeptide. Protein Sci, 2009. **18**(10): p. 2115-24.

Amaravadhi Harikishore, Niang Makhtar, Sreekanth Rajan, Peter Rainer Preiser, Ho Sup Yoon. Small molecule *Plasmodium* FKBP35 inhibitor as potential antimalarial agent (Manuscript in Submission).

Amaravadhi Harikishore, Kalyan kumar Pasunooti, Niang Makhtar, Sreekanth Rajan, Xuewei Liu, Peter Rainer Preiser, Ho Sup Yoon. Adamantyl derivative as potent inhibitor of Plasmodium FKBP35 (Manuscript in Submission).

Chattopadhaya S, Harikishore A, Si P, Kim DH, Yoon HS. Identification and characterization of novel non-immunosuppressive immunophilin ligand targeting FKBP38 (Manuscript in Submission).

Book Chapter

Souvik Chattopadhaya, Amaravadhi Harikishore and Ho Sup Yoon (2012). Role of FKBPs in Parkinson's Disease, Mechanisms in Parkinson's Disease - Models and Treatments, Juliana Dushanova (Ed.), ISBN: 978-953-307-876-2, InTech, Available from: http://www.intechopen.com/articles/show/title/role-of-fkbps-in-parkinson-s-disease

Conference Presentation(s):

Harikishore Amaravadhi, Niang Makhtar, Peter Praiser, Ho Sup Yoon In-silico Design of Non-Immunosuppressive Immunophilin Ligands as Antimalarial agents. DS Workshop 2011, Aspiration Theatrette, Level 2M, Matrix Building, Biopolis.

Harikishore Amaravadhi, Niang Makhtar, Sreekanth Rajan, Peter Praiser, Ho Sup Yoon. Identification & characterization of PfFKBP35 inhibitor as antimalarial agent. Singapore Malaria Network meeting 2012.

XIV. References

1. Bierer, B.E., et al., *Two distinct signal transmission pathways in T lymphocytes are inhibited by complexes formed between an immunophilin and either FK506 or rapamycin.* Proc Natl Acad Sci U S A, 1990. **87**(23): p. 9231-5.
2. Liu, J., et al., *Calcineurin is a common target of cyclophilin-cyclosporin A and FKBP-FK506 complexes.* Cell, 1991. **66**(4): p. 807-15.
3. Friedman, J. and I. Weissman, *Two cytoplasmic candidates for immunophilin action are revealed by affinity for a new cyclophilin: one in the presence and one in the absence of CsA.* Cell, 1991. **66**(4): p. 799-806.
4. Kang, C.B., et al., *FKBP family proteins: immunophilins with versatile biological functions.* Neurosignals, 2008. **16**(4): p. 318-25.
5. Fischer, G., H. Bang, and C. Mech, *[Determination of enzymatic catalysis for the cis-trans-isomerization of peptide binding in proline-containing peptides].* Biomed Biochim Acta, 1984. **43**(10): p. 1101-11.
6. Fischer, G. and T. Aumuller, *Regulation of peptide bond cis/trans isomerization by enzyme catalysis and its implication in physiological processes.* Rev Physiol Biochem Pharmacol, 2003. **148**: p. 105-50.
7. Kay, J.E., *Structure-function relationships in the FK506-binding protein (FKBP) family of peptidylprolyl cis-trans isomerases.* Biochem J, 1996. **314 (Pt 2)**: p. 361-85.
8. Edlich, F. and G. Fischer, *Pharmacological targeting of catalyzed protein folding: the example of peptide bond cis/trans isomerases.* Handb Exp Pharmacol, 2006(172): p. 359-404.
9. Fanghanel, J. and G. Fischer, *Insights into the catalytic mechanism of peptidyl prolyl cis/trans isomerases.* Front Biosci, 2004. **9**: p. 3453-78.
10. Wang, X.J. and F.A. Etzkorn, *Peptidyl-prolyl isomerase inhibitors.* Biopolymers, 2006. **84**(2): p. 125-46.
11. Albers, M.W., C.T. Walsh, and S.L. Schreiber, *Substrate specificity for the human rotamase FKBP: a view of FK506 and rapamycin as leucine-(twisted amide)-proline mimics.* The Journal of Organic Chemistry, 1990. **55**(17): p. 4984-4986.
12. Park, S.T., et al., *PPIase catalysis by human FK506-binding protein proceeds through a conformational twist mechanism.* J Biol Chem, 1992. **267**(5): p. 3316-24.
13. Zoldak, G., et al., *A library of fluorescent peptides for exploring the substrate specificities of prolyl isomerases.* Biochemistry, 2009. **48**(43): p. 10423-36.
14. Michnick, S.W., et al., *Solution structure of FKBP, a rotamase enzyme and receptor for FK506 and rapamycin.* Science, 1991. **252**(5007): p. 836-9.
15. Szep, S., et al., *Structural coupling between FKBP12 and buried water.* Proteins, 2009. **74**(3): p. 603-11.
16. Van Duyne, G.D., et al., *Atomic structure of FKBP-FK506, an immunophilin-immunosuppressant complex.* Science, 1991. **252**(5007): p. 839-42.
17. Cameron, A.M., et al., *Immunophilin FK506 binding protein associated with inositol 1,4,5-trisphosphate receptor modulates calcium flux.* Proc Natl Acad Sci U S A, 1995. **92**(5): p. 1784-8.
18. Cameron, A.M., et al., *FKBP12 binds the inositol 1,4,5-trisphosphate receptor at leucine-proline (1400-1401) and anchors calcineurin to this FK506-like domain.* J Biol Chem, 1997. **272**(44): p. 27582-8.
19. Wang, T., P.K. Donahoe, and A.S. Zervos, *Specific interaction of type I receptors of the TGF-beta family with the immunophilin FKBP-12.* Science, 1994. **265**(5172): p. 674-6.

20. Wang, T., et al., *The immunophilin FKBP12 functions as a common inhibitor of the TGF beta family type I receptors.* Cell, 1996. **86**(3): p. 435-44.
21. Yang, W.M., C.J. Inouye, and E. Seto, *Cyclophilin A and FKBP12 interact with YY1 and alter its transcriptional activity.* The Journal of biological chemistry, 1995. **270**(25): p. 15187-93.
22. Nyanguile, O., et al., *A nonnatural transcriptional coactivator.* Proceedings of the National Academy of Sciences of the United States of America, 1997. **94**(25): p. 13402-6.
23. Cunningham, J.T., et al., *mTOR controls mitochondrial oxidative function through a YY1-PGC-1alpha transcriptional complex.* Nature, 2007. **450**(7170): p. 736-40.
24. Yao, Y.L., et al., *FKBPs in chromatin modification and cancer.* Current opinion in pharmacology, 2011. **11**(4): p. 301-7.
25. Ahearn, I.M., et al., *FKBP12 binds to acylated H-ras and promotes depalmitoylation.* Mol Cell, 2011. **41**(2): p. 173-85.
26. Liu, J.O., et al., *Regulator of Ras depalmitoylation and retrograde trafficking: a new hat for FKBP.* Mol Cell, 2011. **41**(2): p. 131-3.
27. Deleersnijder, A., et al., *Comparative analysis of different peptidyl-prolyl isomerases reveals FK506-binding protein 12 as the most potent enhancer of alpha-synuclein aggregation.* J Biol Chem, 2011. **286**(30): p. 26687-701.
28. Gerard, M., et al., *FK506 binding protein 12 differentially accelerates fibril formation of wild type alpha-synuclein and its clinical mutants A30P or A53T.* J Neurochem, 2008. **106**(1): p. 121-33.
29. Gerard, M., et al., *Inhibition of FK506 binding proteins reduces alpha-synuclein aggregation and Parkinson's disease-like pathology.* J Neurosci, 2010. **30**(7): p. 2454-63.
30. Fulton, K.F., S.E. Jackson, and A.M. Buckle, *Energetic and structural analysis of the role of tryptophan 59 in FKBP12.* Biochemistry, 2003. **42**(8): p. 2364-72.
31. Weiwad, M., et al., *Comparative analysis of calcineurin inhibition by complexes of immunosuppressive drugs with human FK506 binding proteins.* Biochemistry, 2006. **45**(51): p. 15776-84.
32. Milting, H., et al., *FK506 does not affect cardiac contractility and adrenergic response in vitro.* Eur J Pharmacol, 2001. **430**(2-3): p. 299-304.
33. Doi, M., et al., *Propranolol prevents the development of heart failure by restoring FKBP12.6-mediated stabilization of ryanodine receptor.* Circulation, 2002. **105**(11): p. 1374-9.
34. Eltit, J.M., et al., *Reduced gain of excitation-contraction coupling in triadin-null myotubes is mediated by the disruption of FKBP12/RyR1 interaction.* Cell Calcium, 2011. **49**(2): p. 128-35.
35. Jackson, W.F., *Altered expression and function of ryanodine receptors and FKBP12.6 after subarachnoid hemorrhage: more than meets the eye.* J Cereb Blood Flow Metab, 2011. **31**(1): p. 1-2.
36. Lehnart, S.E., et al., *Stabilization of cardiac ryanodine receptor prevents intracellular calcium leak and arrhythmias.* Proc Natl Acad Sci U S A, 2006. **103**(20): p. 7906-10.
37. Lehnart, S.E., et al., *Sudden death in familial polymorphic ventricular tachycardia associated with calcium release channel (ryanodine receptor) leak.* Circulation, 2004. **109**(25): p. 3208-14.
38. Marks, A.R., *Ryanodine receptors/calcium release channels in heart failure and sudden cardiac death.* J Mol Cell Cardiol, 2001. **33**(4): p. 615-24.

39. Prestle, J., et al., *Overexpression of FK506-binding protein FKBP12.6 in cardiomyocytes reduces ryanodine receptor-mediated Ca(2+) leak from the sarcoplasmic reticulum and increases contractility.* Circ Res, 2001. **88**(2): p. 188-94.
40. Wehrens, X.H., et al., *FKBP12.6 deficiency and defective calcium release channel (ryanodine receptor) function linked to exercise-induced sudden cardiac death.* Cell, 2003. **113**(7): p. 829-40.
41. Wehrens, X.H., et al., *Protection from cardiac arrhythmia through ryanodine receptor-stabilizing protein calstabin2.* Science, 2004. **304**(5668): p. 292-6.
42. Zhang, Y., et al., *Downregulated FKBP12.6 expression and upregulated endothelin signaling contribute to elevated diastolic calcium and arrhythmogenesis in rat cardiomyopathy produced by l-thyroxin.* Int J Cardiol, 2008. **130**(3): p. 463-71.
43. Cerrone, M., et al., *Bidirectional ventricular tachycardia and fibrillation elicited in a knock-in mouse model carrier of a mutation in the cardiac ryanodine receptor.* Circ Res, 2005. **96**(10): p. e77-82.
44. George, C.H., G.V. Higgs, and F.A. Lai, *Ryanodine receptor mutations associated with stress-induced ventricular tachycardia mediate increased calcium release in stimulated cardiomyocytes.* Circ Res, 2003. **93**(6): p. 531-40.
45. Jiang, D., et al., *Enhanced store overload-induced Ca2+ release and channel sensitivity to luminal Ca2+ activation are common defects of RyR2 mutations linked to ventricular tachycardia and sudden death.* Circ Res, 2005. **97**(11): p. 1173-81.
46. Liu, N., et al., *Arrhythmogenesis in catecholaminergic polymorphic ventricular tachycardia: insights from a RyR2 R4496C knock-in mouse model.* Circ Res, 2006. **99**(3): p. 292-8.
47. Xiao, J., et al., *Removal of FKBP12.6 does not alter the conductance and activation of the cardiac ryanodine receptor or the susceptibility to stress-induced ventricular arrhythmias.* J Biol Chem, 2007. **282**(48): p. 34828-38.
48. Zissimopoulos, S., et al., *FKBP12.6 binding of ryanodine receptors carrying mutations associated with arrhythmogenic cardiac disease.* Biochem J, 2009. **419**(2): p. 273-8.
49. Xin, H.B., et al., *Oestrogen protects FKBP12.6 null mice from cardiac hypertrophy.* Nature, 2002. **416**(6878): p. 334-8.
50. Chen, Z., et al., *FKBP12.6-knockout mice display hyperinsulinemia and resistance to high-fat diet-induced hyperglycemia.* FASEB J, 2010. **24**(2): p. 357-63.
51. Noguchi, N., et al., *FKBP12.6 disruption impairs glucose-induced insulin secretion.* Biochem Biophys Res Commun, 2008. **371**(4): p. 735-40.
52. Yang, W.M., Y.L. Yao, and E. Seto, *The FK506-binding protein 25 functionally associates with histone deacetylases and with transcription factor YY1.* EMBO J, 2001. **20**(17): p. 4814-25.
53. Dawson, T.M., et al., *The immunophilins, FK506 binding protein and cyclophilin, are discretely localized in the brain: relationship to calcineurin.* Neuroscience, 1994. **62**(2): p. 569-80.
54. Steiner, J.P., et al., *High brain densities of the immunophilin FKBP colocalized with calcineurin.* Nature, 1992. **358**(6387): p. 584-7.
55. Tanaka, K., et al., *Neuroprotective and antioxidant properties of FKBP-binding immunophilin ligands are independent on the FKBP12 pathway in human cells.* Neurosci Lett, 2002. **330**(2): p. 147-50.
56. Chattopadhaya, S., A. Harikishore, and H.S. Yoon, *Role of FK506 Binding Proteins in Neurodegenerative Disorders.* Curr Med Chem, 2011.
57. Chambraud, B., et al., *The immunophilin FKBP52 specifically binds to tubulin and prevents microtubule formation.* FASEB J, 2007. **21**(11): p. 2787-97.

58. Chambraud, B., et al., *A role for FKBP52 in Tau protein function.* Proc Natl Acad Sci U S A, 2010. **107**(6): p. 2658-63.
59. Shim, S., et al., *Peptidyl-prolyl isomerase FKBP52 controls chemotropic guidance of neuronal growth cones via regulation of TRPC1 channel opening.* Neuron, 2009. **64**(4): p. 471-83.
60. Cheung-Flynn, J., et al., *FKBP Co-Chaperones in Steroid Receptor Complexes.* p. 281-312.
61. Chen, H., et al., *Fkbp52 regulates androgen receptor transactivation activity and male urethra morphogenesis.* J Biol Chem. **285**(36): p. 27776-84.
62. Galigniana, M.D., et al., *The hsp90-FKBP52 complex links the mineralocorticoid receptor to motor proteins and persists bound to the receptor in early nuclear events.* Mol Cell Biol, 2010. **30**(5): p. 1285-98.
63. Periyasamy, S., et al., *FKBP51 and Cyp40 are positive regulators of androgen-dependent prostate cancer cell growth and the targets of FK506 and cyclosporin A.* Oncogene, 2010 **29**(11): p. 1691-701.
64. Sivils, J.C., et al., *Regulation of steroid hormone receptor function by the 52-kDa FK506-binding protein (FKBP52).* Curr Opin Pharmacol.
65. Pratt, W.B., et al., *Role of hsp90 and the hsp90-binding immunophilins in signalling protein movement.* Cellular signalling, 2004. **16**(8): p. 857-72.
66. Silverstein, A.M., et al., *Different regions of the immunophilin FKBP52 determine its association with the glucocorticoid receptor, hsp90, and cytoplasmic dynein.* J Biol Chem, 1999. **274**(52): p. 36980-6.
67. Tatro, E.T., et al., *Modulation of glucocorticoid receptor nuclear translocation in neurons by immunophilins FKBP51 and FKBP52: implications for major depressive disorder.* Brain Res, 2009. **1286**: p. 1-12.
68. Wu, B., et al., *3D structure of human FK506-binding protein 52: implications for the assembly of the glucocorticoid receptor/Hsp90/immunophilin heterocomplex.* Proc Natl Acad Sci U S A, 2004. **101**(22): p. 8348-53.
69. Miyata, Y., et al., *Phosphorylation of the immunosuppressant FK506-binding protein FKBP52 by casein kinase II: regulation of HSP90-binding activity of FKBP52.* Proc Natl Acad Sci U S A, 1997. **94**(26): p. 14500-5.
70. Wilson, K.P., et al., *Comparative X-ray structures of the major binding protein for the immunosuppressant FK506 (tacrolimus) in unliganded form and in complex with FK506 and rapamycin.* Acta Crystallogr D Biol Crystallogr, 1995. **51**(Pt 4): p. 511-21.
71. Taipale, M., D.F. Jarosz, and S. Lindquist, *HSP90 at the hub of protein homeostasis: emerging mechanistic insights.* Nat Rev Mol Cell Biol, 2010. **11**(7): p. 515-28.
72. Gallo, L.I., et al., *Differential recruitment of tetratricorpeptide repeat domain immunophilins to the mineralocorticoid receptor influences both heat-shock protein 90-dependent retrotransport and hormone-dependent transcriptional activity.* Biochemistry, 2007. **46**(49): p. 14044-57.
73. Hubler, T.R., et al., *The FK506-binding immunophilin FKBP51 is transcriptionally regulated by progestin and attenuates progestin responsiveness.* Endocrinology, 2003. **144**(6): p. 2380-7.
74. Ni, L., et al., *FKBP51 promotes assembly of the Hsp90 chaperone complex and regulates androgen receptor signaling in prostate cancer cells.* Mol Cell Biol, 2010. **30**(5): p. 1243-53.
75. Reynolds, P.D., et al., *Glucocorticoid resistance in the squirrel monkey is associated with overexpression of the immunophilin FKBP51.* J Clin Endocrinol Metab, 1999. **84**(2): p. 663-9.

76. Stechschulte, L.A. and E.R. Sanchez, *FKBP51-a selective modulator of glucocorticoid and androgen sensitivity.* Curr Opin Pharmacol, 2011. **11**(4): p. 332-7.
77. Jaaskelainen, T., H. Makkonen, and J.J. Palvimo, *Steroid up-regulation of FKBP51 and its role in hormone signaling.* Curr Opin Pharmacol, 2011. **11**(4): p. 326-31.
78. Denny, W.B., et al., *Squirrel monkey immunophilin FKBP51 is a potent inhibitor of glucocorticoid receptor binding.* Endocrinology, 2000. **141**(11): p. 4107-13.
79. Westberry, J.M., et al., *Glucocorticoid resistance in squirrel monkeys results from a combination of a transcriptionally incompetent glucocorticoid receptor and overexpression of the glucocorticoid receptor co-chaperone FKBP51.* J Steroid Biochem Mol Biol, 2006. **100**(1-3): p. 34-41.
80. Binder, E.B., *The role of FKBP5, a co-chaperone of the glucocorticoid receptor in the pathogenesis and therapy of affective and anxiety disorders.* Psychoneuroendocrinology, 2009. **34 Suppl 1**: p. S186-95.
81. Riggs, D.L., et al., *Noncatalytic role of the FKBP52 peptidyl-prolyl isomerase domain in the regulation of steroid hormone signaling.* Mol Cell Biol, 2007. **27**(24): p. 8658-69.
82. Bracher, A., et al., *Structural characterization of the PPIase domain of FKBP51, a cochaperone of human Hsp90.* Acta Crystallogr D Biol Crystallogr, 2011. **67**(Pt 6): p. 549-59.
83. Li, L., Z. Lou, and L. Wang, *The role of FKBP5 in cancer aetiology and chemoresistance.* Br J Cancer, 2011. **104**(1): p. 19-23.
84. Jinwal, U.K., et al., *The Hsp90 cochaperone, FKBP51, increases Tau stability and polymerizes microtubules.* J Neurosci, 2010. **30**(2): p. 591-9.
85. Lam, E., M. Martin, and G. Wiederrecht, *Isolation of a cDNA encoding a novel human FK506-binding protein homolog containing leucine zipper and tetratricopeptide repeat motifs.* Gene, 1995. **160**(2): p. 297-302.
86. Kang, C.B., et al., *Molecular characterization of FK-506 binding protein 38 and its potential regulatory role on the anti-apoptotic protein Bcl-2.* Biochem Biophys Res Commun, 2005. **337**(1): p. 30-8.
87. Bulgakov, O.V., et al., *FKBP8 is a negative regulator of mouse sonic hedgehog signaling in neural tissues.* Development, 2004. **131**(9): p. 2149-59.
88. Maestre-Martinez, M., et al., *Solution structure of the FK506-binding domain of human FKBP38.* J Biomol NMR, 2006. **34**(3): p. 197-202.
89. Edlich, F., et al., *Bcl-2 regulator FKBP38 is activated by Ca2+/calmodulin.* EMBO J, 2005. **24**(14): p. 2688-99.
90. Edlich, F., et al., *A novel calmodulin-Ca2+ target recognition activates the Bcl-2 regulator FKBP38.* J Biol Chem, 2007. **282**(50): p. 36496-504.
91. Maestre-Martinez, M., et al., *A charge-sensitive loop in the FKBP38 catalytic domain modulates Bcl-2 binding.* J Mol Recognit, 2011. **24**(1): p. 23-34.
92. Choi, B.H., L. Feng, and H.S. Yoon, *FKBP38 protects Bcl-2 from caspase-dependent degradation.* J Biol Chem, 2010. **285**(13): p. 9770-9.
93. Kang, C.B., et al., *The flexible loop of Bcl-2 is required for molecular interaction with immunosuppressant FK-506 binding protein 38 (FKBP38).* FEBS Lett, 2005. **579**(6): p. 1469-76.
94. Choi, B.H. and H.S. Yoon, *FKBP38-Bcl-2 interaction: a novel link to chemoresistance.* Curr Opin Pharmacol, 2011.
95. Wang, H.Q., et al., *Interaction of presenilins with FKBP38 promotes apoptosis by reducing mitochondrial Bcl-2.* Hum Mol Genet, 2005. **14**(13): p. 1889-902.
96. Erdmann, F., et al., *Hsp90-mediated inhibition of FKBP38 regulates apoptosis in neuroblastoma cells.* FEBS Lett, 2007. **581**(29): p. 5709-14.

97. Nakagawa, T., et al., *Anchoring of the 26S proteasome to the organellar membrane by FKBP38.* Genes Cells, 2007. **12**(6): p. 709-19.
98. Barth, S., et al., *The peptidyl prolyl cis/trans isomerase FKBP38 determines hypoxia-inducible transcription factor prolyl-4-hydroxylase PHD2 protein stability.* Mol Cell Biol, 2007. **27**(10): p. 3758-68.
99. Barth, S., et al., *Hypoxia-inducible factor prolyl-4-hydroxylase PHD2 protein abundance depends on integral membrane anchoring of FKBP38.* J Biol Chem, 2009. **284**(34): p. 23046-58.
100. Choi, M.S., et al., *The essential role of FKBP38 in regulating phosphatase of regenerating liver 3 (PRL-3) protein stability.* Biochem Biophys Res Commun, 2011. **406**(2): p. 305-9.
101. Rosner, M., et al., *Cell size regulation by the human TSC tumor suppressor proteins depends on PI3K and FKBP38.* Oncogene, 2003. **22**(31): p. 4786-98.
102. Bai, X., et al., *Rheb activates mTOR by antagonizing its endogenous inhibitor, FKBP38.* Science, 2007. **318**(5852): p. 977-80.
103. Uhlenbrock, K., et al., *Reassessment of the role of FKBP38 in the Rheb/mTORC1 pathway.* FEBS Lett, 2009. **583**(6): p. 965-70.
104. Wang, X., et al., *Re-evaluating the roles of proposed modulators of mammalian target of rapamycin complex 1 (mTORC1) signaling.* J Biol Chem, 2008. **283**(45): p. 30482-92.
105. Dunlop, E.A., et al., *Mammalian target of rapamycin complex 1-mediated phosphorylation of eukaryotic initiation factor 4E-binding protein 1 requires multiple protein-protein interactions for substrate recognition.* Cell Signal, 2009. **21**(7): p. 1073-84.
106. Yoon, M.S., et al., *Phosphatidic acid activates mammalian target of rapamycin complex 1 (mTORC1) kinase by displacing FK506 binding protein 38 (FKBP38) and exerting an allosteric effect.* J Biol Chem, 2011. **286**(34): p. 29568-74.
107. Briscoe, J. and J. Ericson, *Specification of neuronal fates in the ventral neural tube.* Curr Opin Neurobiol, 2001. **11**(1): p. 43-9.
108. Cho, A., H.W. Ko, and J.T. Eggenschwiler, *FKBP8 cell-autonomously controls neural tube patterning through a Gli2- and Kif3a-dependent mechanism.* Dev Biol, 2008. **321**(1): p. 27-39.
109. Saita, S., et al., *Promotion of neurite extension by protrudin requires its interaction with vesicle-associated membrane protein-associated protein.* J Biol Chem, 2009. **284**(20): p. 13766-77.
110. Shirane, M., et al., *Regulation of apoptosis and neurite extension by FKBP38 is required for neural tube formation in the mouse.* Genes Cells, 2008. **13**(6): p. 635-51.
111. Edlich, F., et al., *The specific FKBP38 inhibitor N-(N',N'-dimethylcarboxamidomethyl)cycloheximide has potent neuroprotective and neurotrophic properties in brain ischemia.* J Biol Chem, 2006. **281**(21): p. 14961-70.
112. Walker, V.E., et al., *Co-chaperone FKBP38 promotes HERG trafficking.* J Biol Chem, 2007. **282**(32): p. 23509-16.
113. Willis, M.S. and C. Patterson, *Hold me tight: Role of the heat shock protein family of chaperones in cardiac disease.* Circulation, 2010. **122**(17): p. 1740-51.
114. Wang, X., et al., *Hsp90 cochaperone Aha1 downregulation rescues misfolding of CFTR in cystic fibrosis.* Cell, 2006. **127**(4): p. 803-15.
115. Koren, J., 3rd, et al., *Bending tau into shape: the emerging role of peptidyl-prolyl isomerases in tauopathies.* Mol Neurobiol, 2011. **44**(1): p. 65-70.
116. Fong, S., et al., *Functional identification of distinct sets of antitumor activities mediated by the FKBP gene family.* Proc Natl Acad Sci U S A, 2003. **100**(24): p. 14253-8.

117. Chen, H.W., et al., *Anti-invasive gene expression profile of curcumin in lung adenocarcinoma based on a high throughput microarray analysis.* Molecular pharmacology, 2004. **65**(1): p. 99-110.
118. Okamoto, T., et al., *Hepatitis C virus RNA replication is regulated by FKBP8 and Hsp90.* EMBO J, 2006. **25**(20): p. 5015-25.
119. Okamoto, T., et al., *A single-amino-acid mutation in hepatitis C virus NS5A disrupting FKBP8 interaction impairs viral replication.* J Virol, 2008. **82**(7): p. 3480-9.
120. Wang, J., et al., *Hepatitis C virus non-structural protein NS5A interacts with FKBP38 and inhibits apoptosis in Huh7 hepatoma cells.* FEBS Lett, 2006. **580**(18): p. 4392-400.
121. Monaghan, P. and A. Bell, *A Plasmodium falciparum FK506-binding protein (FKBP) with peptidyl-prolyl cis-trans isomerase and chaperone activities.* Mol Biochem Parasitol, 2005. **139**(2): p. 185-95.
122. Bell, A., B. Wernli, and R.M. Franklin, *Roles of peptidyl-prolyl cis-trans isomerase and calcineurin in the mechanisms of antimalarial action of cyclosporin A, FK506, and rapamycin.* Biochem Pharmacol, 1994. **48**(3): p. 495-503.
123. Sabatini, D.M., et al., *RAFT1: a mammalian protein that binds to FKBP12 in a rapamycin-dependent fashion and is homologous to yeast TORs.* Cell, 1994. **78**(1): p. 35-43.
124. Braun, P.D., et al., *A bifunctional molecule that displays context-dependent cellular activity.* J Am Chem Soc, 2003. **125**(25): p. 7575-80.
125. Kang, C.B., et al., *Solution structure of FK506 binding domain (FKBD) of Plasmodium falciparum FK506 binding protein 35 (PfFKBP35).* Proteins, 2008. **70**(1): p. 300-2.
126. Kumar, R., et al., *The FK506-binding protein of the malaria parasite, Plasmodium falciparum, is a FK506-sensitive chaperone with FK506-independent calcineurin-inhibitory activity.* Mol Biochem Parasitol, 2005. **141**(2): p. 163-73.
127. Bell, A., P. Monaghan, and A.P. Page, *Peptidyl-prolyl cis-trans isomerases (immunophilins) and their roles in parasite biochemistry, host-parasite interaction and antiparasitic drug action.* Int J Parasitol, 2006. **36**(3): p. 261-76.
128. Monaghan, P., et al., *Antimalarial effects of macrolactones related to FK520 (ascomycin) are independent of the immunosuppressive properties of the compounds.* J Infect Dis, 2005. **191**(8): p. 1342-9.
129. Alag, R., et al., *NMR and crystallographic structures of the FK506 binding domain of human malarial parasite Plasmodium vivax FKBP35.* Protein Sci, 2010. **19**(8): p. 1577-86.
130. Alag, R., J. Shin, and H.S. Yoon, *NMR assignments of the FK506-binding domain of FK506-binding protein 35 from Plasmodium vivax.* Biomol NMR Assign, 2009. **3**(2): p. 243-5.
131. Kotaka, M., et al., *Crystal structure of the FK506 binding domain of Plasmodium falciparum FKBP35 in complex with FK506.* Biochemistry, 2008. **47**(22): p. 5951-61.
132. Alag, R., et al., *Crystallographic structure of the tetratricopeptide repeat domain of Plasmodium falciparum FKBP35 and its molecular interaction with Hsp90 C-terminal pentapeptide.* Protein Sci, 2009. **18**(10): p. 2115-24.
133. Marinec, P.S., et al., *FK506-binding protein (FKBP) partitions a modified HIV protease inhibitor into blood cells and prolongs its lifetime in vivo.* Proc Natl Acad Sci U S A, 2009. **106**(5): p. 1336-41.
134. Marinec, P.S., J.K. Lancia, and J.E. Gestwicki, *Bifunctional molecules evade cytochrome P(450) metabolism by forming protective complexes with FK506-binding protein.* Mol Biosyst, 2008. **4**(6): p. 571-8.
135. Florence, L.S. and B. Jurgen, *Virtual Screening Methods that Complement HTS.* Combinatorial Chemistry & High Throughput Screening, 2004. **7**(4): p. 259-269.

136. Irwin, J.J. and B.K. Shoichet, *ZINC--a free database of commercially available compounds for virtual screening.* J Chem Inf Model, 2005. **45**(1): p. 177-82.
137. Sousa, S.F., P.A. Fernandes, and M.J. Ramos, *Protein-ligand docking: current status and future challenges.* Proteins, 2006. **65**(1): p. 15-26.
138. Kitchen, D.B., et al., *Docking and scoring in virtual screening for drug discovery: methods and applications.* Nature reviews. Drug discovery, 2004. **3**(11): p. 935-49.
139. Lee, H.S., et al., *Optimization of high throughput virtual screening by combining shape-matching and docking methods.* Journal of chemical information and modeling, 2008. **48**(3): p. 489-97.
140. Leach, A.R., B.K. Shoichet, and C.E. Peishoff, *Prediction of protein-ligand interactions. Docking and scoring: successes and gaps.* J Med Chem, 2006. **49**(20): p. 5851-5.
141. Yoon, S., et al., *Surrogate docking: structure-based virtual screening at high throughput speed.* Journal of computer-aided molecular design, 2005. **19**(7): p. 483-97.
142. Bohm, H.J., *The computer program LUDI: a new method for the de novo design of enzyme inhibitors.* J Comput Aided Mol Des, 1992. **6**(1): p. 61-78.
143. Warren, G.L., et al., *A critical assessment of docking programs and scoring functions.* J Med Chem, 2006. **49**(20): p. 5912-31.
144. Cross, J.B., et al., *Comparison of several molecular docking programs: pose prediction and virtual screening accuracy.* J Chem Inf Model, 2009. **49**(6): p. 1455-74.
145. Feher, M., *Consensus scoring for protein-ligand interactions.* Drug discovery today, 2006. **11**(9-10): p. 421-8.
146. Perola, E., W.P. Walters, and P.S. Charifson, *A detailed comparison of current docking and scoring methods on systems of pharmaceutical relevance.* Proteins, 2004. **56**(2): p. 235-49.
147. Totrov, M. and R. Abagyan, *Flexible ligand docking to multiple receptor conformations: a practical alternative.* Curr Opin Struct Biol, 2008. **18**(2): p. 178-84.
148. Carlson, H.A., *Protein Flexibility is an Important Component of Structure-Based Drug Discovery.* Current Pharmaceutical Design, 2002. **8**(17): p. 1571-1578.
149. Sherman, W., et al., *Novel procedure for modeling ligand/receptor induced fit effects.* Journal of medicinal chemistry, 2006. **49**(2): p. 534-53.
150. Rueda, M., G. Bottegoni, and R. Abagyan, *Recipes for the selection of experimental protein conformations for virtual screening.* J Chem Inf Model. **50**(1): p. 186-93.
151. Yoon, S. and W.J. Welsh, *Identification of a minimal subset of receptor conformations for improved multiple conformation docking and two-step scoring.* Journal of Chemical Information and Computer Sciences, 2004. **44**(1): p. 88-96.
152. Cavasotto, C.N. and R.A. Abagyan, *Protein flexibility in ligand docking and virtual screening to protein kinases.* Journal of molecular biology, 2004. **337**(1): p. 209-25.
153. Bissantz, C., G. Folkers, and D. Rognan, *Protein-based virtual screening of chemical databases. 1. Evaluation of different docking/scoring combinations.* Journal of medicinal chemistry, 2000. **43**(25): p. 4759-67.
154. Kirchhoff, P.D., et al., *Application of structure-based focusing to the estrogen receptor.* Journal of Computational Chemistry, 2001. **22**(10): p. 993-1003.
155. Crackower, M.A., et al., *Essential role of Fkbp6 in male fertility and homologous chromosome pairing in meiosis.* Science, 2003. **300**(5623): p. 1291-5.
156. Bultynck, G., et al., *Effects of the immunosuppressant FK506 on intracellular Ca2+ release and Ca2+ accumulation mechanisms.* J Physiol, 2000. **525 Pt 3**: p. 681-93.
157. Gerard, M., et al., *Unraveling the role of peptidyl-prolyl isomerases in neurodegeneration.* Mol Neurobiol, 2011. **44**(1): p. 13-27.

158. Ruan, B., et al., *Binding of rapamycin analogs to calcium channels and FKBP52 contributes to their neuroprotective activities.* Proc Natl Acad Sci U S A, 2008. **105**(1): p. 33-8.
159. Revill, W.P., et al., *Genetically engineered analogs of ascomycin for nerve regeneration.* J Pharmacol Exp Ther, 2002. **302**(3): p. 1278-85.
160. Gold, B.G., *FK506 and the role of immunophilins in nerve regeneration.* Mol Neurobiol, 1997. **15**(3): p. 285-306.
161. Gold, B.G., *Neuroimmunophilin ligands: evaluation of their therapeutic potential for the treatment of neurological disorders.* Expert Opin Investig Drugs, 2000. **9**(10): p. 2331-42.
162. Gold, B.G., D.M. Armistead, and M.S. Wang, *Non-FK506-binding protein-12 neuroimmunophilin ligands increase neurite elongation and accelerate nerve regeneration.* J Neurosci Res, 2005. **80**(1): p. 56-65.
163. Gold, B.G. and Y.P. Zhong, *FK506 requires stimulation of the extracellular signal-regulated kinase 1/2 and the steroid receptor chaperone protein p23 for neurite elongation.* Neurosignals, 2004. **13**(3): p. 122-9.
164. Gold, B.G., et al., *Immunophilin FK506-binding protein 52 (not FK506-binding protein 12) mediates the neurotrophic action of FK506.* J Pharmacol Exp Ther, 1999. **289**(3): p. 1202-10.
165. Costantini, L.C., et al., *Immunophilin ligands can prevent progressive dopaminergic degeneration in animal models of Parkinson's disease.* Eur J Neurosci, 2001. **13**(6): p. 1085-92.
166. Klettner, A. and T. Herdegen, *The immunophilin-ligands FK506 and V-10,367 mediate neuroprotection by the heat shock response.* Br J Pharmacol, 2003. **138**(5): p. 1004-12.
167. Dumont, F.J., et al., *The immunosuppressive and toxic effects of FK-506 are mechanistically related: pharmacology of a novel antagonist of FK-506 and rapamycin.* J Exp Med, 1992. **176**(3): p. 751-60.
168. Armistead, D.M., et al., *Design, synthesis and structure of non-macrocyclic inhibitors of FKBP12, the major binding protein for the immunosuppressant FK506.* Acta Crystallogr D Biol Crystallogr, 1995. **51**(Pt 4): p. 522-8.
169. Wilkinson, D.E., et al., *Synthesis, molecular modeling and biological evaluation of aza-proline and aza-pipecolic derivatives as FKBP12 ligands and their in vivo neuroprotective effects.* Bioorg Med Chem, 2003. **11**(22): p. 4815-25.
170. Holt, D.A., et al., *Structure-activity studies of synthetic FKBP ligands as peptidyl-prolyl isomerase inhibitors.* Bioorganic & Medicinal Chemistry Letters, 1994. **4**(2): p. 315-320.
171. ChemDiv, I., *11885 Sorrento Valley Road, San Diego, CA, 92121.*
172. Lipinski, C.A., et al., *Experimental and computational approaches to estimate solubility and permeability in drug discovery and development settings.* Adv Drug Deliv Rev, 2001. **46**(1-3): p. 3-26.
173. Veber, D.F., et al., *Molecular properties that influence the oral bioavailability of drug candidates.* Journal of medicinal chemistry, 2002. **45**(12): p. 2615-23.
174. Accelrys, *Discovery Studio Modeling Environment, Release 3.1* Accelrys Software Inc.,San Diego, 2007.
175. Smellie, A., S.D. Kahn, and S.L. Teig, *Analysis of Conformational Coverage. 2. Applications of Conformational Models.* Journal of Chemical Information and Computer Sciences, 1995. **35**(2): p. 295-304.
176. Smellie, A., S.D. Kahn, and S.L. Teig, *Analysis of Conformational Coverage. 1. Validation and Estimation of Coverage.* Journal of Chemical Information and Computer Sciences, 1995. **35**(2): p. 285-294.

177. Smellie, A., S.L. Teig, and P. Towbin, *Poling: Promoting conformational variation.* Journal of Computational Chemistry, 1995. **16**(2): p. 171-187.
178. InterBioScreen Ltd., *119019 Moscow, P.O. Box 218 RUSSIA.* http://www.ibscreen.com/natural.shtml.
179. Bohm, H.J., *A novel computational tool for automated structure-based drug design.* J Mol Recognit, 1993. **6**(3): p. 131-7.
180. Jones, G., et al., *Development and validation of a genetic algorithm for flexible docking.* J Mol Biol, 1997. **267**(3): p. 727-48.
181. Gehlhaar, D.K., et al., *Molecular recognition of the inhibitor AG-1343 by HIV-1 protease: conformationally flexible docking by evolutionary programming.* Chem Biol, 1995. **2**(5): p. 317-24.
182. Jain, A.N., *Scoring noncovalent protein-ligand interactions: a continuous differentiable function tuned to compute binding affinities.* J Comput Aided Mol Des, 1996. **10**(5): p. 427-40.
183. Muegge, I. and Y.C. Martin, *A general and fast scoring function for protein-ligand interactions: a simplified potential approach.* J Med Chem, 1999. **42**(5): p. 791-804.
184. Muegge, I., *PMF scoring revisited.* J Med Chem, 2006. **49**(20): p. 5895-902.
185. Bohm, H.J., *Prediction of binding constants of protein ligands: a fast method for the prioritization of hits obtained from de novo design or 3D database search programs.* J Comput Aided Mol Des, 1998. **12**(4): p. 309-23.
186. Bohm, H.J., *The development of a simple empirical scoring function to estimate the binding constant for a protein-ligand complex of known three-dimensional structure.* J Comput Aided Mol Des, 1994. **8**(3): p. 243-56.
187. Venkatachalam, C.M., et al., *LigandFit: a novel method for the shape-directed rapid docking of ligands to protein active sites.* J Mol Graph Model, 2003. **21**(4): p. 289-307.
188. Neidhardt, F.C., P.L. Bloch, and D.F. Smith, *Culture medium for enterobacteria.* Journal of bacteriology, 1974. **119**(3): p. 736-47.
189. Bosch, J., et al., *Using fragment cocktail crystallography to assist inhibitor design of Trypanosoma brucei nucleoside 2-deoxyribosyltransferase.* J Med Chem, 2006. **49**(20): p. 5939-46.
190. Minor, Z.O.a.W., *Processing of X-ray Diffraction Data Collected in Oscillation Mode* Methods in Enzymology, 1997. **276**: p. 307-326.
191. McCoy, A.J., et al., *Phaser crystallographic software.* J Appl Crystallogr, 2007. **40**(Pt 4): p. 658-674.
192. Murshudov, G.N., et al., *REFMAC5 for the refinement of macromolecular crystal structures.* Acta Crystallogr D Biol Crystallogr, 2011. **67**(Pt 4): p. 355-67.
193. Emsley, P. and K. Cowtan, *Coot: model-building tools for molecular graphics.* Acta Crystallogr D Biol Crystallogr, 2004. **60**(Pt 12 Pt 1): p. 2126-32.
194. Chen, V.B., et al., *MolProbity: all-atom structure validation for macromolecular crystallography.* Acta Crystallogr D Biol Crystallogr, 2010. **66**(Pt 1): p. 12-21.
195. Ramachandran, G.N., C. Ramakrishnan, and V. Sasisekharan, *Stereochemistry of polypeptide chain configurations.* J Mol Biol, 1963. **7**: p. 95-9.
196. Battye, T.G., et al., *iMOSFLM: a new graphical interface for diffraction-image processing with MOSFLM.* Acta Crystallogr D Biol Crystallogr. **67**(Pt 4): p. 271-81.
197. Christopoulos, H.M.a.A., *Fitting Models to Biological Data using Linear and Nonlinear Regression. A Practical Guide to Curve Fitting*. Oxford University Press2004, New York: Oxford University Press, New York.
198. Jiang, B. and M.S. Cyert, *Identification of a novel region critical for calcineurin function in vivo and in vitro.* J Biol Chem, 1999. **274**(26): p. 18543-51.

199. Delaglio, F., et al., *NMRPipe: a multidimensional spectral processing system based on UNIX pipes.* Journal of biomolecular NMR, 1995. **6**(3): p. 277-93.
200. Goddard TD, K.D., *SPARKY 3.* University of California, San Francisco, 2009.
201. Futer, O., et al., *FK506 binding protein mutational analysis. Defining the surface residue contributions to stability of the calcineurin co-complex.* The Journal of biological chemistry, 1995. **270**(32): p. 18935-40.
202. Ikura, T. and N. Ito, *Requirements for peptidyl-prolyl isomerization activity: a comprehensive mutational analysis of the substrate-binding cavity of FK506-binding protein 12.* Protein Sci, 2007. **16**(12): p. 2618-25.
203. Ikura, T., K. Kinoshita, and N. Ito, *A cavity with an appropriate size is the basis of the PPIase activity.* Protein engineering, design & selection : PEDS, 2008. **21**(2): p. 83-9.
204. Kang, C.B., et al., *1H, 13C, and 15N resonance assignments of FK506-binding domain of Plasmodium falciparum FKBP35.* Biomol NMR Assign, 2007. **1**(1): p. 27-8.
205. DeLano, W.L., *The PyMOL Molecular Graphics System.* DeLano Scientific, Palo Alto, CA, USA, 2002.
206. Wallace, A.C., R.A. Laskowski, and J.M. Thornton, *LIGPLOT: a program to generate schematic diagrams of protein-ligand interactions.* Protein Eng, 1995. **8**(2): p. 127-34.
207. Choi, C., et al., *Use of parallel-synthesis combinatorial libraries for rapid identification of potent FKBP12 inhibitors.* Bioorg Med Chem Lett, 2002. **12**(10): p. 1421-8.
208. Hamilton, G.S. and J.P. Steiner, *Immunophilins: beyond immunosuppression.* J Med Chem, 1998. **41**(26): p. 5119-43.
209. Hamilton, G.S., et al., *Synthesis of N-glyoxyl prolyl and pipecolyl amides and thioesters and evaluation of their in vitro and in vivo nerve regenerative effects.* J Med Chem, 2002. **45**(16): p. 3549-57.
210. Holt, D.A., et al., *Design, synthesis, and kinetic evaluation of high-affinity FKBP ligands and the X-ray crystal structures of their complexes with FKBP12.* Journal of the American Chemical Society, 1993. **115**(22): p. 9925-9938.
211. Guner, O.F., *Pharmacophore Perception, Development, and Use in Drug Design (Iul Biotechnology Series, 2)*2000: Intl Univ Line.
212. Sprague, P., *Automated chemical hypothesis generation and database searching with Catalyst®.* Perspectives in Drug Discovery and Design, 1995. **3**(1): p. 1-20.
213. Fischer, R., *The Principle of Experimentation, Illustrated by a Psycho-Physical Experiment. The Design of Experiments (8th ed.).* Hafner Publishing Co., New York, 1966. **Chapter II**.
214. Babine, R.E., et al., *Design, synthesis and X-ray crystallographic studies of novel FKBP-12 ligands.* Bioorganic & Medicinal Chemistry Letters, 1995. **5**(15): p. 1719-1724.